FAT CRYSTALLIZATION – FRACTIONATION BY ENTRAINMENT AND CHARACTERIZATION USING REFRACTOMETRY

vorgelegt von
M.Sc.
Michaela Horn
geb. in Sindelfingen

von der Fakultät III – Prozesswissenschaften
der Technischen Universität Berlin
zu Erlangung des akademischen Grades

Doktor der Ingenieurwissenschaften
- Dr.-Ing. –

genehmigte Dissertation

Promotionsausschuss:

Vorsitzender:	Prof. Dr. rer. nat. habil. Lothar W. Kroh
Gutachter:	Prof. Dr.-Ing. Eckhard Flöter
Gutachter:	Prof. Dr. Stephan Drusch
Gutachterin:	Dr. Elke Scholten

Tag der wissenschaftlichen Aussprache: 01. Juni 2018

Berlin 2018

The elegant pathway in theory too often turned out to be
a troublesome application in practice.

(Marc Kellens & Gijs Calliauw)

ABSTRACT

In food industry, products containing fats and oils are mainly structured by a functional mixture of high and low melting fats and oils. The provided structuring needs to be controlled because it influences texture, stability, taste, and storage life of a product. The mentioned fats and oils are mainly composed of a mixture of triacylglycerides (TAGs). Since this mixture is not a binary system, the phase behavior is quite complex. A possible distinction of the various fractions in these mixtures is their melting/crystallization temperature.

The source of a fat/ oil determines its composition. TAGs from animal fats are high in saturated fatty acid residues (except of e.g. aquatic organisms) while plant-based oils are mainly high in unsaturated fatty acid moieties (except of tropical oils e.g. coconut oil). The consumption of unsaturated fatty acids is known to be healthy for humans and, thus, oils containing high concentrations of these are recommended with respect to nutritional aspects. If these unsaturated fatty acids are polyunsaturated they are so-called essential fatty acids. Due to processing or the nature of the fats, so-called *trans*-fatty acids occur. These are known to have detrimental effects for the health.

In fat technology, specific demands are made for different products to achieve the desired properties (e.g. shelf life, health, processing). This requires the functionalization of naturally occurring fats and oils, historically done using fractionation, interesterification, and/or hydrogenation. During fractionation, which is performed batch-wise, the fractions are generated due to their distinct melting points. Interesterification exchanges the fatty acid residues at the glycerol backbone of the TAGs randomly. For chemical catalysts, the randomization is complete. Enzymatic catalysts are selective and yield lower reaction rates which makes the resulting composition difficult to predict. The process of hydrogenation is used to achieve different degrees of saturation independent of the raw material. However, during this process, if not conducted completely, *trans*-fatty acids are formed which are known to increase the risk of cardiovascular diseases.

The fractionation process is the only functionalization which does not change the molecular structure of the TAGs. Two commonly applied technologies are outlined shortly. The dry fractionation is the cheapest and most applied process but also the least selective and efficient one. The solvent fractionation is more efficient but expensive and the used solvents can cause problems due to hazardous working conditions.

A continuous fractionation process would be desirable to decrease production time and costs. Hence, we examined the application of a new emulsion fractionation process which is based on a process applied for margarine production. It aims for a continuous process and specific fractionation of the desired TAGs. The idea is that cold water droplets are injected into a warm oil mixture initiating crystallization of the high melting TAGs at the droplet surface due to local supercooling. These crystals stabilize the water droplet, forming a so-called Pickering emulsion. The water droplets stabilized by fat crystals have a higher density than the surrounding liquid oil which makes a separation by centrifugal force possible. This separation step was performed in a lab scale decanter centrifuge achieving a continuous process.

Preliminary tests were conducted using a mixture of rapeseed oil and a predetermined amount of fully hydrogenated fat (hardstock) as a model system to know the exact amount of hardstock before and after emulsion fractionation. In addition, experiments with palm oil as a model system were carried out. It was shown that the two processes of crystallization and separation need to be harmonized well to achieve the best separation efficiency. In general, the separation was possible, but the efficiency was very low. Therefore, a better understanding of the influencing parameters used to control the process in the decanter need to be obtained. An accurate knowledge of the phase equilibrium and the kinetics during the continuous process is crucial to establish the window of the apparatus parameters for a successful application.

To study the phase equilibrium of the applied materials, an analytical method is required to characterize fats and oils. This method should be reliable, fast, and easily applicable for a large number of experiments. Therefore, the application of the new temperature modulated optical refractometry was evaluated.

Fat crystallization is usually investigated by distinct methods to determine phase transitions, the amount of solids, and polymorphic crystal forms. Differential scanning

calorimetry is an established method to determine melting and crystallization in fats and oils. Pulsed nuclear magnetic resonance is normally applied to obtain the solid fat content of a material, which is important as a quality parameter and determines the application range of a fat. Powder X-ray diffraction is a well-known technique to differentiate polymorphic forms in fats which is important for products like chocolate where only one polymorph of cocoa butter delivers the desired product properties.

All of these enumerated methods are quite expensive and partially complex in sample handling. A more convenient and cheaper method proofed to be the temperature modulated optical refractometry (TMOR). It determines the refractive index while a temperature modulation is conducted directly on the prism. This yields beside the mean refractive index a thermal volume expansion coefficient α. The method can be carried out in an isothermal and a dynamic way. Both modes are interesting for the application in fat technology and therefore the applicability of TMOR for the investigation of fats and oils was part of this thesis.

We found that it is possible to determine phase transitions of aliphatic chain components as well as of more complex systems like fats. Additionally, the device was used to obtain the solid fat content by determining the apparent refractive index of various fats such as coconut oil and applying the lever rule. So far, only the potential to determine polymorphic forms using TMOR was shown. In future work this application of TMOR needs to be further investigated.

The applicability of TMOR was shown in this work. In the next step this technique is applied to gain better knowledge of the phase behavior and kinetics so that the process window of the continuous emulsion fractionation can be identified.

In summary, both, the new emulsion fractionation technology and the temperature modulated optical refractometry, could be combined. TMOR could be used as analytic method to determine the melting behavior and the solid fat content of the fractionated material. Thereby, important information about the separation efficiency and the resulting TAG fractions would be obtained supporting the optimization of the process design.

ZUSAMMENFASSUNG

In der Lebensmittelindustrie werden Produkte, die Fette und Öl enthalten, hauptsächlich durch eine funktionelle Mischung aus hoch- und niedrigschmelzenden Fetten und Ölen strukturiert. Die Strukturierung muss kontrolliert werden, da sie die Textur, Stabilität, Geschmack und Haltbarkeit eines Produkts beeinflusst. Die genannten Fette und Öle bestehen hauptsächlich aus einer Mischung von Triacylglyceriden (TAGs). Da diese Mischung kein binäres System ist, ergibt sich ein komplexes Phasenverhalten. Eine mögliche Unterscheidung der verschiedenen Fraktionen in diesen Gemischen ist ihre Schmelz- bzw. Kristallisationstemperatur.

Die Quelle eines Fettes/ Öles bestimmt seine Zusammensetzung. TAGs aus tierischen Fetten sind reich an gesättigten Fettsäureresten (mit Ausnahme von z.B. Wasserorganismen), während Öle auf pflanzlicher Basis hauptsächlich ungesättigte Fettsäurereste enthalten (mit Ausnahme von tropischen Ölen, z.B. Kokosnussöl). Es ist bekannt, dass der Verzehr von ungesättigten Fettsäuren gesund für den Menschen ist. Daher werden Öle, die hohe Konzentrationen an ungesättigten Fettsäuren enthalten, in Bezug auf Ernährungsaspekte empfohlen. Wenn diese ungesättigten Fettsäuren mehrfach ungesättigt sind, werden sie als sog. essentielle Fettsäuren bezeichnet. Aufgrund der Verarbeitung oder der Art der Fette treten sog. Transfettsäuren auf, die dafür bekannt sind, dass sie schädliche Auswirkungen auf die Gesundheit haben.

In der Fetttechnologie werden spezifische Anforderungen an verschiedene Produkte gestellt, um die gewünschten Eigenschaften (z. B. Haltbarkeit, Ernährungsphysiologie, Verarbeitung) zu erreichen. Dies erfordert die Funktionalisierung von natürlich vorkommenden Fetten und Ölen, die historisch durch Fraktionierung, Umesterung und/ oder Hydrierung durchgeführt wurden. Während der Fraktionierung, die chargenweise durchgeführt wird, werden die Fraktionen aufgrund ihrer Schmelzpunkte erzeugt. Die Umesterung tauscht die Fettsäurereste am Glycerol-Rückgrat der TAGs zufällig aus. Bei chemischen Katalysatoren erfolgt eine vollständige Zufallssteuerung. Enzymatische Katalysatoren sind dagegen selektiv und zeigen niedrigere Reaktionsgeschwindigkeiten, was die Vorhersage der resultierenden

Zusammensetzung erschwert. Der Prozess der Hydrierung wird verwendet, um unterschiedliche Sättigungsgrade unabhängig vom Rohmaterial zu erreichen. Bei diesem Prozess werden jedoch, wenn er nicht vollständig durchgeführt wird, Transfettsäuren gebildet, von denen bekannt ist, dass sie das Risiko von Herz-Kreislauf-Erkrankungen erhöhen.

Die Fraktionierung ist der einzige Funktionalisierungsprozess, der die molekulare Struktur der TAGs nicht verändert. Zwei gängige Technologien werden in Kürze vorgestellt. Die Trockenfraktionierung ist der billigste und am meisten angewendete Prozess, aber auch der am wenigsten selektive und effiziente. Die Lösungsmittelfraktionierung ist effizienter, aber teuer. Zudem können die verwendeten Lösungsmittel aufgrund von gefährlichen Arbeitsbedingungen Probleme verursachen.

Ein kontinuierlicher Fraktionierungsprozess wäre wünschenswert, um Produktionszeit und -kosten zu verringern. Daher haben wir die Anwendung eines neuen Emulsionsfraktionierungsverfahrens untersucht, das auf einem Verfahren zur Margarineherstellung basiert. Die Ziele sind ein kontinuierlicher Prozess und eine spezifische Fraktionierung der gewünschten TAGs. Die Idee ist, dass kalte Wassertropfen in ein warmes Ölgemisch injiziert werden, die die Kristallisation der hochschmelzenden TAGs an der Tropfenoberfläche aufgrund lokaler Unterkühlung initiieren. Diese Kristalle stabilisieren den Wassertropfen und bilden eine sog. Pickering-Emulsion. Die durch Fettkristalle stabilisierten Wassertropfen haben eine höhere Dichte als das sie umgebende flüssige Öl, was eine Trennung durch Zentrifugalkraft ermöglicht. Dieser Trennschritt wurde in einer Dekanterzentrifuge im Labormaßstab durchgeführt, womit ein kontinuierlicher Prozess erreicht wurde.

Vorversuche wurden unter Verwendung einer Mischung aus Rapsöl und einer vorbestimmten Menge an vollständig hydriertem Fett (Hardstock) als Modellsystem durchgeführt, um die genaue Menge an Hardstock vor und nach der Emulsionsfraktionierung zu kennen. Darüber hinaus wurden Versuche mit Palmöl als Modellsystem durchgeführt. Es wurde gezeigt, dass die beiden Kristallisations- und Trennprozesse gut aufeinander abgestimmt werden müssen, um die beste Trennleistung zu erzielen. Im Allgemeinen war die Trennung möglich, aber die Effizienz sehr gering. Daher muss ein besseres Verständnis der Einflussparameter, die zur Steuerung des Prozesses im Dekanter verwendet werden, entwickelt werden. Eine

genaue Kenntnis des Phasengleichgewichts und der Kinetik während des kontinuierlichen Prozesses ist entscheidend, um das Prozessfenster der Geräteparameter für eine erfolgreiche Anwendung zu ermitteln.

Um das Phasengleichgewicht der verwendeten Materialien zu untersuchen, ist eine analytische Methode zur Charakterisierung von Fetten und Ölen erforderlich. Diese Methode sollte zuverlässig, schnell und leicht für eine große Anzahl von Experimenten anwendbar sein. Daher wurde die Anwendung der neuen temperaturmodulierten optischen Refraktometrie evaluiert.

Die Fettkristallisation wird üblicherweise durch verschiedene Verfahren zur Bestimmung von Phasenübergängen, der Menge an Feststoffen und polymorpher Kristallformen untersucht. Die dynamische Differenzkalorimetrie ist eine etablierte Methode zur Bestimmung des Schmelzens und Kristallisierens in Fetten und Ölen. Gepulste Kernspinresonanz wird normalerweise angewendet, um den Festfettgehalt eines Materials zu ermitteln, welcher als Qualitätsparameter wichtig ist und den Anwendungsbereich eines Fettes bestimmt. Die Röntgenbeugungsanalyse ist eine weit verbreitete Technik, um polymorphe Kristallformen in Fetten zu unterscheiden. Dies ist für Produkte wie Schokolade wichtig, in denen nur ein Polymorph der Kakaobutter die gewünschten Produkteigenschaften liefert.

Alle oben genannten Verfahren sind ziemlich teuer und teilweise komplex in der Probenbehandlung. Eine praktische und billigere Methode ist die temperaturmodulierte optische Refraktometrie (TMOR). Die Methode bestimmt den Brechungsindex, während eine Temperaturmodulation direkt am Prisma durchgeführt wird. Dies ergibt neben dem mittleren Brechungsindex einen thermischen Volumenausdehnungskoeffizienten α. Das Verfahren kann isotherm und dynamisch durchgeführt werden. Beide Modi sind interessant für die Anwendung in der Fetttechnologie. Daher war die Anwendbarkeit von TMOR für die Untersuchung von Fetten und Ölen Teil dieser Arbeit.

Wir zeigten, dass es möglich ist, Phasenübergänge von aliphatischen Ketten sowie von komplexeren Systemen wie Fetten zu bestimmen. Zusätzlich wurde das Gerät verwendet, um den Festfettgehalt zu ermitteln, indem der scheinbare Brechungsindex für verschiedene Fette wie Kokosnussöl bestimmt und das Hebelgesetz angewendet wurde. Bisher wurde nur das Potenzial zur Bestimmung polymorpher Formen mit

TMOR gezeigt. In zukünftigen Arbeiten muss diese Anwendung von TMOR weiter untersucht werden.

Die Anwendbarkeit von TMOR wurde in dieser Arbeit gezeigt. Im nächsten Schritt wird diese Technik verwendet, um das Phasenverhalten und die Kinetik besser zu verstehen, so dass das Prozessfenster der kontinuierlichen Emulsionsfraktionierung identifiziert werden kann.

Zusammenfassend können sowohl die neue Emulsionsfraktionierungstechnologie als auch die temperaturmodulierte optische Refraktometrie kombiniert werden. TMOR könnte als analytische Methode verwendet werden, um das Schmelzverhalten und den Feststoffgehalt der verschiedenen Fraktionen zu bestimmen. Dadurch könnten wichtige Informationen zur Trenneffizienz und den gewonnenen TAG-Fraktionen generiert werden, die wiederum die Optimierung des Prozessdesigns unterstützen.

ACKNOWLEDGEMENTS

This thesis was written at the department of Food Process Engineering at the Technical University of Berlin and financially supported by the Elsa-Neumann Scholarship of the federal state of Berlin.

First of all, I would like to thank Prof. Dr.-Ing. Eckhard Flöter for the supervision of my thesis, the familiar work atmosphere he provides, and his supporting character. He was always open for questions, discussions, and gave helpful advices throughout the thesis.

I owe thanks to Prof. Dr. Stephan Drusch and Dr. Elke Scholten for taking the time to assess my thesis.

I want to especially thank Susanne, who spent lots of time reading and discussing my research. Thank you for being always supportive, helpful, and empowering.

A special thanks goes to the people who were the reason why work did not always feel like work: Karl Schlumbach, Maria Scharfe, and Miro Kirimlidou. Thank you for being more than colleagues, thank you for being friends.

I also want to thank my Bachelor students (Dewi Dewanga Suprana, Frederike Deckwerth, Wiebke Wilms Schulze-Kump, Valeska Hutschenreuter) and Master students (Philipp Martin, Ratna Ayu Savitri) who worked with me throughout the last years and helped me to develop.

A big thanks also goes to all colleagues at the department of Food Process Engineering: Karin, Martha, Ruth, Julia, Evelyn, Alexandra, Gabi, Valentina, Simone, Marco, Tim, Juliane, Melina, Jonathan, Stephan, Susanne.

I´m grateful for having parents who are proud of me, support me at every stage of my life, and love me unconditionally. I also thank my friends all over the world who care about me and make my life brighter every day.

Last, I want to thank my husband Philipp for his advice, gratitude, and support. You cheer me up when I´m down and help me to be the best version of myself.

LIST OF PUBLICATIONS

Parts of the study were presented as follows

Publications in journals

1. Häupler, M., Flöter, E. (2018) Determination of the Crystallization Behavior of Lipids by Temperature Modulated Optical Refractometry; *Food Analytical Methods*, doi.org/10.1007/s12161-018-1217-y

2. Häupler, M., Savitri, R.A., Hutschenreuter, V., Flöter, E. (2018) Application of Temperature Modulated Optical Refractometry for the Characterization of the Crystallization Behavior of Palm Oil; *European Journal of Lipid Science and Technology,* doi.org/10.1002/ejlt.201700511

3. Häupler, M., Kirimlidou, M., Wilms Schulze-Kump, W., Parisi, A., Wagner, L., Flöter, E. (2018) On the feasibility of continuous emulsion fractionation, *submitted to the European Journal of Lipid Science and Technology*.

4. Häupler, M., Hutschenreuter, V., Rudolph, S., Flöter, E. (2018) Feasibility study on the determination of the solid fat content of fats using temperature modulated optical refractometry, *submitted to the European Journal of Lipid Science and Technology*.

Oral and poster presentations

1. Häupler, M., Schwarz G. Henriques, S., Flöter, E., (2015) Determination of Melting Point and Polymorphic Form of Edible Fats via Temperature Modulated Optical Refractometry (TMOR), *Euro Fed Lipids Congress*, Florence, Italy.

2. Häupler, M., Flöter, E. (2016) Continuous Emulsion Fractionation of Fats, *Euro Fed Lipids Congress*, Ghent, Belgium.

3. Häupler, M., Kirimlidou, M., Flöter, E. (2017) Lab Scale Continuous Emulsion Fractionation of Edible Fats, *Euro Fed Lipids Congress*, Uppsala, Sweden.

4. Häupler, M. Kirimlidou, M., Flöter, E. (2018) Kontinuierliche Emulsionsfraktionierung von Speisefetten im Labormaßstab, *ProcessNet*, Berlin, Germany.

CO-AUTHORSHIP

The work presented in this thesis was partially conducted with other scientists of the Department of Food Process Engineering, TU Berlin. Dr. Susanne Rudolph was involved in outlining and writing the publications as well as in scientific discussions concerning all chapters. Dr. Fernanda Peyronel and Dr. Alejandro G. Marangoni provided scientific input and the opportunity to use different devices at the Food Science Department, University of Guelph. With Prof. Dr.-Ing. Eckhard Flöter, who supervised the whole PhD thesis, all chapters were discussed scientifically.

- Chapter 4
  Michaela Häupler designed, planned, conducted, supervised, and analyzed the experimental work. The experimental work was partially carried out by Wiebke Wilms-Schulze Kump, Miro Kirimlidou, Alessandra Parisi, and Leonie Wagner

- Chapter 5
  Michaela Häupler designed, planned, conducted, and analyzed the experimental work.

- Chapter 6
  Michaela Häupler designed, planned, conducted, and analyzed the experimental work. Parts of the experimental work were carried out by Frederike Deckwerth.

- Chapter 7
  Michaela Häupler designed, planned, supervised, and analyzed the experimental work. The experimental work was partially carried out by Ratna Ayu Savitri and Valeska Hutschenreuter.

- Chapter 8
  Michaela Häupler designed, planned, conducted, and analyzed the experimental work. Parts of the experimental work were carried out by Valeska Hutschenreuter. The results were discussed with Susanne Rudolph.

- Chapter 9
  Michaela Häupler designed, planned, conducted, and analyzed the experimental work.

SYMBOLS AND ABBREVIATIONS

Symbols

α	thermal expansion coefficient	-
c_0	speed of light in vacuum	m s^{-1}
c_m	speed of light in material	m s^{-1}
d	diameter	mm
ϕ_ω	phase shift at angular frequency	-
g	acceleration of gravity	m s^{-2}
G	Gibbs free energy	J
ΔH_m	specific melting enthalpy	J g^{-1}
Im(α)	imaginary part of α	-
λ	wave length	nm
m	mass	g
μ	chemical potential	-
n	refractive index	-
η	dynamic viscosity	mPas
ρ	mass density	g cm^{-3}
r	specific refractivity	cm^3 g^{-1}
R	gas constant	J $mol^{-1}K^{-1}$
Re(α)	real part of α	-
θ	angle	°
t	time	s
T	temperature	°C
T_c	crystallization temperature	°C
T_m	melting temperature	°C
$\dot{V}$	volume flow	L h^{-1}
x_i	mole fraction	mol mol^{-1}
ω	angular frequency	s^{-1}

Abbreviations

AOCS	American Oil Chemists Society
CBE	cocoa butter equivalent
CO	coconut oil
DAG	diacylglyceride
DSC	differential scanning calorimetry
FA	fatty acid
FAME	fatty acid methyl ester
FFA	free fatty acid
FHPO	fully hydrogenated palm oil
FHRO	fully hydrogenated rapeseed oil
FID	flame ionization detector
fps	frames per second
GC	gas chromatography
HLB	hydrophilic-lipophilic balance
IV	iodine value
LRT	linear response theory
MAG	monoacylglycerides
MCT	medium-chain length triacylglyceride
MUFA	monounsaturated fatty acid
MTBE	methyl-*tert*-butylether
NMR	nuclear magnetic resonance
OOO	triolein
O/W	oil-in-water emulsion
PHPO	partially hydrogenated palm oil
PLM	polarized light microscopy
PMF	palm mid fraction
PO	palm oil
POP	*sn*-1,3-palmitoyl-2-oleoyl triacylglyceride
PPP	tripalmitate

PUFA	polyunsaturated fatty acid
rpm	rounds per minute
SFC	solid fat content
SFI	solid fat index
SSS	tristearate
TAG	triacylglyceride
TMOR	temperature modulated optical refractometry
TMSH	trimethylsulfoniumhydroxide
W/O	water-in-oil emulsion
XRD	X-ray diffraction

TABLE OF CONTENTS

1 INTRODUCTION

In food industry, the processing of fat containing products requires good knowledge of the composition of the fats and their crystallization behavior. Fats are multicomponent systems which are mainly composed of triacylglycerides (TAGs). Structuring fats are used e.g. to stabilize water or air in products like margarine or ice cream. In addition, the proper crystallization influences shelf life, mouthfeel, and spreadability of the desired products. Decades ago, the application of so-called hydrogenated fats as structuring fats was popular. These were obtained by the saturation of oils with hydrogen (hydrogenation) leading to fats with different degrees of saturation and, hence, different melting profiles which increased the application range dramatically.

However, the use of hydrogenated fats in food industry diminished drastically, it almost vanished. The reason is that during hydrogenation of oils and fats if the process is not completed, *trans*-fatty acids are formed. In the past, by choosing the right degree of hydrogenation, such partially hydrogenated oils were useful to adjust the desired product properties. Even though if hydrogenation is completed no *trans*-fatty acids are formed the public acceptance of the process is low as it is difficult to teach the differences between partial and full hydrogenation to the consumer. Therefore, the industry searched for alternatives to the hydrogenation process. Another modification process is interesterification, where the fatty acids at the glycerol backbone of the TAGs are chemically or enzymatically exchanged. Nevertheless, this exchange occurs randomly and, thus, the prediction of the product properties is difficult.

In this thesis, the selected modification technique was a fractionation process. In contrast to hydrogenation and interesterification, which use chemicals to modify the properties of oils and fats, fractionation is a solely physical process. The invention of the technology of fractionation to separate high from low melting fat is ascribed to Hippolyte Mège Mouriès (1817–1880) in the late 1860s. It uses the differences in the melting points of different fractions, for example of palm oil, to separate the low melting part (olein) from the high melting part (stearin). This separation can be performed several times to yield even more specific fats for certain applications.

Nowadays, three different fractionation methods are known. Only two of them are usually applied, solvent fractionation for specialty fats and dry fractionation for larger amounts of fat to be fractionated (like palm oil). Both are batch processes. The first

one uses solvents like hexane or acetone to decrease the viscosity of the slurry containing crystallized and liquid fat. However, an expensive solvent recovery is indispensable to obtain a fat which is food grade. Another disadvantage of this process is the hazardous working environment.

In dry fractionation, the feed is crystallized so that large crystals are formed which do not entrap liquid oil forming a slurry with the surrounding liquid phase. The slurry is separated by membrane press filtration. Due to the lack of the washing step, the separation efficiency is lower for the dry than for the solvent fractionation. However, sequential fractionation steps can yield diverse fractions showing desired properties for different applications, respectively. The third method, which is not frequently used today, is the detergent fractionation process. It uses surfactants to emulsify the yielded fat fraction which is then separated by centrifugation.

The new process of emulsion fractionation, which was started to be developed in this thesis, combines the mechanism of forming stable droplets as for the detergent fractionation process with a continuous separation step but actually without the use of a detergent. The aim of the emulsion fractionation process is the direct fractionation of the valuable fraction of high melting TAGs like PPP. Normally, to generate this fraction, several fractionation steps need to be performed in the dry fractionation process.

The process is as follows. A cold water stream is injected into a warm liquid oil stream, composed of a high and a low melting fraction. At the cold surface of the water droplet the high melting fraction of the fat crystallizes and stabilizes the droplets, forming a Pickering emulsion. This emulsion is fed into a decanter centrifuge where continuous separation between the liquid phase and the water droplets stabilized by crystallized fat occurs. The process only uses water as an entrainer which can be recycled and is relatively cheap. Moreover, the continuous process has advantages over a batch process because it decreases the inter-batch variability of the resulting products and saves energy costs. Additionally, the particle size distribution of the product is more uniform.

To decrease the complexity of the process, both steps, the crystallization and the separation, were studied independently using palm oil and a mixture of rapeseed oil with a defined amount of high melting fat (hardstock) as model systems. The ultimate

objective is the use of seed oils like sunflower or rapeseed as the raw material for the fractionation process. However, due to the low amount of saturated TAGs in seed oils, first the process needs to be fully understood before a highly effective fractionation method can be designed.

The parameters like crystallization temperature need to be determined precisely to design the process explained above. A reliable and robust alternative to well-established but expensive laboratory devices would be desirable for both research and industry. Therefore, this thesis includes the feasibility study of a new method to determine phase transitions which are crucial for the food industry. The crystallization of fats is decisive for the new fractionation process but also for the product quality and, thus, the resulting shelf life. For example, the melting sensation of chocolate is based on the proper crystallization of cocoa butter during the production.

Moreover, the investigation of the melting behavior is directly linked to the crystallization process because it determines the consumer acceptance. For example, this comes into focus if the consumer uses the margarine right from the fridge which should be spreadable at this temperature. In the last decades, the investigation of crystallization and melting behavior of fats is done by differential scanning calorimetry. This method monitors the heat flow during heating and cooling of the sample, which changes if a phase transition occurs. Other methods to characterize product properties are pulsed nuclear magnetic resonance and powder x-ray diffraction. However, all of the mentioned methods are mainly applicable for laboratory work since the devices are expensive, the handling is quite complex, and the procedures are often time-consuming.

Hence, a reliable but robust, cheap and fast method to determine the phase transitions of fats would be desirable. This is why in this thesis the determination of the refractive index is taken into account as another possibility to characterize fats and oils. The refractive index differs for the solid and the liquid state of a fat. This phenomenon was used to study the phase behavior of lipid components and fats using temperature modulated optical refractometry (TMOR).

In addition to traditional refractometry, this device can modulate the temperature around a set mean temperature with a predefined amplitude and period. This modulation and the resulting phase shift of the answer of the refractive index is used to compute the thermal expansion coefficient α which then indicates the temperature

of phase transition. Additionally, the thesis illustrates that TMOR can be used to determine the SFC of fats and oils or even polymorphic transitions.

In this thesis, the possibility to perform a continuous emulsion fractionation process was evaluated. Therefore, the process was studied by dividing it into the two single processes, crystallization and separation, as well as by studying the entire process.

The aim of the study was to show that it is possible to separate a model fat system by continuous emulsion fractionation technology. Thus, the following questions need to be answered to design a reliable continuous emulsion fractionation process.

1. Which centrifugal forces need to be applied to separate the liquid phase from the water droplets stabilized by fat crystals?
2. How is the temperature development over the process (melting of the crystals)?
3. Which parameters take influence on the separation efficiency, e.g. flocculation, viscosity, throughput, temperature?
4. What are the parameters influencing the crystallization in general and on the water droplet surface?

In addition to the process, also questions concerning the analysis need to be addressed.

1. Is temperature modulated optical refractometry (TMOR) an applicable method to determine the crystallization and melting behavior of alkyl components and thus to characterize systems before emulsion fractionation?
2. What is the proper sample handling to use TMOR as a method to determine the phase behavior of fats and oils?
3. Is it possible to determine the phase behavior of fats and oils with TMOR?
4. Can the application of TMOR be expanded to the determination of SFC and polymorphic transitions?

The characterization of different properties of fats and oils like melting behavior or solid fat content by TMOR could be used to determine the best conditions for the outlined emulsion fractionation process.

First, to answer all the stated questions, the required fundamentals of this thesis are elucidated in chapter 2 to generate an overview of the basic knowledge. The chapter covers the composition of triacylglycerides, the principles of their crystallization behavior, explains the phenomenon of polymorphism and gives background information needed to perform the emulsion fractionation process like the formation of a Pickering emulsion. Subsequently, the experimental and analytical methods used in this thesis are explained (see chapter 3).

The results and discussion section is divided into two sections concerned with either the emulsion fractionation or the TMOR method. The results of the separation step during the emulsion fractionation depending on the emulsion composition are given. The experiments conducted in a batch-wise operating benchtop centrifuge and in a continuous decanter centrifuge are discussed in this part of the results and discussion section (see chapter 4).

The investigations of the applicability of TMOR to study pure substances like *n*-hexadecane, palmitic acid and tripalmitate are shown in chapter 5. The adaption of the sample handling and proper measurement procedure for fats and oils is subsequently given in chapter 6. This procedures were applied to determine the crystallization and melting behavior of edible fats (e.g. partially and fully hydrogenated palm oil) by TMOR (see chapter 7). This section is completed by the applicability of TMOR to determine the SFC of edible fats (e.g. coconut oil, palm oil) which is evaluated in chapter 8. In addition, the possibility to determine polymorphic transitions using TMOR is given in chapter 9.

In the last part of the thesis, a conclusion of all conducted experiments is given (see chapter 10). In addition, advices for future experiments are specified and further areas of research are elucidated.

2 FUNDAMENTALS

This chapter is dedicated to the important topics related to fats and oils and are required as the background information for this thesis. First, the composition of fats and oils is explained including the principle structure of triacylglycerides as well as a brief explanation of minor components and their respective influence on physical and chemical properties. The increasingly used palm oil is key to this thesis and, thus, one chapter about its origin and composition is presented. In addition, the phase behavior of fatty acids, triacylglycerides (TAGs), fats, and oils is described shortly because this knowledge is relevant to understand the crystallization behavior of fats and oils explained in 2.2.

The subchapter on fat crystallization explains nucleation and growth. Furthermore, the phenomenon of polymorphism is elucidated and its importance during fat crystallization and especially fat fractionation is clarified. Particular attention is subsequently paid to fractionation as a common fat modification technique.

After a short introduction into hydrogenation and interesterification, the focus is on the various fractionation techniques available. The solvent and detergent fractionation are explained followed by the description of the dry fractionation process. Finally, the new idea of emulsion fractionation is presented and substantiated with literature about Pickering emulsions and the crystallization of fat at the water/oil interface of emulsions as well as the separation in a decanter centrifuge.

2.1 Fats & Oils

What we refer to as fat is always a multicomponent system and therefore its behavior depends on the composition of the raw material (Flöter, 2012). Therefore, the structure of the main components of fats and oils is given in the following chapter.

2.1.1 Composition of Fats & Oils

The basic molecules of fats and oils are triacylglycerides (TAGs, Figure 2.1c), accompanied by minor amounts of mono- and diacylglycerides as well as other minor components such as phospholipids, phytosterols and tocols (Gunstone, 2013). TAGs are made of fatty acids, which are either based on *n*-alkanes (Figure 2.1a) or *n*-alkenes referring to saturated and unsaturated fatty acids, respectively. While *n*-alkanes and *n*-alkenes end with a methyl group, fatty acids end with a carboxyl group (see Figure

2.1b) In the nomenclature e.g. C16:0 for palmitic acid (Figure 2.1b), 16 refers to the number of C-atoms of the alkane or alkene-chain and 0 refers to the fact that there are no double bonds. So for example C18:1 is a fatty acid with 18 C-atoms in the alkene chain and a double bond (oleic acid) or C18:2 with 18 C-atoms and two double bonds in the alkene-chain (linoleic acid). TAGs are composed of a glycerol backbone esterified with three fatty acids (carbon chains) (Sato, 2001; Himawan, Starov and Stapley, 2006; Douaire *et al.*, 2014).

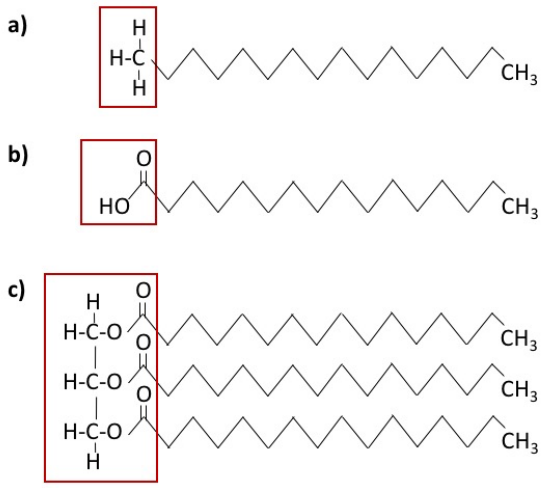

Figure 2.1: Structure of a *n*-alkane (*n*-hexadecane (a)), a fatty acid (palmitic acid (b)) and a triacylglyceride (tripalmitate (c)).

TAGs are the main components with a mass percentage up to 98 % in oils. Their structure is given schematically in Figure 2.2. R_I, R_{II} and R_{III} are fatty acid residues which determine the physical properties of the TAGs. To describe the position of the fatty acids at the glycerol molecule the so called stereospecific numbering (*sn*) is used. The biological synthesis of TAGs is enzyme-promoted and the pathway typically results in vegetable fats with an unsaturated fatty acid at the *sn*-2-position (R_{II}) of the glycerol backbone whereas the *sn*-1,3-positions (R_I and R_{III}) are preferentially occupied by saturated fatty acids (Gunstone, 2013).

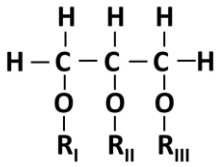

Figure 2.2: Composition of a triacylglyceride molecule with the fatty acid residues R_I, R_{II} and R_{III} (modified, Sato 2001).

The fatty acids can be subdivided into the three categories depending on their degree of saturation, shown in Figure 2.3. Saturated fatty acids have no double bonds whereas monounsaturated fatty acids (MUFAs) have one double bond. If two or more double bonds occur the fatty acids are called polyunsaturated (PUFAs). The group of PUFAs can be further subdivided into ω-3 and ω-6 fatty acids depending on the C-atom at which the first double bond is present counting from the methyl end group (ω-end). The double bonds are in vegetable oils naturally aligned in *cis*-configuration, whereas the *trans*-configuration is not common.

In addition, the fatty acids can differ in the number of carbon atoms (the chain length) or have additional functional residues like hydroxyl or epoxy groups (Gunstone, 2013). Furthermore, the arrangement of fatty acids residues on the glycerol backbone takes influence on the physical properties like the melting point of the TAGs (Gunstone, 2013; Douaire *et al.*, 2014). Hence, the composition of fats with respect to fatty acids determines their physical, nutritional and chemical properties and is therefore crucial for the application of lipids in foods (Gunstone, 2013).

The composition of TAGs with respect to fatty acids is different depending on the source. For example, fat originating from coconut or palm kernel, so called lauric oils, is highly saturated. In contrast, soybean and rapeseed oil have a higher amount of linolenic acid (C18:3). In general, these oils consist of 80 % of mono- and polyunsaturated fatty acids (Noureddini, Teoh and Clements, 1992; Przybylski, 2011). All in all, palmitic, oleic and linoleic acid are the most common fatty acids in vegetable oils. Cocoa butter is an exception and has an unusual TAG composition with mainly so-called HUH TAGs (H = saturated fatty acid with 16 or 18 carbon atoms, U = unsaturated fatty acid). In contrast to vegetable oils, animal fats contain mainly saturated fatty acids (Gunstone, 2013).

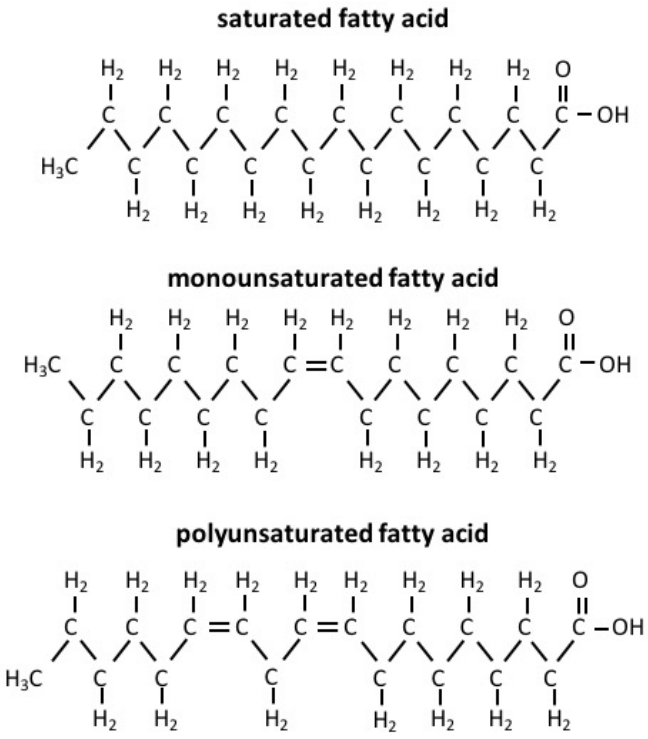

Figure 2.3: Fatty acid structures: saturated (stearic acid), monounsaturated (oleic acid) and polyunsaturated (linoleic acid).

A minor component of general interest are *trans* fatty acids (see also 2.1.2). *Trans* fatty acids are a result of incomplete hydrogenation of vegetable oils (Uauy *et al.*, 2009). The *trans* configuration in at least one double bond is necessary to call a fatty acid "*trans* fatty acid". The reason why *trans* fatty acids came into focus is that they were found to be related to an increased risk for cardiovascular diseases caused by the increase of the serum cholesterol level (Mozaffarian, Rimm, *et al.*, 2004; Mozaffarian and Clarke, 2009). There is also evidence to assume that breast cancer as well as systemic inflammation is related to a high intake in *trans* fatty acids (Mozaffarian, Pischon, *et al.*, 2004; Dhaka *et al.*, 2011). High uptake can also shorten pregnancy and could have an influence on growth and development of the central nervous system especially of infants and kids. According to some studies, there is also a clear correlation between *trans* fatty acids intake and colon cancer, diabetes, and obesity (Uauy *et al.*, 2009; Dhaka *et al.*, 2011). The main *trans* fatty acid originating from industrial hydrogenation is elaidic acid (*trans*-18:1).

The complete exclusion of fats and oils in nutrition is, however, not an appropriate option to avoid these risks. An intake of less than 20 % of the daily calorie intake coming from oils and fats can actually result in a bad absorbance of vitamins, in particular vitamin E, and a lack of essential fatty acids which cannot be synthesized by the body itself (Dhaka *et al.*, 2011). This could disturb processes in the body like immune response or skin appearance.

In order to reduce *trans* fatty acids in fats, the hydrogenation process needs to be modified in pressure, temperature or catalyst. The hydrogenation process is used to modify unsaturated fatty acids by the addition of hydrogen atoms and yields fatty acids at the TAGs with different degrees of saturation and, hence, different application possibilities of the TAGs (see also 2.3.1). Other promising strategies reducing *trans* fatty acids include inter alia interesterification (see also 2.3.2) or the exchange of partially hydrogenated oils by oils with a different TAG composition (Uauy *et al.*, 2009; Dhaka *et al.*, 2011). A very promising possibility to gain structuring lipids is the fractionation of palm oil (see chapter 2.3.3). Thus, the subsequent chapter focuses on palm oil, its cultivation, production and its exceptional composition.

2.1.2 Palm Oil

Palm oil already gained much attention in the beginning of the 1990s for its widely use in confectionary, shortening or margarine production (D'Souza, DeMan and DeMan, 1990). At the beginning of this century, palm oil got even more attention as replacement of hydrogenated fats due to the desired elimination of *trans* fatty acids in food production. This elimination became a challenge for food processing because the physical properties of the products have to be maintained, while simultaneously an increase of the nutritional value was demanded (Gunstone, 2013). These challenges could be overcome using fractionated palm oils (see 2.3.3).

Malaysia and Indonesia are the leading countries in palm oil plantation. The oil palm (*Elaeis guineensis*) was brought to Malaysia in the mid 19th century and, since then, its plantation area has grown rapidly (Basiron, 2005). Today, the *tenera* hybrid (crossbreeding of *dura* and *pisifera*), which yields around four tons oil per hectare, is the most planted oil palm (MPOB, 2009; Lin, 2011). In trials, other oil palm varieties yielded over eight tons per hectare, which makes the oil palm the most efficient among

all vegetable oil producing plants (Basiron, 2005). However, he *tenera* hybrid is mainly used due to its high yield per bunch and the fatty acid composition of the harvested oil. The various fatty acid composition at the TAGs offers the possibility to yield many different fractions with distinct properties.

The oil palm has so called fresh fruit bunches, which are composed of many small palm fruits having the size of a walnut. The unripe palm fruits have a black color, while the red or orange colored ones are ready to be harvested. The palm fruit contains a mesocarp and a palm kernel, which is surrounded by an endocarp (see Figure 2.4). The palm oil is obtained from the mesocarp and is mainly composed of palmitic and oleic acid (MPOB, 2009).

Figure 2.4: Fruit bunch of the oil palm with palm fruits composed of the kernel (white), the shell (black) and the mesocarp (yellow) (https://blog.wwf.de/palmoel-studie/, accessed 05. December 2017)

In the mill, the fresh fruit bunches are loosened up to separate the oil palm fruits from each other. The oil yield per bunch can vary between 18 and 24 %. After the fruits have been discharged a sterilization step is done using steam before threshing the palm fruits. The sterilization is required to avoid further hydrolysis which could lead to the transformation of TAGs into partial glycerides and free fatty acids. Further consequences of the sterilization are the preconditioning of the mesocarp for the subsequent processing and to ease the separation of the mesocarp from the palm kernel. Crude palm oil is extracted after digestion which increases the release of oil. The process to obtain palm kernel oil is similar and described elsewhere (Basiron, 2005).

During further processing in the mill free fatty acids (FFAs) are removed to prevent the oil from lipid oxidation. In addition, color and flavor are removed to make its application range as wide as possible and provide a longer storage time without product changes. In the degumming step, the phospholipids in the crude palm oil are precipitated by phosphoric acid and subsequently removed with bleaching clay along with other undesired components like trace metals or remaining water. Afterwards, the slurry of oil and bleaching earth is set under vacuum at 95-110 °C for at least half an hour to ensure a proper process and then filtered to gain a light orange palm oil. If elevated levels of free fatty acids are present a neutralization step is executed prior to bleaching. Otherwise, the free fatty acids are removed in the subsequent step. In the deodorization step, the oil is heated under vacuum up to about 250 °C to remove undesired volatile compounds like ketones and aldehydes as well as free fatty acids (Basiron, 2005). The flow chart of the above described process to obtain the so called light-colored RBD palm oil (refined, bleached, deodorized) is depicted in Figure 2.5

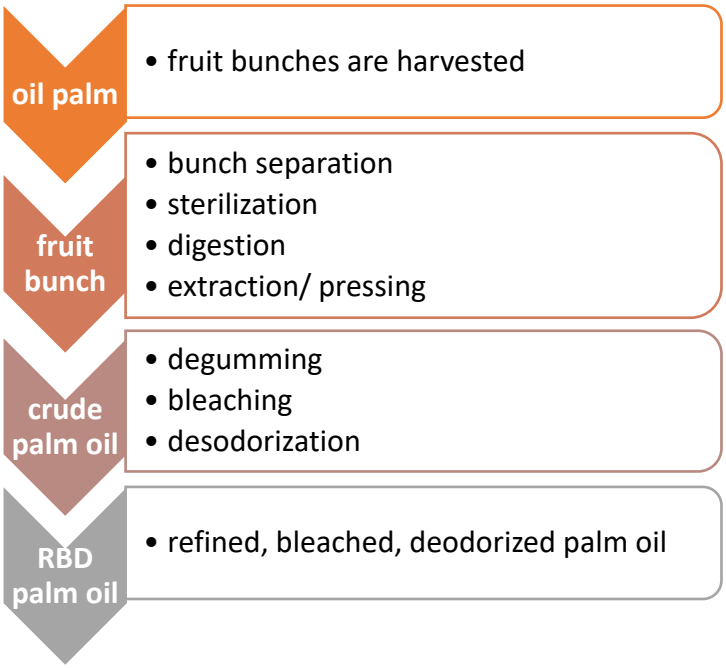

Figure 2.5: Flow chart of the RBD palm oil extraction process.

The fatty acid and TAG composition of palm oil is quite unique because it is roughly composed of equal amounts of saturated and unsaturated fatty acids. Braipson-Danthine and Gibon (2007) found a typical TAG distribution in different palm oils of about 43-49 % HUH (monounsaturated TAGs), 38-44 % HUU (diunsaturated TAGs), 5-9 % HHH (trisaturated TAGs), and 6-8 % UUU (triunsaturated TAGs). The main fatty acids present in palm oil are palmitic (P), oleic (O), stearic (S) and linoleic acid (L). They are combined to the main TAGs POP (30.0 %), POO (25.0 %), POL (10.3 %), POS (5.9 %), PPP (5.3 %), and OOO (4.6 %). Typical percentages of the occurrence of these TAGs in palm oil are given in brackets. Thus, palm oil became a very popular raw material for the fractionation process since it yields different fractions with distinctive properties.

A typical fractionation tree of palm oil is shown in Figure 2.6. Palm stearin, the high melting fraction, and palm olein, the low melting fraction, can be further subdivided into hard and mid stearin or soft palm mid fraction and super olein, respectively. These fractions have distinctive chemical compositions and are thus used to achieve the desired physical state of diverse final products. The iodine value (IV) shown in Figure 2.6 gives the degree of saturation (the higher the IV the lower the degree of saturation) (Kellens *et al.*, 2007). However, one needs to be careful because various combinations of TAGs yield similar iodine values.

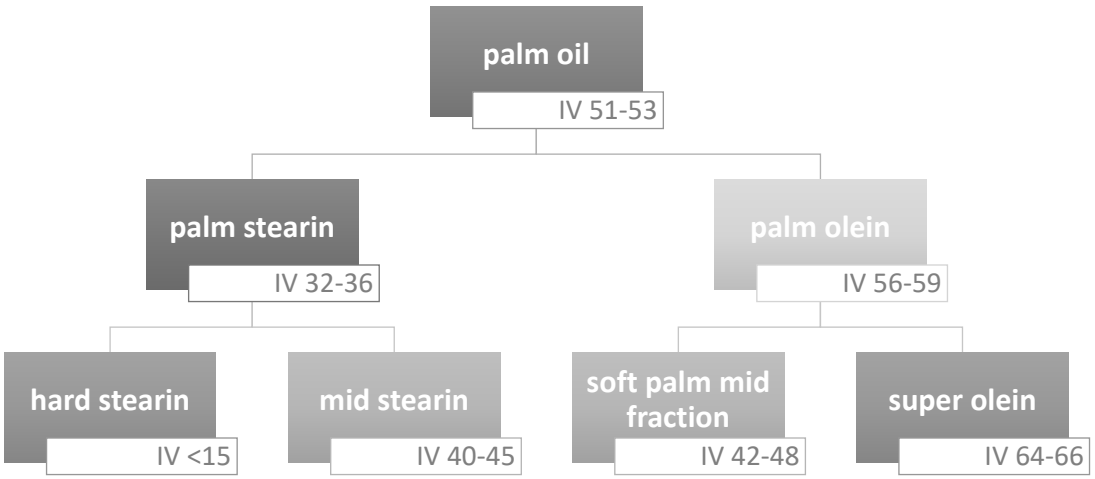

Figure 2.6: Schematic fractionation tree of palm oil (adapted and modified from Timms 1997 and Kellens et al. 2007).

Table 2.1: Main TAG composition of palm oil, palm stearin and palm olein (M= myristic acid (C14:0), P= palmitic acid (C16:0), St= stearic acid (C18:0), O= oleic acid (C18:1), S= saturated fatty acid, U= unsaturated fatty acid) (modified from Kellens et al. 2007).

TAG	palm oil (%)	palm stearin (%)	palm olein (%)
PLL/MOL	2.7	1.5	0.6
OOL	1.9	1.1	2.1
POL/StLL	10.7	5.9	12.0
PLP/MOP	10.4	7.5	10.9
POO	22.7	12.9	24.5
POP/PLSt	30.3	27.5	30.2
PPP	6.1	26.5	1.7
StOO	2.5	1.5	3.1
POSt	5.5	4.8	6.0
PPSt	1.2	5.3	0.2
UUU	6.0	3.3	6.7
SUU-USU	38.6	21.8	42.9
SSU-SUS	47.5	40.7	48.3
SSS	7.9	34.1	2.1

The variations in the TAG composition of palm oil, stearin and olein are listed in part in Table 2.1. Palm stearin is rich in saturated fatty acids whereas palm olein consists of TAGs with a higher amount of unsaturated fatty acids.

Beside TAGs, which are the major components of edible fats and mainly determine the physical behavior of fats during processing and production, minor components like mono- and diacylglycerides (MAGs and DAGs) as well as FFAs or phospholipids are also present (Smith *et al.*, 2011). Even though many more components are present in edible fats only the three minor components MAGs and DAGs as well as phospholipids are shortly described in the following. Most of these other small minor components are removed during refining. However, in palm oil, a high amount of diglycerides remains because their vapor pressure is too low to be removed during the deodorization step (Smith *et al.*, 2011; Gunstone, 2013). The amount of partial glycerides in the end product varies depending on the feedstock and the fractionation method used (Smith *et al.*, 2011).

The difference between MAGs and DAGs is the number of fatty acid moieties esterified to the glycerol backbone. MAGs have a glycerol backbone with only one fatty acid residue (see Figure 2.7a). The other two sites are occupied by a hydroxyl group,

giving the molecule a polar head and thus increasing its surface-active properties. The MAGs are either formed during biosynthesis or by hydrolysis of di- and triglycerides (Gunstone, 2013). In a DAG molecule, two sites instead of one of the glycerol backbone are esterified with a fatty acid moiety (see Figure 2.7b). Also, DAGs show surface-active properties and are often used as emulsifiers (in the same way like MAGs) in the cosmetics and food industry. Jacobsberg and Ho (1976) found no correlation between the free fatty acid and the diglyceride content but concluded that the DAGs resulted from an incomplete biosynthesis of TAGs and not from TAG hydrolysis (Jacobsberg and Ho, 1976). In Figure 2.7c a phospholipid is depicted schematically. It is similar to DAGs but with a phosphate group esterified to the third glycerol hydroxyl group. Lecithin, which is ordinarily a mixture of different phospholipids, is used in the food industry as emulsifier (Smith *et al.*, 2011).

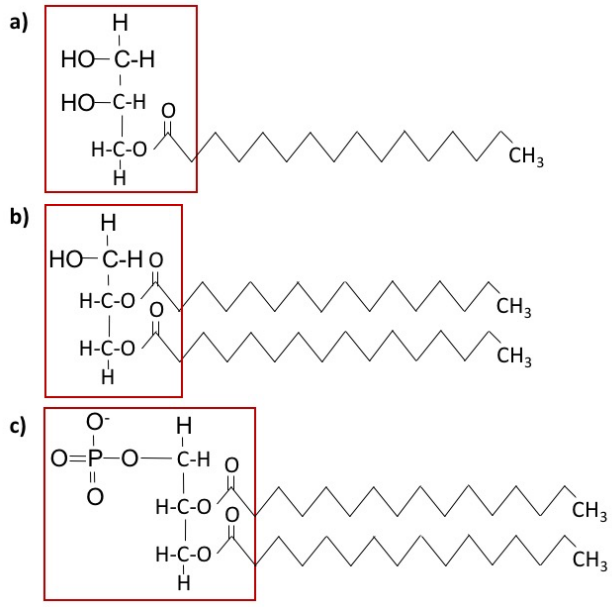

Figure 2.7: Three schematically displayed minor components based on glycerol with varying moieties: monoacylglyceride (a), diacylglyceride (b), and phospholipid (c).

All present minor components as well as the various TAGs in edible fats influence the crystallization of palm oil and thus impact the fractionation process and by that the end products (Jacobsberg and Ho, 1976). So far, the influence of all the components on crystallization are not yet completely understood. For example, Smith and coworkers (2011) found promoting effects on crystallization for some phospholipids

while other phospholipids inhibit crystallization. Consequently, the occurrence of the aforementioned minor components is essential for the characteristics of the final product.

2.1.3 Phase Behavior

Before discussing the phase behavior of mixtures of various TAGs, a brief introduction into phase behavior in particular on solid-liquid equilibria should be given. In Figure 2.8, three possible solid-liquid phase equilibria in a binary system are schematically depicted. The phase behavior in graph a) shows complete miscibility in the solid and the liquid phase and a two phase solid-liquid region. At higher temperatures there is a single liquid phase which consists of A and B in all compositions (Flöter, 2014a). If complete immiscibility in the solid phase occurs (Figure 2.8b), component A and B exist as pure solids. The eutectic point describes the point at which the single liquid phase coexists with the solid A and the solid B. (Flöter, 2014a).

A so-called hylotrope can be found in systems with complete miscibility in the solid and the liquid phase. However, due to interactions between the molecules of component A and B the liquid-solid two-phase region exhibits either a temperature maximum or minimum (see Figure 2.8c). The hylotrope is the point at which the coexisting liquid and solid phase have the same composition at either the maximum or minimum temperature. As a consequence, the liquid-solid two-phase region is divided into two sections. In the one section the liquid phase coexists with a solid phase s_β which is rich in component B. In the other section, the liquid phase coexists with a solid phase s_α which is rich in component A (Flöter, 2014a).

The phase behavior of binary systems explained above are quite simple because there exists either a mixture of components A and B or there is complete immiscibility. Further complexity arises if one mixed crystal rich in B coexists with a mixed crystal rich in A. Three examples of this kind of phase behavior are depicted in Figure 2.9. An immiscibility at low temperatures of the two components leads to a solid-solid two-phase region with an upper critical solution temperature (top of the $s_\alpha + s_\beta$ region). At higher temperatures than the upper critical solution temperature there is a single solid phase with complete miscibility of components A and B. At even higher

temperatures there is a liquid-solid two-phase region. Above the two-phase region there is a single liquid phase (see Figure 2.9a).

In Figure 2.9b, a system with complete miscibility in the liquid phase, an eutecticum and two coexisting solid phases, one rich in A (s_α) and one rich in B (s_β) is shown. At low temperatures there is a solid-solid two-phase region. A solid phase s_α which is rich in component A but also contains component B coexists with a solid phase s_β which is rich in component B with some component A included. The composition of the solid phases s_α and s_β changes slightly with the temperature up to the eutectic temperature. For temperatures higher than the eutectic temperature the changes in the composition of s_α and s_β are more pronounced when s_β becomes richer in B and s_α becomes richer in A. At the eutectic temperature one observes coexistence of the liquid phase l and the two solid phases s_α and s_β. At higher temperatures before only one single completely miscible liquid phase is observed. One finds two different liquid-solid two-phase regions, the s_α-l and the s_β-l region (Flöter 2014).

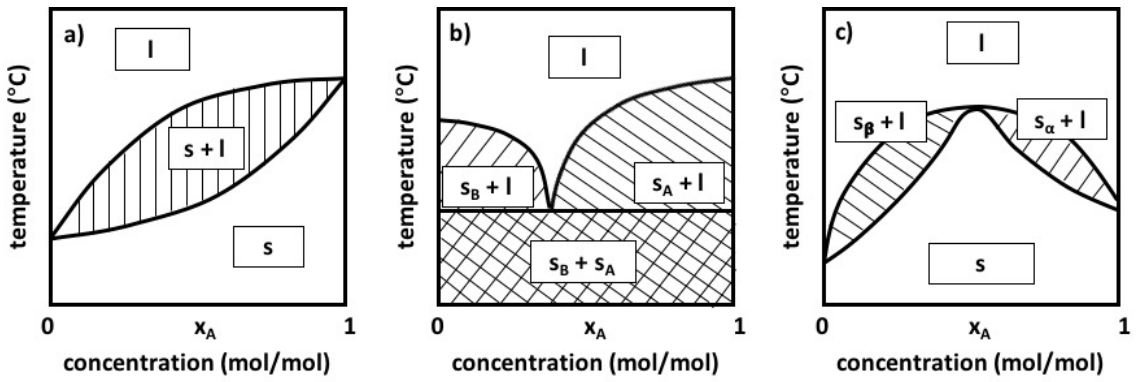

Figure 2.8: Solid-liquid phase diagrams; a) nearly ideal mixing, solid and liquid phase are completely miscible; b) eutectic behavior, A (s_A) and B (s_B) are completely immiscible in the solid phase; c) complete miscibility of the liquid and the solid phase with a high temperature hylotrope, where the coexisting solid and liquid phase have the same composition (modified, Flöter 2014a).

A system exhibiting peritectic behavior is displayed in Figure 2.9c. Similar to a system with an eutectic point, at the peritectic temperature there is a phase equilibrium of a solid phase rich in A (s_α) and a solid phase rich in B (s_β) as well as a single liquid phase (l). However, different than for the eutectic temperature one observes a single

liquid-solid two-phase region (here: s_α in coexistence with l). At temperatures lower than the peritectic temperature a liquid-solid and a solid-solid two-phase region as well as two single solid phases occur. This behavior is found for systems consisting of components with large difference in the pure component melting points (Flöter 2014).

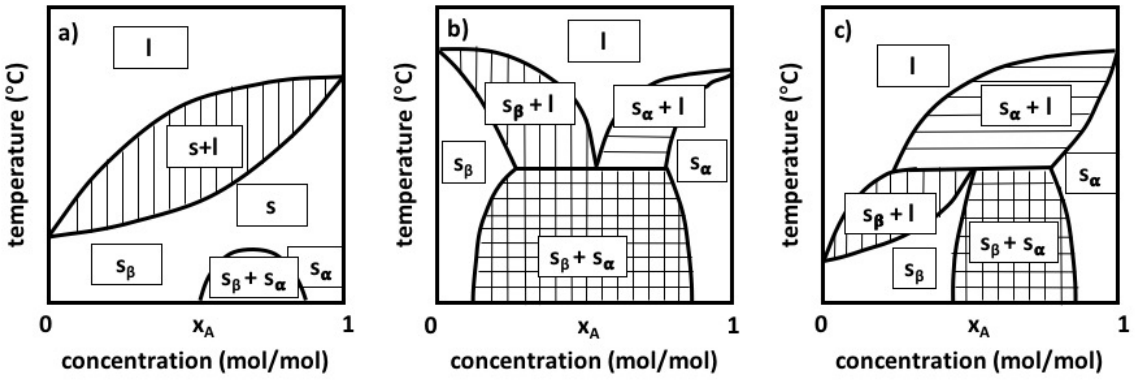

Figure 2.9: Solid-liquid phase behavior, solid phase with partial immiscibility; a) complete miscibility in the liquid phase and partial immiscibility in the solid phase at low temperatures; b) eutectic system with mixed crystals s_α and s_β; c) peritectic system (modified, Flöter 2014a).

So far, the explanations were given for systems consisting of two pure components. However, fats and oils are multicomponent systems of *n*-alkanes, fatty acids, and TAGs. Consequently, the phase behavior of fats and oils is more complex than all the depicted phase diagrams shown in Figure 2.8 and Figure 2.9. However, the phase behavior of these binary systems form the base for the understanding of the complex phase behavior of fats and oils. In general, it can be stated that the complexity increases for mixtures consisting of *n*-alkanes to fatty acids to TAGs.

The melting point of *n*-alkanes is basically determined by their chain length and increases with increasing chain length. In addition, it has been shown that the complexity of the phase behavior of binary systems containing *n*-alkanes of which the aliphatic chains differ by two carbon atoms also increases with increasing chain length (Mondieig *et al.*, 2004).

The phase behavior of binary systems of fatty acids is in itself even more complex but at the same time the changes in the behavior is dramatically systematic. A summary of different studies is given by Floeter et al. (2018) showing that binary systems of two saturated fatty acids differing by two, four or six carbons atoms show a similar complex

phase behavior though at different temperatures. In addition, the temperature range in which the liquid-solid two-phase regions occurs decreases with increasing chain length of the fatty acids. If a saturated fatty acid is mixed with a monounsaturated fatty acid, the phase behavior is less complex than for a system of two saturated fatty acids; though it still shows eutectic behavior. The asymmetry of the phase diagram increases with increasing chain length of the saturated fatty acid shifting the eutectic composition towards the pure monounsaturated fatty acid. Thereby, the double bond of the monounsaturated fatty acid hampers the packing of the saturated and unsaturated fatty acid adjacent to each other within one crystal structure and thus the phase behavior with respect to the occurrence of the solid phase. Binary mixtures of two monounsaturated fatty acids or a monounsaturated and a saturated fatty acid show a systematic change of the phase behavior with the chain length as shown in Figure 2.10.

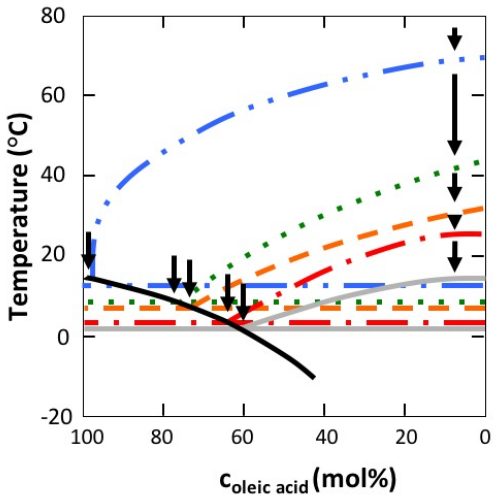

Figure 2.10: Phase behavior of oleic acid (black solid) mixed with stearic (blue, dashed double dotted), lauric (green, dotted), petroselinic (orange, dashed), gondoic (red, dashed dotted) and asclepic (grey solid) acid (adapted from Floeter et al. 2018).

Figure 2.10 gives the phase behavior of oleic acid mixed with stearic, lauric, petroselinic, gondoic or asclepic acid. All mixtures reveal eutectic behavior whereat the composition of the eutectic point shifts to higher concentrations of oleic acid and the eutectic temperature decreases in the order of stearic (C18:0) → lauric (C12:0) → petroselinic (C18:1, Δ6ω12) → gondoic (C20:1, Δ11ω9) → asclepic acid (C18:1,

Δ11ω7). It can be summed up that the phase behavior of fatty acids is influenced by the degree of saturation and the chain length of the fatty acid as well as the position of the double bond in the unsaturated chain (Floeter, Haeupler and Sato, 2018). The complexity of the phase behavior increases even more if more than one double bond is present.

The combination of fatty acids to triglycerides makes the phase behavior of systems containing TAGs even more complicated. Studies are often limited to one or two TAGs in order to decrease the intricacy. Natural fats are, however, composed of a mixture of TAGs (Calliauw *et al.*, 2010). Beside the influence of mixing TAGs, the polymorphic behavior of each TAG needs to be additionally considered. TAG miscibility in the solid phase ultimately depends on the polymorphic form (Takeuchi, Ueno and Sato, 2003; Himawan, Starov and Stapley, 2006; Floeter, Haeupler and Sato, 2018).

The packing of the TAGs depends on both, the fatty acid moieties as well as their respective position on the glycerol backbone. Sometimes TAGs pack more easily together if the fatty acid order at the TAG is not the same (e.g. POP/OPO) (Himawan, Starov and Stapley, 2006). In the phase behavior one distinguishes between complete miscibility in the solid phase, occurrence of an eutecticum, and the formation of so-called molecular compounds which are actually mixed crystals with a fixed ratio of components A and B (Floeter, Haeupler and Sato, 2018). For example, eutectic behavior was found for all polymorphs for POP-PPO mixtures due to the steric hindrance due to the double bond of the unsaturated fatty acid residue (Sato, 2001).

Depending on the conditions, TAGs occur in different polymorphic forms. Consequently, at some conditions a mixture of two specific TAGs are completely miscible, at other conditions they form an eutecticum (Kellens *et al.*, 1991; Takeuchi, Ueno and Sato, 2003).

One important aspect for the work at hand is the study of the solid-liquid phase behavior of system containing fats and/or oils. As pointed out above, fats and oils are a mixture of a number of components. With each component the phase behavior becomes more complicated (Floeter, Haeupler and Sato, 2018). For pure components such as e.g. *n*-alkanes, methods such as DSC or other calorimetry allow a quite accurate determination of the solid-liquid phase transition (e.g. melting point) though parameters as heating or cooling rates affect the accuracy of the determination. For

multicomponent systems, the determination of the solid-liquid phase behavior is more complex as already the systematic phase diagrams of binary systems (Figure 2.8 and Figure 2.9) show (Zhou and Hartel, 2006).

The use of fats and oils as substitutes for animal fats or *trans*-fats requires the knowledge, in particular, of the phase transition from the liquid to the solid phase. As fats and oils are multicomponent systems there is not one single transition point but a number of points describing the transition from the liquid phase to the liquid-solid two-phase region depending on temperature, pressure and composition of the liquid phase. In general, these phase transitions can be described by the equality of the chemical potentials of a component i (which is one of the constituents of the system) in the coexisting phases (= phases in equilibrium at given temperature and pressure), e.g. at the eutectic temperature of a system displaying the phase behavior as given in Figure 2.9b. This is given by the following equation

$$\mu_{i,L} = \mu_{i,s_\alpha} = \mu_{i,s_\beta} \qquad \textbf{Eq. 2.1}$$

where $\mu_{i,L}$ is the chemical potential in the liquid phase, $\mu_{i,\alpha}$ the chemical potential of component A, and $\mu_{i,\beta}$ the chemical potential of component B in the coexisting phase (Flöter, 2012).

In general, the chemical potential of a component i in phase K (as K is liquid or solid) can be described by

$$\mu_{i,K} = \mu_{i,K}^{0} + RT\ln(x_i \cdot \gamma_i)_K \qquad \textbf{Eq. 2.2}$$

where $\mu_{i,K}$ is the chemical potential in the phase K, $\mu_{i,K}^{0}$ the chemical potential of the pure component i, R the gas constant, T the temperature, x_i the mole fraction of component i in phase K and γ_i the activity coefficient of component i (Himawan, Starov and Stapley, 2006).

Using this equation for the description of the solid-liquid phase equilibrium and simplifying the equation leads to the so-called Hildebrand equation:

$$\ln x_i \approx \frac{\Delta H_{m,i}\Delta T}{RT_{m,i}T} \approx \frac{\Delta H_{m,i}}{R}\left(\frac{1}{T} - \frac{1}{T_{m,i}}\right) \qquad \textbf{Eq. 2.3}$$

with the mole fraction x_i of component i, $\Delta H_{m,i}$ the heat of fusion of component i, $T_{m,i}$ the melting temperature of component i, R the gas constant and T the experimental temperature. This equation is quite commonly used to estimate the

solubility of component I in a liquid phase (or in other words to describe the liquidus area). For fats and oils it can be only used as a first approximation as fats are multicomponent mixtures occurring in more than one solid phase

2.2 Fat Crystallization

The crystallization of fats is one of the most important and complex processes in the food industry. It is both, important for the desired final product and for intermediate processes like fractionation. In food technology it is one of the crucial steps for products containing fats as a structure giving component. Examples for its commercial application are margarine, ice cream or chocolate. Dependent on the application, fat crystals give melting stability at ambient temperature (margarine), provide the desired mouthfeel (chocolate) and incorporate and stabilize air bubbles (ice cream). The so-called mouthfeel is related to the size of the crystals, which are detectable by humans at around 20-25 μm (Flöter, 2014a).

The crystallization behavior is primarily given by the TAGs in the mixture. Furthermore, minor components like di- and monoacylglycerides, waxes or phospholipids influence the crystallization process (Sato, 2001). The resulting crystals contribute to shelf life, functionality and consumer perception (Hartel, 2013).

The crystallization process can be considered as the transformation from a mainly disordered liquid into an ordered solid state (Flöter, 2014a). Regarding the crystallization process, especially nucleation and growth rate decisively contribute to the size and amount of formed crystals, which is in turn important for the final product properties. In order to obtain the proper product characteristics or the desired fractionation, nucleation, growth, and polymorphic transformations need to be optimized. In the previous chapter the phase behavior in general and in detail of systems containing fats was discussed. The displayed phase diagrams give the equilibrium conditions. However, during the processing of fats equilibrium is not achieved. The equilibrium conditions give the circumstances which can optimally be reached and thus give the lower value of the gradient representing the driving force for a process. Additionally it has to be taken into account that the equilibrium is often

achieved very slow in the given systems and this process is probably not completed within the shelf life of systems like chocolate or margarine (Flöter, 2012).

Crystallization consists mainly of two steps: nucleation and growth. Nucleation is the accumulation of molecules into a cluster until it reaches the so-called critical nucleus size to favor the incorporation instead of the dissolution. During crystal growth, material from the liquid phase is attached onto the already formed crystal (Flöter, 2014a). In crystallization not only the phase equilibrium needs to be known and studied but also kinetic aspects and driving forces. Among these, supersaturation and recrystallization need to be considered because of their influence on the initiation of crystallization and the resulting shelf life of the products, respectively (Hartel, 2013). To decrease the complexity, the explanations given are mainly limited to pure TAG systems. This needs to be considered if the crystallization behavior of fats and oils as complex mixtures is considered.

2.2.1 Nucleation

The initiation of nuclei can be important for the further progression of a process. Hence, it is necessary to briefly discuss this first step during crystallization. In his review, Hartel (2013) defines the nucleation as "the formation of crystals from liquid state". In the work at hand this means that nucleation can also be described as an accumulation of molecules and is the crucial step to control if solid phases occur. This accumulation needs to be present long enough to start crystal growth for which the nuclei serve as growth sites (Flöter, 2014a). During this step, the TAGs start to align in an ordered way to form a nucleus which later serves as a growth site. Supersaturation as a driving force is a required prerequisite for nucleation (Hartel, 2013). It can be explained as the state at which the concentration of the solutes in a solvent is higher than the solubility at given conditions. Thus, it is the difference in composition between the actual state and the equilibrium state (Flöter, 2014a).

Though commonly the supersaturation is used to determine the driving force for crystallization it is more accurate to use the difference in the chemical potential. The chemical potential describes the partial molar Gibbs energy of a component i in a phase K. Here, one would use the differences between the chemical potential of component i in the supersaturated solution and the chemical potential of component i in the

saturated solution (the equilibrium state). When using the chemical potential difference instead of solely the concentration difference (supersaturation) also the interactions between al molecules in solution are taken into account.

As already mentioned above, the chemical potential is the partial molar Gibbs energy. In classical thermodynamics the Gibbs energy is used to determine the energetically favorable state, in other words which phase is stable at a given temperature and pressure. In general, the phase which is described by the smallest Gibbs energy is the phase which is stable (see Figure 2.11). In Figure 2.11 the Gibbs energy of a pure component is given as function of temperature. G_s gives the Gibbs energy of the solid phase, G_L the one of the liquid phase. At the melting temperature T_m where the solid and liquid phase coexist, e.g. are in equilibrium, the Gibbs energy of the liquid phase is equal to the Gibbs energy of the solid phase. At temperatures higher than the melting temperature, the Gibbs energy of the liquid phase is smaller than the one of the solid phase. Thus, the liquid phase is the stable one in this temperature region. At temperatures lower than the melting temperature T_m, the Gibbs energy of the solid phase is smaller and, hence, the solid phase is stable.

If kinetics are slow, the equilibrium state, e.g. the phase which is stable at a given temperature and pressure, is not achieved immediately. Then a metastable state occurs. This happens if a solution contains a solute in a concentration which is higher than in its saturated state. The difference in the Gibbs energy of the metastable state and the equilibrium state is the real driving force. In the case of a pure component, if the liquid phase is subcooled, e.g. the components exist in the liquid state even though temperature and pressure are such that the solid state is the energetically most favorable, the liquid phase is the metastable state. The Gibbs energy difference ΔG gives the driving force required to overcome the activation energy to change into its stable state (see Figure 2.11, T_1) (Flöter, 2014a).

The formation of molecule clusters (nucleation) makes the formation of an interface necessary which requires energy input. The transfer of molecules from the liquid into the crystal releases energy. The difference in the energy of these processes mainly determines the required driving force to form crystals (Flöter, 2014a).

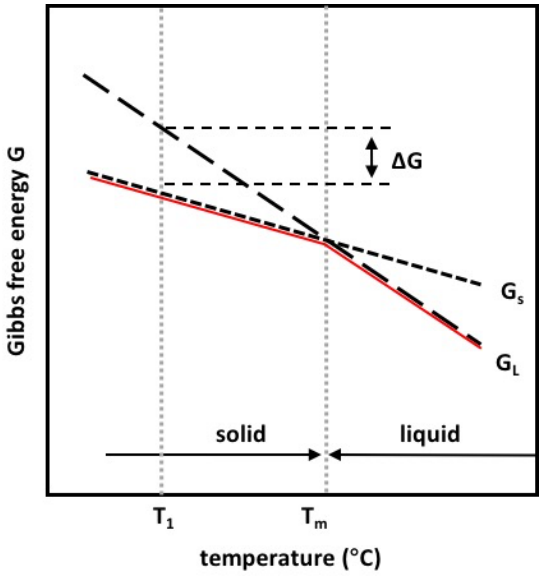

Figure 2.11: Schematic illustration of the relationship between temperature and Gibbs free energy for a pure component at constant pressure; ΔG is the driving force for crystallization at T_1, T_m is the melting point of the pure component, G_s the Gibbs energy of the solid phase (short dashed line), G_L the Gibbs energy of the liquid phase (long dashed line); the red line indicates the most stable state at the corresponding temperature (modified, Flöter 2014).

A nucleus needs to overcome a critical size r* before it is energetically favorable to grow further (see Figure 2.12). Therefore, the molecules need to accumulate into clusters larger than this critical size (r*). Otherwise it is energetically more favorable for the molecules in the cluster to dissolve again. Because the detection of the critical nucleus is often impossible, the term "induction time" is introduced which describes the time until the detection of crystals. Logically, it depends on the detection method applied (Jacobsberg and Ho, 1976; Flöter, 2014a).

During nucleation three ways of nuclei formation are possible. First, there exists homogeneous nucleation in which the molecules collide in a homogeneous liquid phase. Second, heterogeneous nucleation at impurities like dust or at irregularities of the crystallizing equipment can occur. The third possibility is nucleation initiated by already existing crystals. This can be either called seeding (nucleation on purpose) or secondary nucleation (unintentional nucleation) (Hartel, 2013; Flöter, 2014a).

Although homogeneous nucleation is used to describe the phenomenon of nucleation, it plays a minor role in the industry. Heterogeneous nucleation occurs preferentially since it is energetically more favorable than homogeneous nucleation.

During heterogeneous nucleation, the energy required to form a surface is less, in particular if the interfacial tension between the crystal and the foreign surface is low. Commonly, heterogeneous nucleation rather occurs at low levels of supersaturation. At higher supersaturation, homogeneous nucleation appears dominant due to the higher driving force which allows to overcome the activation energy and thus does not require existing surfaces for crystallization (Flöter, 2014a).

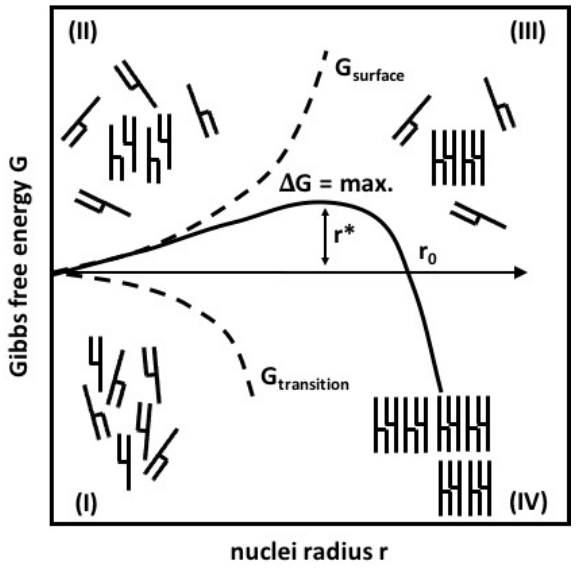

Figure 2.12: Dependency of Gibbs free energy G on the size of formed nuclei r; r* is the critical radius of nucleus, r_0 is the radius where ΔG=0; liquid state (I), accumulation of molecules below the critical size r* (II), nucleus with sufficient size r > r* (III), crystal with r > r_0 (IV) (modified, Flöter 2014).

The advantages of seeding (controlled heterogeneous secondary nucleation) are the control of the crystal size distribution, the requirement of a lower level of supersaturation also due to improved secondary nucleation and the templating effect of the seeds for the desired structure of the crystal (Calliauw *et al.*, 2010, Flöter, 2014a). Subsequent to nucleation, crystal growth is the second step in the crystallization process and is explained in detail in the following sub-chapter.

2.2.2 Crystal growth

A prerequisite for crystal growth is a liquid system in a supersaturated state with present nuclei of critical size. The molecules need to diffuse from the bulk to the crystal surface and attach onto it. In Figure 2.13 the concentration of the solution forming the

crystal is illustrated. The diffusion of molecules towards the crystal surface happens due to differences in the chemical potential. Due to enthalpy differences of the liquid solution and the crystal, attachment of molecules on the crystal results in the release of heat (so-called latent heat). If this heat is not transported away from the crystal surface, a local temperature increase which changes the equilibrium conditions and thus decreases the driving force, is deserved. Other limitations of crystal growth are, e.g. a limited diffusion of new molecules to the growth site or a reduced availability of growth sites and slow conformational processes at them (Hartel, 2013; Flöter, 2014a).

Even though nucleation is a prerequisite for growth, after growth has started nucleation and growth occur simultaneously. Crystal growth already happens at a low level of supersaturation if growth sites are present. If these are rare, apparent bulk crystallization is limited. In general, with increasing supersaturation the nucleation rate, and therefore the number of growth sites, increases. The consequence is a higher crystal growth rate. With a high nucleation rate the crystals grow in a small distribution of sizes. Thus, the resulting crystal size can be controlled by choosing a specific temperature or temperature range during crystallization. For example, increasing the temperature after generating nuclei reduces the nucleation rate. In this case, persisting crystal growth can solely lead to larger crystal sizes. In contrast, small crystal sizes, which are favored in the food industry because of their ability to stabilize and structure more efficient compared to large crystals is, achieved by simultaneously producing a large number of nuclei during crystal growth (Flöter, 2014a).

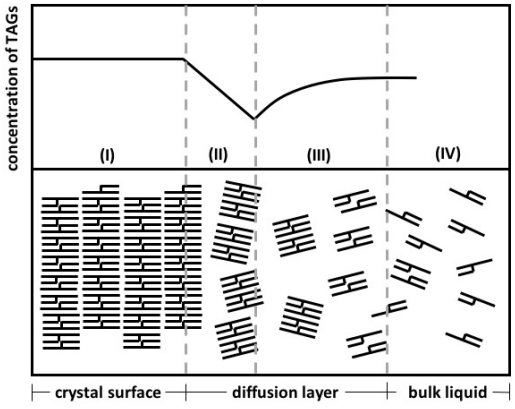

Figure 2.13: Attachment of material from the liquid onto the already solidified and ordered material (here for TAGs); crystallized TAGs (I), adsorption of TAGs onto the growth site (II), diffusion of TAGs (III), composition of the bulk (IV) (modified, Flöter 2014).

When studying fat crystallization besides supersaturation, nucleation and growth also recrystallization needs to be considered. It is driven by the difference between the manufactured metastable and the equilibrium state and can cause product defects like coarsening of ice crystals or the formation of fat bloom in chocolate (Hartel, 2013).

2.2.3 Polymorphism

Many long chain compounds possess the ability to form different crystal structures due to a variety of possible arrangements of the molecules in the unit cell. This phenomenon is called polymorphism and is of technical and scientific interest (Sato and Garti, 1988; D'Souza, DeMan and DeMan, 1990; Gunstone, 2013; Hartel, 2013; Flöter, 2014a). As a consequence of the different molecular packing, different polymorphic forms of the same material have distinct properties, most prominently different melting points (Gunstone, 2013). The knowledge of the polymorphic behavior of fats and oils is crucial for many food products like chocolate or margarine. Depending on the product the best properties can actually be achieved with specific polymorphic forms which are metastable (D'Souza, DeMan and DeMan, 1990; Metin and Hartel, 2005; Himawan, Starov and Stapley, 2006; Sato and Ueno, 2011; Marangoni *et al.*, 2012).

Some authors relate the polymorphism in TAGs to their stereo chemical configuration (Jacobsberg and Ho, 1976). The occurrence of different solid phases (polymorphism) has been studied for a large number of pure components. For fats, which are multicomponent systems, less is known. This is due to the fact that the complexity of the polymorphic behavior increases with the number of distinct TAGs in the mixture. In particular, differences in chain length and unsaturation of the esterified fatty acids have a strong influence (D'Souza, DeMan and DeMan, 1990).

In polymorphism, monotropic and enantiotropic behavior need to be distinguished. The different forms of polymorphism can be explained using the Gibbs energy as function of the temperature (see Figure 2.14). In general, G_L describes the Gibbs energy of the liquid phase, $G_{S,I}$ of the solid phase I and $G_{S,II}$ of the solid phase II. At a given temperature the stable phase is the phase which is characterized by the smallest value of Gibbs energy. The points at which the curves cross give the phase equilibria of the respective phase.

In Figure 2.14a, the so-called monotropic polymorphism is shown. The intersections of the curves describing G_L, $G_{S,I}$ and $G_{S,II}$ occur, one intersection of G_L and $G_{S,I}$ and one of G_L and $G_{S,II}$. In the given temperature range, the curve for $G_{S,I}$ lays under the curve for $G_{S,II}$. This indicates that the solid form S,II is not the stable phase in the given temperature range. If this phase is observed, then it is in the metastable state. This behavior is called monotropic polymorphism because only one of the solid phases is stable.

In Figure 2.14b, the so-called enantiotropic polymorphism is depicted. Here more than two intersections of the Gibbs energy curves are found, intersection of G_L and $G_{S,I}$ at $T_{m,SI}$, intersection of G_L at $G_{S,II}$ at $T_{m,SII}$, and $G_{S,I}$ and $G_{S,II}$ at $T_{I\rightarrow II}$. For temperatures $T > T_{m,SI}$ the liquid phase is stable, for $T_{m,SI} < T < T_{I\rightarrow II}$ the solid phase SI is stable and for temperatures $T < T_{I\rightarrow II}$ the solid phase SII is stable. The respective other phases are metastable and would not be observed if equilibrium is established immediately.

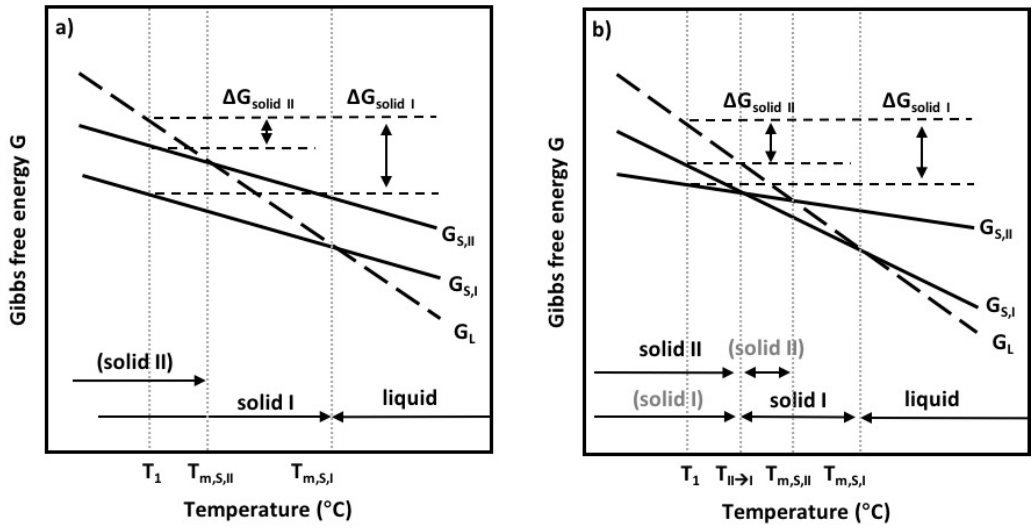

Figure 2.14: Gibbs free energy of solid and liquid phases of a pure component over temperature, ΔG=driving force at T_I. a) monotropic polymorphism, $T_{m,S,I}$= melting point solid SI, $T_{m,S,II}$ = melting point solid SII; b) enantiotropic polymorphism, $T_{m,S,I}$= melting point solid SI, $T_{m,S,II}$ = melting point solid SII, $T_{II\rightarrow I}$= transition temperature of solid I and II (modified, Flöter 2014).

As already mentioned above, due to kinetics the equilibrium state is not established immediately so that the metastable phases can be observed sometimes for very long time. The so-called Ostwald´s rule of stages says that a system rather favors the conversion into an energetically similar state instead of converting it into the energetically most favorable one (Ostwald, 1897). This means that the metastable phase might occur instead of the energetically favored stable phase. The kinetics of polymorphic transitions such as the transition from SII to SI at $T_{I \rightarrow II}$ depend on the crystal composition, the structure and temperature, shear or pressure (Flöter, 2014a).

Above polymorphism is explained using an example of a component which forms two different solid states. Depending on the nature of the component more than two solid forms can occur.

For glycerides, Larsson (1966) defined three polymorphic forms differing in their sub cell structure. Wille and Lutton (1966) found six polymorphic forms for cocoa butter to be differentiated. In Figure 2.15 the most common polymorphic forms of TAGs are shown and explained in the following.

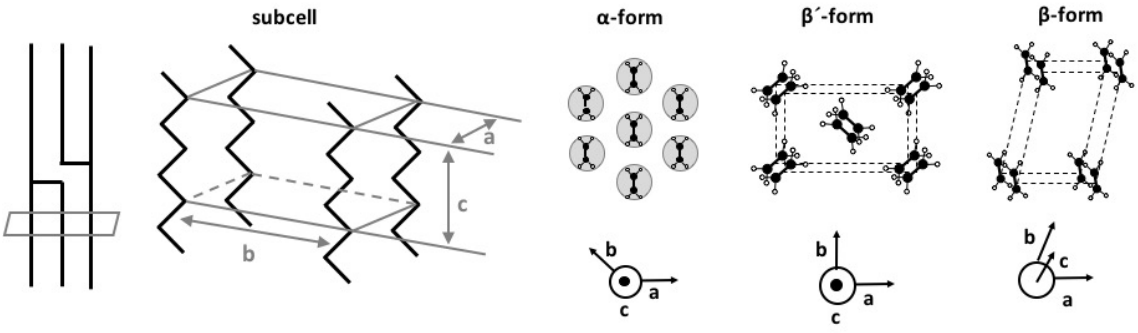

Figure 2.15: Subcell structures of the polymorphic forms α, β' and β (modified, Sato and Ueno 2005; Lopes et al. 2015).

The α polymorph shows a hexagonal sub cell structure and is the energetically least favorable one. It has the lowest melting point and thus it is also the least stable form due to its lose molecular packing (Gunstone, 2013). The fatty acid residues are aligned in a double chain length structure (see Figure 2.16b). In the double chain packing, the TAG molecules can either align in the turning fork or the chain configuration as shown in Figure 2.16a (Flöter, 2014a).

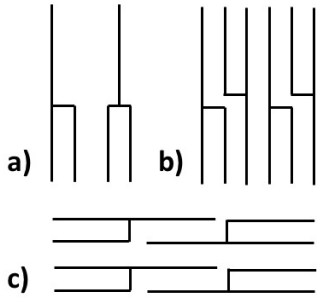

Figure 2.16: Different configurations of TAGs: a) chair (left) and tuning fork (right) configuration, b) double chain length structure, c) triple chain length structure (modified, Sato and Ueno 2005).

The β' and β polymorphs (see Figure 2.15, right) are the more stable forms and provide a more efficient packing due to the tilted arrangement of the alkyl chains (Gunstone, 2013). The fatty acids can either be arranged in a double chain (Figure 2.16b) or a triple chain (Figure 2.16c) length structure. For example, the triple chain length occurs if the *sn*-2-position of the TAGs is occupied by an unsaturated fatty acid (Flöter, 2014a). The sub cell of the β' polymorph is orthorhombic.

In particular, TAGs with an unsaturated fatty acid at the *sn*-2-position and two long chain saturated fatty acids at the *sn*-1- and *sn*-3-positions (HUH) show good structuring properties (e.g. βV form of cocoa butter), slow polymorphic transition and have been found to form stable β-crystals causing chocolate bloom or POP graininess (D'Souza, DeMan and DeMan, 1990; Koyano, Hachiya and Sato, 1990; Sato, 2001; Bot and Flöter, 2013; Kang *et al.*, 2013).

The β polymorph shows a triclinic parallel packing and along with the triple chain length structure (see Figure 2.16c) the densest packing of the molecules is favored (Koyano, Hachiya and Sato, 1992; Sato, Ueno and Yano, 1999). Symmetrical TAGs have a tendency to form stable β crystals, whereas unsymmetrical compounds favor the β' form due to the possible molecular packing (Gunstone, 2013). Each polymorphic state corresponds to a different packing of the hydrocarbon chains and depends on the chain length and the angle of tilt due to double bonds if present in the fatty acid moieties (Jacobsberg and Ho, 1976).

The generation of distinct polymorphs is a matter of primary nucleation kinetics and the application of adequate driving force, e.g. supersaturation. In Figure 2.17a the relation between nucleation/ cooling rates and preferred occurrence of polymorphic form is given. In Figure 2.17b the curves for the respective Gibbs energy are given. The α form can be induced by fast cooling. Once its respective supersaturation is reached, it nucleates faster than the β' form or the β form (Gunstone, 2013; Flöter, 2014a). The nucleation and growth of α lead to a reduced driving force (supersaturation) for β'.

Nevertheless, β' nucleation takes place. Once β' nuclei grow further the driving force for the α nucleation vanishes due to the depletion of molecules available for crystallization due to their incorporation into β' crystals. As a consequence, β' crystals continue to grow further while α crystals dissolve completely (Flöter, 2014a). In principle, the same mechanism between the β' polymorph and the stable β polymorph during growth is observed. However, due to kinetics the metastable β' crystals exist for extended periods of time.

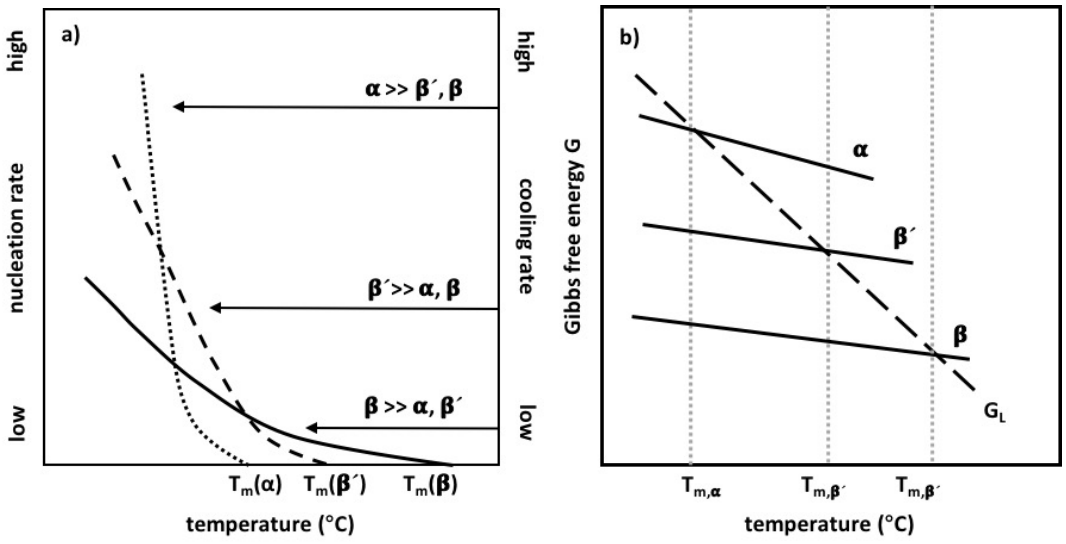

Figure 2.17: a) Nucleation rate of different polymorphic forms in relationship with the cooling rate, nucleation of α (dotted line), nucleation of β´(dashed line), nucleation of β (solid line); $T_m(\alpha)$ = melting point of polymorph α, $T_m(\beta')$ = melting point of polymorph β´, $T_m(\beta)$ = melting point of polymorph β (modified, Flöter 2014); b) Gibbs free energy over temperature for three different polymorphs with the liquidus line GL; α-form: highest G and lowest melting point ($T_{m,\alpha}$), β´-form: medium G and medium melting point ($T_{m,\beta'}$), β-form: lowest G and highest melting point ($T_{m,\beta}$) (modified, Sato 2001).

In general, each polymorph can be crystallized directly from the melt. The transition from one polymorph into another is only possible from the less to the more stable one ($\alpha \rightarrow \beta' \rightarrow \beta$). The understanding of the parameters influencing the phase transition is complicated but some rules of thumb exist. For example, with increasing chain length of the TAG residues the transition rates with respect to the transitions from one polymorph to the other decreases (Jacobsberg and Ho, 1976).

The TAGs present in a fat determine the polymorphic and crystallization behavior. For fats like cocoa butter and palm oil, POP and SOS are the common and dominant TAGs. D'Souza and coworkers (1990) stated, that asymmetric TAGs, which means the same fatty acid residue at the *sn*-1,3- and *sn*-2-position but a different one at the *sn*-1,3-position, yield mostly a β' crystal structure. In contrast, for symmetric TAGs where the *sn*-2-position fatty acid moiety differs from the residues at the *sn*-1,3-position, the β polymorph is the favorable state.

The desired product characteristics determine which polymorphic form needs to be formed. For example, in margarines and spreads the β' polymorph gives a smooth texture, whereas the β-form may lead to disadvantageous structural defects such as graininess (D'Souza, DeMan and DeMan, 1990). A possibility to achieve the proper polymorphic form is the addition of seed crystals which occur in the desired polymorphic form. The addition of seed crystals during the process leads to a crystallization at higher temperatures (Sirota and Herhold, 2000). If seeds are added in the metastable zone where the driving force is already high enough to start nucleation excessive homogeneous nucleation is prevented. Often, this is done during chocolate manufacturing to directly crystallize in the βV-form so that a tempering step to avoid chocolate bloom is not required (Metin and Hartel, 2005).

The process of seeding typically involves the same type of material as the one to be crystallized. Alternatively, crystals of a similar material can be used. This effect is called templating and could also be considered as heterogeneous nucleation. Koyano and coworkers (1990) claimed that successful seeding with foreign crystals requires similarities in chain length and polymorphic properties. Here the nucleation site shows a similar surface structure to the molecules to be crystallized (e.g. emulsifiers with same fatty acid composition in fat crystallization at an oil/water interfaces) (Flöter, 2014a).

2.3 Fat Modification

Since the requirements for the widespread applications of edible fats and oils it is crucial that their physical properties can be adjusted. In the following section, the three modification techniques hydrogenation, interesterification and fractionation are explained.

2.3.1 Hydrogenation

The oldest of the three modification processes explained in this chapter is hydrogenation. It was invented to improve the stability against oxidation of fats containing polyunsaturated fatty acids ultimately leading to the saturation of the fatty acid. Hydrogenation is an exothermic reaction during which hydrogen molecules are added to the fatty acids. The catalyst (predominantly nickel) and the concentration of hydrogen molecules are the main factors which determine the reaction kinetics (Dijkstra, 2014b).

The process conditions need to be balanced in concern for the proper working temperature since on the one hand higher temperatures promote the formation of *trans* fatty acids but are favorable for the selectivity of the hydrogenation process on the other hand (Dijkstra, 2014b). Because of this competition between isomerization and hydrogenation during hydrogenation *trans* fatty acids may be formed. Hydrogenation, even if completely executed, is immediately related to *trans* fatty acids in the public discussion and, thus, the application of this technique is very limited (Kellens and Calliauw, 2013). Therefore, isomerization of double bonds is favored if the catalytic effect is diminished. The formation of *trans* fatty acids is undesired since they are related to an increased risk for e.g. cardiovascular diseases (Dhaka *et al.*, 2011; Kellens and Calliauw, 2013).

The so-called iodine value (IV) is often used in chemistry to determine the degree of unsaturation of fatty acids. It relates to the fact that the double bonds of unsaturated fatty acids react with iodine. The higher the iodine value, the more double bonds are present. The relationship between the iodine value and *trans* fatty acid content in fish, soybean and palm oil is shown in Figure 2.18. As expected the iodine value found for fish oil is larger than for soy bean oil than for palm oil. The *trans* fatty acid content if

plotted as function of the iodine value expresses a maximum. This maximum is commonly found at the typical mean iodine value of the specific oil. For all shown oils it shows also that for low iodine values (< 20) the *trans* fatty acid content is less than 15 %. The oils are so-called partially hydrogenated until the iodine value reaches a low value (IV < 5). These fats are called fully hydrogenated and can be used for the structuring of fat-containing food products since they are low in *trans* fatty acids.

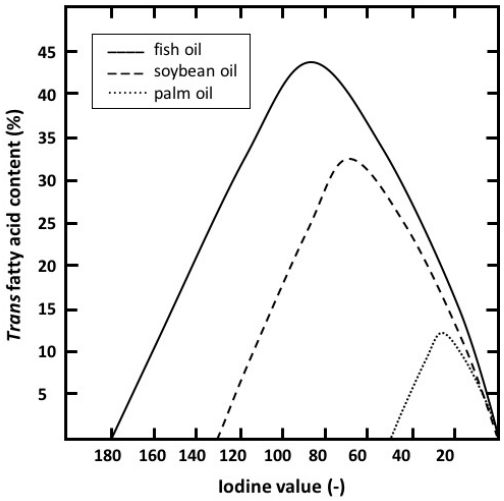

Figure 2.18: Relationship between iodine value and trans fatty acid content of fish oil (solid line), soybean oil (dashed line) and palm oil (dotted line) (modified, Kellens and Calliauw 2013).

In summary, the hydrogenation process yields a higher degree of saturation of the fatty acids and changes an oil into a fat. In addition, the melting point increases with increasing degree of saturation (Kellens and Calliauw, 2013). The progress of hydrogenation can be measured by the decrease of the iodine value and the increase of the melting point (Dijkstra, 2014b). An advantage of hydrogenation is, hence, that the sourcing of the oils is less important because different oils could be processed into fats of desired properties.

2.3.2 Interesterification

Another method to modify physical properties, e.g. melting of fats, such that they fit the product requirements is the interesterification. Therefore, the fatty acids attached to the glycerol backbone of the fat are exchanged. The technology of interesterification was invented in the 19th century.

So far, two variations of the process namely the chemical and enzymatic interesterification are applied. Both have the advantage to be applicable for a wide range of possible raw materials (Dijkstra, 2014a).

Interesterification was firstly used in the 1920s during the search for cheaper butter and became more famous in the 1950s, when researchers started to use sodium methoxide as a catalyst enhancing the chemical interesterification. (Kellens and Calliauw, 2013). The main parameters influencing the process are the oil quality, the type, and the concentration of the catalyst. In addition, the optimized amount of catalyst yields less by-products and thus results in less oil loss (Kellens and Calliauw, 2013). Interesterification is always followed by a deodorization step to remove minor components such as formed FFAs which are prone to oxidation (Dijkstra, 2014a).

During the process, which is performed batch-wise in the industry, the fatty acid residues of the TAGs are statistically rearranged over the TAGs present. Figure 2.19 shows a possible interesterification between a trisaturated TAG (SSS) and a triunsaturated TAG (OOO). In this example, the interesterification yields a TAG with two saturated fatty acids at the *sn*-1,3-position and an unsaturated fatty acid residue at the *sn*-2-position (SOS). These HUH TAGs are important in the production of cocoa butter equivalents (CBEs) due to their structure providing properties. It is important to mention here that the depicted TAG resulting from the interesterification is just one of many possible fatty acid residue combinations. For chemical interesterification, sodium methanolate is a common used chemical catalyst (Dijkstra, 2014a). Probably, even though not completely verified, a carbonyl addition is the basic principle during this reaction (Kellens and Calliauw, 2013). However, the TAGs resulting from chemical interesterification cannot be controlled in a targeted manner. Thus, apart from the TAG SOS (12.5 %) shown in Figure 2.19, also the TAGs SSO (25 %), OSO (12.5 %), OOS (25 %), SSS (12.5 %), and OOO (12.5 %) possibly result from the interesterification process. The probabilities for each TAG composition to occur are given in the brackets assuming a randomly performed process and a statistical distribution.

A fast reaction normally takes about 30 min. It can be stopped by addition of water, leading to the formation of soaps and free fatty acids. Addition of e.g. citric acid reduces the soap formation. The formation of both, free fatty acids (FFAs) and fatty acid methyl esters (FAMEs) is undesired because of the lower yield of the desired TAGs.

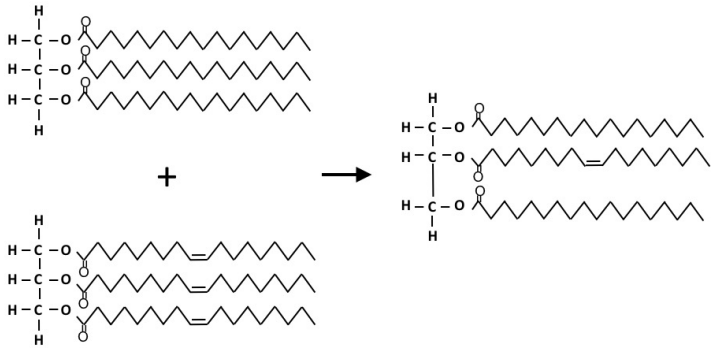

Figure 2.19: Interesterification example; a trisaturated TAG (top left, 3x stearic acid) interesterified with a triunsaturated TAG (bottom left, 3x oleic acid) can yield a HUH TAG (right, 2x stearic (*sn*-1,3-position), 1x oleic acid (*sn*-2-position)).

The interesterification process can alternatively be performed enzymatically as mentioned above. This process can be conducted at milder conditions and provides a stereotypic acyl exchange (Kellens and Calliauw, 2013). It uses lipases to catalyze the abovementioned rearrangement of the fatty acids at the glycerol backbone. There are *sn*-1,3-position selective and non-selective lipases available. The stereo specificity is very helpful to produce cocoa butter equivalents (CBEs) from palm mid fraction by exchanging some of the palmitic acid residues at the *sn*-1,3-positions with stearic acid moieties (Cowan, 2014). Starting from the same feedstock, the TAG composition resulting from a stereo selective lipase and from a chemical approach can differ greatly.

2.3.3 Fractionation Technologies

The main reasons to apply fractionation is the enrichment of valuable TAGs, the removal of undesired minor components or the production of different valuable fractions each with different application ranges and thus presenting alternatives to hydrogenated fats (Timms, 1997). In fat fractionation, fractional crystallization is combined with a separation step to receive different fractions with distinct properties. The solubility of each TAG in the different fraction determines the separation. The separation step depends on the melting points of the various fractions. Therefore, fractionation is currently the only technology which yields fats with specific properties solely based on a physical process (Timms, 1997; Dhaka *et al.*, 2011).

The undesired wide melting range of palm oil is due to the variety of reasonably similar TAGs in the mixture. Because of this it is possible to separate palm oil into different fractions with distinctive properties (Stöver, Eggers and Stein, 1983). Therefore, palm oil became the most fractionated fat in the world (Talbot, Smith and Cain, 2006). It is produced in large amounts (around 64 Mio. tons between 2016 and 2017) and is highly productive (4 t/ha/yr., other vegetable oils ~0.5 t/ha/yr.) (MPOB, 2009; Yan, 2017).

During palm oil fractionation, mainly a good quality olein is aimed due to its application as Asian table or salad oil (Stöver, Eggers and Stein, 1983; Braipson-Danthine and Gibon, 2007; Kellens *et al.*, 2007). However, applying various subsequent fractionation steps leads to a variety of different fractions for divergent applications (Kellens *et al.*, 2007). Once hydrogenation was abandoned, palm oil and its fractions became increasingly important for the food industry. The following explanations are hence focused on palm oil fractionation.

In a simplified way, palm oil can be subdivided into four groups of TAGs with a different melting point each: PPP (65 °C), PPO/POP (34 °C), POO/OPO (18 °C) and OOO (5 °C). These different TAG groups can be separated using fractional crystallization. The mixture of TAGs is crystallized at a certain temperature before separating the two fractions. If no liquid oil remains in the solid fraction, the separation efficiency (SE) of the process is 100 %. To achieve a separation efficiency of 90 % or higher, solvent fractionation needs to be used whereas dry fractionation leads to a SE of max. 60-70 % (Harris, 2014).

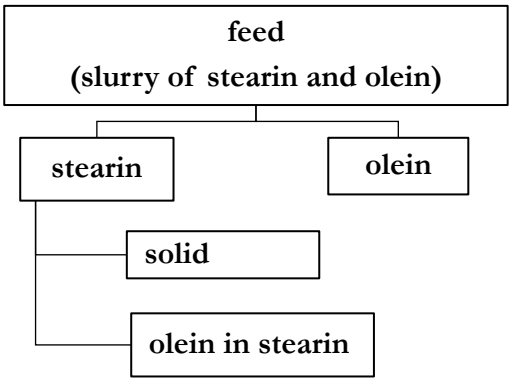

Figure 2.20: Schematically depicted fractionation of a slurry into stearin (solid fraction with entrained olein) and olein (liquid fraction).

In Figure 2.20 fractionation is schematically shown. The yield of the fractionation is given by

$$\mathbf{yield_{stearin}} = \frac{\mathbf{m_{stearin}}}{\mathbf{m_{feed}}} \qquad \textbf{Eq. 2.4}$$

In Eq. 2.4, $m_{stearin}$ is the mass of the stearin fraction after separation and m_{feed} the mass of the slurry at the start of the process.

The separation efficiency (SE) is a measure how successfully the high melting components (solids) were separated from the feed. It is expressed by the ratio of the mass of solid (m_{solid}) and the mass of stearin (Flöter, 2014b).

$$\mathbf{SE} = \frac{\mathbf{m_{solid}}}{\mathbf{m_{stearin}}} \qquad \textbf{Eq. 2.5}$$

With the solid fat content of the feed

$$\mathbf{SFC_{slurry}} = \frac{\mathbf{m_{solid}}}{\mathbf{m_{feed}}} \qquad \textbf{Eq. 2.6}$$

the yield can be expressed by

$$\mathbf{yield_{stearin}} = \frac{\mathbf{SFC_{slurry}}}{\mathbf{SE}} \qquad \textbf{Eq. 2.7}$$

Both parameters, separation efficiency and yield, are used to determine the quality and the efficiency of a fractionation process. If the valuable fraction is stearin, the entrainment of olein should be as low as possible and a maximum separation efficiency is targeted. To increase the separation efficiency, large cubic crystals are desirable to facilitate the removal of olein out of stearin. Possibilities are the solvent or detergent fractionation which increase the separation efficiency even further (Flöter, 2014b).

In general, three different fractionation technologies (dry, solvent and detergent) are applied for oils. Special fractionation processes like supercritical carbon dioxide extraction or molecular distillation are too expensive and not applicable for bulk oil and are therefore not discussed within this work (Kellens and Calliauw, 2013).

All fractionation processes include four steps in common: melting, nucleation, crystal growth, and separation. The oil is melted completely before nucleation is initiated by controlled cooling. Nucleation and growth are done by specific temperature regimes. Once the crystals have grown to the desired size, the crystallized material is separated from the liquid (Timms, 2006).

In the dry fractionation technology, the fat is crystallized from the slurry without any additives such as solvents or surfactants and subsequently filtered. To increase the yield the filter cake is additionally squeezed in e.g. a membrane filter press (Kellens and Calliauw, 2013).

In solvent fractionation solvents such as hexane are used to dissolve the fat and thus increase the separation efficiency (Harris, 2014). The presence of the solvent not only generates a significantly increased volume of feedstock, it also reduces the crystallization temperature significantly. This makes the process only usable for high value fractions.

The third method is the detergent fractionation also known as Lanza or Lipofrac method. Here, the crystals are emulsified in the aqueous phase by addition of a detergent to the slurry prior to the separation in a centrifugal field.

The process parameters and the complexity of the process depend on the desired valuable fraction. This means, for instance, that different fractionation techniques are required whether a low melting fraction or HUH TAGs are the desired fraction. (Hamm, 1986). In addition, the separation of trisaturated TAGs (HHH) from triunsaturated TAGs (UUU) is less complicated because they are not soluble in each other. More complicated is the separation of HUH and HHU TAGs from each other because they have both similar melting points and the solubility in the solid phase is about the same. The entrainment of liquid oil (mainly UUU and HUU) in the resulting filter cake made of the solid fraction (mainly HHH or HUH) and determine he separation efficiency. There are two possible mechanisms responsible for entrainment, the inter- and intra-particle entrainment of the liquid phase. The first one refers to the entrainment between crystal aggregates, whereas the second option relates to the entrapment of oil inside the crystal aggregates (Hamm, 1986).

Dry fractionation is the cheapest fractionation technique whereas solvent and detergent fractionation show higher separation efficiencies. However, both are afflicted with high costs, diminishing consumer acceptance, and hazardous working conditions. Nevertheless, all three mentioned fractionation methods are still of importance and are therefore explained in detail in the following chapter.

2.3.3.1 Dry Fractionation

Palm oil is often fractionated using the discontinuous dry fractionation process which is composed of two main steps, crystallization and separation. The first step can be described as a fractional crystallization based on the distinctive melting points of the different fractions. This means that at a certain temperature, one fraction is already crystallized while the other is still in the liquid state. This invention is attributed to Hippolyte Mége-Mouriés who tried to separate different fractions from tallow to produce cheaper butter. In addition, traders and sailors, who imported palm oil, observed that natural fractional crystallization happened on the ship. In this way, the slight shaking helped the denser crystals to settle yielding a more cold resistant oil behind on top of the crystallized material in the barrels (Kellens and Calliauw, 2013).

Supercooling is necessary to initiate the crystallization, which can also lead to the attachment of undesired lower melting material onto the crystal surface yielding a poorer separation efficiency (Stöver, Eggers and Stein, 1983). Ng and Oh (1994) found that the high melting fraction of palm oil needs to undergo a supercooling of 22 °C before crystallizing. In contrast, a lower supercooling was necessary for the low melting fraction, probably because the high melting fraction crystals acted as seed crystals. In addition, during crystallization transformation from one polymorphic form into another can occur which causes release of the latent heat. The latter is linked to a local temperature increase which can stop the crystallization for a short time which then results in an increase in supersaturation (Stöver, Eggers and Stein, 1983).

In the following section, the process shown in Figure 2.21 is explained in detail. The feed slurry is melted in the feed tank until no crystals remain. Subsequently, the melt is cooled down in the crystallizers to the temperature at which the high melting fraction of the mixture crystallizes. This step is, so far, a batch process. The cooling rate is crucial for the final separation efficiency because it impacts the size of the crystals and the amount of liquid oil incorporated into them. The higher the cooling rate, the smaller the formed crystals which are on the one hand accompanied with a lower amount of incorporated oil but on the other hand have a relatively large surface at which liquid oil can attach. In contrast, a slower cooling leads to less nuclei resulting in larger crystals (Petersson, Anjou and Sandström, 1985).

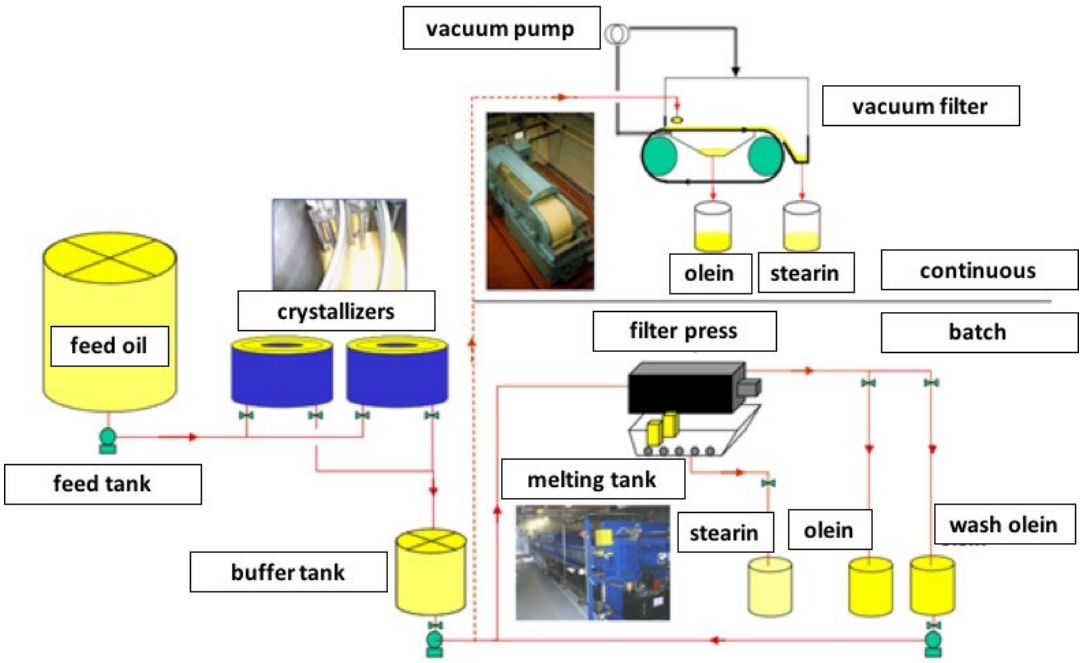

Figure 2.21: Schematic setup of a dry fractionation process with a continuous (top) and a batch (bottom) separation (modified, Calliauw 2017).

The crystal size and shape are important for both, the final product application as well as the fractionation performance. While in product applications, small crystals are desired due to their flexible structuring properties, for a good fractionation performance, large crystals with a low tendency to bind liquid oil are desirable resulting in a less porous filter cake (Stöver, Eggers and Stein, 1983; Bot and Flöter, 2013). The challenge is, hence, to find an adequate balance between the size of the crystals and the amount of oil remaining in the crystals. The generation of larger crystals is done by increasing the temperature after generating enough nuclei to exclusively promote crystal growth instead of the formation of further nuclei (Flöter, 2014a).

In other words, the supersaturation is changed stepwise. Thereby, it needs to be large enough to create a driving force for the crystallization of the desired crystals, but should not be too large so that undesired crystal formation and growth can be prevented (Kellens and Calliauw, 2013). In addition, the viscosity of the slurry should stay moderate during the increase of the amount of crystallized material to avoid slowing down the process too strongly (Calliauw *et al.*, 2010).

The formed slurry consists of the crystallized high melting fraction and the still liquid low melting fraction. It is kept in a buffer tank until it is separated in the second step, the separation (Calliauw, 2014). The separation step was developed and enhanced from vacuum belt to membrane press filters or centrifuges (Timms, 2006; Kellens and Calliauw, 2013). In the batch process, after the first filtration a membrane filter press is used to squeeze the filter cake so that the stearin (high melting fraction) releases as much of the liquid olein (low melting fraction) as possible. For the continuous process either vacuum filters or decanter centrifuges are used for the separation of stearin and olein. However, the continuous process is rarely used in the industry.

In palm oil dry fractionation, two ways of generating a palm mid fraction (PMF) can be applied. Either the olein is generated in the first step and separated from the stearin which is further fractionated or the stearin is removed in the first step leaving the olein fraction for further fractionation. The advantage of the first approach is that the high melting TAGs of the stearin help to nucleate the fractions in both steps and the PMF is obtained more easily (Talbot, Smith and Cain, 2006). In addition, during the fractionation of stearin, also a hard stearin fraction is generated with a sharp melting range. While for dry fractionation two steps are required to obtain hard stearin for solvent fractionation only one step is necessary.

One disadvantage of the dry fractionation is its usually batch-wise operation. Moreover, dry fractionation shows a lower separation efficiency and precision with respect to the separation of the fractions compared to other methods. The precision is rather low due to liquid sticking onto crystals or liquid being trapped in agglomerates so that it is hard to separate the olein from the stearin (Stöver, Eggers and Stein, 1983).

Further, the kinetics of the crystallization is rather slow. The crystallization time mainly determining the processing time ranges from 5 hours to 3 days (Kellens and Calliauw, 2013). Such a long processing time is one of the other main disadvantages of the dry fractionation process.

2.3.3.2 Solvent Fractionation

In the process of solvent fractionation, solvents like acetone or hexane are used to increase the separation efficiency. The solvent addition to the feedstock leads to a variation of the solubility of the TAGs and a very low-viscous filtrate. Moreover,

solvent fractionation often generates a higher separation efficiency compared to dry fractionation because the stearin filter cake can be washed with solvent purging the solid from the trapped olein (Stöver, Eggers and Stein, 1983; Kellens and Calliauw, 2013).

Like dry fractionation, the solvent fractionation process is composed of the aforementioned two steps crystallization and separation. Now, the crystallization happens in a solvent like acetone or hexane. These components are used as solvents due to the high solubility of minor and major components and their low heat of evaporation leading to less energy required for the solvent recovery (Harris, 2014).

Due to the addition of solvents, the crystallization temperature decreases which leads to a viscosity increase (Vanhoutte *et al.*, 2003). However, the solvent present in the liquid phase (e.g. acetone with 0.3 mPa) reduces the viscosity of oils which ranges at relevant fractionation temperature from 30-100 mPa when no solvents are present. The subsequent increased molecular diffusion leads to faster crystallization (30 min in solvent fractionation) and possibly even to a continuous crystallization (Harris, 2014). The lower viscosity helps during filtration because it limits the entrainment of liquid oil in the filter cake and this leads to an increase of the separation efficiency (Timms, 1997; Kellens *et al.*, 2007; Harris, 2014). To sum up, solvent fractionation generally yields a cleaner product resulting in a sharp melting stearin, a higher stearin yield as well as a higher process efficiency due to a one step process, and fast crystallization (Harris, 2014).

As mentioned, one of the most important process steps in fractionation technology is the nucleation of fat crystals. Therefore, the metastable zone, needs to be considered. This degree of supersaturation without substantial nucleation is practically the difference between the temperatures at the cloud point, where some nuclei are already visible, and the clear point (Talbot, Smith and Cain, 2006). Another important factor to consider are the shape and size of the crystals correlating with the washing of the liquid fraction from the solid crystals. The macroscopic appearance of the crystals can be modified by adjustment of the crystallization conditions (Vanhoutte *et al.*, 2003). For palm oil fractionation, hexane and acetone show the same selectivity. However, better olein qualities are achieved, if hexane is used as a solvent. In contrast, acetone should be used if the palm mid fraction is rich in POP (Timms, 2006).

The remaining lower melting TAGs can either be entrapped in the crystals or remain in the bulk oil (Timms, 2006). The removal of the liquid from the solid crystals can be critical in solvent fractionation. Crystals generally tend to entrain more liquid oil during solvent fractionation compared to dry fractionation. Better separation is achieved by washing the stearin with fresh solvent after filtration. This leads to the removal of the remaining liquid oil, which is a mixture of oil and solvent, yielding 90 % SE. The solvent needs to be fully recovered. This particularly means the decrease to a level of 100-200 ppm in the low melting product. Moreover, the slurry must be further cooled down. All these aspects lead to a significant increase of the production costs in comparison to the dry fractionation. Consequently, the higher separation efficiency and yield of solvent fractionation can compensate the higher costs only for high value products (Hamm, 1986). Furthermore, solvent fractionation plants pose a substantial higher hazard potential for operators and the environment. Hence, the use of solvent fractionation is only economical if a high separation efficiency is necessary such as for specialty fats like cocoa butter equivalents or replacers (Stöver, Eggers and Stein, 1983; Timms, 1997; Kellens *et al.*, 2007; Bot and Flöter, 2013; Harris, 2014).

2.3.3.3 Detergent Fractionation

The detergent fractionation, which is also named Lipofrac or Lonza method, is composed of a crystallization step identical to the dry fractionation procedure, but additionally followed by the usage of a detergent solution and a separation in a centrifuge (Stöver, Eggers and Stein, 1983; Timms, 2005). It can thus be assigned to the dry fractionation technologies (Hamm, 1986). The process is based on emulsion technology because a detergent solution composed of water and surfactants or wetting agents is used (Deffense, Tirtiaux and Charleroi, 1985).

After crystallizing the feedstock, the added detergent suspends the already formed crystals in the aqueous solution and hence entrain them from the lipid phase. The density difference between the aqueous detergent solution with the entrained fat crystals and the lower melting liquid oil fraction makes the separation easier using centrifugal force (Timms, 2005). Normally, a wetting agent like sodium lauryl sulfate with an electrolyte (e.g. magnesium sulfate) is used during this process (Kellens *et al.*,

2007). The high costs of the used detergent solution and its recovery are reasons why the detergent process is at present practically not applied in the fractionation industry.

2.3.3.4 Comparison of Fractionation Technologies

In Table 2.2, a summary of different parameters concerning the dry, solvent and detergent fractionation is given. It shows that dry fractionation has the lowest separation efficiency but the lowest costs. In addition, it is not as hazardous as solvent fractionation and produces less waste than the other two fractionation technologies. Both fractionation techniques, in which crystallization is performed from the molten lipid phase (dry and detergent fractionation), show higher entrainment compared to solvent fractionation, which includes a washing step with solvent (Hamm, 1986). However, the hazard and costs make this process less popular. In contrast, the cheaper and environmentally more friendly process of dry fractionation has a separation efficiency inferior to solvent and detergent fractionation. This limits the functionality of the fat phases produced by dry fractionation. Thus, there is a demand for a new fractionation technique, which yields high separation efficiencies without the excessive use of time, supplementary material or energy. The proposed new approach for the fractionation of edible fats is key to this thesis and is subsequently discussed in detail.

Table 2.2: Comparison of costs, yield, efficiency, advantages and disadvantages of the three fractionation methods dry, solvent and detergent.

	Dry	Solvent	Detergent
Costs	lowest[9]	highest[9]	medium[9]
Duration	5 h – 3 d[1] 10 h[3]	30 min cryst.[4]	3-4 h[7]
Stearin yield (%)	17[2] 40[6] 20-21[10]	10-11[2] 37-40[10]	20[6] 17-23[10]
IV Stearin	32[2] 46.7[6]	8[2]	24.9[6]
Entrainment of oil (% of stearin)	30[2] 47-50[10]	5[2]	35-52[10]
Liquid to solid ratio (L/S)	0.5-1.0 (press filtration)[9] > 1.0 (vacuum filtration)[9]	< 0.5[9]	0.5-1.0[9]
Advantages	- cheap[9]	- high selectivity[5] - short crystallization time[8] - easier filtration due to lower viscosity[8] - easier heat transfer[8] - less entrained oil[8]	- cheaper than solvent[5]
Disadvantages	- long residence time[1] - low separation efficiency[10]	- high energy costs[5] - high material costs[5] - safety issues[1] - consumer acceptance[1]	- chemical costs[5] - recovery of polluted water[5] - consumer acceptance[1]

[1](Kellens and Calliauw, 2013) [2](Timms, 2006) [3](Stöver, Eggers and Stein, 1983) [4](Harris, 2014) [5](Ricci-Rossi and Deffense, 1984) [6](Deffense, Tirtiaux and Charleroi, 1985) [7](Cornelius, 1977) [8](Timms, 2005) [9](Hamm, 1986) [10](Timms, 1997)

2.4 Emulsion Fractionation

A continuous fractionation process would be an energetically favorable and thus a desirable process. A possibility would be emulsion fractionation which is, like all other fractionation techniques, based on the two distinct sub-processes of crystallization and separation. The combination of the above into a continuous process decreases the inter-batch variability, improve energy efficiency and yield a more uniform crystal size distribution (Kellens and Calliauw, 2013). In such a process one starts with an emulsion. On the interface between droplets and continuous liquid phase crystallization of the respective fraction of fat occurs. Separation of these droplets with crystals from the liquid phase would lead to the desired fraction. The combination of these processes into one continuous process requires the knowledge about the respective underlying process steps. Therefore, the theoretical background of the crystallization at the oil and water interface along with the separation in a decanter centrifuge as well as the systematic setup idea of the emulsion fractionation technology are given in the following sub-chapters.

2.4.1 Emulsions and Pickering Stabilization

An emulsion is a thermodynamic unstable two-phase system composed of a continuous phase and a dispersed liquid phase. Two different types of emulsions are relevant for the food industry. The first one is water-continuous with oil droplets as the dispersed phase (O/W emulsion). The second one is oil-continuous with dispersed water droplets (W/O emulsion). These emulsions are stabilized either by the addition of an emulsifier (Figure 2.22a and b), by Pickering, e.g. the stabilization of the droplets due to particles on the droplet surface (Figure 2.22c) or a combination of both (Figure 2.22d).

Emulsifiers are usually amphiphilic molecules characterized by a lipophilic and a hydrophilic part. These molecules arrange themselves in a way that the lipophilic tail reaches into the oil phase while the hydrophilic head is in contact with the water phase. These molecules decrease the surface tension between the oil and the aqueous phase, thus, generate the emulsion with droplets surrounded by surfactants. A potential prolongation of the stability of an emulsion depends on the type of emulsifier and in

particular on the steric hindrance of the droplets avoiding coalescence. Emulsifiers can be classified by their so-called HLB-value (hydrophilic-lipophilic-balance). The HLB-value describes the affinity of the emulsifier to stabilize O/W (8-15) or W/O (3-8) emulsions. Emulsifiers with HLB-values lower 3 show anti-foaming properties. Emulsifiers with HLB-values higher than 15 are used to enhance solubilizing (Schuchmann and Köhler, 2012).

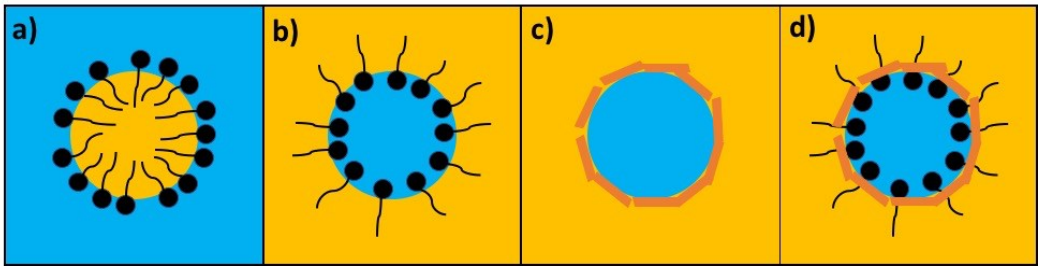

Figure 2.22: Different types of emulsion: a) oil-in-water emulsion stabilized by emulsifiers, b) water-in-oil emulsion stabilized by emulsifiers, c) water-in-oil emulsion stabilized by fat crystals/ particles, d) water-in-oil emulsion stabilized by emulsifiers and fat crystals/ particles.

There are different mechanisms for emulsion stabilization. For example, charged moieties of emulsifiers lead to a repulsion of the droplets whereas large moieties of emulsifiers stabilize an emulsion due to steric hindrance. This special case of emulsion stabilization by particles is called Pickering stabilization. Pickering was the first one who observed that solid particles can serve as stabilizing agent for emulsions (Pickering, 1907). Hence, emulsions stabilized in a steric manner by fat crystals after their adsorption onto the interface are called Pickering emulsions and are important in food products like margarine, mayonnaise or ice cream (Pawlik *et al.*, 2016).

In the case of the aforementioned food products, fat crystals are the stabilizing agents as shown in Figure 2.22c. In cosmetic and pharmaceutical products, other particles can also be used to stabilize emulsions. The particles at the interface in a Pickering emulsion lead to less coalescence and a decreased mass transfer of components from inside the droplets to the surrounding liquid phase due to their function as barrier or shell at the interface (Pawlik *et al.*, 2016).

An oil-continuous matrix in which the emulsion droplets are stabilized by fat crystals is important for many food products. Depending on the nature of the fat crystals in combination with the continuous phase the emulsion is stabilized or dissolved (Hodge and Rousseau, 2005). In a system with a water continuous phase, they mostly lead to partial coalescence of the droplets. In contrast, at the interface fat crystals in oil continuous systems may serve as Pickering particles, thus having a stabilizing effect. Due to adsorption of fat crystals onto the interface sedimentation, flocculation, and coalescence are avoided (Hodge and Rousseau, 2005). Platelet shaped and small crystals as well as crystals formed by in situ crystallization are known to increase the stability of W/O emulsions (Frasch-Melnik, Norton and Spyropoulos, 2010; Douaire *et al.*, 2014).

The stabilizing effect of fat crystals can be enhanced by the addition of surfactants. These increase the polarity of the naturally not amphiphilic fat crystals (Frasch-Melnik, Norton and Spyropoulos, 2010). Moreover, crystallization directly at the interface can be promoted by so-called templates, which lower the activation energy (see Figure 2.22d). These templates impact the crystal arrangement, which in turn influences the emulsion stability itself (Douaire *et al.*, 2014). Improved stabilization was observed if the hydrophobic part of the applied emulsifier has a similar length and structure as the TAGs in the oil (Awad, Hamada and Sato, 2001). Furthermore, the addition of emulsifiers increases the crystallization temperature (Douaire *et al.*, 2014). This was also fond for higher crystal concentrations (Frasch-Melnik et al., 2010).

The addition of mono- and diglycerides with a higher melting point lead to a crystalline interface ("shell") in W/O emulsions (Douaire *et al.*, 2014). Additionally, added saturated monoglycerides for example could serve both as surfactants and as seed for TAGs to crystallize. Small crystals are preferred for the production of Pickering emulsions because they give a high surface coverage of the droplets and by this a better stabilization. Low crystal concentrations lead to less stable emulsions. The desired small and numerous crystals are formed at high cooling rates, hence at larger driving force for the in situ crystallization. In addition, the increased amount of available growth sites at high cooling rates leads to a faster depletion of high melting components for crystal growth (Flöter, 2014a).

In addition to the faster nucleation and the higher amount of produced crystals, added emulsifiers influence polymorphism due to templating. Due to present crystals the creation of the in situ formed crystals is influenced. This control of the polymorphic form can be crucial for the stability of emulsions, e.g. needle-shaped crystals (β) tend to destabilize emulsions, whereas platelets improve the stabilization. Some authors found that specific additives lead to specific polymorphic forms (Douaire *et al.*, 2014).

However, one needs to be careful because crystallization in emulsions differs from bulk systems (see chapter 2.2). As mentioned above, in situ crystallization depends on the emulsion type, the nucleation process, the lipid phase composition and the molecular packaging. The crystallization of oil in an O/W emulsion requires more supercooling (thus supersaturation) because the amount of impurities in the droplets is statistically low (Douaire *et al.*, 2014). Nevertheless, for this thesis, O/W-emulsions play a minor role. The focus is on Pickering W/O-emulsions, where the crystallization mainly takes place on the water droplet surface and not in the bulk. From this sub-chapter, it can be concluded that the existence of an oil/water interface has the potential to severely influence the TAG crystallization and that additives allow to manipulate the nucleation process. In summary it can be said that the functionality of the Pickering particles can be influenced by the continuous phase but also by the choice of emulsifier (Pawlik *et al.*, 2016).

2.4.2 Decanter Centrifuge

The separation of two materials with different densities can be performed in a centrifuge. If a continuous process is desired, a horizontal decanter centrifuge can be used. These are often used to clarify liquid, classify particles or to remove moisture from solids (Gleiss and Nirschl, 2015). Decanters can be applied in a wide range of concentration of solids (up to 60 %) and particle sizes (Beiser *et al.*, 2004). In the oil and fat industry, decanter centrifuges are so far used, for example, in the olive oil industry to separate the oil from the seeds after squeezing (Altieri, Di Renzo and Genovese, 2013). Here, the process executed is a sedimentation process under increased driving forces.

A decanter mainly consists of a bowl and a screw. A setup is schematically shown in Figure 2.23. The bowl has a conical (right side, Figure 2.23) and a cylindrical part (left side, Figure 2.23). At the end of the cylindrical part in the middle of the decanter, the feed is inserted. There exist various parameters which influence the separation in a decanter. Concerning the material, the particle size of the dispersed phase as well as the viscosity of the continuous phase influences the process and also the amount of feed.

Stokes law can be used to calculate the sedimentation velocity v of a particle p in a continuous phase c:

$$\mathbf{v = \frac{g \cdot (\rho_p - \rho_c)}{18\eta_c} \cdot d_p^2} \qquad \textbf{Eq. 2.8}$$

This velocity is influenced by the density of the particles ρ_p, the density ρ_c and the viscosity η_c of the continuous phase, and the diameter of the particles d_p.

In addition, the g-force plays a decisive role and can be varied in the decanter by changing the rotation speed of the bowl. In the used equipment (Lemitec MD 80), the g-force during the separation can be varied between 200-3,000 g. Further parameters are the differential speed between the screw and the bowl (1-200 rpm) as well as the length and the angle of the drying section (both constant in the used device). The retention time of the liquid also influences the separation of the material and can be adjusted by the volume flow into the decanter and the filling volume of the device. The latter can be changed by the addition of different weirs, which increase the filling level.

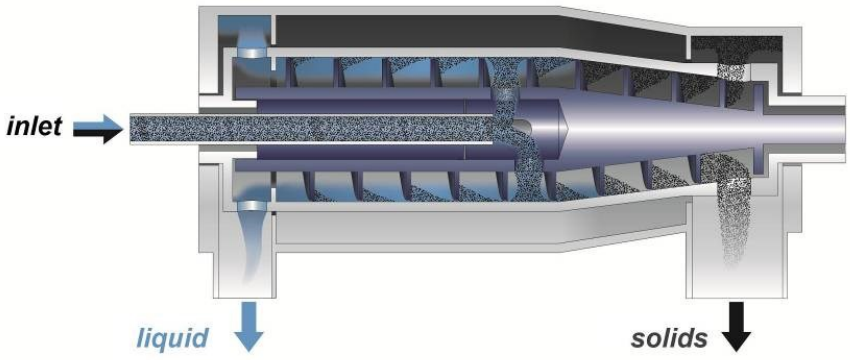

Figure 2.23: Lab scale decanter (Lemitec MD 80) with an inlet (left), an exit for the liquid phase (left, bottom), an exit for the solids (right, bottom) and a weir to adjust the filling level (small grey dash).

The conical part of the decanter is necessary to dry the separated solids. The drying zone prior to the ejection of the material is visualized in Figure 2.24. The length of both, the drying and the clarifying zone can be theoretically adjusted by the height of the weir, illustrated with the yellow arrows in Figure 2.24. If the weir inner diameter is decreased and thus the height of the weir increases, the amount of liquid in the decanter and hence the filling level increases. This leads to a shorter drying zone at the conical end of the decanter in which the solids are transported by the inner screw. This movement is generated because the bowl and the screw rotate at different speeds (1-200 rpm in the case of a Lemitec MD 80).

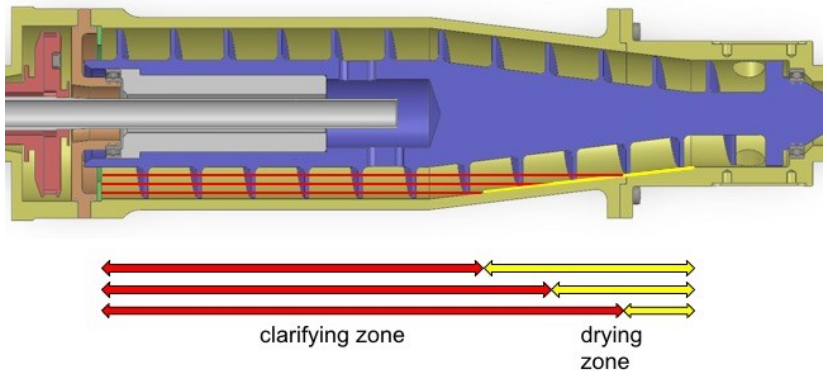

Figure 2.24: Working principle of a decanter with a clarifying zone (left, red lines and arrows) and a drying zone (right, yellow line and arrows).

In this thesis, a lab scale decanter built by the company Lemitec was used for the emulsion fractionation. In contrast to an industrial decanter (the largest conveying 250,000 l/h (Beiser *et al.*, 2004)), the lab scale decanter (see in Figure 2.25) has a comparatively low throughput of approximately 40 l/h enabling small-scale experiments.

Figure 2.25: Lab scale decanter (Lemitec MD 80)

2.4.3 Concept of Emulsion Fractionation

The conceptual setup of the continuous emulsion fractionation process is depicted in Figure 2.26. The basic idea is to continuously generate a Pickering emulsion by sending cold water droplets into a hot oil stream. This process initiates the crystallization of the high melting fat fraction at the water droplet surface (step 1). The resulting slurry, a Pickering emulsion, water droplets (blue dots after step 1) stabilized by fat crystals (orange dashes) dispersed in liquid oil (yellow background).

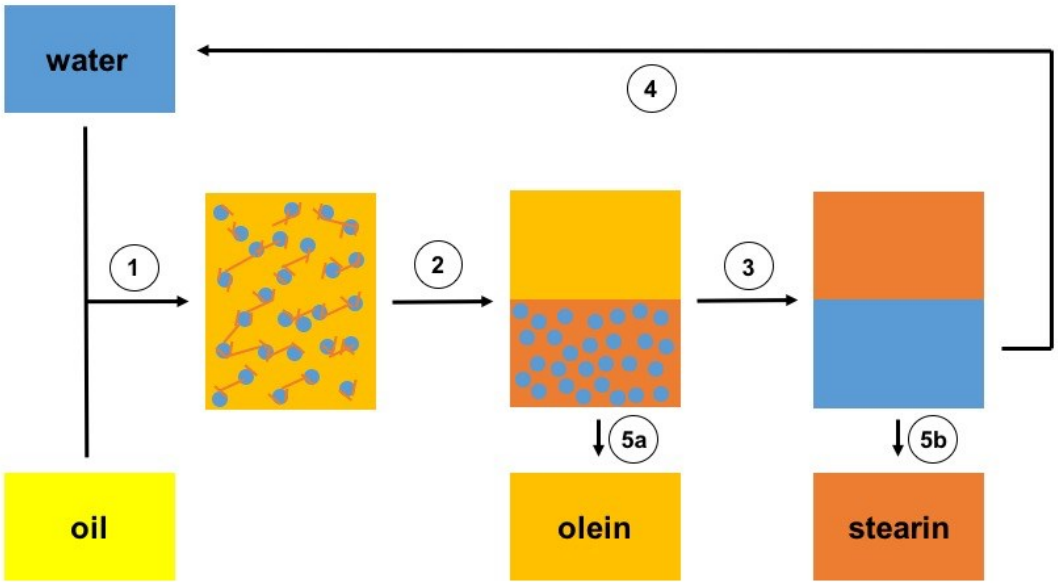

Figure 2.26: Theoretical setup of the continuous emulsion fractionation process; 1) crystallization of fat at water droplet surface, 2) separation of high and low melting fraction in decanter, 3) separation of high melting fraction and water in decanter, 4) recycling of water, 5a) yielded low melting fraction (olein), 5b) yielded high melting fraction (stearin)

In step 2, the separation in the decanter centrifuge takes place. Due to density differences, the denser water droplets carrying a high melting fat crystal shell sediment out of the oil phase. The density of the oil is approximately 0.92 g/cm^3 (Coupland and McClements, 1997), the density of the water droplets is 1.00 g/cm^3 (Coupland and McClements, 1997) and the density of fat crystals is stated to lay between 1.02 g/cm^3 (Sato *et al.*, 2001) and >1.04 g/cm^3 (Bailey and Singleton, 1945). During this process step, olein which is the low melting fraction exits the decanter as the liquid fraction (step 5 a). After the separation of the olein from the slurry, the water droplets with attached fat crystals are heated up until the fat melts. Subsequently, the resulting undefined emulsion is separated into an aqueous and a lipid phase by means of a centrifuge (step 3). In this step the second product, the high melting fraction stearin, is obtained (step 5b). The outlined process allows to reuse the water (step 4) and optimize energy consumption by recovering thermal energy from the streams generated.

The ambition of the outlined emulsion fractionation process is to operate continuously at low conversion costs compared to solvent or detergent fractionation. It is further aiming at selective crystallization by the choice of the appropriate crystallization conditions, exclusive use of water as entrainer, and high separation efficiencies.

3 EXPERIMENTAL METHODS

This chapter is dedicated to the main experimental methods used in this thesis. Both the basic measurement principle and the used procedures are outlined for differential scanning calorimetry, temperature modulated optical refractometry, gas chromatography, nuclear magnetic resonance, polarized light microscopy, and powder X-ray diffraction. In addition, their relevance and application in the field of fat technology are highlighted.

3.1 Differential Scanning Calorimetry

Phase transitions like melting and crystallization as well as glass transitions can be determined by differential scanning calorimetry (DSC). Thus, it is a widely applied technique in the food industry (Menard and Sichina, 2000). This subchapter gives an overview of its basic principle and its main applications in the area of fat technology.

3.1.1 Principle of determination

The DSC method is based upon the differences in the thermal conductivity of two samples. The setup is shown in Figure 3.1, where a reference and a sample pan are placed in a temperature controlled cabinet. During heating or cooling, the difference in the voltage between the two pans is recorded by the instrument and converted into temperature differences. The sensors are located at positions for the reference and sample crucible.

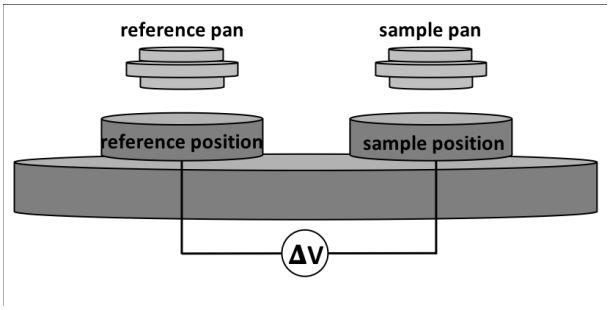

Figure 3.1: Schematic setup of a heat-flux DSC with a reference pan and a sample pan for the determination of the voltage difference ΔV.

The temperature difference is converted into a thermogram where the heat flow is depicted as a function of temperature. This conversion is shown in Figure 3.2. where the temperature of the reference pan, indicated by the grey line, increases linearly over time. In contrast, the temperature recorded for the sample pan (black line) shows a plateau starting at time t_1. At that time, a phase transition commences in the sample which means that the thermal energy is either absorbed (melting) or emitted (crystallization) by the sample but not used to heat or cool the pan. Thus, the temperature stays constant until the phase transition is completed and the temperature increases again linearly.

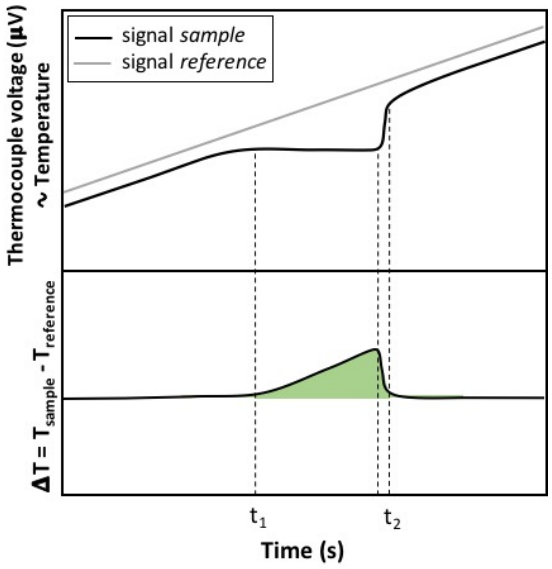

Figure 3.2: Experimental data of a heat flux DSC; upper graph: thermocouple voltage (proportional to temperature) plotted against time, sample signal (black line) and reference signal (grey line); lower graph: converted voltage signal into temperature difference of the reference and the sample (modified, Netzsch 2017).

The detected temperature difference is converted into peaks which are plotted against the temperature, the so called thermograms. Two possible resulting schematic thermograms are depicted in Figure 3.3. A phase diagram of a system constituted of a high and a low melting component is given. The red, dashed line shows the liquid to solid transition of a mixture with an overall composition of x_a. The area between the solidus and the liquidus line describes the mixture of a solid and a liquid phase. There, the low melting component of the mixture in its pure state would already be liquid

while the high melting one would still be solid. The width of this two-phase region (with respect to temperature) decreases approaching the composition of the pure components. For a pure component, the resulting melting peak (red solid curve) is almost discrete, meaning that the transition from solid to liquid occurs at one distinct temperature. For a mixture, a broader melting peak is obtained because at each temperature two phases (solid and liquid) of different compositions exist. Only after the liquid phase has reached the overall composition x_a the phase transition has been completed.

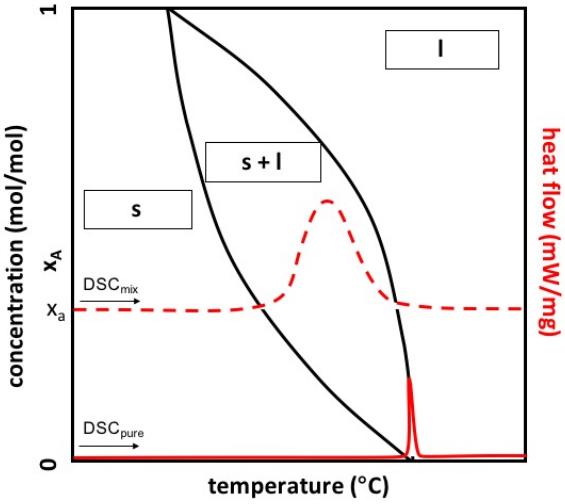

Figure 3.3: Phase diagram of a two-component mixture with schematic DSC thermograms of a mixture (red, dashed line) and of a pure component (red, solid line).

Hence, the composition of the mixture influences the shape of the peak. Conversely, the shape of the peak can be used to characterize a sample. Moreover, parameters like the peak temperature (transition temperature) as well as the onset and offset temperature of the phase transition are helpful parameters for the characterization of a mixture. The onset temperature of a phase transition in a mixture can be considered as the crossing of the solidus line into the two-phase region. Subsequently, the crossing of the liquidus line can be related to the offset temperature of the transition. In addition to the different characteristic temperatures, the heat of fusion (ΔH) can be determined for not too complex systems by the area under the peak. Since the heat of fusion depends on the mass of the sample, the mass needs to be

determined as exactly as possible. The determination of all four parameters is shown in the schematic thermogram for a crystallization and a melting process in Figure 3.4. An important term for this data processing is the baseline. The zero baseline is based on the equal heating of the empty reference pan and the sample pan without a phase change. A proper baseline is required to calculate the enthalpy of fusion. In addition, the intersection of the extension of the baseline and the tangents of the peak (grey dashed lines in Figure 3.4) are necessary to determine the onset and offset of phase transitions.

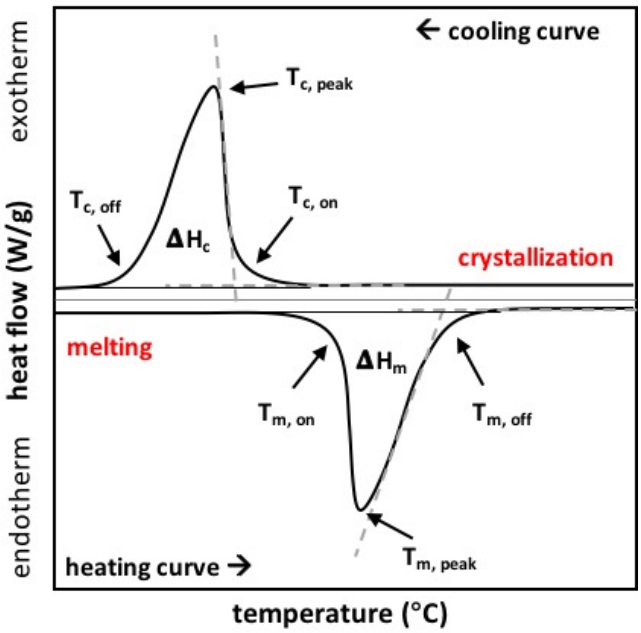

Figure 3.4: DSC thermogram of crystallization and melting; T_{on} = onset temperature, T_{peak} = peak temperature T_{off} = offset temperature, c = crystallization, m = melting.

Commonly, a positive peak in a DSC thermogram refers to a crystallization process which is an exothermic process (release of heat). A melting process is an endothermic process showing a negative peak in the DSC thermogram because of the negative heat flow due to the uptake of heat.

Besides the composition, also the scan rate influences the width of the peak. For example, a too high cooling rate during the crystallization of a pure component would lead to a temperature lag in the sample behind the temperature in the system. Thus, the peak becomes broader and the transition temperature is found at a higher crystallization

temperature than the actual equilibrium temperature. To decrease the influence of the thermal lag a small scan rate would be desirable. This also leads to a higher resolution. However, while enhancing the sensitivity, a small scan rate may also increase the noise (Chiu and Prenner, 2011). Hence, a good balance between resolution and sensitivity needs to be found for DSC measurements.

3.1.2 Application in the field of fat technology

DSC is applied widely in the field of fat technology to determine phase transitions. Fats and oils are composed of a mixture of various TAGs. This can make the interpretation of the DSC thermograms more complicated but if the method is applied with care the data can be used to characterize different fats and oils. The received experimental data is influenced by both, the chemical composition of the fat as well as the applied parameters (scan rate, sample mass).

Considering the composition of fats, it can be said that fats with high amounts of saturated fatty acids need more energy to be melted which results in a higher specific melting enthalpy. However, one must be careful determining the enthalpy from DSC thermograms because the baseline may differ before and after the phase transition (peak) (Tan and Che Man, 2002b). In addition, as mentioned above, the heat of fusion is an extensive property which makes it necessary to determine the weight of the sample properly.

Hence, to gain proper data, the sample mass needs to be determined precisely in advance since it has an impact on the resulting thermograms and the determined transition temperatures. Saeed and coworkers (2016) showed that the specific melting enthalpy increases slightly with increasing sample mass. The determination of the melting temperature was affected at lower sample masses (< 5 mg) while no effect was seen at larger sample masses (> 5 mg). Therefore before comparing data, it is important to always weigh in the samples in the same weight range.

In addition, Saeed and coworkers (2016) presented that the scan rate influences the peak temperature and the specific melting enthalpy for mainly pure components. The same was found by Tan and Che Man (2002), who showed the effect of the scanning rate on the thermal profile of different fats. They examined four scanning rates (1, 5, 10, 20 °C/min) from 80 °C to -80 °C and back to 80 °C. High scanning rates resulted

in a smooth melting curve with less peaks than lower rates. This may lead to a loss of information. Furthermore, high scanning rates resulted in an increase of the determined melting point and the computed area under the peak. Also Vanden Poel and Mathot (2006) found that at high cooling rates the crystallization temperature is shifted towards lower temperatures while high heating rates lead to a shift of the determined melting temperature to higher temperatures. In addition, the offset temperature can be affected by the scanning rate shifting to higher values with increasing scanning rate (Tan and Che Man, 2002b). Consequently, it might be interesting prior to analysis to investigate comparable samples with different scan rates to identify the best scan rate for the given investigation.

Besides the peak, onset and offset temperatures, also the number of peaks can change with the scanning rate. Often more than one endothermic peak occurs during melting which can be explained by the variety of composition in TAGs (SSS, SUS, SUU, UUU) or the appearance of polymorphism (melting-recrystallization). Overall it can be said that the complexity increases with the number of different TAGs comprising the mixture (Tan and Che Man, 2002b).

DSC should be used with caution to differentiate polymorphic forms. More peaks could be visible at slow scanning rates because the TAGs have more time to rearrange. This leads to the conclusion, that the scan rate takes a big influence on the determination of the crystallization behavior of TAGs. The higher the scanning rate the lower the determined exothermic peak temperature. Furthermore, the slow scanning rate gives the TAGs more time to re-organize which results in more interactions and thus leads to co-crystallization (Tan and Che Man, 2002b).

3.1.3 Procedures

To determine the crystallization and melting behavior a device from Netzsch (DSC 204 F1 Phoenix, NETZSCH-Geraetebau GmbH, Selb, Germany) was used. 5-10 mg of sample was weighed into aluminum pans. Then, the samples in the DSC pans were molten by increasing the temperature to 80 °C and holding it there for 10 min.

Afterwards the samples were cooled at defined rates (2 °C/min, 5 °C/min or 10 °C/min) to the desired stabilization temperature, which varied between -50 °C and 5 °C. After a defined crystallization time (between 10 min at -50 °C and 30 min at 5 °C, respectively) the samples were heated to 80 °C again at predefined rates (2 °C/min, 5 °C/min or 10 °C/min) to determine the melting profile.

In addition to the determination of the phase transitions, DSC data received at a scan rate of 5 °C/min were also used to calculate the solid fat index (SFI). Therefore, the area under the peak was subdivided and partially integrated. The relation between the partial area and the complete area under the peak was defined as the amount of solids at the specific temperature (Bentz and Breidenbach, 1969; Nassu and Guaraldo Gonçalves, 1995). All experiments were at least performed in duplicate. The analysis of all thermograms was performed with the NETZSCH Proteus – Thermal Analysis software version 6.1.0 provided by the manufacturer.

3.2 Temperature Modulated Optical Refractometry

The measurement of phase transitions is crucial in fat technology to determine e.g. organoleptic properties. The standard method is the well-established DSC which is described above. Alternatively, the temperature modulated optical refractometry (TMOR) could be applied. It uses the difference in the refractive index *n* between a solid and a liquid phase to compute the phase transition temperature. Its basics like refractometry and temperature modulation are explained in the following chapter along with the principle of TMOR and its previous applications apart from fat crystallization.

3.2.1 Refractometry

The refractive index *n* of a substance or component is its property to diffract light and is expressed as the relationship between the propagation speed of light in the medium c_m in comparison to vacuum c_0 (see Eq. 3.1). The refractive index is also called optical density and, hence, a denser material leads to a higher *n*.

$$\mathbf{n} = \frac{\mathbf{c_0}}{\mathbf{c_m}} \qquad \textbf{Eq. 3.1}$$

The difference in the refractive indices of two materials is a result of their distinct refraction of light. In Figure 3.5, an incident ray is going through medium 1 with the refractive index n_1. At the interface between the two media, the beam is partly reflected (with the same angle as it is impinged upon the interface θ_1) and partly refracted. The angle of the refracted ray θ_2 depends on the refractive index n_2 of medium 2. The so-called Snell´s law gives this relation between the refractive indices and the angles of the beam (Carlton, 2011):

$$\mathbf{n_1 \cdot \sin \theta_1 = n_2 \cdot \sin \theta_2} \qquad \textbf{Eq. 3.2}$$

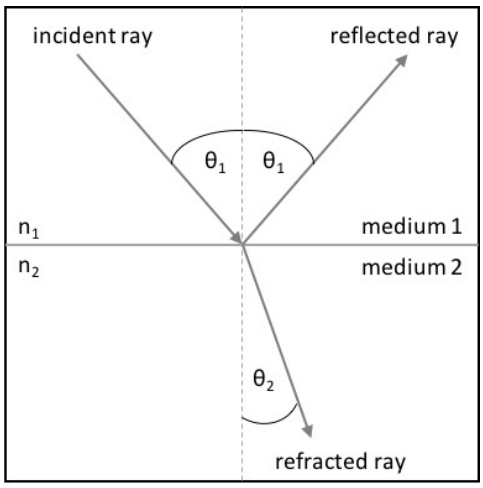

Figure 3.5: Refractive index n_1 of medium 1 and n_2 of medium 2 (modified, Carlton 2011).

The determination of the refractive index is temperature dependent and quite easy if a pure component is investigated. A mixture of two components makes the determination of the refractive index more complex. However, it might be possible to calculate the ratio of two miscible components with different refractive indices from the resulting refractive index. The change of the refractive index over the composition range is based on the mixing rule. Hence, the amount of each component can be calculated as indicated in Figure 3.6.

For the investigations of fat, both isothermal and dynamic measurements are helpful. In addition, a robust and convenient device would be desired if the method should be applied in practice e.g. in a factory. Therefore, the application of a refractometer with additional temperature modulation was investigated to determine the crystallization and melting behavior of fats and alkyl components.

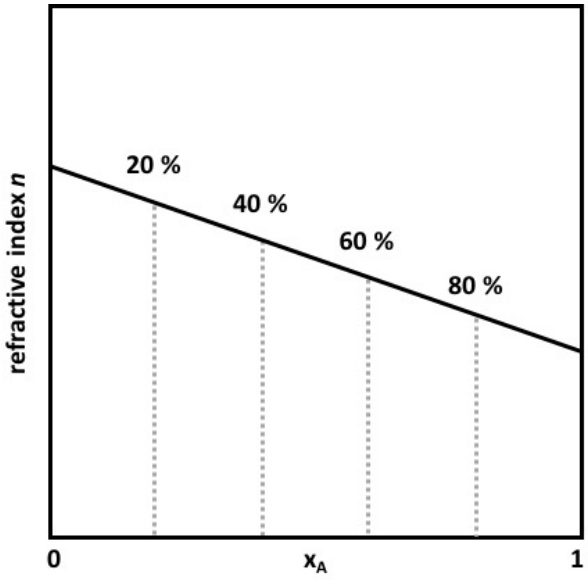

Figure 3.6: Mixing rule of a binary system composed of two miscible components with distinct refractive indices.

3.2.2 Fundamentals of the Temperature Modulated Optical Refractometry

The total reflection is required to determine the refractive index of a solid or a turbid liquid sample. To generate a total reflection of the beam, the incident ray needs to enter the sample with an angle larger than the critical angle of total reflection θ_c (see Figure 3.7).

In addition to basic refractometry, the temperature modulated optical refractometry (TMOR) provides more information due to an additional applied temperature undulation. The temperature of the prism is precisely controlled by a Peltier element. Prior to the measurement, a period (in seconds) and an amplitude (in °C) of the undulation are set. The equations given in this sub-chapter to enhance the understanding of TMOR are taken from Müller et al. (2013).

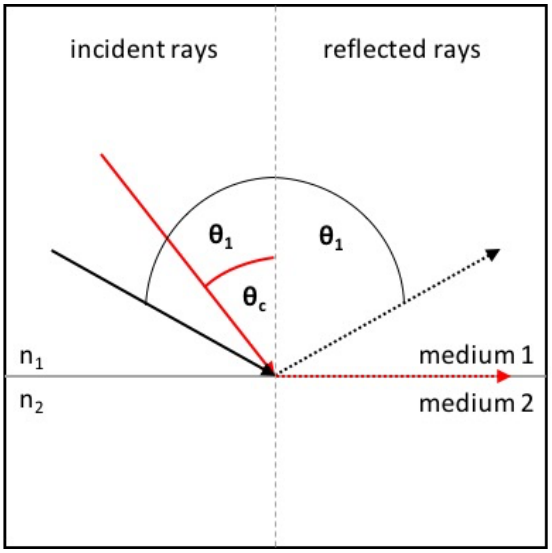

Figure 3.7: Total reflection of a beam: at a critical angle of the incident ray (θ_c) the beam is reflected at the interface between medium 1 and 2 (red arrows), rays with an entrance angle larger than θ_c are completely reflected (θ_1, black arrows).

The basis for TMOR is the correlation between the refractive index *n* and the mass density of a substance ρ. Both are related to the specific refractivity *r*, which is the molar refractivity of a component divided by its density. This is expressed by the Lorentz-Lorenz relation:

$$\frac{\mathbf{n^2-1}}{\mathbf{n^2+2}} = \mathbf{r \cdot \rho} \qquad \textbf{Eq. 3.3}$$

The relationship between the density and the refractive index allows that the refractive index can be used to determine the volume expansion coefficient α. It is calculated from the refractive index *n* and its change over temperature *T* ($\Psi = \frac{dn}{dT}$):

$$\boldsymbol{\alpha} = \frac{\mathbf{-6n}}{\mathbf{(n^2+2)(n^2-1)}} \cdot \boldsymbol{\Psi} \qquad \textbf{Eq. 3.4}$$

To obtain data on phase transitions with only the determination of the refractive index and its dynamic temperature derivative, the linear response theory (LRT) is used. It relates the temperature perturbations to the variations of the refractive index of a sample. The determination of the thermo-optical properties of a sample Ψ_ω^* makes a sinusoidal perturbation of the temperature with a suitable amplitude $A_{T,\omega}$ necessary. The amplitude needs to be small so that LRT can be applied because a linear response is crucial for the modulation (Müller et al. 2013).

Additionally, the phase shift at a given angular frequency Φ_ω and the static equilibrium refractive index n_0 need to be considered for the calculation of the frequency dependent refractive index

$$|\mathbf{n}^*_\omega(\mathbf{t})| = \mathbf{n_0} + |\mathbf{\Psi}^*_\omega| \cdot \mathbf{A_{T,\omega}} \cdot \mathbf{sin}(\boldsymbol{\omega}\mathbf{t} - \mathbf{\Phi}_\omega) \qquad \textbf{Eq. 3.5}$$

The applied sinusoidal temperature modulation results in a delayed but also sinusoidal answer of the refractive index (see Figure 3.8).

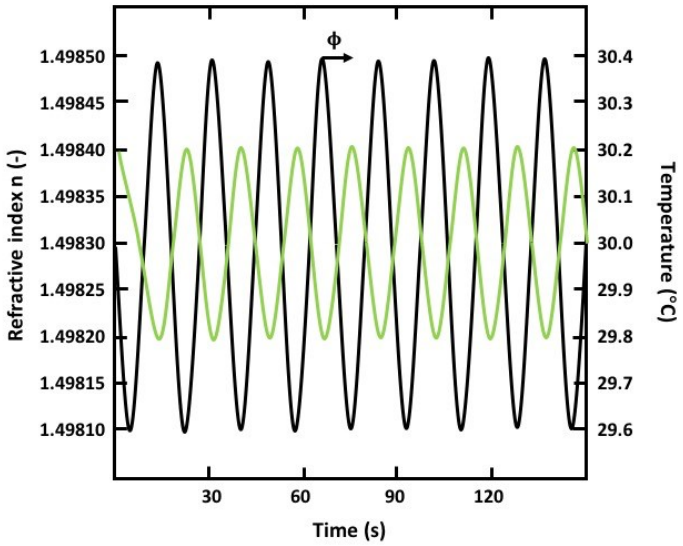

Figure 3.8: Modulation of TMOR: undulated temperature (black solid curve) and the answer of the refractive index (green solid line) delayed by the phase shift ϕ (modified, Müller et al. 2013).

TMOR delivers reliable values for Ψ and n_0 (average refractive index in one modulation period). These are used to calculate the complex volume expansion coefficient α^*_ω with Eq. 3.6, which is based on

$$|\boldsymbol{\alpha}^*_\omega| = \frac{-\mathbf{6n_0}}{(\mathbf{n_0^2}+\mathbf{2})(\mathbf{n_0^2}-\mathbf{1})} \cdot |\mathbf{\Psi}^*_\omega| \qquad \textbf{Eq. 3.6}$$

The phase shift Φ caused by the delayed answer of the refractive index is used to compute the real and imaginary part of the volume expansion coefficient α

$$\boldsymbol{\alpha}' \equiv \mathbf{Re}(\boldsymbol{\alpha}^*_\omega) = |\boldsymbol{\alpha}^*_\omega| \cos(\mathbf{\Phi}_\omega) \qquad \textbf{Eq. 3.7}$$

$$\boldsymbol{\alpha}'' \equiv \mathbf{Im}(\boldsymbol{\alpha}^*_\omega) = |\boldsymbol{\alpha}^*_\omega| \sin(\mathbf{\Phi}_\omega) \qquad \textbf{Eq. 3.8}$$

The computed complex volume expansion coefficient is needed for the calculation of the real *Re (α)* and imaginary *Im (α)* part. The real and imaginary volume expansion coefficient allows to identify transition temperatures such as glass transition or phase transitions such as crystallization or melting. These phase transitions can either be glass transitions or crystallization and melting processes. The melting behavior of a TAG over temperature is schematically represented in Figure 3.9. The mean refractive index decreases with increasing temperature, thus it is higher in the solid state than in the liquid state. The phase transition temperature is indicated by peaks of the imaginary thermal expansion coefficient (*Im (α)*). A peak of the real volume expansion coefficient (*Re (α)*) indicates a real phase transition such as crystallization or melting whereas a step shows a glass transition. In the figure below, the mean refractive index shows a drop and both *Re (α)* and *Im (α)* show peaks at the phase transition temperatures.

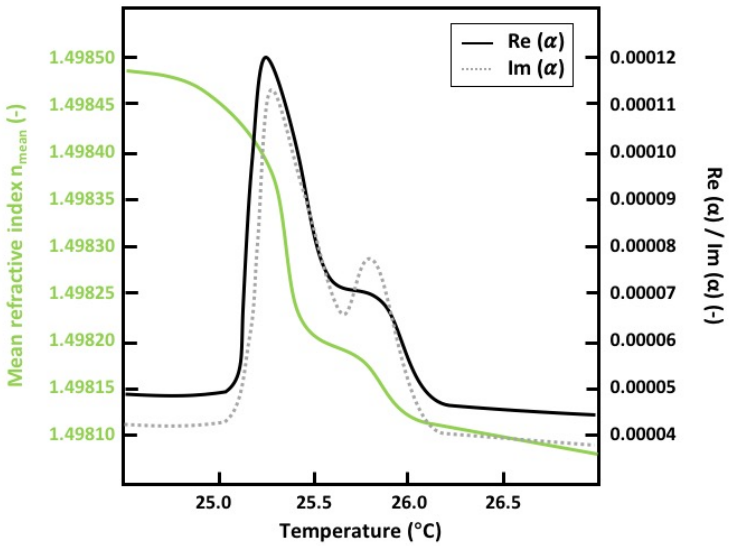

Figure 3.9: Schematic melting process of a TAG determined by TMOR; mean refractive index (n_{mean}) and real (Re (α)) and imaginary (Im (α)) part of the volume expansion coefficient α over temperature.

The thermal volume expansion coefficient can also be determined over time, which makes sense if one temperature is chosen and the undulation is performed around this temperature. This quasi-isothermal measurement allows the determination of e.g. the induction time of a glass transition or a crystallization. A ramp at a certain scan rate is required for a dynamically determined transition temperature. With the dynamic

measurement the melting and crystallization behavior of fats and oils in the allowed temperature range of TMOR could be investigated. Since the investigation of lipid systems by refractometry is not new, the next subchapter shortly summarizes this application area.

3.2.3 Refractometry in Fat Technology

Even more complex than the application of refractometry for single components or TAGs is the investigation of fats and oils. There is not only a two-component but a multi-component system present. The application of refractometry for fats and oils needs to be performed with care. Not only the liquid phase influences the determination of the refractive index for mixtures as occurring during fat crystallization but also the solid one. The group of Kaufmann and Thieme (1954) investigated the crystallization of fats, e.g. cocoa butter and coconut oil, with refractometry. The investigation of the only solid phase was performed by crystallizing the sample on the prism directly from the solution or by melting it on the prism. They found that even though the sensitivity of the determination refractive index is less for solid than for liquid phases, it is still possible. The refraction index increases with increasing fatty acid chain length and increasing amount of double bonds (Kaufmann and Thieme, 1954). In addition, they identified a minimum stabilization time of about 15 min before a stable value of the refractive index was achieved (Kaufmann, Thieme and Wöhlert, 1955).

They also found that the curve of the refractive indices as a function of temperature differed for distinct polymorphic forms of cocoa butter. This leads to the assumption that also the solid phase of a fat mixture takes influence on the refractive index. Furthermore, it seems that less stable solid phases have a higher refractive index compared to more stable ones. This could be due to the fact that less stable crystal modifications have a lower melting point. Hence at the same temperature, they contain a higher liquid fraction compared to a more stable polymorph. Consequently, the refractive index already decreases at a lower temperature. The transformation from one polymorphic form into another is a zero order reaction which means the rate of transition is independent of the previous present amount of polymorph (Kaufmann and Thieme, 1954; Kaufmann, Thieme and Wöhlert, 1955).

Kaufmann and Thieme (1954) also stated that the refractive index of mixtures lies in between the refractive index of the liquid and the one of the solid phase. Thus, this refractive index can be calculated with the mixing rules. In addition they indicate that the refractometer determines a geometric mean of the refractive indices of the liquid and the solid fraction (Kaufmann and Thieme, 1954). This relationship is depicted in Figure 3.10. The measured refractive index can be related to a certain solid fat content (SFC). Moreover, it can be plotted against temperature resulting in a melting curve which is determined by the measurement of the apparent refractive index.

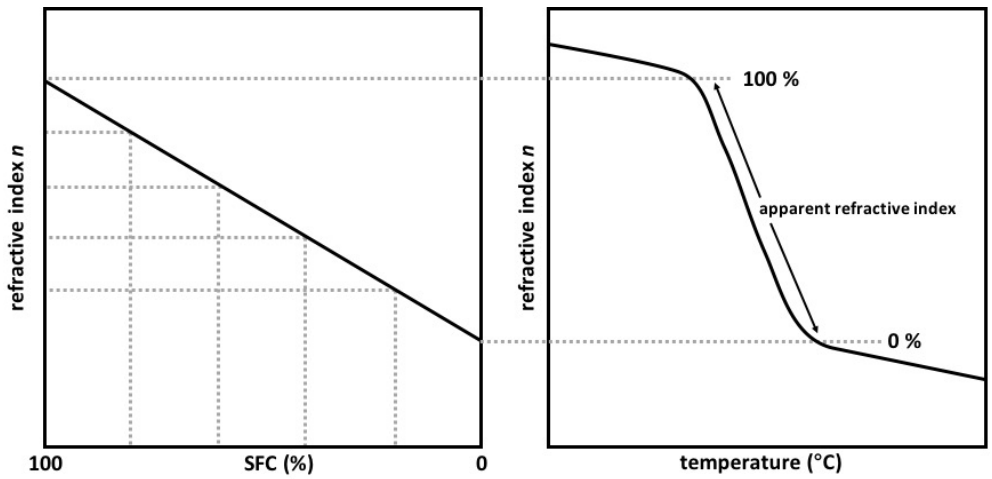

Figure 3.10: Refractive index n plotted schematically against SFC (left) and temperature (right).

The crystals of TAGs, fatty acids, fatty acid alcohols, and hydrocarbon chains show anisotropic behavior, which results in different refractive indices for introduced light with different angles. In contrast, the melted sample shows an isotropic refractive curve, which means that the introduced light is reflected in the same way in all directions (Kaufmann and Thieme, 1954).

In the liquid phase of TAG mixtures they found that the refractive index decreases by 0.00038 per 1 °C. Moreover, the sharpness of the melting interval can be used to identify the present fat (Kaufmann and Thieme, 1954).

3.2.4 Procedures

The refractometer used for the TMOR measurements was an Abbemat 350 displayed in Figure 3.11 (Anton Paar OptoTec GmbH, Seelze-Letter, Germany). It uses the angle of the total reflection at 589 nm to precisely determine the refractive index. The principle of the refractometer is explained shortly. The device uses reflecting light instead of transmitting light. The LED beam hits the sample which is placed on the prism at different angles. At the interface between prism and sample, a part of the beam is reflected and another part is refracted by the sample as explained above (see Figure 3.7). The reflected light is used to determine the critical angle of total reflection and is used to calculate the refractive index of the sample in relation to air (taken from the Abbemat 350/550 manual).

Figure 3.11: Refractometer Abbemat 350 used for temperature modulated optical refractometry.

The applicability of TMOR is the best for transparent soft matter. However, this thesis shows, that also opaque materials like fats and lipid components after crystallization can be analyzed. One needs to be careful because the approach can only be used if the refractive index changes linearly in one period of modulation. For the interpretation of the data, it needs to be considered if phase separation ("fractionation") of the sample took place during the measurement. This could lead to results which are not representative for the complete sample. Therefore, the sample is only analyzed in a volume directly at the prism with the dimensions 1 mm x 1 mm x 1 μm.

Three different procedures were performed to determine phase transitions temperatures, solid fat content, and polymorphic behavior.

For the determination of phase transition temperatures all samples were placed directly on the prism and subsequently heated to 80 °C under the predetermined conditions. Subsequently, after a stabilization time of 10 min the samples were cooled down to 5 °C. All samples were at least performed in duplicate. As the method was never used before for the experimental determination of phase transition temperatures of fats or TAG mixtures, the method was used with three different emphases. First, distinct scan rates (2 °C/min, 5 °C/min, and 10 °C/min) were checked on their applicability. Second, different amplitudes (0.25 °C, 0.5 °C, and 0.75 °C) were under investigation. Finally, distinct periods (30 s, 60 s, and 120 s) were applied.

For the determination of the solid fat content (SFC) the AOCS temperature profile for non-stabilizing fats was applied (AOCS, 2009a). The fat was heated up to 80 °C and kept at this temperature for 10 min. After cooling to 60 °C and a stabilization time of 10 min, the sample was cooled down to 0 °C. This temperature was held for 60 min before the sample was heated to the desired temperature, respectively 10 °C, 15 °C, 20 °C, …, 60 °C. The stabilization time was 30 min during which the undulation was applied with a period of 30 s and an amplitude of 0.5 °C. The temperature profile is depicted in Figure 3.12 (black solid line). The mean refractive index was used to calculate the SFC. Before each measurement, the heating to 80 °C with the following stabilization steps at 60 °C and 0 °C was performed with each sample. To shorten the required time, three different approaches were taken. First, a stepwise heating was applied after 30 min of stabilization at each temperature (see Figure 3.12, grey solid line). Second, the time for stabilization was decreased from 30 min to 5 min (see Figure 3.12, black dashed line). Third, the stepwise concept was done starting at 60 °C for 30 min before the sample was cooled stepwise in 5 °C steps to respectively 55 °C, 50 °C, 45 °C, …, 0 °C (see Figure 3.12, grey dashed curve).

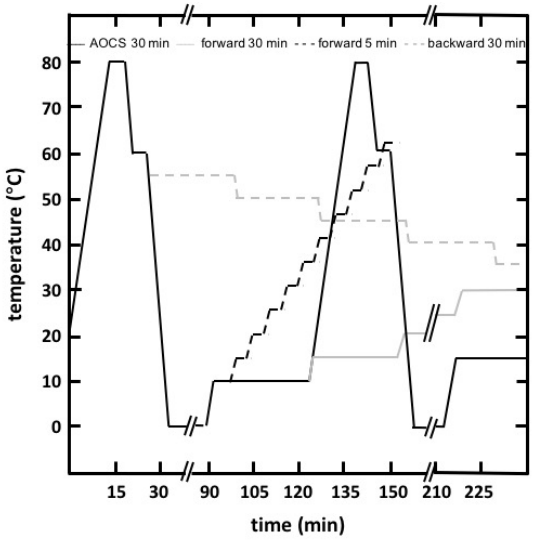

Figure 3.12: Temperature profiles of the SFC determination with TMOR, AOCS method with 30 min stabilization time (black solid line), forward proceeding measurement with 5 min (black dashed line) and 30 min stabilization time (grey solid line), backward proceeding measurement (grey dashed line).

Two methods were almost equally applicable. The AOCS procedure always lead to good results. In addition, the forward-approach with a stabilization time could replace this procedure for reasons of measurement time reduction. Both, the forward-approach with a stabilization time of 5 min and the backward-approach did not lead to satisfactory results. The reasons could be not enough time to yield a stable sample at the measurement temperature in the first case or to lack a driving force for crystallization in the second case.

For the determination of polymorphic transitions the samples were molten on the prism and kept for 10 min at 80 °C. Subsequently, the sample to generate a less stable polymorph was cooled down to 4 °C at a scan rate of 10 °C/min and kept there for 10 min. Next, the sample was heated to 80 °C at 2 °C/min, with the modulation parameters of a period of 30 s and an amplitude of 0.5 °C. The real and imaginary part of the volume expansion coefficient α were then computed. To yield a more stable polymorphic form, the sample was cooled to 45 °C after the stabilization time of 10 min at 80 °C. Afterwards, the sample was kept at this temperature for 60 min before it was heated at the same conditions as described above. The two temperature profiles are given in Figure 3.13.

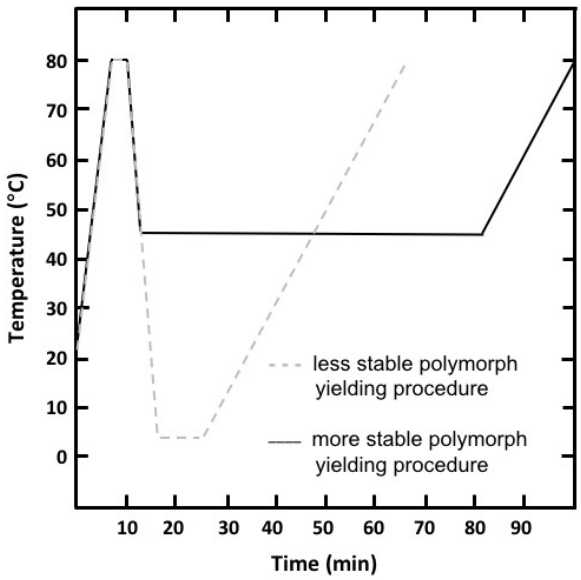

Figure 3.13: Temperature profiles used for TMOR to yield a less stable polymorph (grey dashed line) or a stable polymorph (black solid line).

3.3 Pulsed Nuclear Magnetic Resonance

One of the important techniques for fat technologists is the pulsed nuclear magnetic resonance (pNMR). Its principle is described only briefly below before its application in the field of fat technology is outlined. Furthermore, the followed procedure is explained.

3.3.1 Principle of pNMR

In general, NMR is used to characterize material based on its protons and neutrons. In particular, only the principle of NMR applied in fat technology is outlined due to the fact that a deeper background would be beyond the scope of this thesis.

A sample exposed to a strong magnetic field will experience the orientation of its protons where each hydrogen nucleus acts as a little magnet (Van Putte and Van Den Enden, 1974; van den Enden *et al.*, 1978). The magnetization of the sample is proportional to the number of protons present (Van Putte and Van Den Enden, 1974). After the sample is placed in a static electromagnetic field the nuclei align themselves.

The application of pNMR in the area of fat technology is based on the assumption, that the hydrogen nuclei of fat relax differently in the liquid and the solid state leading

to a different spin-spin relaxation time t_2 (van Boekel, 1981). This t_2 is determined by the receiver coil of the pNMR. Since there exists a difference in t_2 for solids (10 μs) and liquids (10-20 ms), a solid-to-liquid ratio can be determined by pNMR (Van Putte and Van Den Enden, 1974).

The application of a strong radio frequency pulse perpendicular to the existing magnetic field (90°) leads to a change of the orientation of the protons (Petersson, Anjou and Sandström, 1985). If a pulse of a different frequency is applied, the magnetization is disturbed and the reorganization of the molecules in the magnetic field differs for different nuclei (Van Putte and Van Den Enden, 1974).

Subsequently, the removal of the pulse results in the relaxation of the sample, which returns to its equilibrium state. The relaxation time from this disorientation into the former orientation is recorded with the NMR (spin-spin relaxation time). This time differs between protons in solid or liquid phases. The relaxation time in a solid is faster because the protons are packed closer in a dense network and can exchange their energy faster (van den Enden *et al.*, 1978; Petersson, Anjou and Sandström, 1985). In addition, the number of present protons influences the signal at the receiver coil. If the energy fades, the system relaxes and returns to its initial state (Petersson, Anjou and Sandström, 1985).

Peyronel and Marangoni (2014a) describe the background of pNMR in more detail. However, for this thesis only the application in fat technology is relevant, which is outlined in the following sub-chapter.

3.3.2 Application of pNMR in fat technology

The solid fat content (SFC) is an important property if one is concerned with the sensorial behavior of fat containing products, e.g. the quantification of the structuring potential (Augusto *et al.*, 2012). Thus, the knowledge of the solid fat index (SFI) or content (SFC) is crucial for formulations and process control in fat technology (Chapman and Sunlight, 1959; Van Putte and Van Den Enden, 1974; Mills and van de Voort, 1981a; Petersson, Anjou and Sandström, 1985).

Nowadays, the determination of the SFC is mostly performed using pNMR. Before, other methods such as dilatometry, density meters, wide-line NMR or DSC were used (Walker and Bosin, 1971; Mills and van de Voort, 1981b; Petersson, Anjou

and Sandström, 1985). Dilatometry, which is based on the change of the specific volume at different temperatures is only applicable up to 50 % solids. It is an empirical but reproducible method (Mills and van de Voort, 1981a). It is based on the different densities of the solid and liquid phase of fats (Van Putte and Van Den Enden, 1974). Until the 1980s it was the most accepted method to determine the solid-liquid content in fats and oils (Mills and van de Voort, 1981b).

Today, the most often applied method to determine the SFC is pNMR (see Figure 3.14). It can be performed in an indirect and a direct manner. The direct method uses

$$\%\mathbf{solids} = \frac{\mathbf{f \cdot s'}}{\mathbf{f \cdot s' + l}} \cdot \mathbf{100} = \frac{\mathbf{s}}{\mathbf{s + l}} \cdot \mathbf{100} \qquad \textbf{Eq. 3.9}$$

to calculate the amount of solids. Here, s' is the solid signal after ca. 10 µs, f the correction factor for the dead time of the receiver coil, s the "true" solid signal and l the liquid signal after ca. 70 µs.

The indirect method is the more accurate one and uses the equation

$$\%\mathbf{solids\ at\ t°C} = \mathbf{100} - \frac{\mathbf{l_T}}{\mathbf{l_{60}}} \cdot \mathbf{100} \cdot \frac{\mathbf{l_{s,60}}}{\mathbf{l_{s,T}}} \qquad \textbf{Eq. 3.10}$$

Here, l_T represents the liquid signal of the sample at T °C, l_{60} is the liquid signal at 60 °C, $l_{s,T}$ and $l_{s,60}$ are the signals of a reference oil (e.g. soybean oil) at T °C and 60 °C, respectively and $\frac{l_{s,60}}{l_{s,T}}$ as a correction factor (Petersson, Anjou and Sandström, 1985).

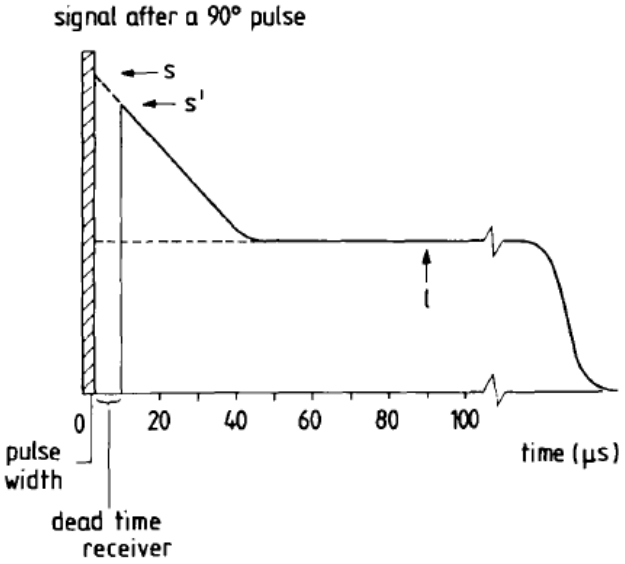

Figure 3.14: Principle of pulsed nuclear magnetic resonance, decay of the signal after a 90° pulse ((van Boekel, 1981).

The direct method determines the signal immediately after the 90° pulse. However, a correction factor *f* is necessary which takes the solid fat protons into account to compensate the signal due to the dead time of the NMR receiver (van Putte and van den Enden, 1973; Mills and van de Voort, 1981a). The *f*-factor depends on the dead time itself as well as the composition of the solid (polymorphic form, type of fat, crystal size) and should therefore be chosen carefully (van Putte and van den Enden, 1973; van den Enden *et al.*, 1978; Petersson, Anjou and Sandström, 1985). A mean factor can only be used if the applied temperature regime is the same and the samples have a similar composition (van Boekel, 1981). A mean *f*-factor of 1.37 is used instead of determining it by the indirect method. This is a mean value for oils and fats. The more accurate way would be to determine the *f*-factor separately for each fat under investigation (Van Putte and Van Den Enden, 1974). The fact that the *f*-factor decreases with increasing solid fat content should be kept in mind (van Putte and van den Enden, 1973).

The indirect pNMR method uses the signal of the liquid phase to determine the SFC (van Boekel, 1981). It is characterized by the signal of the liquid part after 70 μs (number of protons in the liquid) in relation to the signal of the completely melted sample (total number of protons). To ensure good results, the spin-lattice relaxation time t_1 is crucial. Hence, the number and time between pulses need to be chosen carefully. For example, the t_1 for α crystals is shorter compared to β crystals (Van Putte and Van Den Enden, 1974). Therefore, also the polymorphic form and thus for tempering fats the correct sample handling prior to the measurement is crucial because fats high in POP, SOS, POS (2-oleodisaturated TAGs) take a longer time to stabilize (Petersson, Anjou and Sandström, 1985). One needs to mention, that this method neglects that the number of protons in the liquid and solid phase can slightly differ (van Putte and van den Enden, 1973).

The SFC curve generated by the pNMR, whereby the percentage of solids is plotted over temperature, is also called N-line. This curve is used as an important quality parameter for every oil and fat. Typical SFC curves for cocoa butter and palm oil are depicted in Figure 3.15.

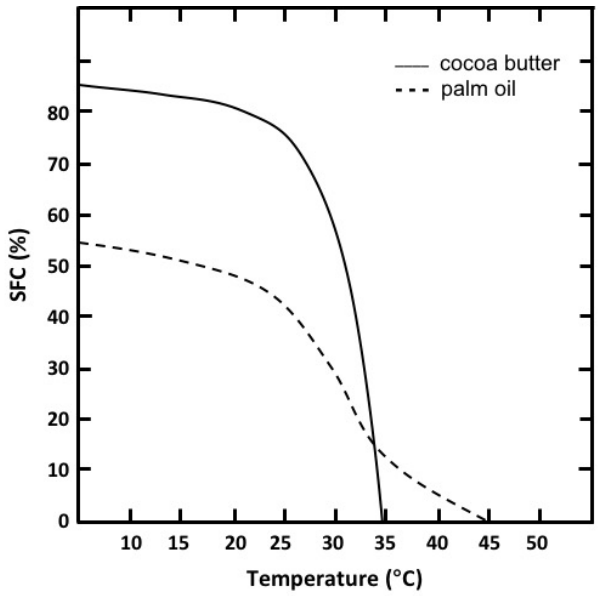

Figure 3.15: SFC lines for cocoa butter (black solid line) and palm oil (black dashed line).

In addition to the mentioned principles, empirical models can be used to describe N-lines. Based on NMR and DSC data from different literature sources, Augusto et al. (2012) used three different models to describe the sigmoidal appearance of a SFC curve. The aim is to model changes in the SFC behavior in a process before trying it. The Gompertz model describes the SFC curve the best compared to the other two models (power decay and logistic) especially at high and low SFC values. The power and the decay model tend to overestimate the SFC values at a low solids content and to underestimate the SFC at a high amount of solids. In addition, polynomial functions do not describe the S-shape of the SFC curve and can only be used in a certain part of the curve to describe it (Augusto *et al.*, 2012). The use of a model can be helpful to describe the SFC of different fats and fat mixtures without the need to determine experimental data over the whole temperature range.

Since the pNMR in fat technology is often used as a benchtop equipment, NMR glass tubes are used as sample holder (AOCS, 2009b). Errors can occur if the crystallization is different over the whole NMR tube, both in height or width of the tube. In addition, the determination of the solid fat content with pNMR via the orientation of the hydrogen nuclei is only an approximation of the SFC which can lead to errors. Also, the usage of the direct or indirect method can result in differences in the SFC value. Thus, the same method needs to be used if values should be compared.

3.3.3 SFC Determination Procedure

As mentioned before, the tempering of fats is crucial for the proper determination of the SFC. Tempering is the systematic heating and cooling of a fat sample to achieve a desired crystal network (Moens *et al.*, 2015). This is important for fats which show a complex polymorphic behavior like cocoa butter (Petersson, Anjou and Sandström, 1985). The same temperature and tempering history leads to better comparability between the two methods of NMR and dilatometry (Madison and Hill, 1978). For fats like cocoa butter, which have an oleic acid at the *sn*-2-position, tempering is even more important to receive comparable SFC results due to their characteristic crystallization properties (Petersson, Anjou and Sandström, 1985). Van Putte and van den Enden (1973) discovered that a tempering step enhances the accuracy of the NMR method and leads to a lower content of solids compared to the in the meantime applied dilatometry. The tempering leads to a smaller number of solids below the tempering temperature (Fulton, Lutton and Wille, 1953; Walker and Bosin, 1971).

The tempering procedure of the direct AOCS method Cd 16b-93 for non-stabilizing fats and oils like margarine was slightly modified and used in this thesis (AOCS, 2009b). It is composed of the following four steps:

1. Melt the sample at 80 °C for 10 min
2. Stabilize the sample at 60 °C for 10 min
3. Keep the sample at 0 °C for 60 min
4. Heat the sample to the desired measurement temperature and keep it there for 30-35 min before the measurement

3.4 Gas Chromatography

The analysis of the fatty acid composition is performed using gas chromatography (GC). The basic principle is outlined before the required preparation procedure for the determination of fatty acids is explained. Subsequently, the applied procedure is elucidated.

3.4.1 Principle of Gas Chromatography

The GC is used to detect volatile components in the mixture. In this study, the different components in a mixture are separated within the GC column due to their distinct molecular weight. The separation efficiency is influenced by the choice of the packing material of the column and the applied flow rates and temperatures. Basically, the equipment is composed of a column in an oven which can be heated at a defined temperature rate and can be kept constant at a desired temperature. The device is completed by a detector. For the detection, the temperature at which the volatile components are evaporated needs to be established. At the end of the column a detector analyzes the volatile substances. A carrier gas, nitrogen in the example shown in Figure 3.16, carries the volatile compounds through the column after the sample injection. The smaller components move faster through the column in comparison to larger and, thus, heavier compounds leading to an earlier detection of the smaller components. The chosen column affects the retention of the components depending on its packing material and their interaction with the sample. In the given case, a flame ionization detector (FID) is used which generates a flame by the combination of air and hydrogen. The volatile substance is ionized in the flame and the released electrons are detected. The detected electrons are converted into a peak which is plotted over time leading to a chromatogram. The retention times can be used after calibration to assign a peak to a component and to compare their concentration in the sample.

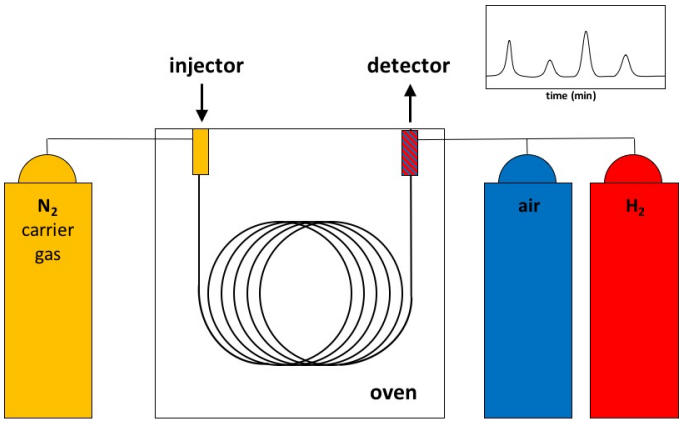

Figure 3.16: Principle of a gas chromatograph with nitrogen (N_2) as carrier gas, an injector on the top left of the column in the oven and air and hydrogen (H_2) to generate the flame for the FID (flame ionization detector) at the top of the oven recording a chromatograph of the fatty acid methyl esters.

The determination of fatty acids is crucial in the fat technology because different fatty acids esterified onto the glycerol backbone lead to different physical and chemical properties. The analysis of fatty acids using gas chromatography require volatile substances. Unfortunately, neither TAGs nor fatty acids are volatile and need to be modified. Thus, the fatty acids are first removed from the glycerol backbone. Subsequently, the fatty acids are methylated to generate the volatile fatty acid methyl esters (FAMEs). For both steps the addition of a methylation agent (e.g. trimethylsulfonium hydroxide) is required (see Figure 3.17). The FAMEs are then injected into the GC for analysis.

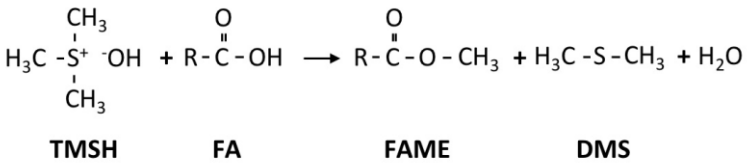

Figure 3.17: Chemical reaction of trimethylsulfonium hydroxide (TMSH) with a fatty acid (FA) with a carboxyl chain residue R leading to a fatty acid methyl ester (FAME), dimethyl sulfide (DMS) and water.

Errors can occur if the methylation of the TAGs has not been conducted completely or if residues of former measurements are still on the column. The latter was tried to be avoided by rinsing the column after every measurement with methyl *tert*-butyl ether (MTBE).

3.4.2 Procedure

The sample of which the composition should be analyzed is dissolved in MTBE. About 10-20 mg were weighed in and 4 ml of MTBE were added. After the sample was dissolved, 100 µl of the sample solution were transferred into a GC vial. 100 µl of internal standard solution (C17:0 in MTBE) were added together with 10 µl of a trimethylsulfonium hydroxide (TMSH) solution (Machery-Nagel GmbH & Co. KG, Düren, Germany). The latter was used to get volatile FAMEs. The internal standard ensures a reliable quantification. The sample was left at room temperature for 2 h to ensure proper methylation.

For the analysis of the FAMEs a gas chromatograph (GC-2010 Plus) equipped with an auto injector (AOC-20i) from Shimadzu was used (Shimadzu Corporation, Tokyo, Japan). The carrier gas was nitrogen (6.8 ml/min), hydrogen and air were used to ignite the flame in a ratio of 1/10 (40 ml/ 400 ml). The GC was equipped with a silica capillary column from Fisher Scientific (Trace™ TR-FAME GC Column, Shimadzu Corporation, Tokyo, Japan) with a diameter of 0.25 mm and a length of 120 m. The stationary phase in the column has a film thickness of 0.25 µm. After injection, the GC oven was kept at 100 °C for 5 min. Subsequently, the oven was heated to 250 °C at a rate of 4 °C/min. The end temperature of 250 °C was kept for 45 min. Each GC run lasted for 85 min and was performed in duplicate. The data processing was done with the software provided by the manufacturer (Lab Solutions, Version 5.85, Shimadzu Corporation, Tokyo, Japan).

3.5 Polarized Light Microscopy

One of the main microscopic methods used for the investigation of fat crystallization is polarized light microscopy (PLM). Its principle and procedure are outlined below.

3.5.1 Principle of PLM

Light microscopy uses transmitting light to display a specimen using different objectives to achieve different magnifications. A special case is the use of polarized light to display only birefringent specimen. Anisotropic materials reflecting a beam of light in two perpendicular directions due to differences in the refractive index depending on the polarization of light, are called birefringent (Wright, Narine and Marangoni, 2000). This birefringence is utilized in the polarized light microscopy (PLM). In Figure 3.18 the principle of the PLM is displayed. The light from the bottom of the microscope is oriented by a polarizing filter so that it can only pass in one direction. On the top of the microscope an analyzer is placed. Both the polarizer and the analyzer are arranged perpendicular to each other (90°) thus no light is coming through. If a birefringent specimen is placed between the condenser (bundling the beam) and the objective (magnification) a bright object appears in the micrograph whereas isotropic materials stay dark.

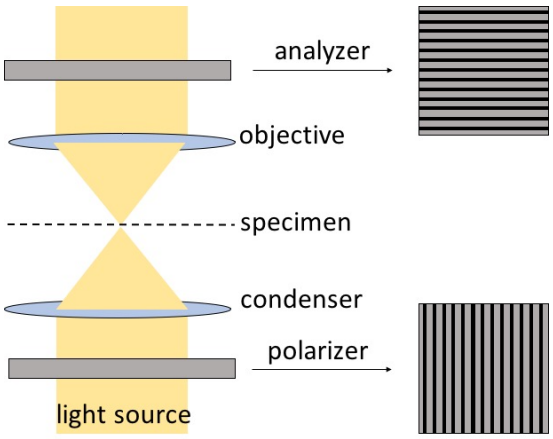

Figure 3.18: Schematic setup of a polarized light microscope with two filters (grey rectangles), a polarizer (at the light source) and an analyzer after the specimen framing two lenses (light blue ovals), the condenser and the objective as well as the specimen.

Errors in the analysis of polarized light micrographs can occur if the polarizer and analyzer are not set properly aligned in a 90° angle to generate the correct optical path. Additionally, the preparation of the sample could always influence the macroscopic appearance. The coverage by the glass slide could have an impact e.g. on the crystallization behavior if the sample is not completely molten before inserting the microscopy slide in the Linkam stage. The used glass slides need to be clean e.g. to avoid any nucleation sites for crystallization.

3.5.2 PLM for the investigation of fat crystals

Since fat crystals show birefringence, their macroscopic appearance can be investigated by polarized light microscopy. The polarized light micrographs were captured at 5x, 10x or 20x magnification using a Zeiss AxioScope (Carl Zeiss Jena GmbH, Jena, Germany) equipped with a camera (AxioCam ICm1, Carl Zeiss Jena GmbH, Jena, Germany). The image analysis was done with the ZEN Software provided by the manufacturer (Carl Zeiss Jena GmbH, Jena, Germany). If an exact temperature or a temperature profile was required a temperature-controlled stage from Linkam Scientific Instruments (Surrey, UK) was used. Depending on the desired experiments, heating and cooling scan rates of 2 °C/min, 5 °C/min or 10 °C/min were applied. The respective temperature profiles are given in the corresponding chapters.

3.6 Powder X-Ray Diffraction

The correct determination of the polymorphic form of the solid phase is crucial for many food products like chocolate or margarine. Hence, powder X-ray diffraction (XRD) is an important method in this area. Subsequently, its basic principle is explained and adopted to the field of fat technology.

3.6.1 Principle of XRD

This method uses an X-ray beam to investigate the internal structure of a material by scattering the impinging beam. X-rays have a short wavelength and thus a high energy level (~120 eV to ~120 keV). Therefore, they can penetrate the matter under investigation (Peyronel and Marangoni, 2014b).

A requirement to generate peaks in X-ray diffraction patterns is that the sent X-ray and the scattered beam are in-phase. Hence, Braggs law, given in equation Eq. 3.11, can be used to determine a typical XRD pattern where the intensity is plotted against the diffracted angle (usually 2θ).

$$\boldsymbol{\lambda = 2 \cdot d_{hkl} \cdot \sin(\theta)} \qquad \textbf{Eq. 3.11}$$

The spacing in between two lamellar planes is indicated by d_{hkl}, where the indices *hkl* are referred to a family of atomic planes based on the Miller indices which are given to explain the orientation of the atomic planes (Peyronel and Marangoni, 2014b).

A typical setup of a diffractometer is shown in Figure 3.19. The X-ray tube and the detector always move at the same time to keep the ratio of θ/2θ. In this study, they move up to 25° 2θ to allow X-rays from all desired angles to hit the sample (2θ = angle of diffracted beam). Normally, the specimen is hold on a temperature controlled sample holder.

A systematic error can occur if the sample mold is continuously over or under filled because the device takes the proper flat filling level of the cavity as the zero position for the procedure. In addition, during data processing errors can occur if the baseline and the peak fits are not set properly or equally.

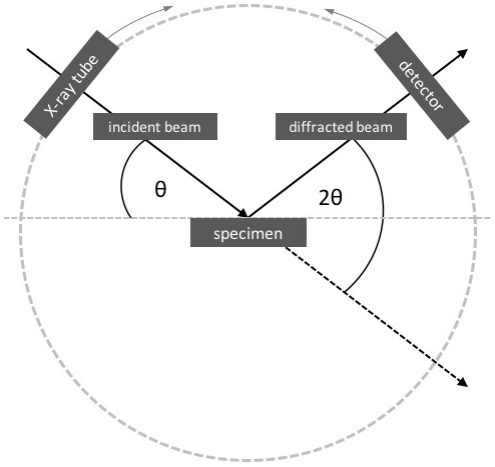

Figure 3.19: Setup of a X-ray diffractometer (modified, Peyronel & Marangoni 2014).

3.6.2 Application of XRD in Fat Technology

XRD is one of the main methods to study fat polymorphism. There are two main sections which are mainly investigated in fat technology: the long spacing (1-15° 2θ) and the short spacing (16-25° 2θ), where 2θ represents the angle of the diffracted beam. The long spacing is also known as the small angle X-ray scattering (SAXS) region and the short spacing as the wide angle X-ray scattering (WAXS) region. The extension of the SAXS region angle depends on the chain length of the fatty acids because it corresponds to the planes formed by the methyl end groups. In contrast, the short spacing is independent of the chain length of the fatty acids and corresponds to the cross sectional packing (D'Souza, DeMan and DeMan, 1990; Peyronel and Marangoni, 2014b).

The cross sectional packing correlates with the polymorphic form. The main forms in fat technology are the so-called α, β´, and β polymorphs. The α form corresponds to a hexagonal cross sectional packing while the β´ aligns in an orthorhombic manner. The β polymorph is characterized by a triclinic structure (Sato and Ueno, 2005). The determination of the polymorphic form is crucial due to their different structure and thus distinctive melting points. More detailed information is given in the fundamentals section (chapter 2.2.3). The specific procedures applied in this thesis are explained in the following sub-chapter.

3.6.3 Procedure

For the determination, a Multiflex powder X-ray diffractometer (RigakuMSC Inc., Toronto, Canada) was used. Approximately 150 µl were placed on the sample holder and analyzed at the corresponding temperature. The copper X-ray tube (λ=1.54Å, Cu/Kα1) was operated at 40 kV and 44 mA together with a 0.5° diversion slit and scatter slit. In addition, a 0.3 mm receiving slit was used. The analysis was performed moving the X-ray tube and the detector from 1.0-3.0° 2θ and from 17.0-25.0° 2θ to cover the relevant ranges in the wide and small angle region at a scan speed of 1°/min with a step size of 0.02°. The XRD patterns were analyzed using the Jade 9.0.1 XRD software (Rigaku MSC Inc., Toronto, Canada). Two different procedures were performed to identify different polymorphic forms of fully hydrogenated palm oil namely α, β´, and β. To generate the less stable polymorphic form, the sample was placed onto the slide in the liquid state and transferred directly into the fridge at 4 °C where it was kept for 10 min. The sample holder in the X-ray diffractometer was cooled to 4 °C by a water bath to keep the same temperature during the examination. The more stable polymorph was generated by keeping the sample for 60 min at 45 °C. The sample holder was set at 45 °C during the measurement.

4 ON THE FEASIBILITY OF CONTINUOUS EMULSION FRACTIONATION

Michaela Häupler*, Miro Kirimlidou, Wiebke Wilms-Schulze Kump, Alessandra Parisi, Leonie Wagner, Eckhard Flöter

TU Berlin, Department of Food Process Engineering, Seestrasse 13, 13353 Berlin, Germany

Submitted to the European Journal of Lipid Science and Technology (2018).

The following chapter is a submitted manuscript.

Abstract

In this study, the feasibility of a continuous emulsion fractionation process was evaluated. The conceptual design of the process entails that a cold-water stream is emulsified into a hot oil stream such that a Pickering emulsion emerges. The water droplets serve as entrainer which is removed conjointly with the attached fat crystals continuously in a decanter centrifuge.

Results on the kinetics of crystallization give guidance for the process design in the future. The sedimentation experiments in the benchtop centrifuge showed on the one hand that the prepared emulsions were often insufficiently stabilized to withstand the centrifugal forces (3,000 g). On the other hand, flocculation occurred as a problem since the highly porous sediments cause prohibitively low separation efficiencies. The results for the decanter centrifuge lead to the conclusion that an accumulation of hardstock at the solid discharge took place because a significantly increased levels of water droplets in the solid discharge were accompanied by decreased levels of hardstock in the lipid phase.

The findings show the difficulty to identify the correct process window for this new process and indicate further research needs. Even though general feasibility was illustrated by the data obtained currently achievable separation efficiencies are unacceptably low.

Key words: *Emulsion fractionation, Pickering emulsion, centrifugation, emulsion stabilization, palm oil fractionation*

Practical applications

A new continuous emulsion fractionation process is developed as an alternative for the typical palm oil fractionation process. the designed process aims at a more specific fractionation of tripalmitate, higher separation efficiencies as well as a more energy efficient operation.

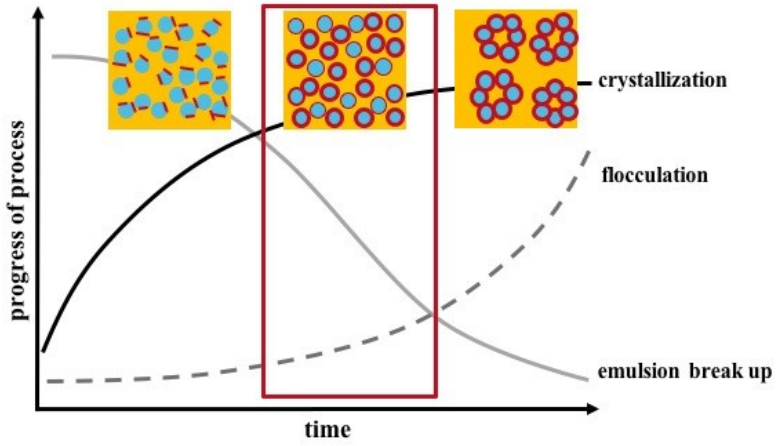

Figure 4.1: Graphical abstract of the process window for the continuous emulsion fractionation process.

4.1 Introduction

The production of functional fat phases necessitates the application of oil modification techniques. The process to eliminate partially hydrogenated fats started in the second half of the nineties of the previous century due to concerns about the health risk associated with the consumption of *trans*-fatty acids. Since then the consumer awareness with respect to chemical modification of food materials has significantly grown. Even though chemical interesterification has widely been substituted by enzyme catalyzed reactions, processes which leave the molecular structure of raw materials unchanged appear to be most desirable considering consumer acceptance. Fractionation which is widely applied to palm oil is such a process. During fractionation a fat composition is divided into fractions, high melting stearin and low melting olein, by solely physical processes. Typically fractional crystallization in combination with a separation, often in a membrane filter press, is performed to separate the solid high melting triacylglyceride (TAG) fraction from the low melting one (Deffense, Tirtiaux and Charleroi, 1985; Kellens *et al.*, 2007; Bot and Flöter, 2013; Kellens and Calliauw, 2013). Palm oil can be separated into different fractions with varying purposes like olein (frying or salad oil), stearin (margarine, shortening), or palm mid fraction (cocoa butter equivalent, coating) on repeated application of the process (Timms, 1997; Kellens *et al.*, 2007).

However, fat fractionation processes are performed batch wise or semi-continuously. Hence, a continuous process would be a desirable alternative (Kellens and Calliauw, 2013). Shorter process times omitting the slow crystallization process and improved separation efficiencies would be meaningful targets. The separation efficiency is in essence the content of solid material in the high melting fraction. In other words, it expresses how much liquid low melting fraction is included in the filter cake. In dry fractionation achievable separation efficiencies are usually limited to levels below 60 %. This value can be improved by dilution of the system with organic solvents, wet fractionation. A raft of disadvantages, however, accompanies the wet fractionation process. Higher energy consumption, larger volumes to process, and increased safety precautions render wet fractionation only suitable for high value fractions, such as in the production of cocoa butter equivalents (CBE). The suggested emulsion fractionation process possibly offers a solution since a direct fractionation of high melting TAGs could be possible in a continuous way. The basic idea is that cold water droplets are injected into a hot oil stream, which contains high and low melting TAG fractions to be separated. If process conditions are set accordingly the high melting TAGs crystallize around the water droplets forming a Pickering emulsion (Pickering, 1907; Flöter, 2009) in analogy to the margarine manufacturing process. The process design entangles that this possibly transient emulsion is subsequently separated from the liquid low melting fraction in a decanter centrifuge. The separation in a centrifugal field is promoted by the fact that the water droplets function as entrainer. The process steps are illustrated in Figure 4.2.

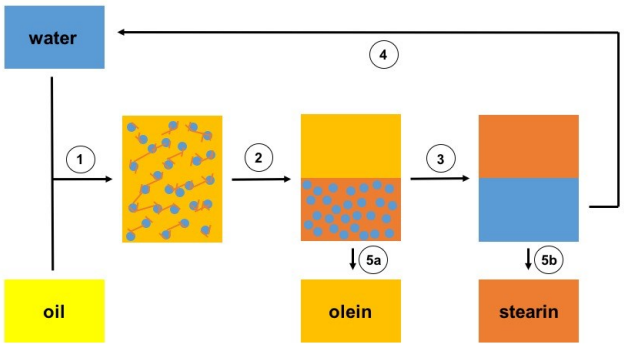

Figure 4.2 Principle of emulsion fractionation process, crystallization of high melting TAGs at water droplet surface (1), separation of water droplets and liquid oil (2), heating and separation of high melting fraction and water (3), recirculation of water (4), resulting products olein (5a) and stearin (5b).

Obviously, the process has some resemblance to the Lonza process. But in the case considered here the two crucial elements of the process, crystallization and separation have also to be considered with respect to their kinetics. Taking a closer look at the different processes occurring either simultaneously or sequential it becomes apparent that the identification of a viable process window is far from easy. Figure 4.3 schematically depicts the process window looked for. The crystallization at the water droplet surface has to progress to the level that the target TAG's are crystallized up to equilibrium level to deliver a high relative yield. Secondly, the solid material needs to be able to stabilize the interface. These processes, crystallization and surface coverage depend on among others thermal energy balances, heat and mass transfer and the cumulative droplet surface area. The separation in a decanter centrifuge allows for several process parameters to be set. These are primarily the actual centrifugal force by means of rotational speed of the bowl, the differential speed between bowl and screw, and the residence time. Inside the decanter the emulsion should neither break, loss of entrainment, nor flocculate because this will negatively affect the density differences and separation efficiency. Density difference being an obvious must (Gleiss and Nirschl, 2015) for successful process implementation. It is envisaged that deformation of fat covered droplets at the inner surface of the bowl is beneficial for the separation efficiency because the porosity of the droplet packing would be reduced.

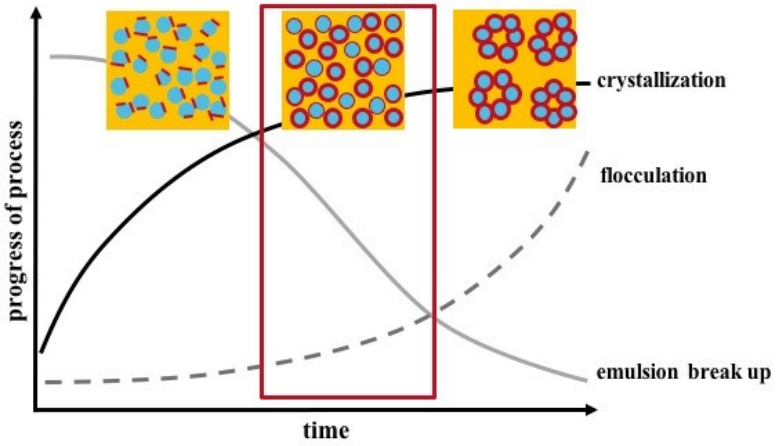

Figure 4.3: Schematic position of the process window for emulsion fractionation, progress of processes over time leading to crystallization (black solid line), emulsion break up – subject to centrifugal force (grey solid line), and flocculation (grey dashed line).

Additional means to manipulate the boundaries of the process window are, a priori not desired though, the addition of other components. For example, could surfactants serve as templates to speed up crystallization and lead to the desired TAGs accumulating at the water/oil interface (Awad and Sato, 2001, 2002; Awad, Hamada and Sato, 2001). To increase density differences between droplets and oil phase materials such as salts or sugars could be dissolved in the aqueous phase.

To this end the study presented here documents the initial experiments to evaluate the feasibility of the continuous emulsion fractionation process.

4.2 Materials and Methods

A commercially available stored Pickering emulsion was used as a model system to investigate the process. This emulsion was expected to be the most difficult to separate. Pronounced flocculation including a space-filling network is indicated by the fact that 20 % of dispersed phase combined with less than 2 % crystalline fat material result in a homogeneous, non-sedimenting thin paste. This 20 % water and 80 % oil/fat mixture contained additionally a small amount of emulsifier (lecithins).

A so-called freshly prepared Pickering emulsion was prepared containing 20 % distilled water and 80 % oil/fat. The oil mixture was composed of 95 % rapeseed oil, 0.5 % distilled monoglycerides, and 4.5 % fully hydrogenated palm oil. Both oils were provided by ADM (Hamburg, Germany). The oil mixture was heated to 80 °C and kept at this temperature while stirring for at least 30 min to remove all crystal memory. Subsequently, the oil mixture was poured into a cylinder and distilled water (80 °C) was added. The emulsion was prepared using a disperser (T25 Ultra-Turrax®, IKA® Werke GmbH & Co. KG, Staufen, Germany) for 1 min at 8.000 rpm and for 1 min at 24.000 rpm. To initiate crystallization, the emulsion was put in an ice bath and sheared with the disperser for 5 min at 8.000 rpm.

The so-called dynamic Pickering emulsion was not prepared batch wise but continuously by mixing cold water (1°C) and a mixture of rapeseed oil and fully hydrogenated palm oil (60 °C) in a T-piece in a ratio of 20 % water and 80 % oil mixture. The oil mixtures contained 90 to 95 % rapeseed oil, 9.0 to 4.5 % fully hydrogenated palm oil, and between 1.0 and 0.5 % distilled monoglycerides (Dimodan®

HR-Kosher, DuPont Nutrition Biosciences ApS, Braband, Denmark) to serve as a template for the crystallization of fully hydrogenated palm oil at the water droplet surface. This static mixing set up resulted into the formation of a Pickering emulsion.

The samples were poured into centrifuge tubes directly after preparation and centrifuged at 4,500 rpm (~3,000 g) in a lab scale centrifuge (Sigma 2-15, Sigma Laborzentrifugen GmbH, Osterode, Germany) for 60 min, taking a photograph every 10 min. For the dynamic emulsions only one photograph after 10 min was taken since the emulsion was not stable.

The Pickering emulsions were also separated continuously in a lab scale decanter centrifuge (MD 80, Lemitec, Berlin, Germany) at different accelerations and differential speeds.

The crystallization and melting behavior of materials and fractions was investigated by differential scanning calorimetry (DSC) using a device from Netzsch (DSC 204 F1 Phoenix, NETZSCH-Geraetebau GmbH, Selb, Germany). Samples were heated to 80°C and the temperature was kept for 10 min to erase the crystal memory. Subsequently, the samples were cooled down to -50 °C at 10 °C/min. The samples were kept at -50 °C for 10 min prior to heating to 80 °C at 10 °C/min. About 10 mg of each sample was weighed into aluminum pans. An empty aluminum pan served as reference. The peak analysis was done with the software provided by the DSC manufacturer (NETZSCH Proteus – Thermal Analysis software version 6.1.0).

The microscopy was performed using a polarized light microscope from Zeiss (AxioScope A.1, Carl Zeiss Jena GmbH, Jena, Germany) equipped with a digital camera (AxioCam ICm1, Carl Zeiss Jena GmbH, Jena, Germany). Either a 10x or a 20x magnification was used and the micrographs were recorded at room temperature. The ZEN Software provided by the manufacturer was applied to do the image analysis (Carl Zeiss Jena GmbH, Jena, Germany).

The samples were analyzed by gas chromatograph (GC) to determine the fatty acid composition of the obtained fractions. In detail, 10-20 mg were dissolved in 4 ml of MTBE. 100 µl of sample solution and 100 µl of internal standard solution (C17:0 in MTBE) were added together with 10 µl of a trimethylsulfonium hydroxide (TMSH) solution (Machery-Nagel GmbH & Co. KG, Düren, Germany). The sample was left at room temperature for 2 h to ensure proper methylation. The FAME analysis was done

with a gas chromatograph (GC-2010 Plus, Shimadzu Corporation, Tokyo, Japan). A silica capillary column (Trace™ TR-FAME GC Column, Shimadzu Corporation, Tokyo, Japan, 120 m x 0.25 mm x 0.25 μm) was used with nitrogen as the carrier gas (6.8 ml/min) for the analysis. The sample was heated from 100 °C to 250 °C at a rate of 4 °C/min. Data analysis was done with the software provided by the manufacturer (Lab Solutions, Version 5.85, Shimadzu Corporation, Tokyo, Japan).

4.3 Results & Discussion

4.3.1 Preliminary study on surface crystallization

Inherently the process design described above necessitates that the dispersion of a cold aqueous phase in the hot oil stream induces crystallization at the droplet surface. This could in general be achieved in two manners. In one embodiment the mixing of the two streams results in a temperature low enough to create the desired amount of solids at thermal equilibrium conditions. To achieve this the fraction of the aqueous stream and its cooling capacity need to be large enough and the mixing time sufficiently long to allow for elimination of temperature gradients. Additionally nucleation of crystals at the surface and mass transfer to the growing crystals has to occur in the same timeframe. This results in a stable Pickering emulsion. Alternatively, the situation of a crystalline shell surrounding the water droplets could be transient. This means that even though the heat balance of the mixed two streams does not result in temperatures low enough for crystallization, initial crystallization takes place at the cold droplet surface prior to the system assuming thermal equilibrium. Obviously, the latter process has the advantage to be more energy efficient. However, to identify the desired transient state with sufficient solid material deposited before the interphase region is heated up is difficult and might prove even impossible.

Some observations of the study on the crystallization of a hardstock (fully hydrogenated palm oil) out of a warm oil mixture (50 % w/w rapeseed oil, 50 % hardstock) onto the surface of a cold water droplet are shown in Figure 4.4. The selection of a sequence of high speed camera images reveals that from the moment the water droplet (4°C) touches the oil surface it takes approximately 1 s to initiate significant crystallization. After additional 0.7 s the surface of the droplet (ca. 1 mm

diameter) is completely covered with crystals. The crystalline shell stays intact for at least the next 5 s.

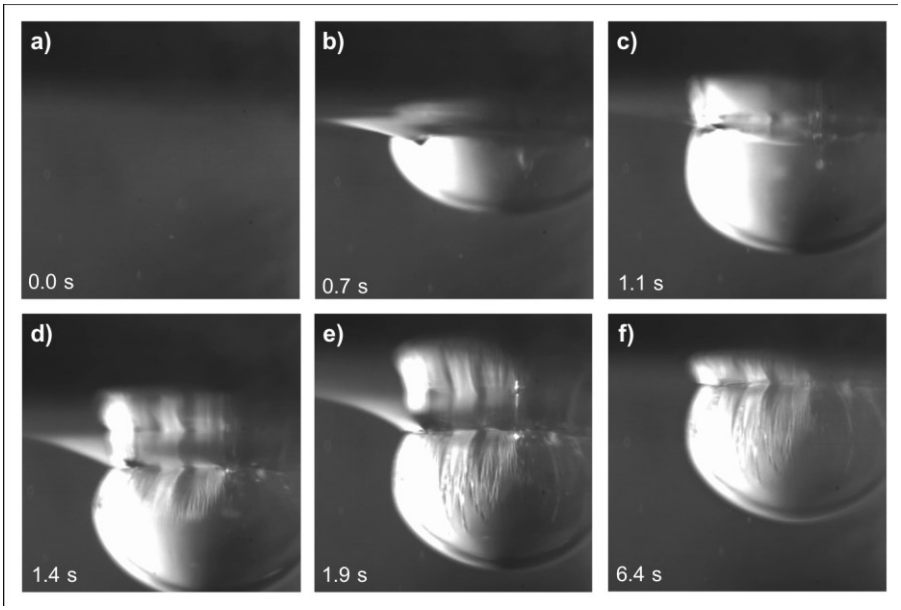

Figure 4.4: High speed camera images of a cold water droplet (4 °C) injected into a warm oil mixture (60 °C, 50 % rapeseed oil, 50 % fully hydrogenated palm oil)

In the interpretation of the different results of cold, dripping droplets it has to be taken into account that a dramatic excess of hot oil (60 °C) is present and no agitation takes place. These results indicate that the crystallization at the surface is possible for even very asymmetric settings. Furthermore, it was found that the appearance of the crystal shell is actually rather quick compared to its melt off. The initial results on the kinetics of crystallization and melting show that even a transient crystalline state could allow to separate the water droplets surrounded by fat crystals from the liquid warm oil before thermal equilibrium is reached.

For further evaluation, a dynamic Pickering emulsion was prepared with an oil temperature of 75 °C to ensure that the hardstock (fully hydrogenated palm oil) was completely molten. Hardstock levels of 10 % and 20 % (w/w) were studied to evaluate effects of concentration and supersaturation. The ratio of water to oil stream was set at 40 to 60 throughout the experiments. The target temperature was set below 35 °C since the crystallization of the fully hydrogenated palm oil in the oil mixture was observed at 35 °C.

Assuming the system adiabatic, which in the current setup is certainly not the case, one can calculate the resulting average temperatures based on the heat capacities of water ($c_{p,H2O}$ = 4.18 kJ/kgK) and oil ($c_{p,oil}$ = 1.67 kJ/kgK), and the temperatures of the both streams. Based on Equation 1 the reference curve (grey circles) in Figure 4.5 is derived.

$$T_{end} = \frac{Q_{H_2O,in} + Q_{oil,in}}{c_{p,H_2O} \cdot m_{H_2O} + c_{p,oil} \cdot m_{oil}} \qquad \textbf{Eq. 12}$$

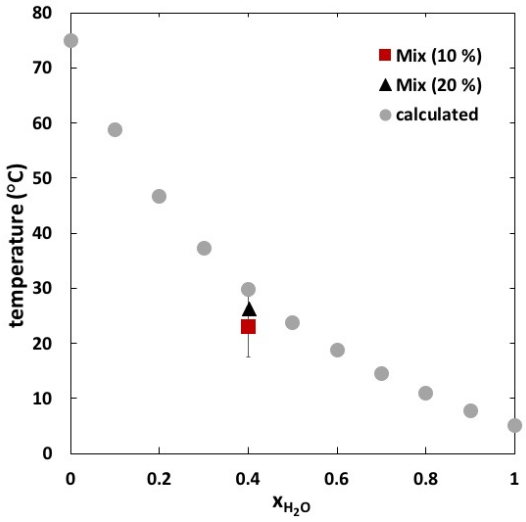

Figure 4.5: Predicted oil temperature depending on the amount of water (5°C) injected into oil (75 °C), experimental data from an oil mixture containing 10 % hardstock (red square) and 20 % hardstock (black triangle).

Figure 4.5 reveals that the experimental emulsion temperatures were lower than those calculated by simple energy balances. Additionally it was found that higher levels of dissolved hardstock and hence higher levels of crystalline material result in higher final temperatures. This is not surprising. In the first place, the system is not adiabatic and the heat flux to the environment reduces the emulsion temperature. Secondly, the temperature increase on higher solid levels corresponds well with back of the envelop calculations that crystallization of 10 % material causes a temperature increase of almost 5 °C.

4.3.2 Emulsion Stability and Flocculation

The high speed camera pictures revealed that the surface coverage by crystals was achieved. Next to this, the emulsion stability is important to allow for separation according to the suggested process. The emulsion stability depends on parameters like the droplet size, the coverage of the surface by Pickering particles, amount and conformation of fat crystals, the applied g-force, and the residence time in the centrifugal field. Therefore, the stability of three different Pickering emulsions against centrifugal force was examined.

4.3.2.1 Centrifuge separation

Dynamic Pickering Emulsion

For the dynamically prepared emulsions three different volume flows (100 – 250 ml/min) were tested to vary the mixing process time. The temperature settings were chosen such that the crystalline material remained present throughout the experiment. However, all samples resulted in a complete emulsion break up on centrifugation at 3,000 g for up to 10 min. Hence, no water droplets surrounded by fat crystals remained intact and the emulsions separated into a continuous aqueous phase topped by a lipid phase. One reason might be that the droplets generated by the T-piece were not small enough and hence mechanically stable enough to withstand the compression in the centrifuge.

Freshly prepared Pickering Emulsion

The micrograph, recorded with a polarized light microscope, of the freshly prepared Pickering emulsion is shown in Figure 4.6. The white areas in the image represent crystalline material which is located mainly at the surface of water droplets. These have a mean size of 7.36 ± 2.07 μm. The micrograph shows that the Pickering stabilization was established. Figure 4.7 depicts the fresh Pickering emulsion after centrifugation intervals of 10 min. After 30 min, the maximum separation seemed to be achieved as further centrifugation does not lead to the release of more free oil. It has to be noted that after 20 min a small amount of water appeared at the bottom of the centrifuge tube. This sediment does not increase over time indicating possibly an

original fraction of the emulsion not well stabilized. Overall, the emulsion was considered stable.

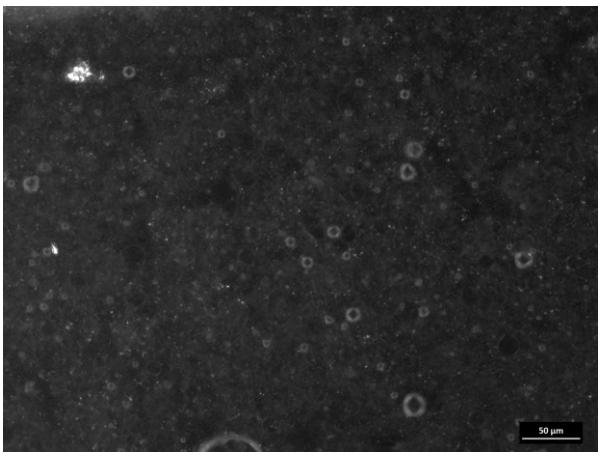

Figure 4.6: Polarized light micrograph of the fresh Pickering emulsion. Scale bar represents 50 µm.

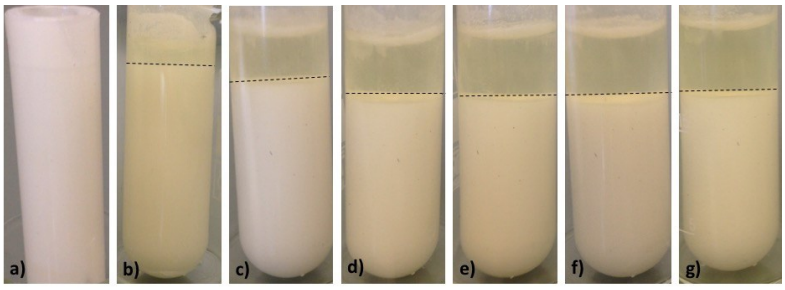

Figure 4.7: Freshly prepared Pickering emulsion centrifuged for a) 0 min, b) 10 min, c) 20 min, d) 30 min, e) 40 min, f) 50 min, g) 60 min.

The DSC thermograms of the freshly prepared Pickering emulsion before and after centrifugation are shown in Figure 4.8. The large melting peak at 0 °C in Figure 4.8a is associated with water. The melting peaks at -20 °C and 40 °C, see also insert, can be assigned to rapeseed oil and fully hydrogenated palm oil, respectively. The top layer, characterized in Figure 4.8b, had neither a melting peak of fully hydrogenated palm oil (see insert) nor of water. Not surprisingly, this indicates a clear oil phase well separated from the water/crystal slurry. The bottom layer showed quite the same melting behavior as the feed (see Figure 4.8c). A clear peak of fully hydrogenated palm oil can be identified in the insert of this figure which also seems slightly higher in comparison to the feed. This would lead to the conclusion that fully hydrogenated palm oil was

accumulated in the bottom layer after centrifugation. However, the observations showed that only a limited compaction of the emulsion was achieved during centrifugation. This manifests itself by the limited amount of supernatant, indicating a high degree of flocculation. Such a highly porous sediment needs to be avoided in fractionation processes to achieve acceptable separation efficiencies.

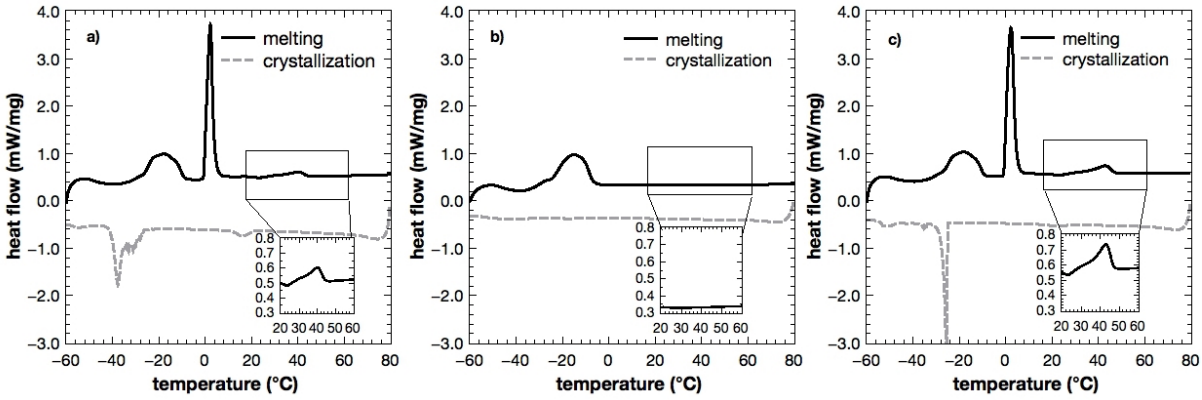

Figure 4.8: Freshly prepared Pickering emulsion with 20 % water and 80 % oil mixture, before (a) and after centrifugation (top layer (b) and bottom layer (c)).

Table 4.1 gives fatty acid concentrations of the phases during processing the freshly prepared Pickering emulsion. The GC analysis shows differences between the different phases. Looking at the data of the supernatant, the upper phase, simple mass balances reveal that approximately 1.5 to 2.0 % of the hardstock was dissolved in the oil. Based on that, the level of solid fat in the different phases was deduced. This yields 2.5 and 3.5 % of solid fat in the starting emulsion and the slurry, respectively. The ratio of these values corresponds very well with the compaction of the emulsion phase shown in Figure 6. Here it was assumed that the crystallized TAGs had a fatty acid composition of 1 to 1 stearic to palmitic acid. However, the solid levels are small and a large portion of the high melting TAG's remains dissolved rendering the process neither delivering a reasonable yield nor an acceptable separation efficiency.

Table 4.1: Fatty acid composition of freshly prepared Pickering emulsion before and after 60 min of centrifugation determined by gas chromatography.

fatty acid	emulsion (%)	upper part (%)	lower part (%)
C 16:0	6.5 ± 0.1	5.3 ± 0.5	7.6 ± 0.1
C 18:0	4.9 ± 0.1	3.2 ± 0.5	6.6 ± 0.1
C 18:1 *cis*	54.6 ± 0.1	54.4 ± 0.4	50.3 ± 0.6
C 18:2 *cis*	18.1 ± 0.1	18.4 ± 0.3	16.7 ± 0.2
C 18:3 alpha	7.2 ± 0.1	7.1 ± 0.1	6.5 ± 0.1

Stored Pickering Emulsion

Analogue to the freshly prepared emulsion the stored Pickering emulsion was centrifuged for 60 min. Photos taken every 10 min during centrifugation are shown in Figure 4.9. For clarity reasons the supernatant is indicated by a dotted line. The volume of supernatant grows from approximately 2.5 % after 30 min to 5 %, 7.5 %, and 15 % after 60 min. The observation is hence very similar to the one made for the freshly prepared emulsions. The images however indicate that the stored emulsion had an even stronger tendency to flocculate and develop a porous sediment phase detrimental to acceptable separation efficiencies.

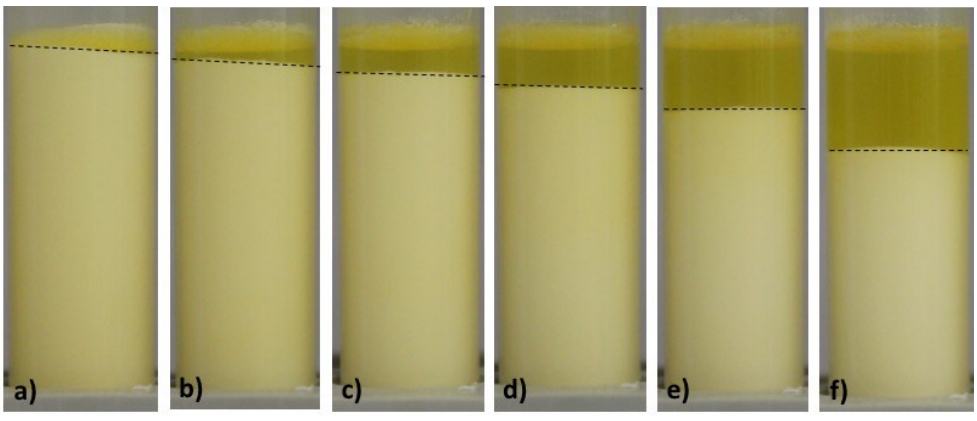

Figure 4.9: Stored stabilized Pickering Emulsion centrifuged at 3,000 g for a) 10 min, b) 20 min, c) 30 min, d) 40 min, e) 50 min, f) 60 min.

In Figure 4.10 the DSC thermograms of the phases from processing the stored Pickering emulsion are shown. For the interpretation of the data it is important to recognize that the hardstock used for this emulsion is fully hydrogenated high erucic rapeseed oil. The TAG's related to this hardstock have a different fatty acid composition (C22:0 and C18:0 at approximately 1 to 1 ratio) resulting in even lower solubility. All melting thermograms show the overlapping peaks between -20 °C and 0 °C. The inserts in Figure 4.10a, b, c reveal that in all phases the high melting TAG's of the hardstock had been crystallized at the low stabilization temperature, -50 °C. The data further reveal that there has been a clear concentration effect of these TAG's in the sediment phase (stearin). This was confirmed by the fatty acid analysis and the thermograms.

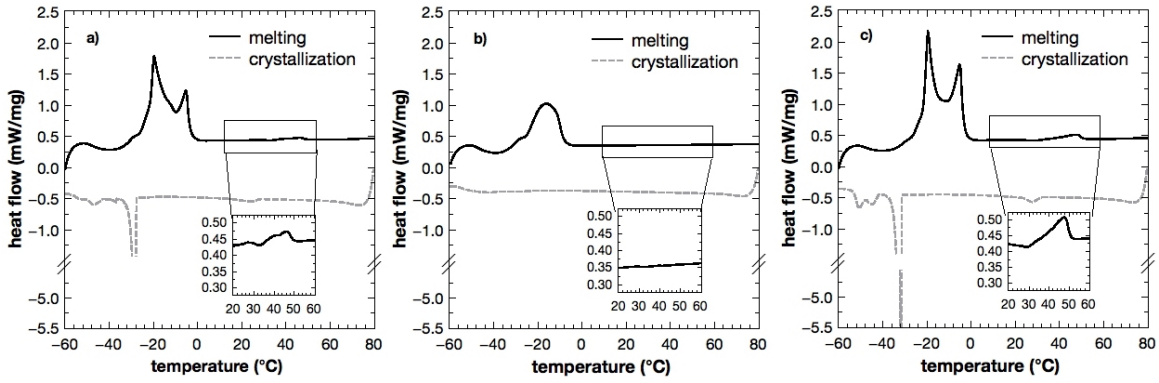

Figure 4.10: DSC thermograms of the stored Pickering emulsion before and after 60 min of centrifugation at 3,000 g: a) before centrifugation, b) top layer after centrifugation, c) bottom layer after centrifugation.

The stored and the freshly prepared Pickering emulsions showed a good emulsion stability since sedimentation could be achieved without the occurrence of free water. However, in both systems the sediment appeared to be very porous so that the compaction of the slurry was insufficient to obtain reasonable separation efficiencies. In contrast, the dynamically prepared emulsion broke after 10 min at 3000 g yielding a continuous aqueous phase. This leads to the conclusion that the state of the emulsion, kinetics of crystallization, stabilization of interphase, and flocculation are of paramount importance for a successful process design. Many sub-processes govern the compromise of stability of emulsion versus flocculation.

4.3.2.2 Separation in a lab scale decanter centrifuge

The separation in the static centrifuge varied depending on the type of sample preparation. Both, the stored and the freshly prepared emulsion were quite stable against centrifugal forces while dynamic emulsions broke up in almost all of the conducted experiments. The samples studied previously were separated in a decanter centrifuge as described above to evaluate effects of this processing step on the flocculation an emulsion stability, ultimately the separation efficiency. As a preliminary test the temperatures of the streams at the inlet and at the discharges of the decanter were determined. The temperatures at the discharges were stable around room temperature indicating some cooling down of the material with inlet temperatures between 25 and 30 °C. This implies that no melting of crystals should occur in the decanter due to dissipation of mechanical energy.

Dynamic Pickering Emulsion

The mixtures of water (4°C) and oil (75°C) resulted in an emulsion temperature of approximately 26 °C at the decanter inlet. The ratio of mixing is 4 to 6. The decanter was operated at an acceleration of 3,000 g and a differential rotational speed of 5 rpm. The DSC thermogram of the oil mixture, composed of 5 % fully hydrogenated palm oil and 1 % emulsifier dissolved in rapeseed oil, is shown in Figure 4.11a. In both, Figure 4.11b (liquid discharge) and Figure 4.11c (solid discharge) a water melting peak is visible. This leads to the conclusion that water and thus hardstock was transported to both exits and no separation occurred.

Not surprisingly, all thermograms show a very similar oil peak. Looking at the inserts of different thermograms it becomes apparent that all oil phases contain the same amount of hardstock. This is also confirmed by the enthalpy values determined, Table 4.2. The data indicate that the hardstock level is equal in both discharge streams. The actual value scales with content of water in both streams that appears to be practically identical as well.

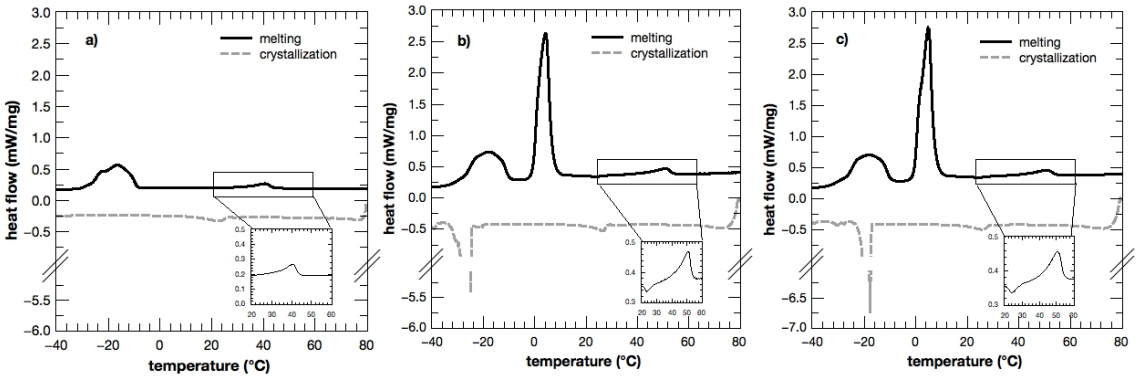

Figure 4.11: Dynamic prepared Pickering emulsion before and after separation in the decanter centrifuge (5 rpm differential speed, 3,000 g); a) oil mixture (5 % fully hydrogenated palm oil, 1 % emulsifier), b) sample from liquid discharge, c) sample from solid discharge.

In line with the results reported above on the centrifuge experiments this indicates that the dynamically prepared emulsion appears to be of insufficient stability to withstand the forces in the centrifugal field applied. Most likely, the emulsion broke up in the decanter and a three–layered system was established. In this situation possibly both discharges were fed from a water layer at the bowl and an inner oil phase with an intermediate layer of fat crystals. Currently the experiments performed did not reveal an operational window of reduced centrifugal force that results in good separation process while maintaining droplet integrity.

Table 4.2: Specific melting enthalpy ΔH of hardstock and water of the dynamic Pickering emulsion separated in the decanter centrifuge (5 rpm differential speed, 3,000 g), products received from the solid and the liquid discharge.

	ΔH hardstock	**ΔH water**
Solid discharge	4.1 J/g	71.3 J/g
Liquid discharge	3.9 J/g	66.4 J/g

Freshly prepared Pickering Emulsion

The thermograms resulting from a decanter experiment with the freshly prepared Pickering emulsion are displayed in Figure 4.12. The samples taken at the entry and at the liquid discharge of the decanter centrifuge show no difference. This is not surprising since no sample was expelled from the solid discharge. These results document the

effect of a reduced centrifugal force, 800 g compared to 3,000 g. Also, this processing setup does not seem to suit the desired application.

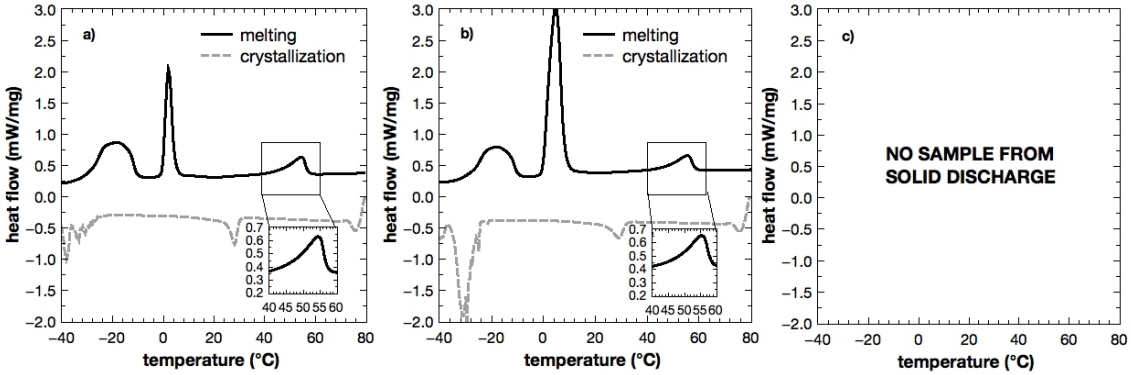

Figure 4.12: DSC thermograms of the freshly prepared Pickering emulsion before and after the separation in a lab scale decanter centrifuge (5 rpm differential speed, 800 g), a) temporary Pickering emulsion, b) product from the exit for liquids, c) product from the exit for solids.

Possible explanations for the lack of any solid discharge stream might be the breakup of the emulsion, insufficient friction at the bowl, or insufficient sedimentation. However, emulsion breakup had most likely occurred during experiments with the dynamically produced emulsions and led to similar streams at both discharges. In case the emulsion remains practically unchanged during the passage of the decanter - no breakup, no sedimentation - it is understandable that the movement of the screw is not able to transport any material to the solid discharge. Up to this point no combination of residence time and centrifugal force could be identified that yields a meaningful separation process for the freshly prepared emulsions.

Stored Pickering Emulsion

Figure 4.13 shows the characterization of the streams produced from processing a stored Pickering emulsion. The process parameters used for the sample shown were 3,000 g and a differential speed of 20 rpm. Again Figures a, b, and c show DSC thermograms of the original stored Pickering emulsion, the stream from the liquid (b) and the solid (c) discharge, respectively. The inserts show a magnification of the section of the thermograms most relevant for the hardstock melting. The data on enthalpy of melting extracted from the thermograms are given in Table 4.3. In this case the data

indicate clearly that the dispersed phase is concentrated in the solid discharge stream. Both the thermal signal for the hardstock as well as the water phase are increased compared to the feed and the liquid discharge. The latter actually appeared to be depleted of hardstock and water. Applying simple mass balances on the data of water the yield of solid discharge stream, the stearin containing emulsion, was approximately 35 %. This corresponds to a stearin yield of approximately 24 %. Even though this combination of feedstock and processing settings appeared to indicate general feasibility, the separation efficiency is still unacceptably low. However, this was owed to the low level of solid material in the system and possibly the insufficient drying of the solid discharge stream. The latter being a function of bowl configuration and differential speed defining the residence time in the drying zone.

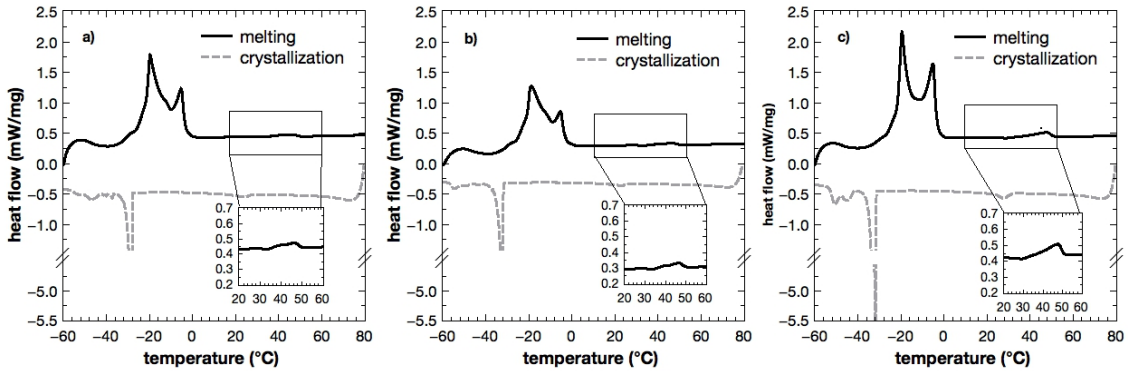

Figure 4.13: DSC thermograms of the stored Pickering emulsion before and after the separation in a lab scale decanter centrifuge (20 rpm differential speed, 3,000 g), a) stored Pickering emulsion, b) product from the exit for liquids, c) product from the exit for solids.

Table 4.3: Specific melting enthalpy ΔH of hardstock and water of the Pickering emulsion and the products received from the solid and the liquid discharge of the decanter centrifuge (3,000 g, 20 rpm differential speed).

	ΔH hardstock	**ΔH water**
Pickering emulsion	2.0 J/g	24.0 J/g
Liquid discharge	1.8 J/g	16.7 J/g
Solid discharge	4.8 J/g	37.1 J/g

4.4 Conclusion

The goal of this study was to investigate the feasibility of the proposed emulsion fractionation process. The conceptual design of the process entails that a cold-water stream is emulsified into a hot oil stream such that a Pickering emulsion emerges. Using the water droplets as means of entrainment the application of a decanter should yield a stream of fat covered water droplets that carry as little adhering oil as possible. It was established that in general the mixing of the two streams allows to generate Pickering emulsions. First results on the kinetics of crystallization at the cold droplet surface could give guidance to further details of the process design. Experiments on the sedimentation of different emulsions in a lab centrifuge revealed that an emulsion prepared directly prior to exposure to the centrifugal field, without a controlled emulsification process, is of insufficient stability to yield meaningful results. Sedimentation experiments with different longer stabilized emulsions with droplet sizes of approximately seven micron showed that the emulsions can withstand high centrifugal forces (3,000g) but that the tendency to flocculate result in highly porous sediments that would cause prohibitively low separation efficiencies. Processing the different emulsions with a decanter centrifuge at different process settings in essence reconfirmed the results of the centrifugation experiments. However, in particular stored, and hence stabilized, emulsions could be processed such that significant differences in the composition of the solid and liquid discharge of the decanter were observed. A significantly increased level of water droplets in the solid discharge was accompanied by decreased levels of hardstock in the liquid lipid phase.

Even though the data presented illustrate the general feasibility of the emulsion fractionation process, its product streams were of inacceptable quality, in particular the separation efficiency. If this approach has the potential to ever become competitive cannot be judged currently. Areas that certainly need more detailed attention are improvement of the drying of the stabilized droplets, by variation of weir height and differential speed, the effect of droplet size on crystallization kinetics and emulsion stability, and the composition of the feed material. Compared to the model systems studied up to now the fractionation of palm or shea oil will pose much bigger challenges with among others larger amounts of solid material to be separated.

5 Determination of the Crystallization Behavior of Lipids by Temperature Modulated Optical Refractometry

Michaela Häupler, Eckhard Flöter

TU Berlin, Department of Food Process Engineering, Seestrasse 13, 13353 Berlin, Germany

Originally published in Food Analytical Methods (2018), 11 (9), 2347-2359
https://doi.org/10.1007/s12161-018-1217-y

Abstract

This study was conducted to examine if the new temperature modulated optical refractometry (TMOR) method is applicable to study the phase behavior of alkyl based components. *n*-Hexadecane, palmitic acid, and glycerol tripalmitate were used as model components. TMOR was benchmarked against differential scanning calorimetry (DSC) and polarized light microscopy (PLM).

For all substances, a good agreement of the DSC data with TMOR was found. For *n*-hexadecane a difference of 2.2 °C for the crystallization and 2.6 °C for the melting temperature was found. Considering palmitic acid, the crystallization temperature differed by 3.3 °C while the melting varied by 2.8 °C. The crystallization temperature of tripalmitate identified by TMOR was 2.7 °C higher and the melting temperature 2.3 °C lower compared to the DSC. The crystallization temperature for TMOR was always higher and the melting temperature always lower if related to DSC. This leads to the conclusion that TMOR is more accurate and direct. In addition, the transition peaks identified by TMOR were narrower compared to the DSC peaks. This is due to slower heating and cooling rates leading to a smaller temperature range of phase transition and less thermal lag.

The study showed that TMOR is an appropriate method to determine the phase transition temperatures for the three examined substances. The results were comparable to the DSC data in both melting and crystallization behavior. Since the accuracy of TMOR is better at lower heating and cooling rates it could be a reasonable extension of the well-known DSC method in the studies of melting and crystallization.

Key words: *crystallization, alkanes, fatty acids, triacylglycerides, temperature modulated optical refractometry (TMOR), phase behavior*

5.1 Introduction

Next to carbohydrates and proteins, lipids represent a major class of nutrients and play an important role in food production. In essence, lipids are characterized by their hydrophobic nature which is also manifested by the existence of aliphatic chains. The solidification behavior of these materials is strongly influenced by chain-chain interactions. Therefore, the investigations of alkanes, fatty acids, partial glycerides, and triacylglycerides form a good base to elucidate overriding principles of physicochemical behavior of alkyl-chain containing molecules. The improved understanding of the phase behavior is beneficial for substances ranging from petroleum waxes to edible fats. In this type of products, the alkyl components and their composition have a big influence on quality, consumer acceptance as well as application field and range (Sirota and Herhold, 1999; Sato, 2001).

n-Alkanes are hydrocarbon chains composed of carbon and hydrogen atoms and can align in a defined position to form crystals. In addition, even-numbered alkanes form a triclinic phase while odd-numbered result in an orthorhombic phase (Wentzel and Milner, 2010). Despite the fact, that even- and odd-numbered alkanes show different crystallization behavior the authors were only interested in even-numbered alkanes due to their appearance in naturally derived fats. Work on the phase behavior of *n*-alkanes and mixtures of *n*-alkanes can be found in abundance (Dorset, 2005).

Fatty acids (FA) or carbonic acids are carboxylated hydrocarbon chains. The aliphatic chain is nonpolar while the carboxyl group builds the polar group. FAs are of big interest because they form the basis for fats and oils as well as for energy storage systems or biofuels (Costa *et al.*, 2009). The packing of fatty acids into a crystal structure is determined by the length and angle of tilt of the FAs. Saturated FAs with no double bond in the hydrocarbon chain allow a denser packing compared to mono- or polyunsaturated FAs (Sato, 2001).

Another important aspect that complicates matters is polymorphism. It is the ability of a material to crystallize in different crystalline structures. Since the different structures have specific interactions this leads e.g. to different melting points and x-ray patterns of the distinguishable polymorphic forms.

Combined with a carboxylic group, *n*-alkanes form fatty acids, which are the main components of triacylglycerides (TAGs) after esterification to a glycerol. For one TAG, three fatty acids need to be esterified onto a glycerol backbone. In general, also partial glycerides with only one or two fatty acid moieties esterified to the glycerol backbone should be considered in this series. However, for the purpose of this work mono- and diacylglycerides as investigated by Hernqvist (1988) will not be considered.

The investigation of the phase behavior of *n*-alkanes, FAs or TAGs is often performed using differential scanning calorimetry (DSC) (Xie *et al.*, 2008; Costa *et al.*, 2009; Ikeda *et al.*, 2010). The DSC method is based on the variation of the heat released or absorbed during thermal processing to observe the melting and crystallization events of a substance. For that purpose, the sample is heated or cooled at a specific rate while the heat flux is monitored to investigate occurring phase transitions. Thermodynamics, in particular the Gibbs' phase rule, dictates that melting of a pure component should take place at a fixed temperature. However, depending on the scan rate of the chosen temperature program a limited thermal lag occurs. This implies that the true transition temperature is actually related to an extrapolation to a scan rate of zero. To execute this directly is for obvious reasons, decreasing signal-to-noise ratio and general execution, not practical.

Studying crystal structures by powder x-ray diffraction (XRD) yields details on the geometry of the crystallographic unit cell because the different crystal structures, polymorphs, have different distances between methyl end planes (small angle) and neighboring fatty acid moieties (wide angle) and hence scatter differently (Timms, 1984; D'Souza, DeMan and DeMan, 1990; Sato, Ueno and Yano, 1999).

Using table top nuclear magnetic resonance (NMR) to determine the level of solidified lipid material in a sample is well established since the 1970s. The solid fat content (SFC) is an important quality parameter for fats and oils (Van Putte and Van Den Enden, 1974; Petersson, Anjou and Sandström, 1985). The measurement is based on the different relaxation times in of hydrogen nuclei in solid and liquid phases after excitation in a magnetic field.

Further investigations have been conducted to validate the potential of this technique to determine polymorphic forms, which was successful for several mono- and triacylglycerides (Van Duynhoven *et al.*, 2002).

All the above-mentioned techniques are used for the investigation of fat crystallization because aliphatic chains are a major building block of the respective molecular structure. Before NMR and XRD were established methods, a rather outdated method called dilatometry was used to characterize phase transitions and polymorphic forms**.** It was established for fats in the early 1930's by Normann (1931) and well understood in the mid 1940´s (Bailey and Kraemer, 1944; Bailey and Singleton, 1945). This simple method was applied to determine phase transitions of various fats by investigating differences in the thermal expansion of solid and liquid phases (Bailey and Kraemer, 1944). The same was applied for saturated fatty acids by Dorinson et al. in 1942. The so called thermal expansion coefficient describes the thermally induced density variations and is directly related to the derivative of the density regarding temperature. Hence, a dilatometer takes advantage of the fact that the liquid phase of a sample is not only characterized by typically lower densities compared to its crystal form, but also that the temperature dependence of the said densities changes. Since density and refractive index have a simple relationship as shown by the Lorentz-Lorenz equation (Eq. 5.1 (Müller *et al.*, 2013)), it was a conceivable step to use the refractive index as a basis for a new method to determine the density changes and simultaneously the thermal expansion.

$$\frac{\mathbf{n^2-1}}{\mathbf{n^2+2}} = \mathbf{r \cdot \rho} \qquad \textbf{Eq. 5.1}$$

The determination of refractive indices of alkanes, FAs and TAGs has up to now been limited to exclusively study the liquid state. In these cases, the refractive index is a sensitive finger print of for example oils that allows to verify the identity of an oil. Here the differences of refractive indices of oils are primarily caused by differences in the level of unsaturated bonds in the aliphatic chains. One could consider the refractive index an optical density which is defined as the velocity of light in vacuum divided by the velocity of light in the medium. To utilize the refractive index for the determination of phase transitions *Anton Paar OptoTec* in cooperation with the group around Prof. Dr. Krüger from the University of Luxembourg developed the temperature modulated optical refractometry (TMOR). So far, the application focussed on the isothermal study of chemically induced glass transitions in polymers (Müller *et al.*, 2013). The actual TMOR prototype used is equipped with a prism, for which the temperature is precisely

controlled (+/- 0.03 °C). The temperature is modulated with a predetermined period (30-120 s) and a given amplitude (0.1-1.0 °C) as shown in Figure 5.1. During the temperature modulation, the refractive index of the sample is carefully recorded (n_D).

In the first place the TMOR determines the change of the refractive index depending on the temperature. This change is expressed as $\frac{dn}{dT}$, which is the basis for the calculation of the thermal expansion coefficient α. It can be calculated by the Lorentz-Lorenz-Model using the following equation

$$\boldsymbol{\alpha = -\frac{6 * n}{(n^2 - 1) * (n^2 + 2)} * \frac{dn}{dT}} \qquad \textbf{Eq. 5.2}$$

where *n* is the refractive index and *T* the temperature (Müller *et al.*, 2013).

If a change in the sample occurs, e.g. glass or phase transition, the undulation of the refractive index is trailing the temperature by a phase shift ϕ (see Figure 5.1). This delay can be expressed by modelling the signal as real and imaginary part of the thermal expansion coefficient α (see Eq. 5.3 and Eq. 5.4).

$$\boldsymbol{Re(\alpha) = |\alpha| * cos(\phi)} \qquad \textbf{Eq. 5.3}$$

$$\boldsymbol{Im(\alpha) = |\alpha| * sin(\phi)} \qquad \textbf{Eq. 5.4}$$

The real part represents the coefficient of thermal expansion (CTE) while the imaginary part is the loss term. A peak in the curve of the imaginary part vs. temperature indicates a phase transition at the corresponding crystallization/melting temperature (see Figure 5.2). In turn, the shape of the real part plotted versus temperature is indicative for the kind of observed phase transition. For example, if melting or crystallization occurred the real part also displays a peak like the imaginary part. Other transitions, such as glass transitions, reveal a step function in the real part of α. This concept has been applied for isothermal phase changes induced by chemical reactions, where the derivation of all formulas and variables is also published (Müller *et al.*, 2013).

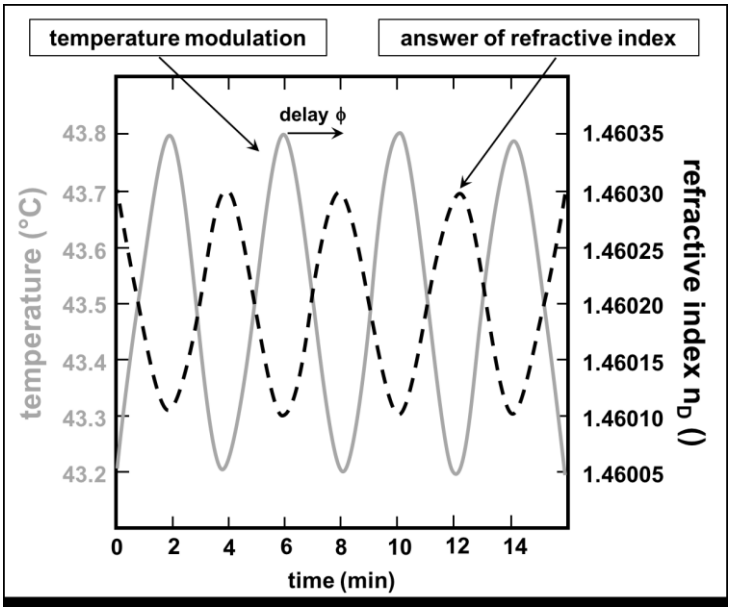

Figure 5.1: Explanation of temperature modulation (grey, solid curve) and answer of the refractive index (black, dashed curve), measured by TMOR.

In addition to the modulation around a constant temperature during isothermal experiments, the TMOR is also able to perform a modulation of the temperature around a given temperature ramp. This feature enables a monitoring of dynamic processes arising from temperature changes and opens the opportunity to realize investigations like those executed with the help of DSC. Therefore, this study aimed to apply TMOR instead of the standard DSC method to determine crystallization and melting behavior of alkyl components. Its application would be desirable because TMOR is potentially an easier and cheaper alternative to all well-established methods to monitor phase transitions. In addition, TMOR seems to have a higher sensitivity compared to other methods and thus yields more detailed information. With the possibility to perform slow scan rates, a reduction of the thermal lag during alkyl component investigation can be achieved. In contrast to high resolution refractometry, TMOR yields peaks during the phase transitions instead of a kink in the refractive index. This should emphasize change of properties of the first order phase transition which becomes in particular important, when mixed systems are going to be studied. Consequently, this manuscript is concerned with the assessment of the potential of the temperature modulated optical refractometry to investigate the crystallization and melting behavior of alkanes, fatty acids and triacylglycerides. The chosen model systems

represent classes of materials such as waxes, edible fats and oils or biofuels. The evaluation of the TMOR entangles benchmarking against conventional methods, even though this is far from straight forward due to different limitations in temperature range and scan rates. Additionally, complementary benefits were looked for.

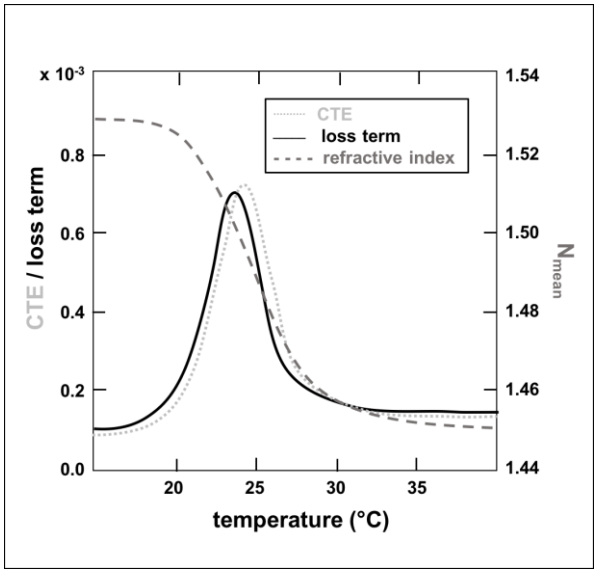

Figure 5.2: Analysis of the loss term (black solid line) and the coefficient of thermal expansion (CTE, light grey pointed line) and the mean refractive index (N_{mean}, dark grey dashed line) as a function of temperature.

To this end, the three substances displayed in Figure 5.3 were investigated. All of them have 16 carbon atoms at each chain and only differ in their residues, which is a methyl group for alkanes (hexadecane, Figure 5.3a), a carboxyl group for fatty acids (palmitic acid, Figure 5.3b) and a glycerol backbone for triacylglycerides (tripalmitate, Figure 5.3c). The purpose of the study was to investigate the applicability of the TMOR method for the determination of crystallization and melting behavior of alkyl components.

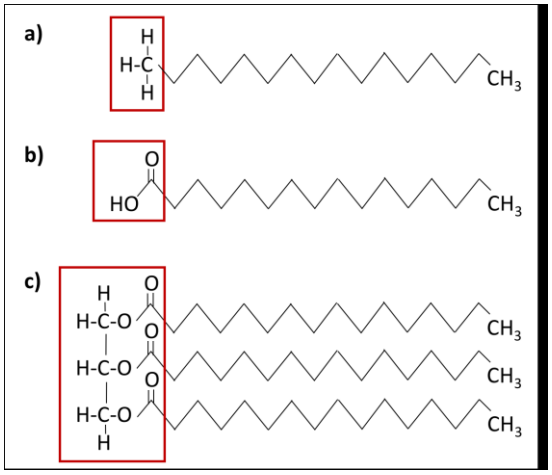

Figure 5.3: Differences between alkane, fatty acid and triacylglycerol marked with red boxes: a) hexadecane (alkane with 16 carbon atoms and two methyl residues), b) palmitic acid (hexadecane with acidic group on the one and a methyl group on the other end), c) tripalmitate (glycerol backbone esterified with three palmitic acid residues).

5.2 Materials and Methods

In this study, three different pure substances (*n*-hexadecane, palmitic acid, tripalmitate) were chosen to evaluate the applicability of TMOR for the investigation of phase transitions in hydrocarbon chain based molecules.

The DSC was chosen as the reference method for the crystallization and melting range, and polarized light microscopy (PLM) as a possibility to determine the microstructure in the solid state. This is because shape and amount of the crystals present could influence the refractive index measured.

n-Hexadecane and palmitic acid were purchased from Merck (Merck KGaA, Darmstadt, Germany) with a specified melting point of 18 °C and 61-63 °C, respectively. The glycerol tripalmitate was purchased from Alfa Aesar (ThermoFisher (Kandel) GmbH, Karlsruhe, Germany) with a melting range between 60-64 °C.

The temperature modulated optical refractometry (TMOR) measurements were performed with a prototype from Anton Paar OptoTec GmbH (Seelze-Letter, Germany). The used modification of the Lorentz-Lorenz model (based on (Beysens and Calmettes, 1977)) is valid if the specific refractivity r is constant. However, Aleksandrova *et al.* (2014) showed for polyacrylamide solutions that the specific refractivity changes if weak bonds are broken (Aleksandrova *et al.*, 2014). Therefore,

the authors assumed like Müller *et al.* (2014), that the specific refractivity remains constant in the range of one period of 30 s which leads to a higher contribution of the volumetric changes to the calculated data. The design of the device is described elsewhere (Müller *et al.*, 2013). Briefly explained, an Abbe-refractometer with a precisely temperature controlled prism is used. The sample is put in a cone-shaped vat directly on the temperature controlled prism. Both, cooling and heating rate were set at 0.5 °C/min, with a modulation period of 30 s and an amplitude of 0.2 °C. In the scope of this paper, the reported ramp of 0.5 °C/min is always referred to as the mean ramp and not to the local ramp of the modulation. The samples were pressed onto the prism using a solid stamp to ensure best contact between the sample and the prism and thus minimizing measurement anomalies. Approximately 100 µL of the sample were molten at 80 °C on the prism, holding the temperature for 10 min to remove all crystal memory. Subsequently, the samples were cooled to 4 °C, holding it for 30 min before heating the sample at the rate of 0.5 °C/min up to 80 °C again. At the beginning of each day, the device was calibrated with distilled water. Currently, the procedures cannot include temperatures of less than 4 °C due to limitations of the prototype equipment. The data was recorded at all stages during the measurement.

The differential scanning calorimetry (DSC) was performed with a device from Netzsch (DSC 204 F1 Phoenix, NETZSCH-Geraetebau GmbH, Selb, Germany) which and indium (T_m = 156.6 °C) was used for calibration. The two temperature profiles were determined at a cooling and heating rate of 2 °C/min and a holding time for 30 min at 4 °C and for 10 min at -50 °C, respectively. This was done to check if differences in the melting profiles occurred due to different crystallization temperatures and kinetic effects that might change due to sample size. Approximately 8 mg of sample were weighed in aluminum pans and sealed hermetically. An empty pan was used as reference.

The micrographs were taken during crystallization at a 10x magnification using a Zeiss AxioScope (Carl Zeiss Jena GmbH, Jena, Germany) equipped with a camera (AxioCam ICm1, Carl Zeiss Jena GmbH, Jena, Germany). The image analysis was done with the ZEN Software provided by the manufacturer (Carl Zeiss Jena GmbH, Jena, Germany). The polarized light microscopy (PLM) was combined with a temperature-controlled stage from Linkam Scientific Instruments (Surrey, UK)

following essentially the same temperature regime as the TMOR except for the scan rate of 2 °C/min. The pictures taken were used to investigate the microstructure during the phase transitions and to generate an assessment of the homogeneity of the sample. TMOR, DSC and PLM measurements were all performed in duplicate. Both the onset and the peak temperatures determined by TMOR, DSC and PLM were compared with each other.

5.3 Results and Discussion

The aim to investigate all samples with the different methods under the same processing conditions was hampered by two difficulties. Firstly, TMOR seems to be more precise at lower scanning rates compared to the DSC, which is normally applied at higher scan rates. Secondly, the DSC can cool down to much lower temperatures than the TMOR prototype. In the evaluation of the applicability of TMOR for the investigation of crystallization and melting behavior of alkyl components these two issues are addressed as well.

To improve the comparability of the two methods, the DSC data are used to extrapolate for the determination of the transition temperature at scan rates of 0.5 °C/min, where the TMOR showed the best results. The procedure applied in this approach is well established to determined values for zero scan rates (Illers, 1974; Richardson and Savill, 1975; Vanden Poel and Mathot, 2006). For higher scan rates, the changes in the refractive index appear to be too fast for the current evaluation algorithms implemented in the prototype equipment.

The extrapolation of the experimental DSC data of *n*-hexadecane, palmitic acid and tripalmitate investigated at three different heating and cooling rates (2 °C/min, 5 °C/min, and 10 °C/min) is depicted in Figure 5.4. As expected, the peak crystallization temperature decreases for all three substances with increasing cooling rate (see in Figure 5.4a).

Table 5.1 gives the crystallization temperature for the different cooling rates including the value determined by extrapolation to a scan rate of 0.5 °C/min.

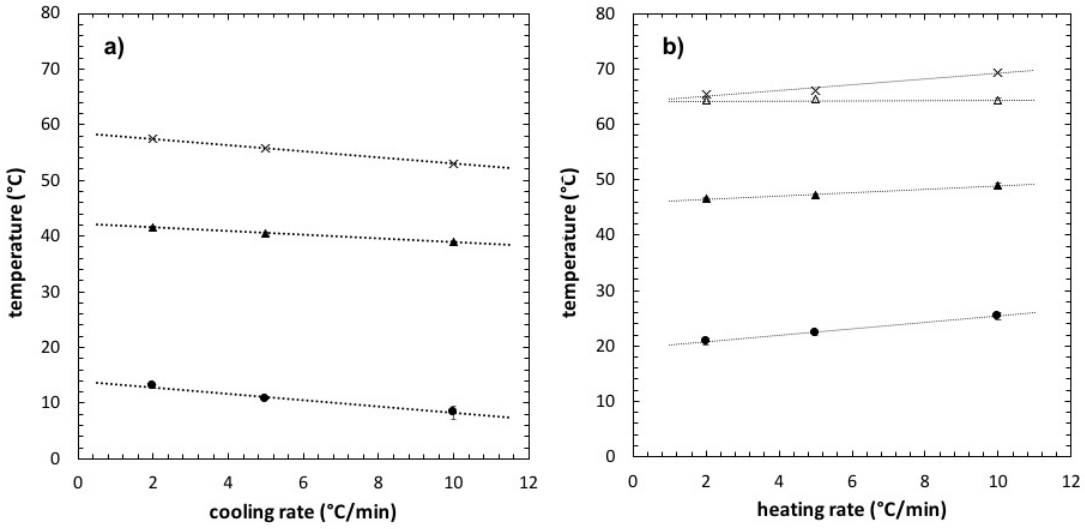

Figure 5.4: Extrapolation of DSC measurements of *n*-hexadecane (circle), tripalmitate (triangle black: first peak; triangle white: second peak) and palmitic acid (cross) at different cooling (a) and heating rates (b).

Table 5.1: DSC peak temperatures at different cooling rates of *n*-hexadecane, palmitic acid and tripalmitate, temperatures at 0.5 °C/min are extrapolated and indicated with italic letters.

cooling rate (°C/min)	*n*-hexadecane (°C)	palmitic acid (°C)	PPP (°C)
10	8.3 ± 1.2	53.0 ± 0.5	39.0 ± 0.2
5	10.8 ± 0.1	55.8 ± 0.6	40.4 ± 0.4
2	13.0 ± 0.4	57.5 ± 0.5	41.6 ± 0.2
0.5	*13.9*	*58.5*	*42.0*

The melting curves were recorded after crystallization of the samples at a scan rate of 2 °C/min. Figure 5.4b shows that the measured melting peak temperatures increase with increasing heating rate for *n*-hexadecane, palmitic acid and the first peak of tripalmitate, as was expected. In the thermogram of tripalmitate a second peak was identified. This peak, related to the melting of a more stable polymorph, shows neither an increase nor a decrease in melting temperature, which means it seems not to be affected by the scan rate. An explanation could be that it relates to a transient state combining the melting of the lower melting polymorph overshadowed by the crystallization of the more stable polymorph. Consequently, this transition is more complete at a scan rate of 2 °C/min than at 5 °C/min, or 10 °C/min. The amount of

crystallized material and the occurring thermal lag due to different scan rates seem to counteract each other. This results in the same melting point of the second peak for all scan rates at 64.3 °C. The calculated melting peak temperatures for 0.5 °C/min are listed in Table 5.2.

Table 5.2: DSC peak temperatures at different heating rates of *n*-hexadecane, palmitic acid and tripalmitate (two melting peaks) crystallized at 2 °C/min, temperatures at 0.5 °C/min are extrapolated and indicated with italic letters.

heating rate (°C/min)	***n*-hexadecane (°C)**	**palmitic acid (°C)**	**PPP (°C)**	
10	25.4 ± 0.7	69.4 ± 0.1	49.0 ± 0.5	64.3 ± 0.4
5	22.4 ± 0.5	66.0 ± 0.1	47.1 ± 0.3	64.5 ± 0.4
2	20.9 ± 0.7	65.5 ± 0.1	46.6 ± 0.1	64.3 ± 0.3
0.5	*19.4*	*64.3*	*46.0*	*64.3*

Before the melting behavior analysis by TMOR was compared to the DSC results, the proper modulation of each measurement was evaluated as shown in Figure 5.5.

Owing to the fact that the piece of equipment and the analytical method are still in their infancy, irregularities that occur during the TMOR measurement leading for example to sharp edges in the curve of the refractive index, the mean refractive index cannot be dealt with automatically. Consequently, the data gathered needed careful consideration prior to further analysis. A sinusoidal oscillation of both temperature and refractive index signal is required for the analysis of the melting behavior which was done based on Re (α) and Im (α), the real and imaginary part, to describe the evolution of the thermal expansion coefficient α, respectively.

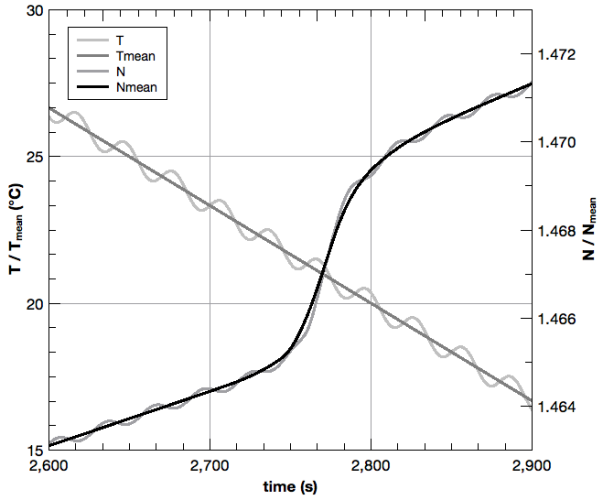

Figure 5.5: Evaluation of proper TMOR measurement, sinusoidal modulation of temperature (grey solid curve: mean temperature, grey dashed curve: modulated temperature) and refractive index (black solid curve: mean refractive index, black dashed curve: modulated refractive index), respectively.

5.3.1 *n*-Hexadecane

All results of PLM, DSC and TMOR for *n*-hexadecane are shown below. For both, PLM and DSC measurements, a cooling and heating rate of 2 °C/min was applied. The aim was to investigate the microstructure and the crystallization and melting behavior, respectively. The sample treatment with the TMOR method was performed at a rate of 0.5 °C/min.

In Figure 5.6, a polarized light micrograph shows a dense network of *n*-hexadecane at 4.0 °C after cooling the sample at 2 °C/min. The crystallization of *n*-hexadecane began at 14.8 °C, which was determined with the PLM, and was completed within a range of 2.0 °C. This narrow range of phase transitions was also found in the DSC measurements (see Figure 5.7), where the crystallization starts at 15.0 °C (T_{peak} = 13.4 °C) and the sample melts at 17.3 °C (T_{peak} = 20.5 °C). The melting point is in line with the manufacturer's specification of 18.0 °C and did not differ between the two chosen stabilization temperatures of -50 °C and 4 °C, respectively (see Table 5.3). This was necessary to achieve a truthful comparison of the DSC and the TMOR method.

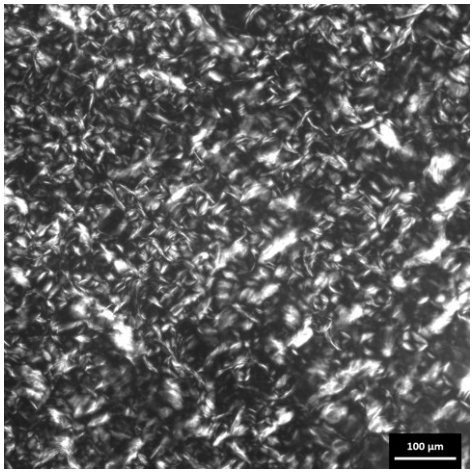

Figure 5.6: Polarized light microscopy of crystallized *n*-hexadecane at 4 °C; scale bar represents 100 µm.

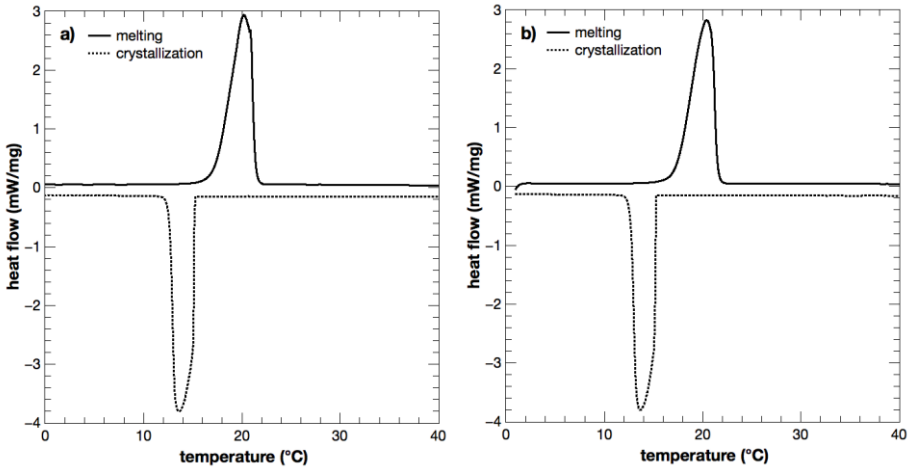

Figure 5.7: DSC thermograms of *n*-hexadecane stabilized at -50 °C (a) and 4 °C (b); cooling and heating rate 2 °C/min.

In Figure 5.8, the crystallization (a) and melting (b) of *n*-hexadecane measured with TMOR is shown. The curve of the refractive index in Figure 5.8a shows a small kink 15.7 °C during crystallization because the change of the refractive index was not linear in one period. However, the resulting Re (α) and Im (α) were calculated properly and hence the crystallization behavior of *n*-hexadecane could be discussed appropriately. Such irregularities can occur since TMOR is still a prototype for which the authors are in the process to develop an experimental protocol, which can be used for different acyl chain components. If one considers the crystallization and melting behavior of *n*-hexadecane during the TMOR measurements similarities to the DSC method can be

seen. The crystallization occurs at around 16.0 °C and the melting at 18.0 °C, respectively, according to the TMOR measurement.

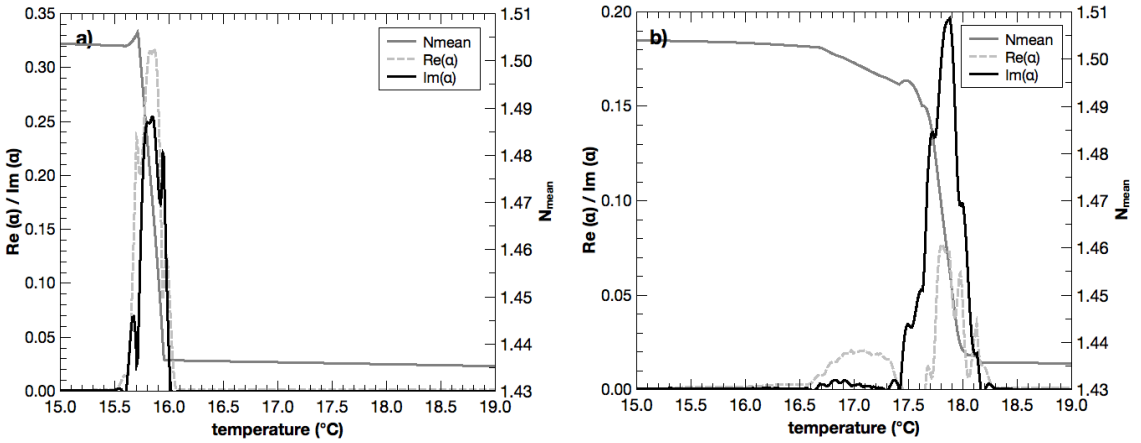

Figure 5.8: Crystallization (a) and melting (b) of *n*-hexadecane investigated by temperature modulated optical refractometry; cooling and heating rate 0.5 °C/min, 30 s period of modulation, 0.2 °C amplitude.

The crystallization begins at 16.0 °C with TMOR, has its peak temperature at 15.8 °C and its offset at 15.6 °C. In comparison, *n*-hexadecane starts crystallizing at 15.2 °C in the DSC measurement and at 14.8 °C if investigated with the PLM. The DSC results show a peak temperature of 13.6 °C and an offset temperature of 12.6 °C. For pure substances, the crystallization temperature should be theoretically at one exact temperature instead of a range. However, the broader peak in the DSC results compared to the TMOR can be explained by the emerging thermal lag of both which should be considered when discussing differences in data obtained by different methods. This is because the cooling and heating rate of the TMOR measurement was lower (0.5 °C/min) compared to the one of the DSC (2 °C/min) because current data evaluation for TMOR is less artifact-prone at lower rates and slower phase changes of the sample. If one extrapolates the peak temperatures of the DSC measurements during cooling at 2 °C/min, 5 °C/min and 10 °C/min (see Figure 5.4a), the peak temperature at a rate of 0.5 °C/min would be 13.7 °C for *n*-hexadecane, which is lower than the 16.0 °C determined with TMOR.

For the heating of *n*-hexadecane, an extrapolation would lead to a melting temperature of 19.4 °C, which is closer but still not matching the TMOR result of

18.0 °C. This leads to the conclusion, that TMOR has a higher sensitivity because the differences in peak temperature cannot be explained by only considering the different scan rates. Both phenomena could be explained by the mentioned difference in the heat transfer to the measured sample volume, whereby both the crystallization and the melting on the TMOR prism starts earlier compared to the DSC or the PLM. Additionally, our observation indicates that the onset of crystallization however suffers less from this phenomenon. The onset temperatures determined with the DSC for crystallization and melting at 15.2 °C and 17.3 °C, respectively, fit better to the TMOR onset and peak temperatures, which were determined at 16.0 °C and 15.8 °C, respectively, and 17.4 °C and 17.8 °C, respectively.

The experiments of the pure substance *n*-hexadecane were promising although other authors stated before that TMOR should only be used to investigate transparent material. However, this study showed that opaque material like *n*-hexadecane in the crystalline state can be examined. Subsequently, the next step was to investigate a substance with a slightly more complicated structure compared to *n*-hexadecane.

5.3.2 Palmitic acid

The sample of palmitic acid showed a different microstructure under the polarized light microscope compared to the other samples (see Figure 5.9). No clear crystal structure was visible but a change of structure occurred at around 60.6 °C. The sample got rigid immediately and changed from translucent to a very bright white color. Therefore, the generation of a proper TMOR signal was not as easy as for the other samples which showed a crystal structure.

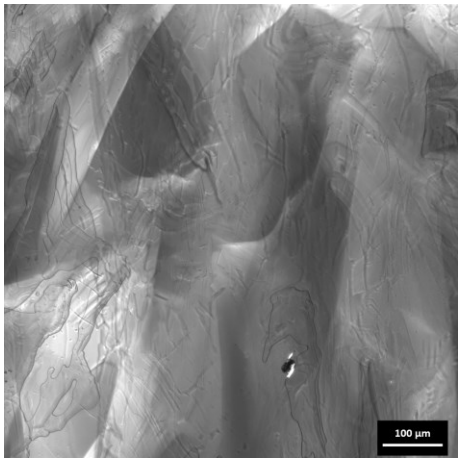

Figure 5.9: Polarized light micrograph of palmitic acid during crystallization at 60.6 °C; scale bar represents 100 µm.

In Figure 5.10, the two DSC thermograms for different stabilization temperatures are displayed. There was no difference observed whether palmitic acid was stabilized at -50 °C (Figure 5.10a) or at 4 °C (Figure 5.10b). The crystallization and melting of palmitic acid investigated with TMOR is depicted in Figure 5.11. During crystallization, the peak temperature was found to be 57.9 °C in the DSC (Figure 5.10a) and 61.2 °C in the TMOR measurement (Figure 5.11a). The sample began to crystallize at 59.9 °C in the DSC and at 61.4 °C on the TMOR prism.

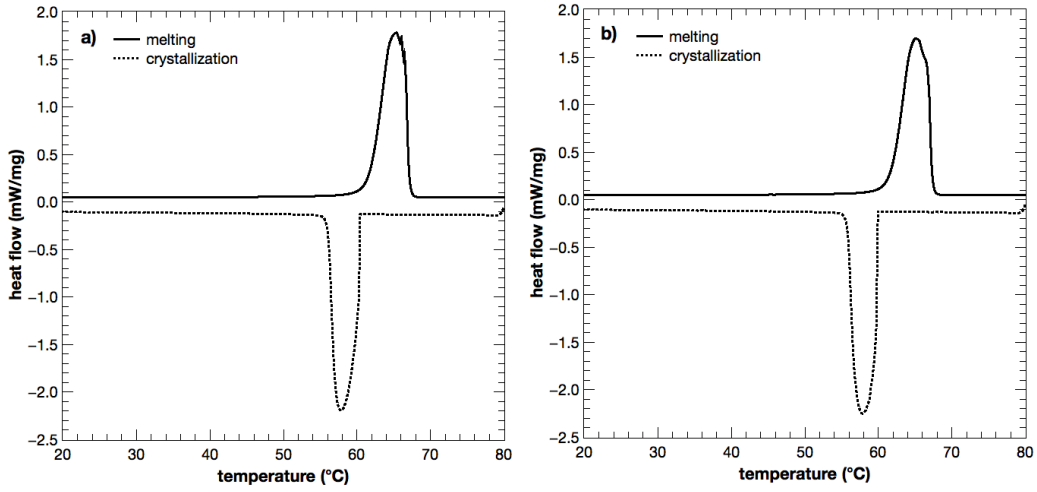

Figure 5.10: DSC thermograms of palmitic acid stabilized at -50 °C (a) and 4 °C (b); cooling and heating rate 2 °C/min.

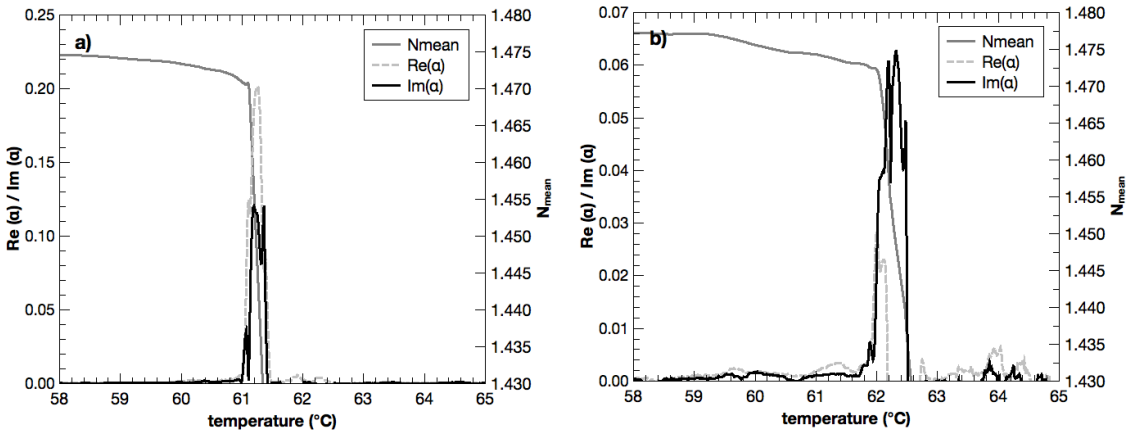

Figure 5.11: Crystallization (a) and melting (b) of palmitic acid investigated by temperature modulated optical refractometry; cooling and heating rate 0.5 °C/min, 30 s period of modulation, 0.2 °C amplitude.

For the melting behavior, 65.1 °C was the peak temperature of palmitic acid investigated by the DSC (Figure 5.10b) whereas the peak melting temperature was 62.3 °C in the TMOR measurement (Figure 5.11b). The DSC onset temperature of the melting peak was at 61.7 °C and the onset determined by TMOR at 61.8 °C. As seen for *n*-hexadecane, the temperatures determined by TMOR are closer to the onset temperature of the DSC than the peak temperature. The supporting data is given in

Table 5.3. The extrapolated values for the peak temperatures during crystallization and melting at 0.5 °C/min with the DSC are 58.5 °C and 64.3 °C, respectively (see Table 5.1 and Table 5.2). These values are closer to the peak temperatures determined with TMOR but also after heating rate correction not in agreement. Again, the higher crystallization and lower melting temperatures cannot be explained by only considering the different scan rates.

The experiments showed that it was also possible to study the phase behavior of palmitic acid as a highly pure substance even though it has a slightly more complicated phase behavior compared to *n*-hexadecane. These results let hope that also even more complicated samples can be analyzed successfully. Therefore, the next step was to analyze tripalmitate to increase the complexity of material.

5.3.3 Tripalmitate

The polarized light micrograph of tripalmitate in Figure 5.12 shows the spherulitic structure of the formed solids. In contrast to *n*-hexadecane and palmitic acid, tripalmitate showed small crystals, which can be identified as white areas. Furthermore, in the solid state at 4 °C also dark areas remained which lead to the conclusion that the tripalmitate crystals formed a network and did not align as properly as the other two substances.

The crystallization peak temperature in the DSC measurement was determined at 41.9 °C and the onset temperature at 44.2 °C (see Figure 5.13). Again, as shown for the other two pure substances, the peak temperature of TMOR (see Figure 5.14a), which is 44.2 °C, fits better to the onset temperature of the DSC measurement instead of the peak temperature (see Table 5.3).

Both DSC thermograms in Figure 5.13 show a recrystallization during melting for both stabilization procedures at -50 °C (Figure 5.13a) and 4 °C (Figure 5.13b), respectively. This indicates that during crystallization a less stable polymorph was formed. The recrystallization into a more stable polymorph appears to be melt mediated. At least the melting of the less stable polymorph is clearly detectable prior to the overlapping crystallization of the more stable polymorph. On further temperature increase the more stable polymorph melts.

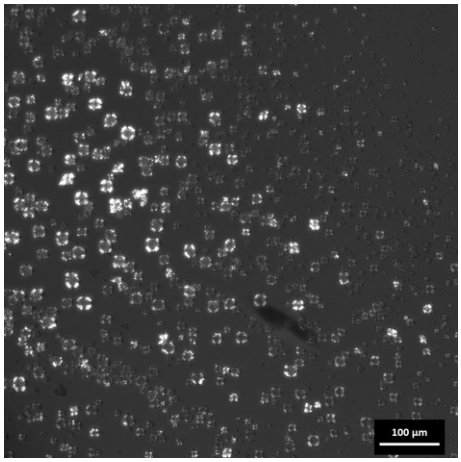

Figure 5.12: Polarized light micrograph during the crystallization of glycerol tripalmitate at 51.0 °C; scale bar represents 100 µm.

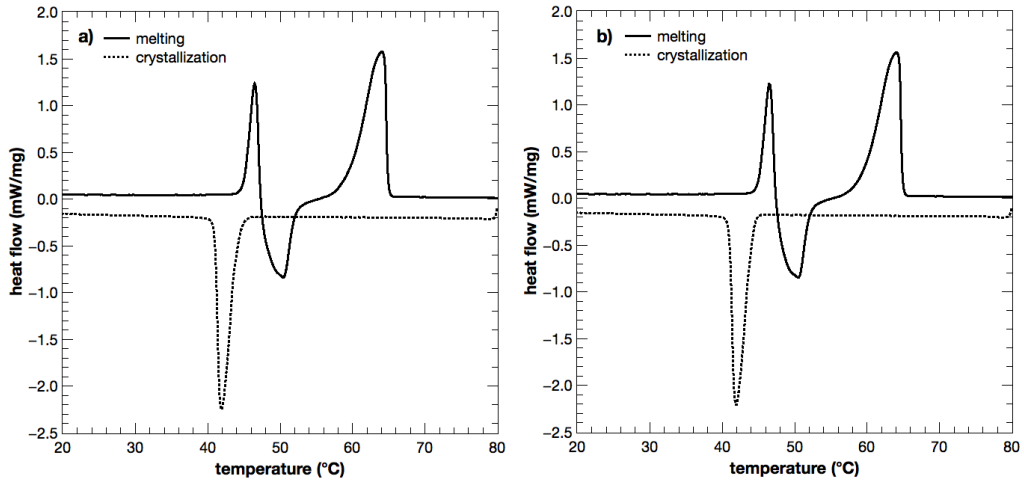

Figure 5.13: DSC thermograms of tripalmitate stabilized at -50 °C (a) and 4 °C (b); cooling and heating rate 2 °C/min.

Also, the signal obtained during melting by TMOR indicates an event at temperatures between 43.0 °C and 47.0 °C. A small bump at 45.0 °C in the imaginary part as well as in the refractive index is visible in the enlarged section in Figure 5.14b. This is an indication that TMOR also detected the melting of the unstable polymorph. A possible explanation for the much less pronounced signal of this melt-mediated polymorphic transition are the slower scan rate and the temperature undulation both promoting a simultaneous progression of melting of the less stable polymorph and crystallization of the more stable polymorph. This overlap of melting and crystallization causes that the net effect appears to be minute compared to separate distinct melting or crystallization events. As the insert in Figure 5.14b reveals, this change of the

polymorphic form is accompanied by a change in physical properties. The slopes of the refractive index over temperature (grey) are different before and after the polymorphic transition. In addition, the thermal expansion coefficient shows a minute difference before (lower arrow) and after (upper arrow) the transition from a less to a more stable polymorph. Both observations trigger deeper investigations of the ability of TMOR to determine polymorphic transitions or polymorphic forms.

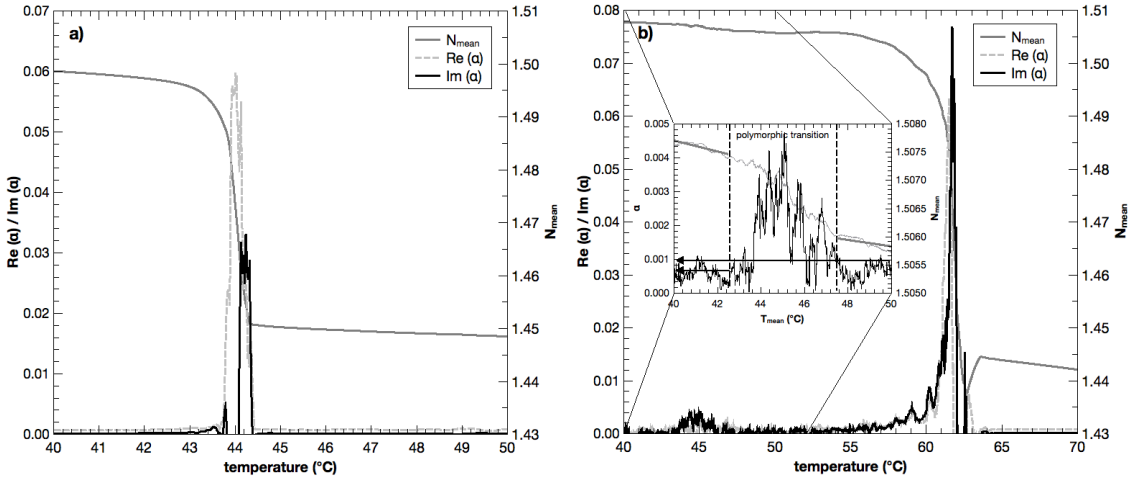

Figure 5.14: Crystallization (a) and melting (b) of tripalmitate investigated by temperature modulated optical refractometry; cooling and heating rate 0.5 °C/min, 30 s period of modulation, 0.2 °C amplitude.

The onset temperatures of melting were determined at 45.0 °C and 59.7 °C and the peak temperatures at 46.5 °C and 64.3 °C, respectively. For the first melting peak the TMOR peak temperature fits exactly the onset temperature determined by DSC. The second melting peak was found at 61.7 °C, which was lower compared to the DSC onset temperature. Even though the temperature of the second melting peak of tripalmitate does not depend on the crystallization of the original material but recrystallization, both peaks can be considered for the extrapolation of the peak temperatures at 2 °C/min, 5 °C/min and 10 °C/min (Figure 5.4b). At a rate of 0.5 °C/min a crystallization peak temperature of 42.0 °C and a melting peak at 46.0 °C were calculated for tripalmitate. This is slightly higher than the determined values with TMOR.

In addition to *n*-hexadecane and palmitic acid, it was also successful to study the crystallization and melting behavior of tripalmitate, a material with an even more complex phase behavior, by TMOR. In summary, all results show that this new technique could be a promising tool to investigate the phase behavior of lipid components independent of the structure or the optical appearance.

5.3.4 Comparison of TMOR and DSC

The collected DSC data is summarized in Table 5.3. For the three substances under investigation, the differences between the stabilization at -50 °C for 10 min and at 4 °C for 30 min are minute, which makes them suitable as reference materials to prove the suitability of the new TMOR method. It was also important to show that the collected data can be compared to both the standard DSC procedure, in which the samples are cooled down to -50 °C, and to literature data collected with this standard method.

The differences between the determined temperatures with both methods cannot be completely explained by the variation in the scan rates because otherwise the TMOR data would have fit the extrapolation of the DSC data. The thermal lag is not only dependent on the scan rate but also on the sample volume which is considered for measurement. This means that not the whole sample volume is important but the volume at the point of measurement. If one considers the heat transfer inside a DSC pan, a volume of approximately 6 mm^3 needs to be heated. In contrast, the refractometer is equipped with a 1 mm^2 photo diode array and its beam enters not even 1 μm. This results in a volume considered for measurement in TMOR which is 6000 times smaller than the DSC sample volume. The thermal lag is a problem which needs to be addressed if phase transitions due to temperature changes are discussed. However, this problem is less pronounced using TMOR because the lower sample volume makes the measurement even more direct than the DSC.

In addition to the thermal lag, it is advantageous that an instantaneous temperature change occurs at the measurement point. Therefore, a very direct measurement is expected. At the same time this coinciding of the heating or cooling surface with the point of measurement is the origin of possible artifacts when measuring multicomponent systems. In these cases, a selective crystallization on the prism,

fractionation of high melting compounds, would cause a dramatic inhomogeneity of the sample and hence affect the measurement results.

Table 5.3: Onset, offset and peak temperatures during the phase transitions of *n*-hexadecane, palmitic acid and tripalmitate determined via DSC measurements at 2 °C/min and TMOR measurements at 0.5 °C/min.

			DSC (2 °C/min)			TMOR (0.5 °C/min)		
	$T_{stab.}$	phase transition	T_{onset} (°C)	T_{peak} (°C)	T_{offset} (°C)	T_{onset} (°C)	T_{peak} (°C)	T_{offset} (°C)
***n*-hexadecane**	-50 °C	crystallization	15.1	13.5	12.6	-	-	-
		melting	17.3	20.4	21.5	-	-	-
	4 °C	crystallization	15.2	13.6	12.6	16.0	15.8	15.6
		melting	17.3	20.4	21.5	17.4	17.8	18.1
palmitic acid	-50 °C	crystallization	60.6	57.8	55.9	-	-	-
		melting	61.9	65.5	67.8	-	-	-
	4 °C	crystallization	59.7	57.9	55.9	61.4	61.2	61.0
		melting	61.7	65.1	67.3	61.8	62.3	62.5
tripalmitate	-50 °C	crystallization	44.2	41.9	41.1	-	-	-
		melting 1st peak	45.0	46.5	47.2	-	-	-
		melting 2nd peak	59.6	64.0	64.9	-	-	-
	4 °C	crystallization	44.2	41.5	41.1	44.4	44.2	44.0
		melting 1st peak	45.0	46.5	47.2	43.6	45.0	46.0
		melting 2nd peak	59.7	64.1	64.9	60.0	61.8	62.0

The surface sensitivity and the directness of measurement is one of the advantages of the new TMOR method. However, one might be concerned about the birefringence of the crystal structure affecting the measurement. If it is assumed that the crystals are randomized, the local birefringence should be averaged in the plane without taking influence on the measurement. Due to the tempering from only one side of the sample an orientation of the crystals could take place. Since s-polarization is used for TMOR the orientation takes place in the z-direction and an ordinary beam is measured. Hence, because the calculation of the TMOR data is based on the measurement of the ordinary beam, the concerns due to potential orientation of the crystals are negligible. Anyhow, ongoing experiments to benchmark the results obtained by TMOR against conventional methods aim to evaluate these effects.

5.4 Conclusion

The new method of temperature modulated optical refractometry (TMOR) is comparable to the DSC in determining crystallization and melting events of pure substances. In evaluation of different crystallization regimes prior to DSC analysis only insignificant variations were encountered. This indicates that possible differences in DSC and TMOR are not due to the crystallization procedure for the material studied. The comparison of DSC onset, offset and peak temperatures with data obtained by TMOR show good agreement. One disadvantage is the limited cooling of the current prototype to minimum 4 °C. Hence, TMOR can be used as a possible device to determine phase transitions of the three investigated substance classes in a temperature range between 4 °C and 85 °C at the present moment. Nevertheless, if the cooling procedure can be extended to temperatures below 0 °C, TMOR could become even more competitive to DSC.

The melting and crystallization peaks measured by TMOR are narrower and thus the phase transitions occur in a shorter temperature range than the ones from DSC measurements and the response of the sample is more direct. This might be due to the slower heating and cooling rate because the peaks get narrower with decreasing rate of temperature change. Furthermore, the results obtained by TMOR could be more accurate due to the smaller sample size considered for measurement and less thermal lag because of more direct heat transfer. Additionally the better exploitation of the signal relating to the thermal expansion coefficient is believed to give rise to more accurate temperature determinations.

Supplementary, TMOR showed accurate data considering phase transitions. The provided time for the transitions is longer at slower scan rates. In addition, the undulation promotes the transition. If one considers the signal for tripalmitate, it could be that it almost diminished due to the overlapping of the melting of the unstable polymorphic form and the crystallization of the more stable polymorph. To determine properties like dn/dT or the thermal expansion coefficient could be a possible route to exploit accurate phase transition temperatures. Also, utilizing the undulation at low scan rates can help to increase the accuracy of the measurement. Besides the investigation of phase transitions, TMOR could be used to study kinetic effects. In addition, it could

be applied to measure suspension systems and calculating therefrom the solid fat content, which is an important parameter in the oils and fats industry. However, while such measurements of inhomogeneous systems and phase transitions are challenging these possibilities are still under investigation at this point.

Apart from the high sensitivity the sample preparation is easy and TMOR has low acquisition costs. The isothermal and dynamic measurements could yield more information about the microstructure and phase behavior of *n*-alkanes, fatty acids and triacylglycerides. To extend the applicability of TMOR, investigations of the phase behavior of edible fats and oils are currently conducted by the authors. This step is desirable because TMOR could be a helpful tool in quality assurance, thermal characterization, and phase transition monitoring in the food industry.

Acknowledgements

The authors would like to thank Anton Paar OptoTec GmbH for the support providing the prototype and room for discussion. In addition, the authors are grateful for the financial support of Anton Paar OptoTec and the Elsa Neumann scholarship of the federal state of Berlin.

6 EVALUATION OF TMOR PARAMETERS FOR THE INVESTIGATION OF FATS

6.1 Theoretical background

The temperature modulated optical refractometry (TMOR) is a novel method based on refractometry with an additional temperature undulation. The device and the method are explained in detail in chapter 3.2. TMOR was for the first time applied investigating the crystallization of fats and lipid mixtures. As mentioned, TMOR is based on refractometry. From this some challenges for the measurements arise such as that the reflection of the fats turning nearly white during crystallization and that fats become brittle during or after crystallization.

In this work, the applicability of TMOR for the determination of liquid-solid transition (crystallization / melting) of fats was studied. Therefore, parameters which could be adjusted for the TMOR measurements were varied. Three different scan rates for three distinct fats were investigated before the influence of the temperature amplitude and the period was examined. The overall goal for these preliminary tests was to determine the best applicable procedure for the investigations of fats using TMOR by the comparison with the established differential scanning calorimetry (DSC). In addition, different fats were used to see if and how the triacylglyceride (TAG) composition impacts the applicability of TMOR. For a reliable comparison, the samples need to be treated equally before each measurement so that the temperature history of the sample is the same.

Beside the fat composition and the scan rate, also the period and amplitude of the modulation during TMOR measurements influence the results. Care needs to be taken because the scan rate and both, the amplitude and the period, can interfere. Therefore, a proper combination of all three parameters needs to be chosen and, thus, the influence of amplitude and period is elucidated.

The graphical explanation of period and amplitude is given in Figure 6.1. The period of a sinus function is the time between two maxima of the wave, also referred to as wave length. The amplitude is the height of the signal. In this study, three different periods and three different amplitudes were investigated.

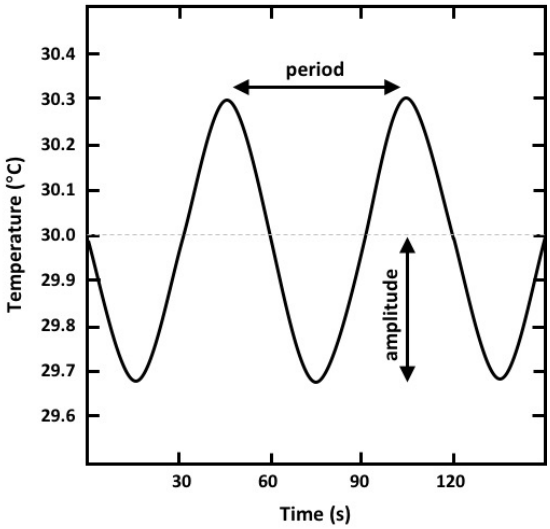

Figure 6.1: Explanation of amplitude and period of a modulated wave; the amplitude is referred to the height of the signal (°C) and the period to the time between two zero-crossings (s).

For the study on the influence of period and amplitude, fully hydrogenated palm oil was used because it shows a very narrow melting and crystallization range, respectively. The peak temperatures are only given for the graphs presented even though the analysis was performed in triplicate. The experiments were conducted at a scan rate of 2 °C/min.

The proper combination of scan rate, period, and amplitude might needs to be changed for other materials. A short explanation is given in Figure 6.2, where two different scan rates with the same modulation amplitude are shown. The red dashed curve represents a scan rate of 3 °C/min while the black dashed line symbolizes a scan rate of 0.75 °C/min. Both curves have the same amplitude of 0.5 °C. For the scan rate of 3 °C/min the modulation and the scan rate do not interfere which is why the temperature of 31.0 °C (upper grey solid line) is only achieved once during this measurement indicated by the yellow diamond. In contrast, the modulation comes across 29.5 °C (lower grey line) for nine times at a scan rate of 0.75 °C/min with the same amplitude. Only the red diamond represents the determination point at which the mean refractive index and the modulated one have the same value. The frequent achievement of one temperature can be crucial if the phase transition is happening at this temperature. Hence, care must be taken if the predefined amplitude impedes a proper measurement with the applied scan rate.

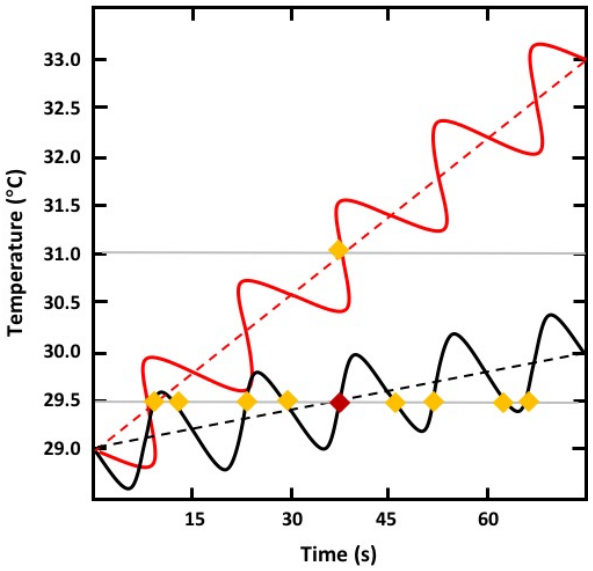

Figure 6.2: Interference of scan rate (red 3 °C/min, black 0.75 °C/min) and amplitude (0.5 °C) during temperature modulation.

6.2 Materials and Methods

6.2.1 Material properties

For the experiments, four different fats (shea butter, coconut oil, palm oil, and fully hydrogenated palm oil) were used and provided by ADM (Hamburg, Germany). Shea butter is mainly composed of stearic acid (C18:0) and oleic acid (C18:1) with minor amounts of palmitic (C16:0) and linoleic acid (C18:2) (Adomako, 1977). The TAG composition of coconut oil is characterized by medium-chain length TAGs (MCT) consisting of e.g. lauric acid (C12:0) and myristic acid (C14:0) (Salas *et al.*, 2009; Chaleepa, Szepes and Ulrich, 2010). These MCTs show a melting range typically around room temperature. Palm oil consists of a mixture of various TAGs, mainly POP (30.0 %), POO (25.0 %), POL (10.3 %), POS (5.9 %), PPP (5.3 %), and OOO (4.6 %), with palmitic (P), oleic (O), stearic (S), and linoleic acid (L) (Braipson-Danthine and Gibon, 2007). This variety causes a complex phase behavior and, thus, palm oil shows many different melting points.

The data collected in Table 6.1 is a summary of values for the melting and crystallization temperatures of the investigated fats determined by DSC. These values were used to evaluate the resulting TMOR data.

Table 6.1: Literature data of the crystallization (T_c) and melting (T_m) temperatures of coconut oil, shea butter and palm oil derived from literature.

sample	scan rate	T_m	T_c	reference
shea butter	-	32.0-45.0 °C	-	Firestone, 1999
shea butter	2 °C/min	38.0-39.5 °C	26.5-30.0 °C	Adomako, 1977
shea butter	5 °C/min	37.0 °C	-	Hajj Ali *et al.*, 2016
coconut oil	-	23.0-26.0 °C		Firestone, 1999
coconut oil	1 °C/min	11.4 °C	0.7 °C	Tan and Che Man,
		21.1 °C	2.7 °C	2002b
coconut oil	5 °C/min	12.4 °C	-0.7 °C	Tan and Che Man,
		22.5 °C	-7.9 °C	2002b
coconut oil	10 °C/min	7.9 °C	-2.9 °C	Tan and Che Man,
		23.6 °C	-16.5 °C	2002b
palm oil	-	33.0-40.0 °C	-	Firestone, 1999
palm oil	1 °C/min	0.9 °C	18.4 °C	Tan and Che Man,
		10.8 °C		2002b
		26.8 °C		
		41.5 °C		
palm oil	5 °C/min	0.2 °C	15.4 °C	Tan and Che Man,
		5.3 °C	6.1 °C	2002b
		21.9 °C	-2.9 °C	
		35.4 °C		
palm oil	10 °C/min	2.9 °C	12.9 °C	Tan and Che Man,
		6.4 °C	-5.7 °C	2002b
		27.2 °C		
		35.8 °C		

6.2.2 Devices

Three different TMOR parameters were investigated: the scan rate (2 °C/min, 5 °C/min, 10 °C/min), the amplitude (0.25 °C, 0.5 °C, 0.75 °C), and the period (30 s, 60 s, 120 s).

The sample preparation for TMOR measurements was done in preliminary tests (data not shown). Approximately 100 µl of sample were placed directly on the prism. The samples were poured into a cylindrical geometry to generate a crystallization/ melting which occurs only vertically. This geometry was applied for the fats with a low degree of saturation like palm oil. For fats with a narrow composition range (e.g. fully hydrogenated palm oil), which means mostly saturated fatty acids in this case, it is recommended to use a stamp to ensure proper contact between the sample and the prism during the whole measurement. These samples which are too hard or brittle needed to be examined carefully.

The samples were heated at different scan rates, 2 °C/min, 5 °C/min, and 10 °C/min, respectively, until 80 °C were reached. This temperature was held for 10 min before the same cooling rate as the heating rate was applied to investigate the crystallization behavior. Due to limitations of TMOR the minimum temperature at which data can be obtained is 5 °C. The parameters for the TMOR measurements were a period of 60 s and an amplitude of 0.25 °C. The sample was placed directly on the prism. The peak temperature analysis of the TMOR data was done for the values of abs (α).

To evaluate the data obtained by TMOR, differential scanning calorimetry (DSC) was used as the reference method. A device from Netzsch (DSC 204 F1 Phoenix, NETZSCH-Geraetebau GmbH, Selb, Germany) was used. The temperature profiles were executed in the same manner like the TMOR measurements. Approximately 8 mg of sample were weighed in aluminum pans and sealed hermetically. An empty pan was used as reference.

All DSC measurements were performed in duplicate while the TMOR measurement was done at least in a triplicate to prove its applicability to properly study fat crystallization.

Polarized light microscopy (PLM) was used to determine the microscopic structure of the samples at various temperatures. A Zeiss AxioScope (Carl Zeiss Jena GmbH, Jena, Germany) equipped with a camera (AxioCam ICm1) was used. A scan rate of 2 °C/min was applied using a temperature controlled stage (Linkam Scientific Instruments, Surrey, UK). The micrographs were captured at different temperatures where the samples were in transient state.

6.3 Influence of fat composition and scan rate

The crystallization and melting behavior of lipid mixtures is influenced by its composition and the applied scan rate. Therefore, the effect of these factors on the TMOR measurements was examined.

The thermogram of shea butter determined by DSC is depicted in Figure 6.3a. The increase of the scan rate results in a crystallization peak temperature which is shifted to lower temperatures and a melting temperature which is detected at higher temperatures. A scan rate of 2 °C/min resulted in a melting peak at 38.9 ± 0.1 °C and a crystallization peak at 13.7 ± 0.1 °C, respectively. The melting peak temperature at a heating scan rate of 5 °C/min was determined at 35.6 ± 0.5 °C by DSC while the crystallization peak was detected at 13.5 ± 0.2 °C. With a scan rate of 10 °C/min, the melting temperature was determined at 29.9 ± 1.3 °C and the crystallization peak temperature at 10.5 ± 0.3 °C.

Figure 6.3b depicts the DSC thermogram of coconut oil crystallized and melted at a rate of 2 °C/min (black line). The crystallization peak temperature was found at 9.8 ± 0.1 °C and the melting peak at 27.1 ± 0.1 °C. Taking a look at a scan rate of 5 °C/min (dark grey line), the melting peak temperature was determined at 26.4 ± 0.6 °C. The crystallization could not be detected because the minimum temperature which could be achieved with TMOR was higher than the temperature at which the coconut oil is completely solid. Therefore, the DSC temperature profile was only conducted until 5 °C. The increase of the scan rate up to 10 °C/min was investigated because it is one of the mostly used scan rates in fat technology. The DSC thermogram shows a melting peak detected at 28.1 ± 0.1 °C while there was no crystallization peak visible for the experiment conducted at 10 °C/min (light grey line).

The investigations by DSC of palm oil at a scan rate of 2 °C/min showed melting peak temperatures at 11.7 ± 0.9 °C, 27.1 ± 2.7 °C, 37.2 ± 1.8 °C, and 43.7 ± 2.7 °C, respectively (see Figure 6.3c, black line). These various melting points occurred because palm oil has a diverse composition of TAGs which all melt at different temperatures (Braipson-Danthine and Gibon, 2007) The crystallization temperature was detected at 19.8 ± 0.7 °C. At 5 °C/min the peak melting temperatures were detected at 10.1 ± 1.0 °C, 33.5 ± 1.1 °C, and 43.9 ± 0.8 °C, respectively (see Figure 6.3c, dark grey line). The crystallization took place at 18.6 ± 0.3 °C. The thermogram at a scan rate of 10 °C/min is indicated by the light grey line in Figure 6.3c. The melting peaks were determined at 11.9 ± 0.5 °C, 35.7 ± 1.7 °C, and 44.0 ± 0.5 °C, respectively while the crystallization peak was detected at 15.9 ± 0.1 °C.

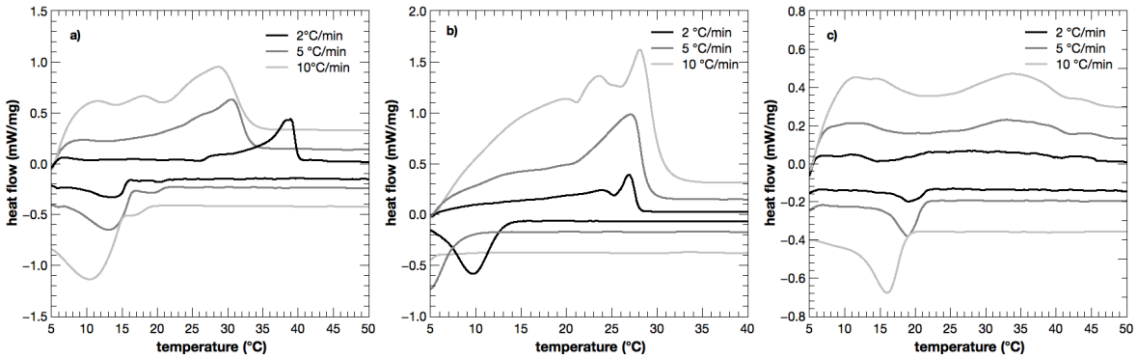

Figure 6.3: DSC thermogram of shea butter (a), coconut oil (b), and palm oil (c) at 2 °C/min (black line), 5 °C/min (dark grey line), and 10 °C/min (light grey line) during melting (positive heat flow) and crystallization (negative heat flow).

The analysis of TMOR graphs was done using the values of the absolute thermal expansion coefficient α (abs (α)). These values were considered because they were always in a positive range while the values of the real and the imaginary part showed sometimes negative values. This was caused by a not suitable combination of the applied scan rate and amplitude leading to calculating artefacts. Hence, these combinations were later excluded as not-suitable for the investigation of the phase behavior of lipid mixtures.

Investigated by TMOR, the melting peak temperature of shea butter was detected at 34.9 ± 1.9 °C (see Figure 6.4a, black line) and the crystallization occurs at a peak temperature of 14.3 ± 0.2 °C (see Figure 6.4b, black line) when a scan rate of 2 °C/min was applied. For 5 °C/min, the crystallization peak was determined at 13.3 ± 0.3 °C (see Figure 6.4a, dark grey line). The melting graph showed three peaks in the thermal expansion coefficient α located at 32.5 ± 2.0 °C, 35.6 ± 2.0 °C, 38.2 ± 2.1 °C (see Figure 6.4b, dark grey line).

The application of a scan rate of 10 °C/min lead to the detection of a crystallization peak temperature at 14.5 ± 0.4 °C (see Figure 6.4a, light grey line). The melting peak temperatures were detected at 31.5 ± 1.2 °C, 37.4 ± 0.9 °C, and 42.5 ± 0.4 °C, respectively (see Figure 6.4b, light grey line).

In comparison, Figure 6.4c and Figure 6.4d show the TMOR measurements of coconut oil during crystallization and melting, respectively. The crystallization temperature with a scan rate of 2 °C/min was found at 5.2 ± 0.3 °C and the melting occurred at 13.5 ± 0.4 °C. TMOR seems to detect the melting behavior at a lower temperature, which means more direct, compared to the DSC. In contrast, the crystallization was detected later which is in contradiction to the results found for shea butter. The melting peak temperature at 5 °C/min was determined at 14.7 ± 2.1 °C while the crystallization occurred at 7.7 ± 0.1 °C. The shift of the melting temperature to a higher temperature compared to a scan rate of 2 °C/min can be explained by the thermal lag. Smaller rates lead to a decrease of the thermal lag while faster rates increase the measured melting temperature and lead to a broadening of the peaks (Tan and Che Man, 2002a; Chiu and Prenner, 2011; Peyronel and Marangoni, 2014a). In comparison to the DSC, a crystallization temperature could be detected by TMOR. This could be an indication that the device indeed has a higher sensitivity compared to the DSC. The TMOR graphs obtained at a scan rate of 10 °C/min show a crystallization peak at 8.3 ± 0.3 °C and two kinks in the refractive index during melting at 15.5 ± 0.3 and 20.5 ± 0.7 °C, respectively.

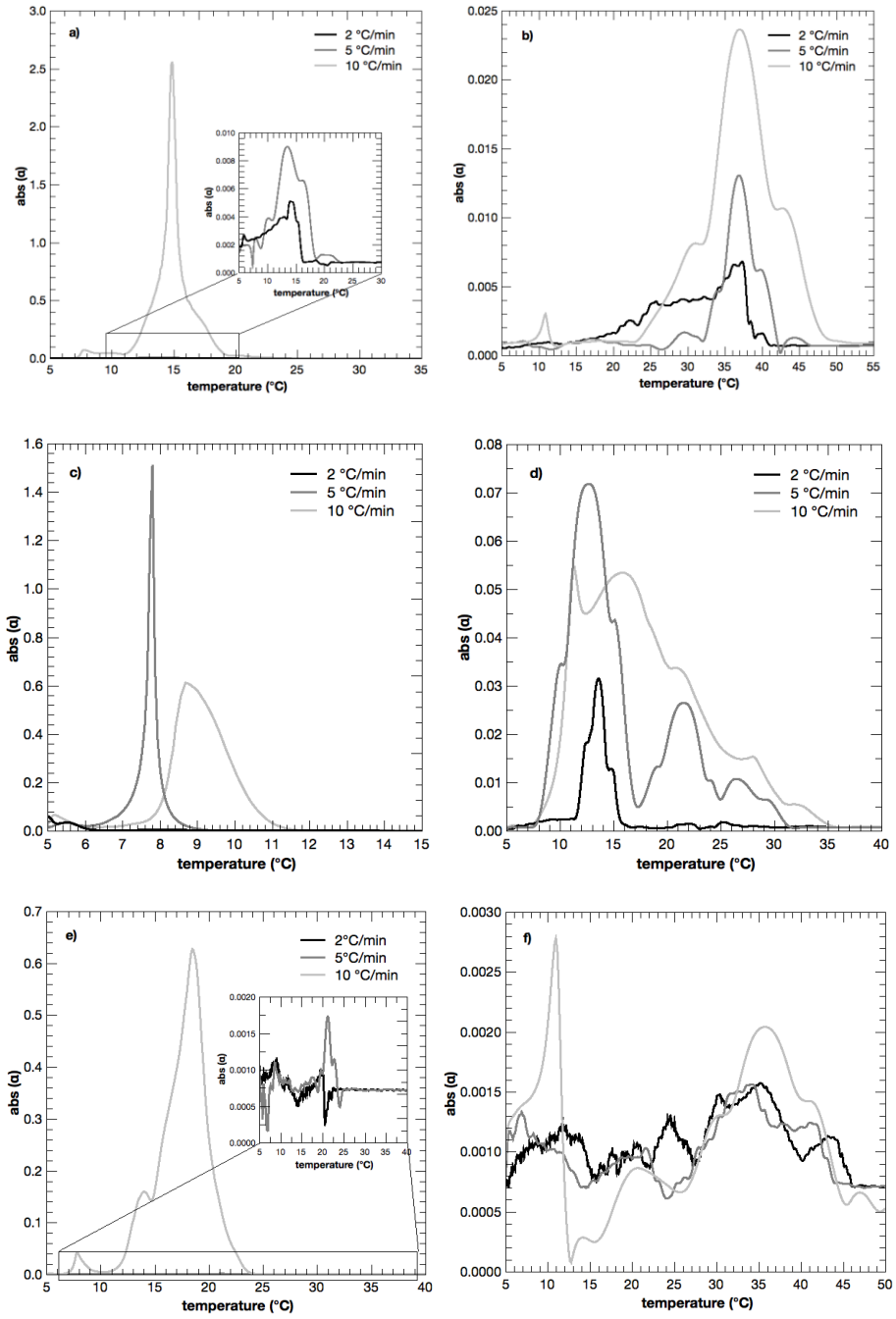

Figure 6.4: TMOR graphs of crystallization (left column) and melting (right column) of shea butter (a and b), coconut oil (c and d), and palm oil (e and f) at 2 °C/min (black line), 5 °C/min (dark grey line), and 10 °C/min (light grey line), period 60 s, amplitude 0.25 °C.

Using TMOR, the melting temperatures using a scan rate of 2 °C/min were determined at 9.9 ± 2.0 °C, 25.3 ± 0.7 °C, 35.9 ± 1.3 °C, and 43.7 ± 0.4 °C for palm oil, respectively (see Figure 6.4e and f, black line). The distinct peaks can be explained by the variety of TAGs in palm oil, each contributing to the complex melting behavior. Beside the last peak, all melting temperatures were lower compared to the DSC

measurement. The higher crystallization peak temperature of 20.7 ± 1.0 °C detected by TMOR could as well as the lower melting temperatures be related to the more direct heat transfer. At a scan rate of 5 °C/min, TMOR detected phase transitions during heating at 7.5 ± 0.9 °C, 23.0 ± 0.9 °C, 34.1 ± 0.3 °C, and 41.6 ± 0.4 °C, respectively, while the crystallization was determined at a peak temperature of 21.0 ± 0.4 °C (see Figure 6.4e and f, dark grey line). The crystallization was determined at a higher temperature by TMOR compared to DSC. In addition, more melting peaks were detected. Both findings support the conclusion that TMOR is more sensitive to phase transitions in comparison to the DSC method.

However, a scan rate of 5 °C/min could be too fast for the investigation of the crystallization behavior of palm oil by TMOR because the applied modulation did not fit to the scan rate properly. This was also visible when TMOR data was recorded at 10 °C/min, which is indicated with the light grey lines in Figure 6.4e and f. Melting peaks were determined at 11.1 ± 0.1 °C, 35.7 ± 0.3 °C, and 41.4 ± 0.2 °C, respectively. It seems that the modulation did not fit properly to the applied scan rate. This becomes even clearer if the crystallization is considered. The peak temperature was detected at 15.9 ± 0.1 °C by DSC and at 18.6 ± 0.1 °C by TMOR. Even though this tendency supports the assumption that TMOR is more sensitive and detects the phase transition earlier compared to DSC, the modulation was not suitable to the applied scan rate. The combination resulted in partially negative peaks which make the data not reliable.

The microscopy pictures were taken to obtain a visualization of the experimental data from DSC and TMOR measurements. The polarized light micrographs at transient states of the three investigated fats are shown in Figure 6.5. The micrographs a, b, and c show the crystallization of shea butter at 21.0 °C, 16.0 °C, and 8.0 °C, respectively. Coconut oil crystallization is depicted in inserts d, e, and f at 11.0 °C, 8.0 °C, and 5.0 °C, respectively. The crystallization of palm oil is shown in the micrographs g-i at 24.0 °C, 19.0 °C, and 5.0 °C, respectively.

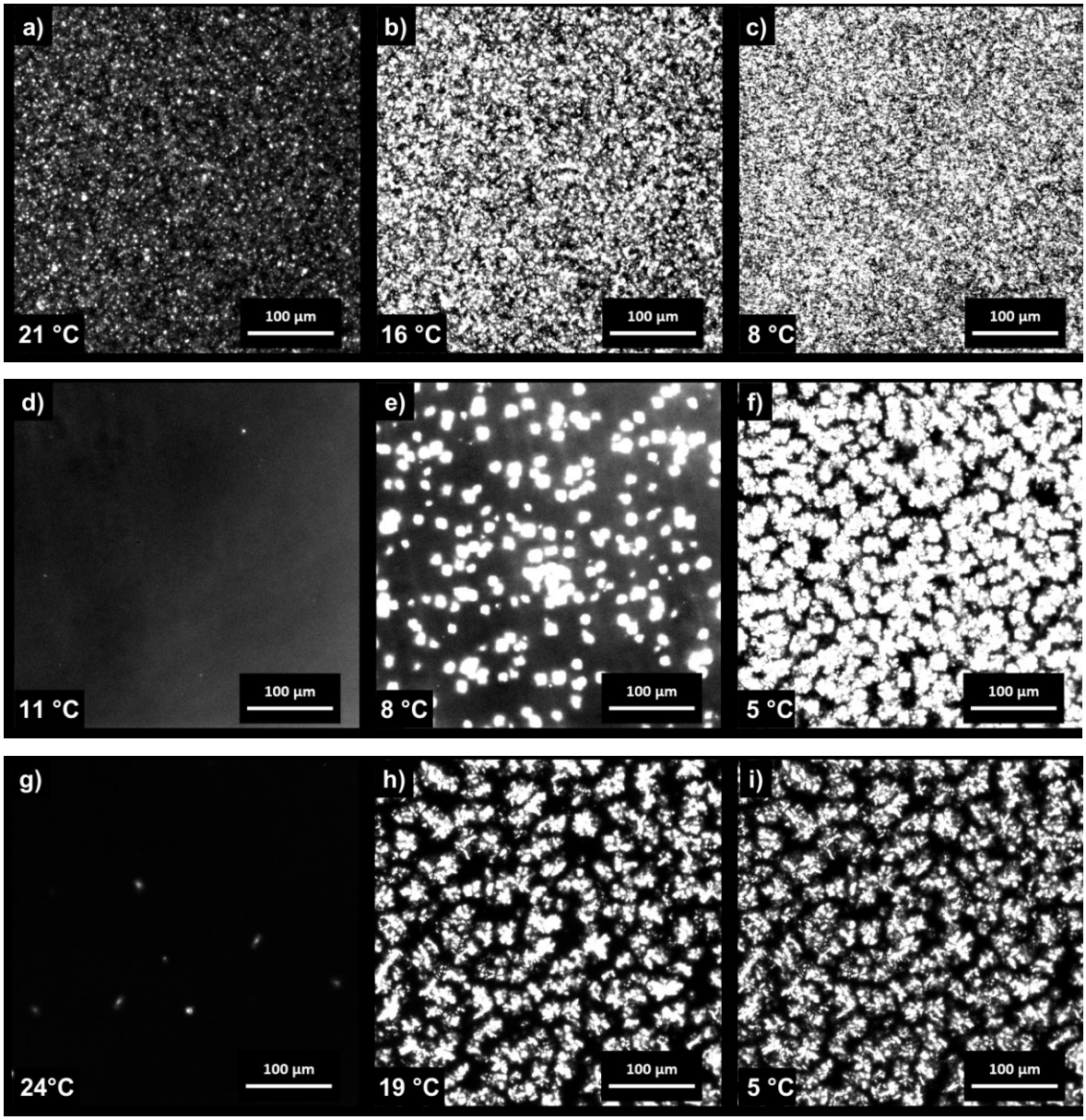

Figure 6.5: Polarized light micrographs of shea butter (a-c), coconut oil (d-f), and palm oil (g-i) during cooling at 2 °C/min, micrographs captured at transient states at 21.0 °C (a), 16.0 °C (b), and 8.0 °C (c), the scale bar represents 100 µm.

Since shea butter is composed half of unsaturated and half of saturated fatty acids the distribution of the crystals and the dark areas is not surprising. It is surprising that the PLM reveals that the sample was already crystallized at 16.0 °C (see Figure 6.5b) while both, DSC and TMOR, detected the phase transition at a lower temperatures. However, the small visible crystals in Figure 6.5a at 21.0 °C indicate the onset of crystallization and could be associated with small bump shown in the DSC thermograms (see Figure 6.3). An explanation for the crystallization at higher

temperatures could be that small particles on the microscope slide acted as nuclei helping inducing secondary nucleation. This could explain the higher crystallization temperature.

The crystals of coconut oil formed at a cooling rate of 2 °C/min are depicted in Figure 6.5d-f. The crystallization starts at around 8.0 °C (see Figure 6.5e). It can be seen that at 5.0 °C, in contrast to shea butter, many crystals are formed of about 25 μm in diameter (see Figure 6.5f). This supports the detected crystallization peak temperatures of both DSC and TMOR. The temperature profile during cooling seems to promote the formation of single crystals.

The PLM micrographs displayed in Figure 6.5g-i show the microstructure during crystallization of palm oil which is initiated at around 24.0 °C (see Figure 6.5g). In the micrograph at 5.0 °C (see Figure 6.6i) dark areas are visible which can be referred to still liquid oil. This means that not the complete palm oil was crystallized at the displayed temperatures and it can be concluded that the fat should have been cooled down further to guarantee complete crystallization. However, the given temperature range of TMOR limited the application. This may lead to the assumption that TMOR should be predominantly applied for fats and oils which are completely solid at 5.0 °C to guarantee the proper analysis of the crystallization and melting behavior.

During heating micrographs were captured at 11.0 °C, 28.0 °C, and 32.0 °C (see Figure 6.6). The dark areas represent the liquid TAGs with mostly unsaturated fatty acids. The crystals have a size of less than 1 μm and are uniformly distributed over the sample.

The micrographs captured during melting show that some areas are already liquid at 28.0 °C (see Figure 6.6b) indicated by the dark parts. The melting is nearly completed at 32.0 °C (see Figure 6.6c). This is lower than the values determined by DSC and TMOR and could be explained by the differences in heat transfer.

The vanishing of the coconut crystal network starts at around 20.0 °C during heating (see Figure 6.6e). Since there are crystals still visible at 20.0 °C during heating, with TMOR probably not all crystals were detected but one measured a partial fraction melting. The kink in the refractive index at around 27.0 °C might be the melting of the last remaining crystals which can also be seen in the micrograph during melting.

The melting transition states of palm oil are shown in Figure 6.6g-i. The melting starts at 42.0 °C (see Figure 6.6h) and is almost finished at 47.0 °C (see Figure 6.6i). The temperatures are slightly higher than detected by DSC and TMOR. This could be explained by the potentially lower heat transition through the glass microscope slide in comparison to the aluminum DSC pan or the TMOR prism.

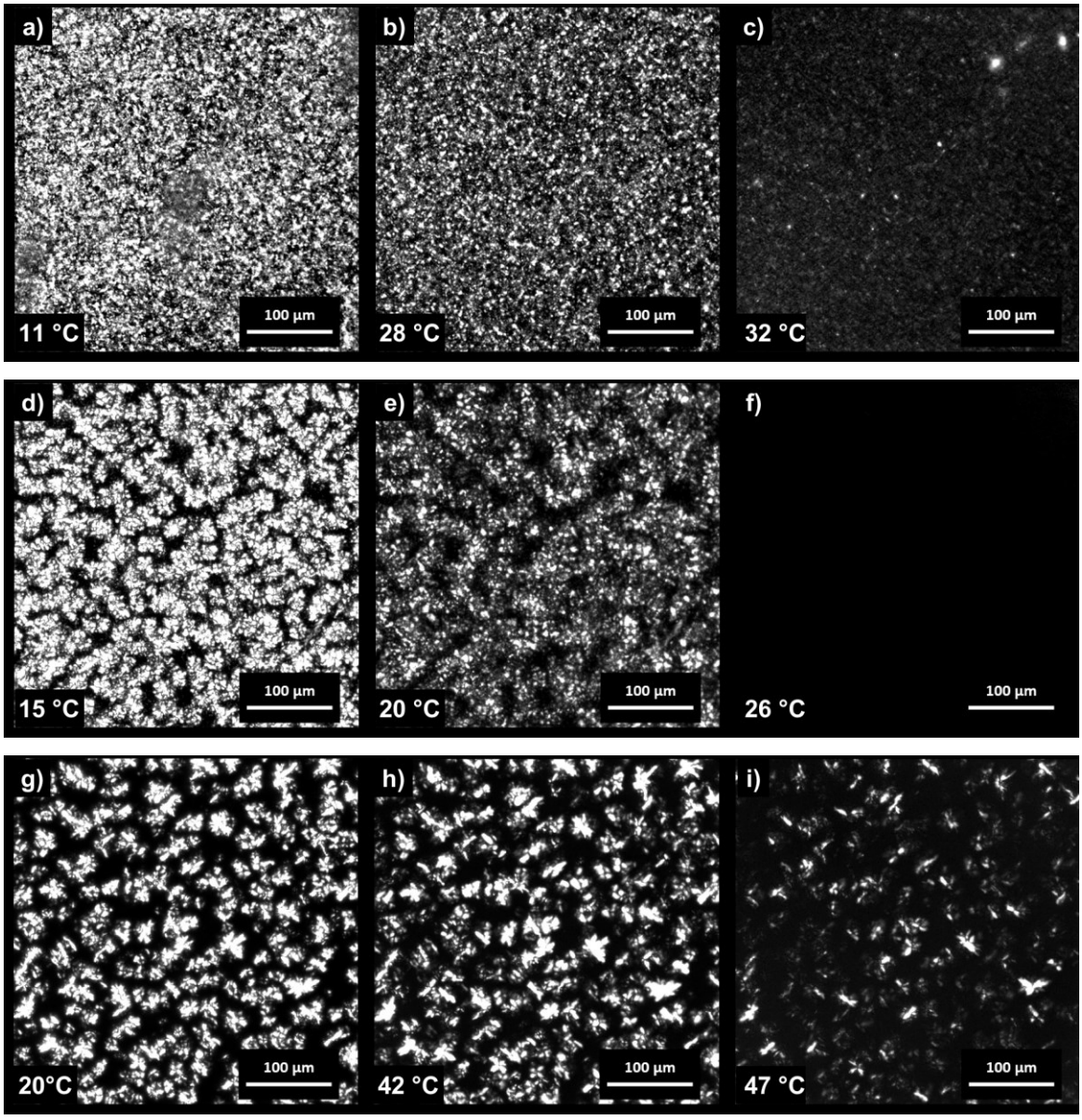

Figure 6.6: Polarized light micrographs of shea butter (a-c), coconut oil (d-f), and palm oil (g-i) during heating at 2 °C/min, micrographs captured at transient states at 11.0 °C (a), 28.0 °C (b), and 32.0 °C (c), the scale bar represents 100 µm.

The comparison of all three scan rates investigated and the literature data of shea butter are listed inTable 6.2. The thermal lag is visible for the DSC measurements for the used scan rates which means that a higher cooling rate leads to a lower crystallization peak temperature. However, during melting, a higher heating rate normally results in a higher melting peak temperature which was not found for shea butter. In contrast, the TMOR data depending on the scan rate progresses in accordance to the theory and shows some thermal lag.

Table 6.2: Melting and crystallization peak temperatures of shea butter determined at different rates (2 °C/min, 5 °C/min, 10 °C/min).

	scan rate	DSC	TMOR	literature
melting	2 °C/min	38.9 ± 0.1 °C	34.9 ± 1.9 °C	38.0-39.5 °C
	5 °C/min	35.6 ± 0.5 °C	35.6 ± 2.0 °C	37.0 °C
	10 °C/min	29.9 ± 1.3 °C	37.4 ± 0.9 °C	
crystallization	2 °C/min	13.7 ± 0.1 °C	14.3 ± 0.2 °C	26.5-30.0 °C
	5 °C/min	13.5 ± 0.2 °C	13.3 ± 0.3 °C	
	10 °C/min	10.5 ± 0.3 °C	14.5 ± 0.4 °C	

Compared to the DSC, the melting temperature is lower and the crystallization temperature is higher if determined by TMOR. This could be due to the direct heat transfer into the sample when using TMOR because the sample is placed directly on the prism whereas during the DSC measurement the sample is placed in a sealed aluminum pan. In addition, the sample volume considered for TMOR is smaller than for DSC (around 0.001 mm^3 vs. 10 - 20 mm^3). At 5 °C/min, the crystallization temperature is in accordance with the DSC measurement, while during the heating more melting peaks were observed using TMOR. The same results were found for a scan rate of 10 °C/min.

For the melting behavior, the detected peak temperatures are in the same range as the literature. However, the crystallization point was determined at much lower temperatures in this study. This could be due to the fact that in the cited literature another method to determine crystallization was used. In addition, a small peak is visible during the crystallization of shea butter at around 22.0 °C, which could be an indication that already at higher temperatures a part of the sample crystallizes. This is also shown in the PLM micrographs in Figure 6.5a. Since the crystallization point determined by DSC and by TMOR are quite similar it could also be that the shea butter used in the cited study has a different composition.

In Table 6.3, the peak melting and crystallization temperatures of coconut oil at different scan rates are listed and compared to literature data. It can be seen, like also shown for shea butter, that the melting is detected at lower temperatures when TMOR is used compared to the DSC. The crystallization was detected by TMOR also at higher rates when there was no phase transition measurable by the DSC. This phenomenon could be a hint that TMOR is a more sensitive method. The comparison to the literature data shows that the data recorded with the DSC in this study always resulted in a higher melting peak temperature. It was confirmed that it was not possible to detect the crystallization since all given crystallization temperatures are below 5.0 °C. However at 2 °C/min there was a peak detected. One explanation could be a different composition of the examined shea butter in comparison to the literature data. The melting peak temperatures measured by TMOR are close to the literature data and show a slight shift to higher temperatures with increasing scan rate. The high accuracy of TMOR made it possible to determine a crystallization temperature for all rates even though the temperature was shifted to higher temperatures. This is rather illogical and could be a result of the poor fit of the modulation and the scan rate.

Table 6.3: Melting and crystallization peak temperatures of coconut oil determined by DSC and TMOR compared with literature data.

	scan rate	DSC	TMOR	literature
melting	2 °C/min	27.1 ± 0.1 °C	13.5 ± 0.4 °C	11.4 °C 21.1 °C
	5 °C/min	26.4 ± 0.6 °C	14.7 ± 2.1 °C	12.4 °C 22.5 °C
	10 °C/min	28.1 ± 0.1 °C	15.5 ± 0.3 °C 20.5 ± 0.7 °C	7.9 °C 23.6 °C
crystallization	2 °C/min	9.8 ± 0.1 °C	5.2 ± 0.3 °C	0.7 °C 2.7 °C
	5 °C/min	n.d.	7.7 ± 0.1 °C	-0.7 °C -7.9 °C
	10 °C/min	n.d.	8.3 ± 0.3 °C	-2.9 °C -16.5 °C

The comparison of the peak temperatures of phase transitions of palm oil determined with TMOR, DSC, and the associated literature data are listed in Table 6.4. Both, DSC and TMOR detected the melting transition peaks at higher temperatures compared to the literature. This could be explained by possible different handling before the measurement which influences the melting behavior or by distinct origins of the samples which cause varieties in the composition. In addition, more peaks were detected at lower scan rates which is in accordance to the literature (Tan and Che Man, 2002b). The thermal lag for the determination of the crystallization temperature was seen for the DSC and the literature data but did occur to a smaller extend for TMOR data.

Table 6.4: Palm oil peak temperatures measured by DSC and TMOR during heating and cooling at different scan rates (2 °C/min, 5 °C/min, 10 °C/min) compared to literature data.

	scan rate	DSC	TMOR	literature
melting	2 °C/min	11.7 ± 0.9 °C	9.9 ± 2.0 °C	0.9 °C
		27.1 ± 2.7 °C	25.3 ± 0.7 °C	10.8 °C
		37.2 ± 1.8 °C	35.9 ± 1.3 °C	26.8 °C
		43.7 ± 2.7 °C	43.7 ± 0.4 °C	41.5 °C
	5 °C/min	10.1 ± 1.0 °C	7.5 ± 0.9 °C	0.2 °C
			23.0 ± 0.9 °C	5.3 °C
		33.5 ± 1.1 °C	34.1 ± 0.3 °C	21.9 °C
		43.9 ± 0.8 °C	41.6 ± 0.4 °C	35.4 °C
	10 °C/min			2.8 °C
		11.9 ± 0.5 °C	11.1 ± 0.1 °C	6.4 °C
		35.7 ± 1.7 °C	35.7 ± 0.3 °C	27.2 °C
		44.0 ± 0.5 °C	41.4 ± 0.2 °C	35.8 °C
crystallization	2 °C/min	19.8 ± 0.7 °C	20.7 ± 1.0 °C	18.4 °C
	5 °C/min	18.6 ± 0.3 °C	21.0 ± 0.4 °C	15.4 °C
				6.1 °C
				-2.9 °C
	10 °C/min	15.9 ± 0.1 °C	18.6 ± 0.1 °C	12.9 °C
				-5.7 °C

In summary, both scan rates of 5 °C/min and 10 °C/min seem not to fit the applied amplitude and period for all samples. On the one hand, the peak temperatures are too high for the melting process. On the other hand, negative values occurred which indicate that the calculation based on the modulation was not done appropriately. This results in a calculation error giving negative values which cannot be used. Thus, the application of a these scan rates for TMOR for the investigation of the investigated oils is not recommended in combination with an amplitude of 0.25 °C and a period of 60 s.

Therefore, a smaller rate should be applied. It was shown that the TMOR method is well applicable for the investigation of the phase behavior of the examined fats at a scan rate of 2 °C/min. Subsequently, the influence of amplitude and period depending on the scan rate needs to be investigated.

6.4 Influence of amplitude and period

6.4.1 Amplitude

The consideration of the amplitude can be crucial because it could impact the determination of the phase transition due to the temperature variation due to the modulation. If a phase transition occurs within a small temperature range a large amplitude can give a too low transition temperature. Since the modulation is required for the calculation of the real and imaginary part of the thermal expansion coefficient it is necessary to determine the suitable amplitude which should be large enough to ensure a proper calculation but not too large to impair the applied scan rate. Three different amplitudes (0.25 °C, 0.5 °C, 0.75 °C) were investigated while the modulation period was kept at 30 s because this was the smallest period which could be applied by the device. For all measurements, the modulation was first checked on its regularity. Second, the calculations of the TMOR peaks during cooling and heating were evaluated.

A modulation amplitude of 0.25 °C was applied on the sample shown in Figure 6.7. Both, the refractive index and the temperature are plotted over time (Figure 6.7a). A deeper insight into the modulation during melting is shown in Figure 6.7b. The grey line refers to the actual temperature while the black dashed line is the mean temperature of one period of modulation. The solid black line represents the determined refractive index depending on the modulated temperature. The red dashed line represents the mean refractive index.

It can be seen that the modulation was not smooth since the solid black line shows spikes and lacks a sinusoidal modulation, like explained in chapter 3.2. Considering the calculated peaks during cooling (Figure 6.8a) and heating (Figure 6.8b) it was shown that despite the fact that the chosen amplitude did not suit the applied scan rate the calculation basically worked since positive peaks are visible in the thermal expansion

coefficient α. The crystallization peak temperature is at 46.7 °C while the melting peak temperature was detected at 50.0 °C and 58.7 °C, respectively. However, the amplitude of 0.25 °C is not recommended in combination with a scan rate of 2 °C/min and a period of 30 s for the investigation of the phase transition of highly saturated fats such as fully hydrogenated palm oil.

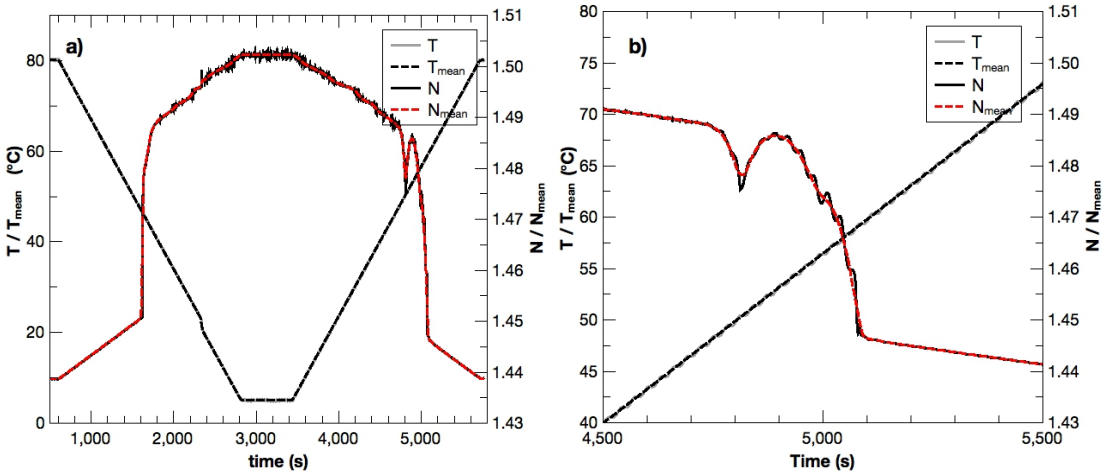

Figure 6.7: Temperature/ mean temperature and refractive index/ mean refractive index of fully hydrogenated palm oil plotted against temperature, 2 °C/min, 0.25 °C amplitude, 30 s period; a) complete time range b) zoom.

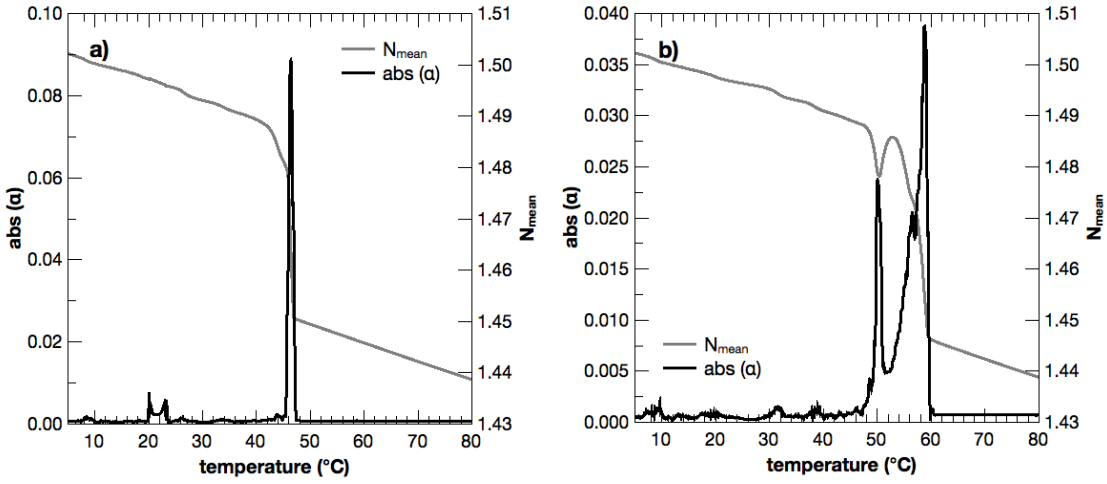

Figure 6.8: TMOR graphs of fully hydrogenated palm oil, 0.25 °C amplitude, 30 s period, a) cooled at 2 °C/min, b) heated at 2 °C/min.

Since the modulation of 0.25 °C prove not to be suitable, the modulation amplitude was increased to 0.5 °C. In Figure 6.9, the temperature and refractive index are plotted over time. The spikes in the refractive index are almost diminished in comparison to the results when using an amplitude of 0.25 °C. The calculated peaks from the modulation are shown in Figure 6.10. The crystallization (a) occurred at a peak temperature of 46.7 °C while the melting point was determined at 49.6 °C and 58.3 °C (b) probably referring to two polymorphic forms. At an amplitude of 0.5 °C the calculation of the peaks seemed to work better than at 0.25 °C.

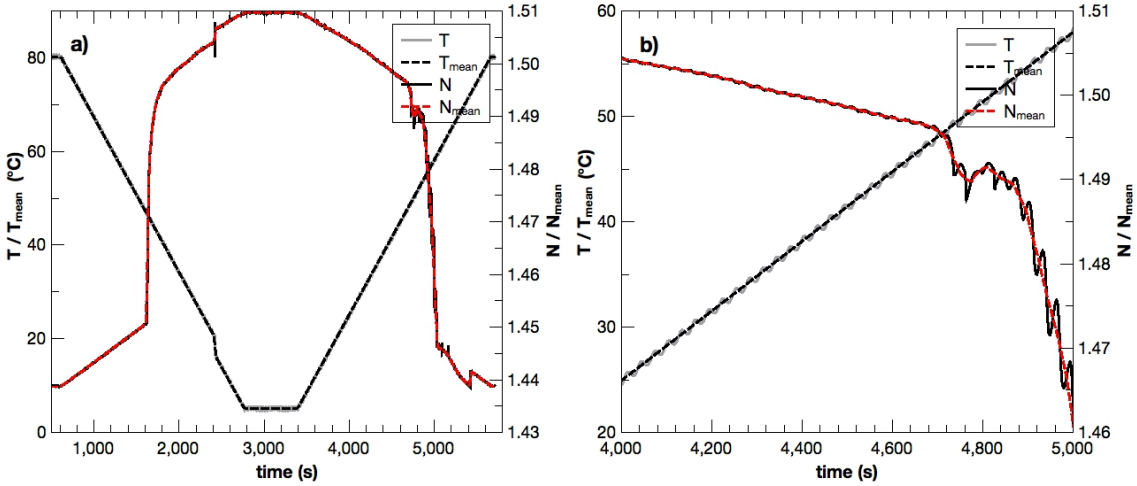

Figure 6.9: Temperature/ mean temperature and refractive index/ mean refractive index of fully hydrogenated palm oil plotted against temperature, 2 °C/min, 0.5 °C amplitude, 30 s period; a) complete time range b) zoom.

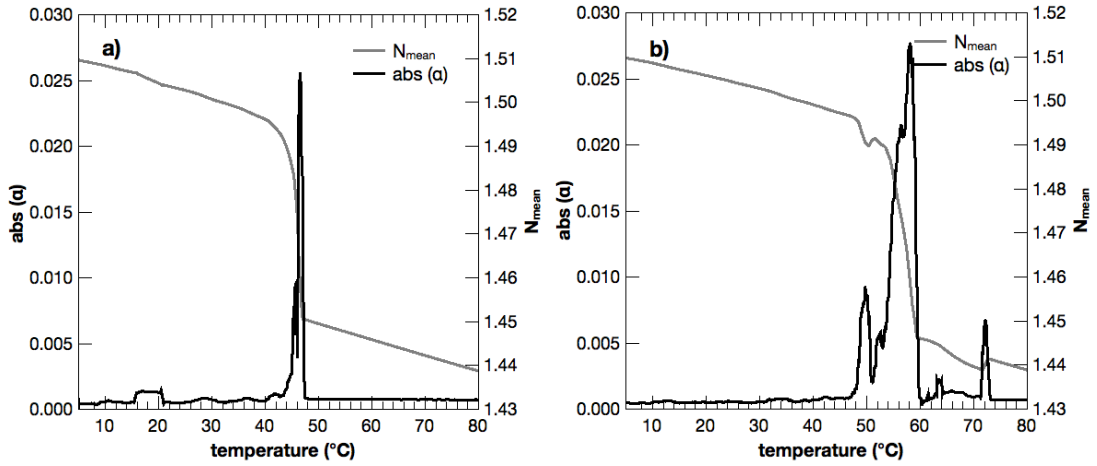

Figure 6.10: TMOR graphs of fully hydrogenated palm oil, 0.5 °C amplitude, 30 s period, a) cooled at 2 °C/min, b) heated at 2 °C/min.

The modulation with an amplitude of 0.75 °C is depicted in Figure 6.11. The spikes in the refractive index are less than the results with an applied amplitude of 0.25 °C but more than for the results obtained with an amplitude of 0.5 °C. The calculation of the crystallization and melting peaks, shown in Figure 6.12a and b, respectively, were done properly as indicated by the lack of negative values for α. The peak temperatures were detected at 46.0 °C for crystallization and at 49.1 °C and 58.1 °C for melting. The crystallization is determined at a lower temperature compared to literature data (49.0 °C) (deMan, deMan and Blackman, 1989). The second melting peak is in accordance with the literature (57.6 °C) while the first melting peak is higher (41.8 °C) (Kloek, Walstra and van Vliet, 2000). This could be because the first melting peak depends on the previous crystallization behavior of the polymorph while the second peak is a result of the melting of the less stable polymorph.

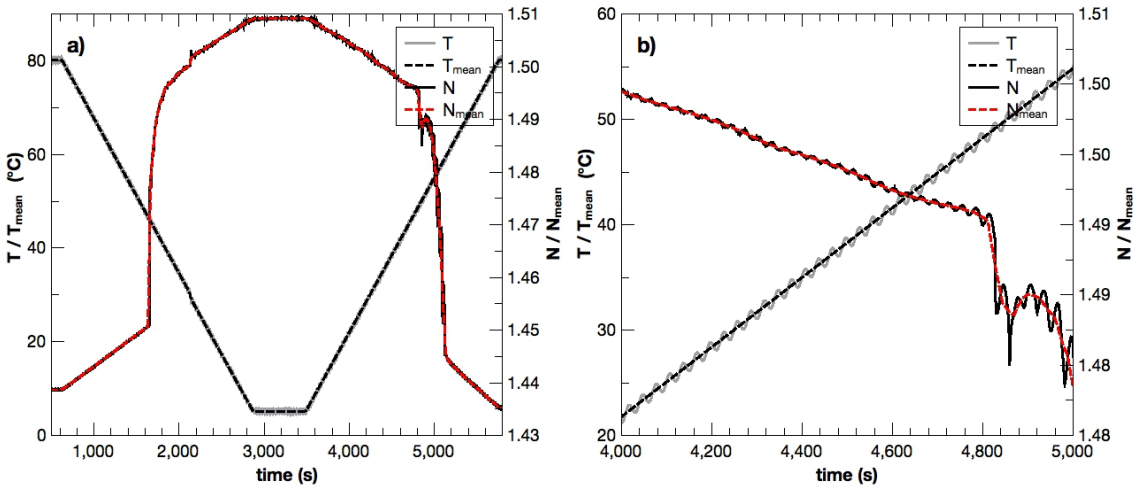

Figure 6.11: Temperature/ mean temperature and refractive index/ mean refractive index of fully hydrogenated palm oil plotted against temperature, 2 °C/min, 0.75 °C amplitude, 30 s period; a) complete time range b) zoom.

Kloek and coworkers cooled their sample at a rate of 20 °C/min. Thus, they treated their samples differently before the analysis of the melting behavior. This can explain the different melting temperatures of the first peak because the samples on the TMOR prism were cooled at 2 °C/min. In addition, the small peak during melting which is referred to a less stable polymorphic form is the most pronounced applying an amplitude of 0.75 °C. The comparison of all three amplitudes shows that temperature

at which the first melting peak is detected decreases from 50.0 °C to 49.6 °C to 49.1 °C. A reasonable explanation could be that the larger amplitude stimulates the phase transition which results in a lower transition temperature. Hence, one could conclude that this amplitude might be the best to apply but the combination of amplitude and scan rate always need to be kept in mind as explained above. In addition, the modulation showed the least spikes with an amplitude of 0.5 °C applied.

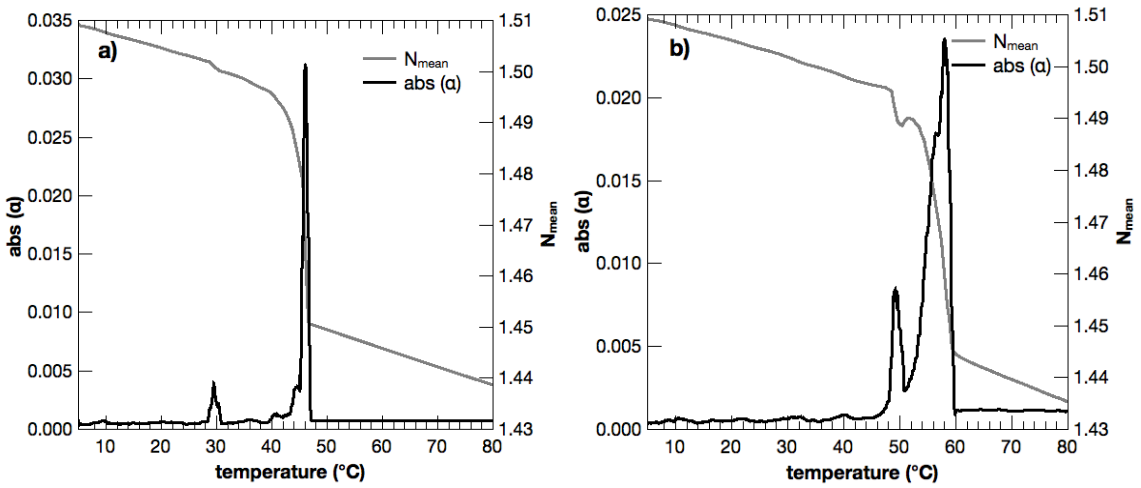

Figure 6.12: TMOR graphs of fully hydrogenated palm oil, 0.75 °C amplitude, 30 s period, a) cooled at 2 °C/min, b) heated at 2 °C/min.

6.4.2 Period

The period λ was varied between 30 s, 60 s, and 120 s, respectively. Overall, for isothermal experiments the statement that larger periods lead to a better calculation is true. In contrast, small periods should be applied if ramps are applied by TMOR. Since a heating and cooling rate of 2 °C/min was used the applied period could influenced the validity of the results. Therefore, it is necessary to investigate which period is suitable for the investigation of phase transitions of fats. The amplitude was kept at 0.5 °C, since this was found to be a suitable range in the experiments outlined above.

The resulting answer of the refractive index based on a temperature modulation of 0.5 °C amplitude and a period of 30 s was already shown in Figure 6.9. Some spikes are visible in the answer of the refractive index but the resulting crystallization and melting peaks depicted in Figure 6.10 are acceptable.

The application of a larger period of 60 s (see Figure 6.13a) showed neither an enhancement nor a deterioration of the answer of the refractive index. The zoom at times between 4,600 s and 5,200 s also revealed an appropriate modulation (see Figure 6.13b). The calculated peak temperatures depicted in Figure 6.14 show good agreement with the literature. The crystallization peak was detected at 46.2 °C and the melting peak at 58.3 °C. So far, there is no severe difference between a period of 30 s and 60 s. Hence, an even larger period of 120 s was investigated.

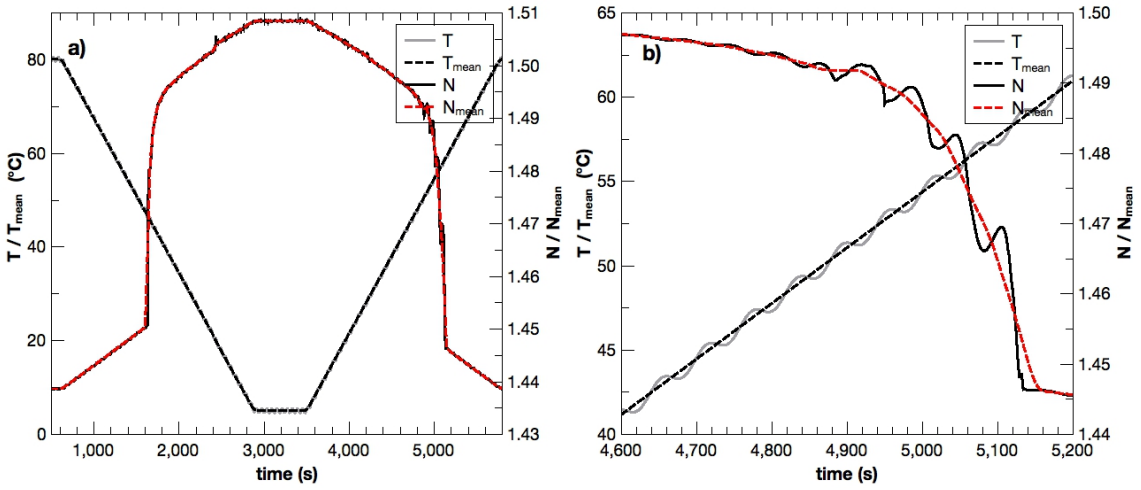

Figure 6.13: Temperature/ mean temperature and refractive index/ mean refractive index of fully hydrogenated palm oil plotted against temperature, 2 °C/min, 0.5 °C amplitude, 60 s period; a) complete time range b) zoom.

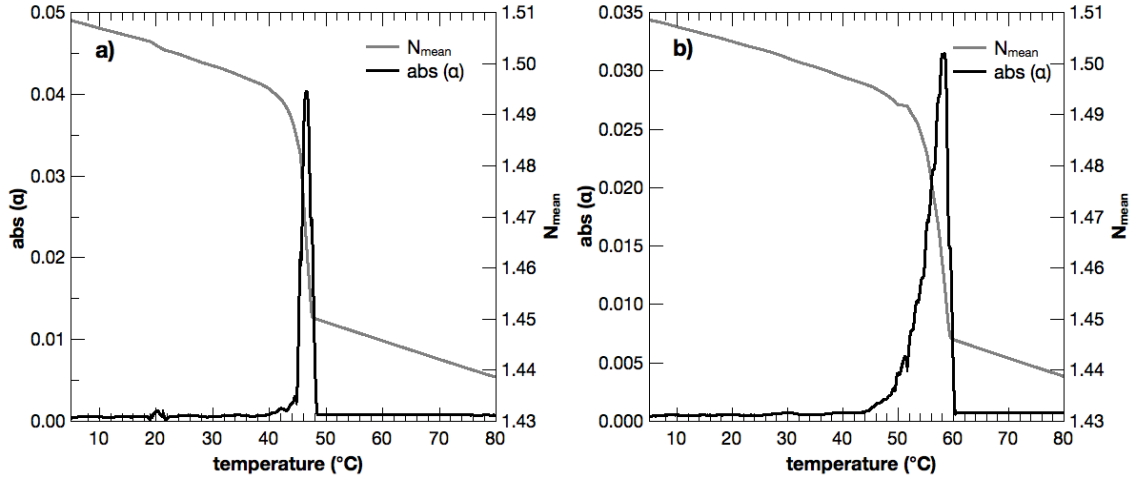

Figure 6.14: TMOR graphs of fully hydrogenated palm oil, 0.5 °C amplitude, 60 s period, a) cooled at 2 °C/min, b) heated at 2 °C/min.

The plot of the temperature and the refractive index over time at a modulation period of 120 s is shown in Figure 6.15. The spikes during the equilibrium states of the system are as small as seen for the periods applied before. However, during the phase transitions the modulation period seems too long because a kink in the measured refractive index (see Figure 6.15a, black solid curve) is visible. Since it is required that e.g. the change of the mean refractive index in one period is linear this means that the phase transition (change in the optical properties) needs to be relatively slow in comparison to the angular frequency ω ($\omega = 2\pi f = 2\pi\frac{1}{\lambda}$) (Müller *et al.*, 2013). Therefore, a period of 120 s at a scan rate of 2 °C/min might be too high to gain good information and to calculate the peaks properly because the change in the refractive index might not be linear anymore. This is also visible in the calculated peaks which are shown in Figure 6.16. The calculated crystallization peak (a) is in the same range like the ones measured at a period of 30 s and 60 s, respectively. However, it is broader which makes the determination less precise. The unsuitable combination of scan rate, amplitude, and period affects the melting peak even more leading to calculation artifacts (data not shown). In addition, the transition from one polymorphic form into another is not visible as good for the 120 s sample as for the other two. Therefore, a period of 120 s seems not applicable for the investigation of phase transition at a scan rate of 2 °C/min.

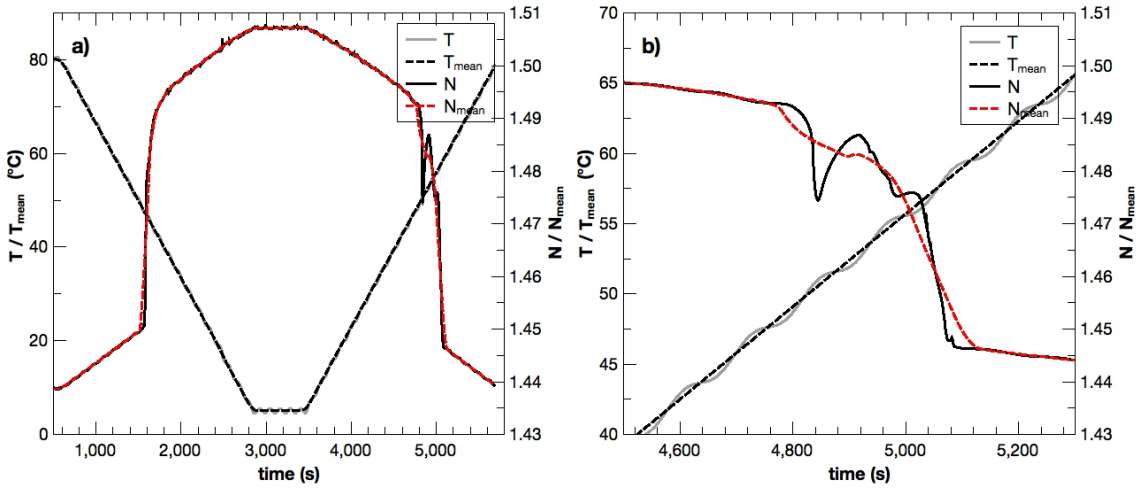

Figure 6.15: Temperature/ mean temperature and refractive index/ mean refractive index of fully hydrogenated palm oil plotted against temperature, 2 °C/min, 0.5 °C amplitude, 120 s period; a) complete time range b) zoom.

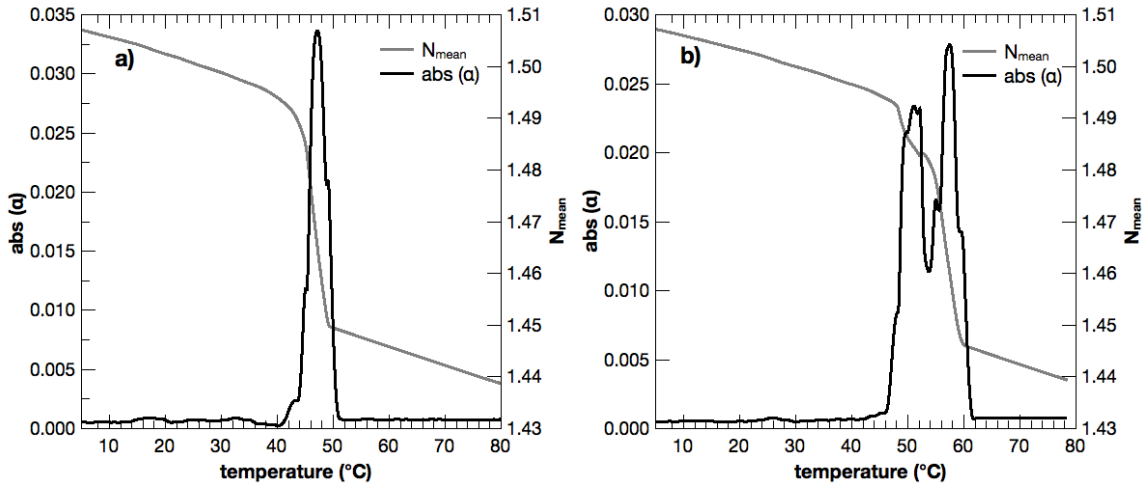

Figure 6.16: TMOR graphs of fully hydrogenated palm oil, 0.5 °C amplitude, 120 s period, a) cooled at 2 °C/min, b) heated at 2 °C/min.

It might be concluded that the combination of period and scan rate is crucial. For the applied scan rate of 2 °C/min both periods of 30 s and 60 s were found to be suitable. Since a smaller period leads to narrower phase transition ranges of the investigated samples a period of 30 s seems to be the most promising for a scan rate of 2 °C/min. However, if the scan rate is decreased it might be worth applying longer modulation periods to gain more proper information.

To sum up the influence of the amplitude and the period on the measurement principle of TMOR one can conclude that the combination of scan rate, period, and modulation is crucial. A too high amplitude in combination with a too long period leads to a non-linear change of the mean refractive index in one period which affects the proper calculation of the peaks of the transition temperatures (Müller *et al.*, 2013). In addition, the scan rate can influence the temperature range of phase transition which itself impacts the period to be selected.

6.5 Conclusion

The subchapters above show that the four parameters of fat composition, scan rate, amplitude, and period influence the quality of the measurement data of TMOR when lipid mixtures are investigated. The three fats examined concerning the scan rate varied in their composition thus in their phase behavior. All showed that a good comparison of DSC and TMOR data was given if a scan rate of 2 °C/min was applied.

However, higher scan rates did not fit with the chosen modulation amplitude resulting in calculation errors. This lead to the conclusion that these combinations were not suitable to generate good experimental data. Therefore, it is recommended to investigate the crystallization and melting behavior with the used amplitude of 0.25 °C at a scan rate of 2 °C/min.

In these experiments, the samples were directly placed on the prism, heated at a defined rate and subsequently cooled. This makes the crystallization process well defined because the sample was liquid before. Nevertheless, the melting behavior is quite unpredictable because it depends on the thermal history of the fat. This might be the reason why the standard deviation was larger for the melting than for the crystallization peak temperatures. Hence, the temperature profile was adapted for the following experiments to establish a defined crystallization procedure to decrease the influence of the thermal history of the sample. The sample was molten and kept at 80 °C for 10 min to remove the crystals and ensure the is no so-called memory effect. Because the sample is completely liquid proper contact between the sample and the prism is generated and good heat transfer is given. The cooling step was performed at the same scan rate as the following heating which was performed after a stabilization time of 30 min at 5 °C. With this procedure reproducible results were obtained.

Since a thermal lag can be seen for peak temperatures but the onset of melting and crystallization might not be as much affected this value could be an opportunity to also take it into account for the comparison with literature data. It seems less dependent on the scan rate and could be used to compare the DSC and the TMOR method excluding the thermal lag (Peyronel and Marangoni, 2014a).

It was outlined that the amplitude plays an important role during the measurement of phase transitions using TMOR. One interesting objective in the future could be isothermal measurements with different amplitudes to investigate polymorphic transitions because of their stimulating effect on phase changes. Preliminary studies to investigate polymorphism are given in chapter 9.

In summary, to study the phase transitions of fats at a scan rate of 2 °C/min an amplitude of 0.5 °C seems to be most suitable. However, it could be required to adapt under investigation. Since the period can also play a crucial role it will be discussed in the following subchapter.

The best scan rate of the ones applied (2 °C/min, 5 °C/min, 10 °C/min) was 2 °C/min for all fats investigated. It might be suitable to go even lower in the scan rate but a balance between the significance of the generated data and the invested time should be kept. Therefore, the further analysis for the phase behavior of fats and oils was done at 2 °C/min. For samples with less complexity and a narrower phase transition range it might be recommendable to examine them at lower scan rates to ensure a change of the mean refractive index in a linear manner (Müller *et al.*, 2013).

In summary, a scan rate of 2 °C/min, a modulation amplitude of 0.5 °C, and a period of 30 s was found to be the most suitable. If the scan rate is changed the suitable setup concerning period and amplitude should be determined since the combination of scan rate, amplitude and period defines the validity of the obtained data. The sample under investigation might also impact the choice of the proper parameters. In addition, the following studies were conducted with an extended stabilization time of 30 min because the device was limited to a temperature of 5 °C.

7 APPLICATION OF TEMPERATURE MODULATED OPTICAL REFRACTOMETRY FOR THE CHARACTERIZATION OF THE CRYSTALLIZATION BEHAVIOR OF PALM OIL

Michaela Häupler, Ratna Ayu Savitri, Valeska Hutschenreuter, Eckhard Flöter

TU Berlin, Department of Food Process Engineering, Seestrasse 13, 13353 Berlin, Germany

Originally published in European Journal of Lipid Science and Technology (2018), 120 (5)

https://doi.org/10.1002/ejlt.201700511

The following chapter is an accepted manuscript.

Abstract

The phase behavior of fats is mainly determined using DSC. Here, the application of temperature modulated optical refractometry (TMOR) was examined to monitor the phase transitions of palm oil with different degrees of saturation.

Studying the phase behavior by both methods revealed systematic differences. At identical scan rates, TMOR yielded up to 2 °C higher crystallization temperatures and identified consistently lower temperatures for melting phenomena. Because the prism serves as heating surface and defines the sample volume considered for the measurement a more direct heat transfer with TMOR is assumed. The sample depth above the prism relevant for the determination is only one micron. Hence, a direct heat transfer is ensured and thermal lag is practically eliminated causing the above-mentioned differences.

Because the TMOR signal is averaged over a defined prism surface area data for inhomogeneous samples can be generated. Although actual values for thermal expansion coefficients appear meaningless the combination of the TMOR signals allows to accurately determine the relevant phase transitions. The identification of different polymorphic forms and levels of solids in palm oil will be studied prospectively building on the promising results reported to identify if TMOR can become a valuable extension of the fat technologists' toolbox.

Key words: *fat crystallization, hydrogenated palm oil, refractive index, temperature modulation, phase behavior*

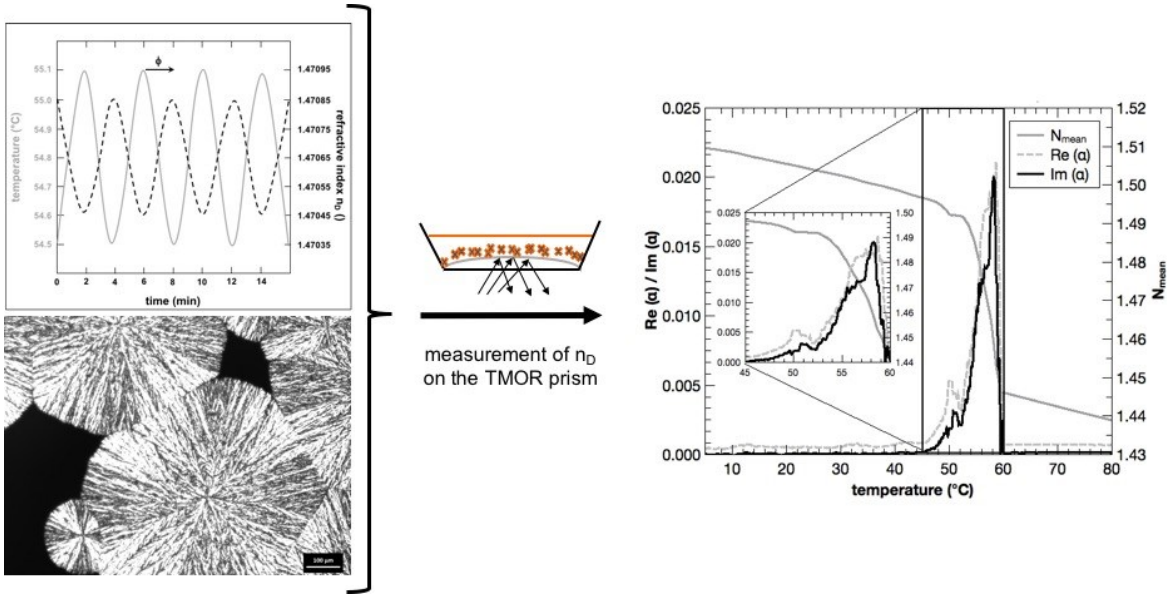

Figure 7.1: Graphical abstract of the investigation of fat crystallization using temperature modulated optical refractometry (TMOR).

Graphical Abstract

It is possible to investigate the crystallization and melting behavior of fats with the new temperature modulated optical refractometry (TMOR). An undulated temperature is applied and the time-delayed answer of the refractive index is measured. Subsequently, the real and imaginary part of the thermal expansion coefficient α are calculated based on the refractive index of the sample and the occurring phase shift (see Figure 7.1). A plot of the real and imaginary part against the temperature leads to peaks at the phase transition temperatures and a resulting thermogram for the sample.

Practical Applications

The new temperature modulated optical refractometry could extend the mainly used differential scanning calorimetry. It works highly accurate at small scan rates (<5 °C/min) in comparison to the DSC. The new method could provide a deeper insight into samples during heating and cooling due to additional temperature undulation as well as the possibility to perform quasi-isothermal measurements.

7.1 Introduction

Fat crystallization is the crucial processing step in many food products (e.g. margarine, chocolate, and ice cream) (Flöter, 2009; Bot and Flöter, 2013; Hartel, 2013). The adequate crystallization determines the later melting behavior, mouthfeel and stability of the products. The resulting crystals and their phase behavior are one of the most studied fields in the context of fat technology. A variety of methods exists which can be combined to reveal a finger print for every single fat. Typical methods applied are pulsed nuclear magnetic resonance (pNMR) to determine the solid fat content, differential scanning calorimetry (DSC) to study the crystallization behavior, and polarized light microscopy (PLM) to identify the basic morphology of the sample. Temperature modulated optical refractometry (TMOR) has been applied to study polymers but has not been evaluated for its applicability to characterize the crystallization of fats and oils (Aleksandrova *et al.*, 2014). The determination of the refractive index of a homogeneous liquid oil is common practise for the purpose of identification.

In cooperation with the group of Dr. Krüger from the University of Luxembourg, Anton Paar OptoTec GmbH (Seelze-Letter, Germany) developed the TMOR technique. It has been used so far to determine chemically induced glass transitions by refractometry accompanied by an accurate temperature modulation (Müller *et al.*, 2013). The device measures the refractive index as a response of the applied temperature, which is sinusoidally modulated (see Figure 7.2). Actually, this modulation distinguishes this device from high accuracy refractometers. The measured refractive index and its trailing to the temperature modulation are the basis to compute the thermal expansion coefficient α. The data gathered was also used to determine phase transition temperatures and to identify if either a glass transition or a first order transition had occurred. However, the systems studied always yielded a homogeneous sample, which is a prerequisite for the application of the Abbe-refractometry. This has some consequences for the study presented here. The fat compositions studied are multi-component mixtures and the solidification thus yields particle suspensions. By default, this implies that the represented data in this study on the refractive indices and the computed thermal expansion coefficients of dispersions are at risk to be flawed.

Nevertheless, the changes of these signals as a function of temperature were assumed to be accurate indicators for transition temperatures in inhomogeneous systems.

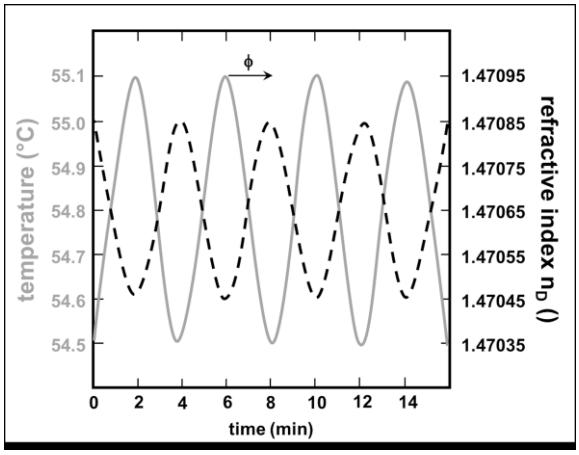

Figure 7.2: Explanation of sinusoidal temperature modulation (solid line) at a given amplitude and period and the answer of the refractive index (dashed line) delayed by the phase shift ϕ.

The outlined approach is thus to some extend reconsidering dilatometry. The application of dilatometry is rather outdated in terms of characterizing phase transitions and polymorphic forms of various fats by density differences. In the beginning of the 1930's, Normann established this method, which was further investigated and understood by the mid 1940´s (Bailey and Kraemer, 1944; Bailey and Singleton, 1945). The basic approach is built on the density difference between liquid oil and crystalline material taking also density differences as a function of temperature, hence, the differences in the thermal expansion of the different states of aggregation into account (Van Putte and Van Den Enden, 1974).

TMOR is capable to perform either isothermal or dynamic measurements. In the first place, the temperature modulation appears most useful during the isothermal mode, hence to study the kinetics of transitions at a constant temperature. In an earlier publication, the application of TMOR to pure aliphatic components, namely, *n*-hexadecane, palmitic acid, and tripalmitate, was reported (Häupler and Floeter, 2018). Studying the crystallization and melting behavior induced by executing temperature scans revealed that TMOR yields reliable and accurate results. Differences found compared to DSC relate possibly to the nature of the measurement, in particular the more direct heat transfer related to the measurement volume causing less thermal lag

in TMOR applications. The present contribution extends this study into more complex, multicomponent and hence inhomogeneous systems.

To this end, the crystallization and melting behavior of three fats with different degrees of saturation were investigated to evaluate the possible application of TMOR to characterize the thermal behavior of fats. Palm oil was chosen amongst others since it is one of the most used materials in structured fat phases (Berger and Idris, 2005; Aini and Miskandar, 2007; Ghosh and Rousseau, 2011). Its crystallization and melting behavior is quite unique due to its balanced composition of unsaturated and saturated fatty acids. The resulting complex TAG composition causes the typical phase behavior with multiple co-existing solid phases (Tan and Che Man, 2002b). Additionally, palm oil based fats with differences in their specific crystallization behavior were chosen, namely partially and fully hydrogenated palm oil, to limit the effects of changes in chain length. This work discusses the advantages of TMOR compared to DSC and PLM, which are the easy sample handling, the limited thermal lag and the sensitivity of the measurement.

7.2 Materials and Methods

Three different edible fats were chosen to investigate the applicability of the temperature modulated optical refractometry (TMOR) for the determination of phase transitions. The fats differed in their degree of saturation, resulting in differences in the crystallization and melting behavior. The DSC was chosen as the reference method for the phase transition and PLM to determine the microstructure in the solid state. The latter was also performed to support the interpretation of the data measured by TMOR.

Refined, bleached and deodorized palm oil as well as partially and fully hydrogenated palm oil were used throughout the studies. All samples were taken from the same batch, respectively, and kindly provided by ADM (Hamburg, Germany). Subsequently, the samples are abbreviated PO (palm oil), PHPO (partial hydrogenated palm oil) and FHPO (fully hydrogenated palm oil). Prior to each experiment the fats were completely molten (at approximately 70-80 °C) to eliminate any remaining nuclei, referred to as crystal memory. All measurements, starting from sample preparation, were performed at least in duplicate.

TMOR measurements were conducted with a prototype equipment from Anton Paar OptoTec GmbH (Seelze-Letter, Germany). Briefly summarized, an Abbe-refractometer with an accurate temperature control of the prism (+/- 0.03 °C) is used to measure the refractive index n_D of the sample. Both, temperature ramps to investigate dynamic phase transitions and quasi-isothermal measurements can be performed. The current temperature is modulated in a predefined period (30-120 s) and amplitude (0.1-1 °C) and thus, quasi-isothermal phase transitions can be investigated. The novelty of TMOR is that it determines a thermal expansion coefficient α based on the change of n_D over the modulated temperature in a measurement period. The predetermined temperature undulation leads to a similarly undulated answer of the refractive index. If a phase change occurs the delay of this answer causes a phase shift which is the basis for the calculations of the real and imaginary part of α, Re (α) and Im (α), respectively. The design of the device and the underlying theory of TMOR is described in detail elsewhere (Müller *et al.*, 2013; Häupler and Floeter, 2018). The refractive index is recorded over the whole measurement time. The software computes the mean temperature as well as the mean refractive index. Both, cooling and heating rate were set at 2 °C/min with a modulation amplitude of 0.5 °C and a period of 30 s. Each measurement was conducted with 100 µL of sample, which was placed on the prism. To create intense contact, the more saturated FHPO was pressed onto the prism using a standardized stamp to avoid sample detachment during the measurement. Both PO and PHPO were placed in a conical geometry. All fats were molten at 80 °C on the prism and kept at this temperature for 10 min to remove all crystal memory. Afterwards, the samples were cooled to 5 °C, held at this temperature for 30 min prior to heating the samples up to 80 °C. Currently, the device is limited to temperatures above 4 °C. Hence, 5 °C was chosen as the stabilization temperature. The data recording was conducted at all stages during the measurement.

The DSC thermograms were recorded with a device from Netzsch (DSC 204 F1 Phoenix, NETZSCH-Geraetebau GmbH, Selb, Germany). Two temperature profiles were executed, cooling and heating rates were 2 °C/min, and stabilization for 30 min at 5 °C and 10 min at -50 °C, respectively. Approximately 8 mg of sample were weighed in aluminum pans and sealed hermetically. An empty pan was used as reference. The

analysis was performed with the NETZSCH Proteus – Thermal Analysis software (version 6.1.0) provided by the DSC manufacturer.

The PLM micrographs were taken during crystallization at a 10x magnification using a Zeiss AxioScope (Carl Zeiss Jena GmbH, Jena, Germany) equipped with a digital camera (AxioCam ICm1, Carl Zeiss Jena GmbH, Jena, Germany) and a temperature-controlled stage from Linkam Scientific Instruments (Surrey, UK). The image analysis was done with the ZEN Software provided by the manufacturer (Carl Zeiss Jena GmbH, Jena, Germany). Also for PLM the stabilization regime outlined above was applied. The micrographs were used to investigate the microstructure during the phase transitions and illustrated the sample's configuration at the prism.

The iodine value (IV) was determined according to the DGF standard method C-V 11e (02) to verify the differences of the fats. However, instead of glacial acetic acid chloroform was used as solvent. The fatty acid composition was determined by the analysis of fatty acid methyl esters (FAME) by gas chromatography (GC). The sample (10-15 mg) was dissolved in 4 ml of methyl *tert*-butyl ether (VWR Chemicals, Radnor, PA) and methylated using trimethylsulfonium hydroxide (TMSH, 0.2 mol/l, Macherey-Nagel GmbH & Co. KG, Düren, Germany). Margaric acid (C 17:0) was used as internal standard (Alfa Aesar, Thermo Fisher (Kandel) GmbH, Kandel, Germany). A capillary column (Trace™ TR-FAME GC Column, 120 m x 0.25 mm x 0.25 µm, Shimadzu Corporation, Tokyo, Japan) and nitrogen as carrier gas were used for the analysis. The oven was heated from 100 °C up to 250 °C at 4 °C/min. The samples were examined in duplicate and analyzed with the software provided by the GC manufacturer (Lab Solutions, Version 5.85, Shimadzu Corporation, Tokyo, Japan).

7.3 Results and Discussion

The iodine value was determined to ensure the differences in the saturation between PO, PHPO and FHPO. The result for palm oil was 53.5 ± 1.3, which in agreement with the literature (Ng and Oh, 1994). The IV of partially hydrogenated palm oil was with 41.6 ± 1.0 expectedly lower (Sarma *et al.*, 2011). Fully hydrogenated palm oil showed an IV of 4.4 ± 0.8, which is higher than the typical value for fully hydrogenated oils around 1.5 (Masuchi *et al.*, 2014).

The fatty acid composition is given in Table 7.1. The composition of palm oil is in accordance with the literature within a range of 3 % which could be related to different origins, plantation conditions, or distinct species (Che Man *et al.*, 1999). As expected, partially hydrogenated palm oil was the only fat investigated showing a high amount of *trans* fatty acids due to its manufacturing process (Kellens and Calliauw, 2013). The amount of palmitic (C 16:0) and stearic acid (C 18:0) in fully hydrogenated palm oil is in accordance with the statement of the manufacturer.

Table 7.1: Fatty acid composition of palm oil (PO), partially (PHPO) and fully hydrogenated palm oil (FHPO) analyzed by gas chromatography.

fatty acid	**PO (%)**	**PHPO (%)**	**FHPO (%)**
C 16:0	42.10 ± 0.11	45.98 ± 0.16	44.13 ± 0.31
C 16:1	1.56 ± 0.09	n.d.	n.d.
C 18:0	4.77 ± 0.01	10.67 ± 0.01	51.69 ± 0.09
C 18:1 *trans*	n.d.	23.70 ± 0.18	n.d.
C 18:1 *cis*	38.65 ± 0.29	16.55 ± 0.09	n.d.
C 18:2 *trans*	1.48 ± 0.08	n.d.	n.d.
C 18:2 *cis*	8.81 ± 0.04	n.d.	n.d.
C 20:2	2.63 ± 0.05	3.11 ± 0.42	4.18 ± 0.40

Since temperature modulation is considered the key to TMOR's benefit over simple accurate refractive index measurement it was necessary to ensure an adequate modulation for the temperature program executed. The data of the preliminary study to identify optimal parameters is not shown. The adequate modulation is the basis for the subsequent calculations, e.g., of the thermal expansion coefficient and therefore crucial to determine the applicability of the TMOR method in the field of fat technology. In addition, the DSC measurement was performed using two different stabilization temperatures, -50 °C according to AOCS method Cj 1-94 and 5 °C, to achieve the best possible comparability with the TMOR temperature program.

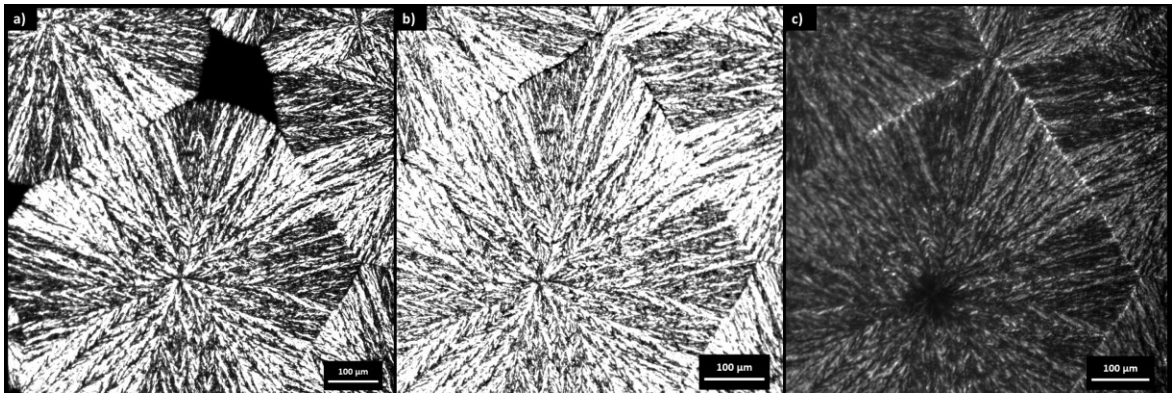

Figure 7.3: FHPO during crystallization and melting at a scan rate of 2 °C/min. Micrographs were taken a) during crystallization at 42 °C, b) after 30 min of stabilization at 5 °C, and c) during melting at 58 °C. Scale bar represents 100 µm.

In Figure 7.3a, the microstructure of FHPO during crystallization at a cooling rate of 2 °C/min is depicted. The micrograph is taken at a transient temperature of 42 °C. The crystallization occurs into large spherulites in line with the expectation that the saturated TAGs of FHPO show such behavior at high growth rates (Shi, Liang and Hartel, 2005). The shape does not change neither after 30 min of stabilization at 5 °C (Figure 7.3b) nor during melting at a heating rate of 2 °C/min (micrograph taken at 58 °C, Figure 7.3c). In addition to the indication of the onset temperatures of crystallization and melting, the microstructure illustrates the sample structure at the surface of TMOR's prism.

Table 7.2: Onset, offset and peak temperatures during the phase transitions of fully hydrogenated palm oil (FHPO) determined via DSC and TMOR measurements at 2 °C/min, DSC stabilization temperatures of 5 °C (30 min) and -50 °C (10 min), TMOR stabilization temperature of 5 °C (30 min).

	$T_{stab.}$	phase transition	T_{onset} (°C)	T_{peak} (°C)	T_{offset} (°C)
FHPO	DSC -50 °C	crystallization	46.00 ± 0.10	42.75 ± 0.55	40.50 ± 0.60
		melting	47.15 ± 0.05	49.50 ± 0.10	50.00 ± 0.10
			55.25 ± 0.35	60.15 ± 0.55	61.40 ± 0.60
	DSC 5 °C	crystallization	46.10 ± 0.00	43.50 ± 0.40	41.90 ± 0.80
		melting	46.90 ± 0.30	49.10 ± 0.40	49.70 ± 0.40
			54.75 ± 0.25	59.10 ± 0.80	60.20 ± 0.80
	TMOR 5 °C	crystallization	47.53 ± 0.12	46.34 ± 0.25	44.13 ± 0.05
		melting	46.86 ± 0.69	49.89 ± 0.23	51.34 ± 0.65
			57.03 ± 0.09	58.12 ± 0.12	60.17 ± 0.23

The following discussion takes the peak temperatures into account and considers the real part of the thermal expansion coefficient (Re (α)) for the TMOR data analysis. The on- and offset temperatures of the DSC and TMOR measurements can be found in Table 7.2. Considering the crystallization behavior of FHPO it was found that the peak temperatures in the DSC thermograms are located at 42.75 ± 0.55 °C and 43.50 ± 0.40 °C, respectively. The assessment by TMOR in contrast revealed a crystallization temperature of 46.34 ± 0.23 °C. The higher crystallization temperature identified by TMOR could be related to the more direct thermal exchange between the prism and the relevant specimen volume. These differences indicate the sensitivity of the induction time and the metastable limit to the experimental method applied.

The peak temperatures in both the DSC and the TMOR thermograms are discussed in the following paragraph. The mean values and standard deviations for the on- and offset temperatures of the triplicate (TMOR) and duplicate (DSC) determinations are listed in Table 7.2. The DSC thermograms of FHPO in Figure 7.4 indicate that recrystallization from a less stable to a more stable polymorph took place during the heating process. This leads to two melting peaks at 49.50 ± 0.10 °C and 60.15 ± 0.55 °C for the sample stabilized at -50 °C and at 49.10 ± 0.40°C and 59.10 ± 0.80 °C for the sample stabilized at 5 °C, respectively. The data shows good

agreement with the literature for both the polymorphic transition and the melting point (Nassu and Guaraldo Gonçalves, 1999; Kloek, Walstra and van Vliet, 2000). Additionally, it was found that FHPO is not sensitive to variation in the stabilization temperature since both stabilization regimes yield practically the same results.

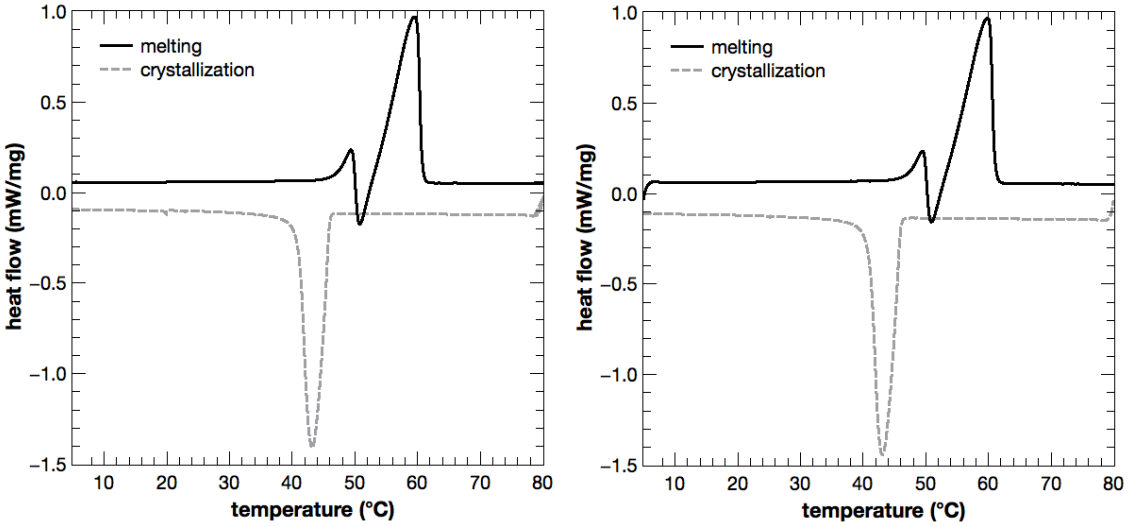

Figure 7.4: DSC data of FHPO. Left: cooled and heated at 2 °C/min, stabilized at -50 °C for 10 min. Right: cooled and heated at 2 °C/min, stabilized at 5 °C for 30 min.

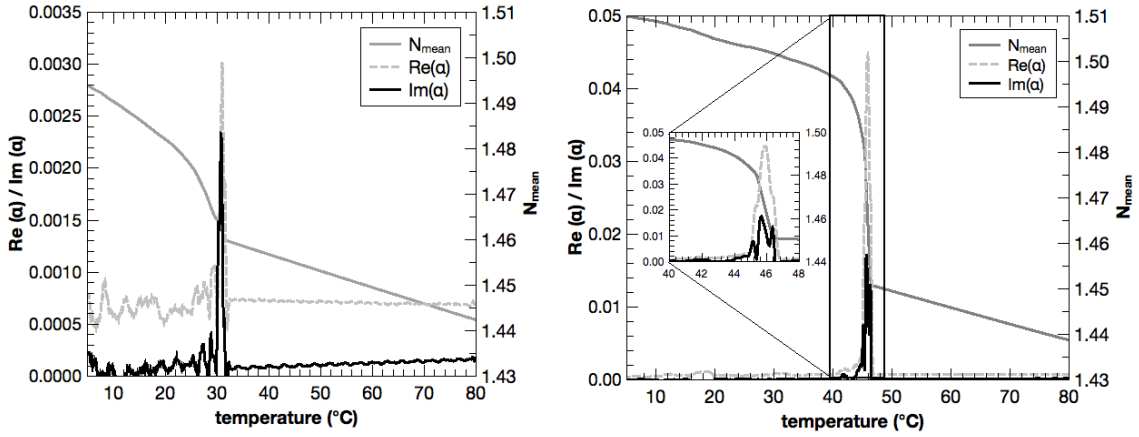

Figure 7.5: Crystallization (left) and melting curve (right) of FHPO measured with TMOR at a cooling and heating rate of 2 °C/min. Sample was stabilized at 5 °C for 30 min prior to melting.

The TMOR data of FHPO in Figure 7.5 showed a small bump in the real part at 49.89 ± 0.23 °C and a steep peak at 58.12 ± 0.12 °C. The phase transition, whether crystallization or melting, always results in a positive peak in the TMOR thermograms different than DSC, which distinguishes between exothermal and endothermal events.

The first melting peak, considered either the melting of the α polymorph followed by the crystallization of a more stable polymorph or a direct polymorphic transition, is located at similar temperatures, 49.89 ± 0.23 °C and 49.5 ± 0.10 °C, for TMOR and DSC measurements, respectively. The difference in the temperature found for the second melting peak, 58.12 ± 0.12 °C to 59.10 ± 0.80 °C, could result from the differences of the sample volume considered during the measurement. TMOR appears to show a rather instantaneous temperature control of the relevant sample volume because only a depth of the specimen of up to 1 μm is measured. In contrast, the DSC signal prevails until the whole specimen is molten. This so-called thermal lag of the DSC could be compensated by extrapolation of measurements at different scan rates to a zero-scan rate.

The difference between the melting peak temperature and the slip melting point of FHPO at 60.7 °C according to the manufacturer is due different methods used. The slip melting point appears to better relate to the offset temperatures, which are 60.20 ± 0.80 °C and 60.17 ± 0.23 °C determined with DSC and TMOR, respectively. The lower temperature found with TMOR could be explained again by the more direct heat transfer and the smaller amount of sample considered for measurement. This could also be an explanation for the higher onset and offset temperatures of crystallization found for TMOR compared to both DSC measurements (see Table 7.2). The onset temperature of the melting process is slightly higher in the TMOR data. The small difference could be explained by difficulties to identify the onset. The onset and offset of the second melting peak occurred at lower temperatures compared to the DSC as found before.

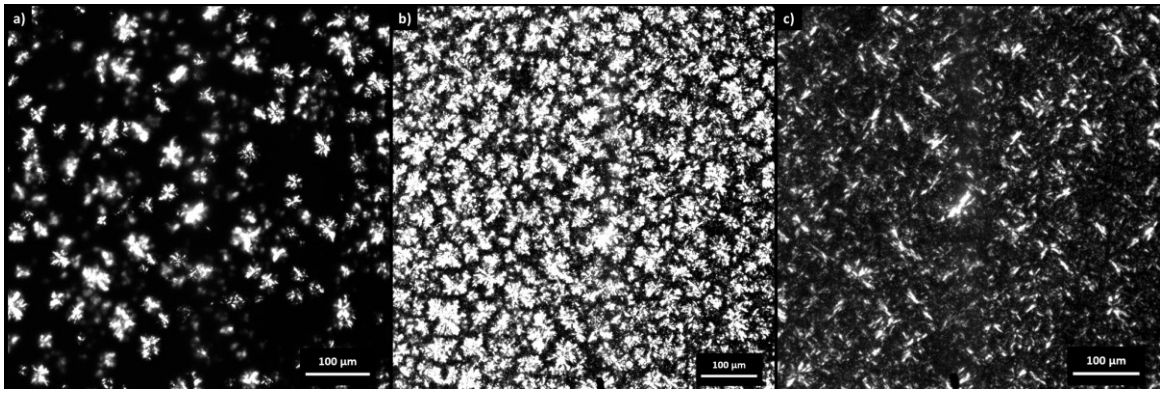

Figure 7.6: Crystallization and melting of PHPO at 2 °C/min. Micrographs taken at three different temperatures; a) during crystallization at 33 °C, b) after stabilization at 5 °C for 30 min, c) during melting at 45 °C. Scale bar represents 100 µm.

In comparison to FHPO one expects differences in the crystallization and melting behavior of PHPO due to the presence of different unsaturated fatty acids. Figure 7.6a refers to PHPO during crystallization at 33 °C with a scan rate of 2 °C/min, Figure 7.6b depicts PHPO after 30 min stabilized at 5 °C and Figure 7.6c shows the microstructure during melting at 45 °C with a scan rate of 2 °C/min. Looking at the micrographs, Figure 7.6, the dark areas reveal a significant portion of non-crystalline material in contrast to the micrographs of FHPO (Figure 7.3). This is not surprising because of the presence of a multitude of different TAGs with different melting points. The occurrence of multiple co-existing mixed solid phases in this sample also influences the kinetics of nucleation and growth (Bot and Flöter, 2013). This is indicated by the high number of small crystals found.

The DSC cooling curve of the sample stabilized at 5 °C shows two distinct peaks at 29.65 ± 0.15 °C and 27.40 ± 0.20 °C, respectively (see Figure 7.7). The TMOR showed a strong peak at 31.03 ± 0.33 °C (see Figure 7.8). These temperatures were slightly higher than determined by DSC. The irregularities in the different properties of the TMOR thermogram, e.g., the change of slope in the refractive index, possibly also indicate the second crystallization step. Analogous to the melting event the detection of crystallization events at higher temperatures by TMOR could most likely relate to better heat transfer kinetics.

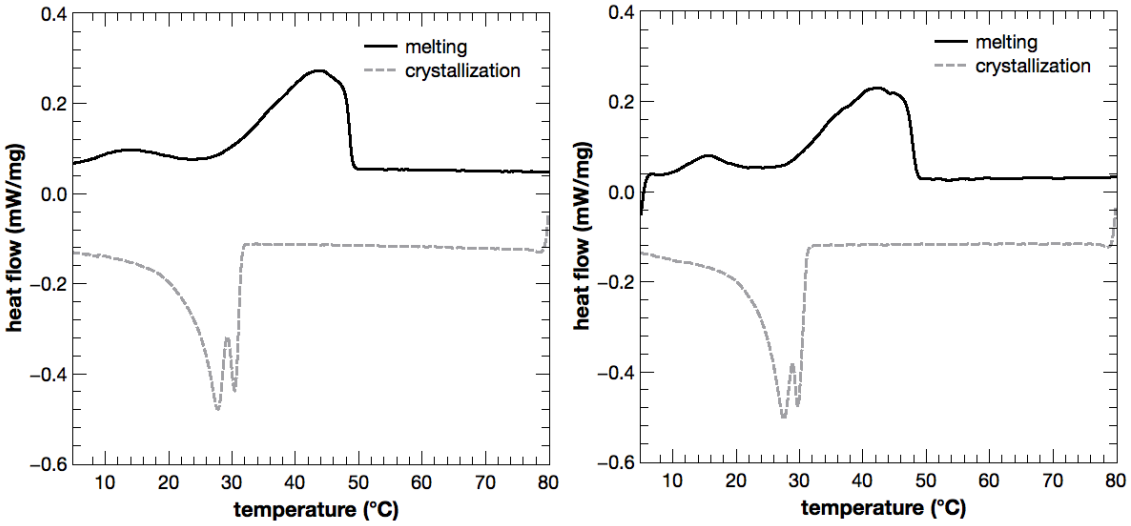

Figure 7.7: DSC data of PHPO; left: cooled and heated at 2 °C/min, stabilized at -50 °C for 10 min; right: cooled and heated at 2 °C/min, stabilized at 5 °C for 30 min.

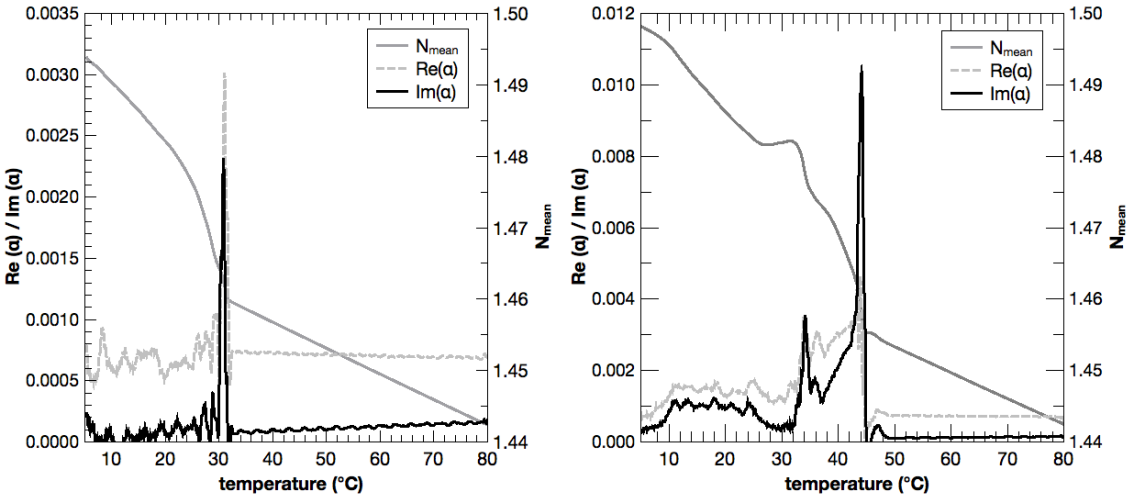

Figure 7.8: Phase behavior of PHPO recorded with TMOR at 2 °C/min, left: crystallization; right: melting. Sample was stabilized at 5 °C for 30 min prior to melting.

The mean values and standard deviations of the triplicate (TMOR) and duplicate (DSC) determinations of PHPO are listed in Table 7.3. The peak temperatures are discussed in the following section. The DSC-thermograms shown in Figure 7.7 reveal two distinct melting peaks at 14.10 ± 0.20 °C and 43.95 ± 0.15 °C for the sample stabilized at -50 °C and 15.60 ± 0.30 °C and 41.55 ± 0.55 °C for the sample stabilized at 5 °C. However, the shape of the peaks indicates that more than two solid phases co-existed. The TMOR thermogram indicates a melting range between 10 °C and

25 °C. This range can be recognized either as a broad hump in the contribution to thermal expansion coefficient or as a change of slope in the refractive index. The most pronounced peak of five small peaks in the broad bump of the real part of the thermal expansion coefficient was identified at 16.32 ± 0.02 °C.

Table 7.3: Onset, offset and peak temperatures during the phase transitions of partially hydrogenated palm oil (PHPO) determined via DSC and TMOR measurements at 2 °C/min, DSC stabilization temperatures of 5 °C and -50 °C, TMOR stabilization temperature of 5 °C.

	$T_{stab.}$	phase transition	T_{onset} (°C)	T_{peak} (°C)	T_{offset} (°C)
PHPO	DSC -50 °C	crystallization	31.70 ± 0.20	30.70 ± 0.20	30.00 ± 0.40
			31.80 ± 0.20	28.40 ± 0.60	23.55 ± 0.05
		melting	5.30 ± 0.30	14.10 ± 0.20	21.00 ± 0.70
			30.05 ± 0.05	43.95 ± 0.15	49.40 ± 0.30
	DSC 5 °C	crystallization	31.00 ± 0.20	29.65 ± 0.15	29.30 ± 0.20
			29.80 ± 1.00	27.40 ± 0.20	23.60 ± 0.50
		melting	10.25 ± 0.25	15.60 ± 0.30	19.60 ± 0.20
			28.50 ± 0.50	41.55 ± 0.55	48.50 ± 0.00
	TMOR 5 °C	crystallization	32.21 ± 0.01	31.03 ± 0.33	30.13 ± 0.03
		melting	11.20 ± 0.13	16.32 ± 0.02	19.75 ± 0.11
			30.71 ± 2.98	34.79 ± 2.57	35.69 ± 0.77
			40.25 ± 2.67	45.44 ± 1.05	49.07 ± 2.00

TMOR data revealed for PHPO two distinct peaks at 34.79 ± 2.57 °C and at 45.44 ± 1.05 °C during the melting process leading to a more detailed analysis of the broad peak shown in the DSC thermogram (Figure 7.8). Both measurements, DSC and TMOR, show lower melting points compared to the manufacturers specification. The slip melting point of the partially hydrogenated palm oil stated by the manufacturer was 48.5 °C. Since the PHPO had a lower IV value than the material specified in literature the higher melting point found, 41.55 ± 0.55 °C for DSC and 45.44 ± 1.05 °C for TMOR compared to 38-40 °C, was to be expected (Sakata, Takahashi and Sonehara, 1985). Therefore, the comparison with the stated melting point of the manufacturer is more appropriate. Like shown for FHPO, the stated melting point is closer to the offset temperatures determined by DSC (48.50 ± 0.00 °C) and TMOR (49.07 ± 2.00 °C)

which could be explained by the method applied by the manufacturer. TMOR again indicated lower melting point temperatures at both peak and offset temperature, respectively (see Table 7.3). Even though the DSC and TMOR measurements were performed at identical rates, 2 °C/min, the TMOR showed two peaks, one before the melting peak determined by DSC and one after. This is probably due to the intense contact of the thin layer used for the refractive index determination with the prism, which makes the TMOR operation more precise at smaller scan rates in comparison to DSC.

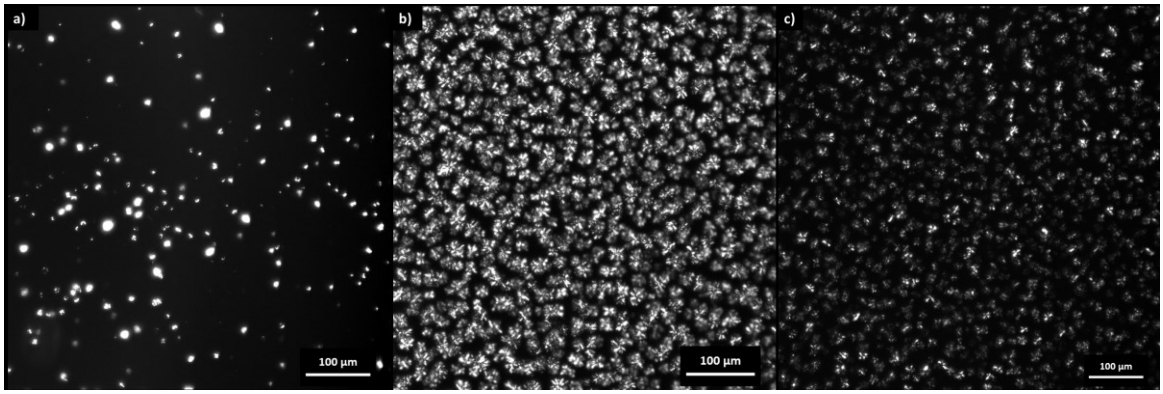

Figure 7.9: PO crystals at three different temperatures; a) during crystallization at 23 °C, b) after stabilization at 5 °C for 30 min, c) during melting at 42 °C; experiments were performed at a heating and cooling rate of 2 °C/min. Scale bar represents 100 µm.

Figure 7.9 shows the micrographs of palm oil (PO) during crystallization with a cooling rate of 2 °C/min at 23 °C (micrograph a), at 5 °C after 30 min of stabilization (micrograph b), and at 42 °C (micrograph c) during melting at a heating rate of 2 °C/min. Also in this case, the solid fat content at 5 °C is far from 100 % as large areas of liquid oil are shown as dark areas.

The complex mixture of different TAGs with varying levels of unsaturation and conformation caused a complex crystallization behavior and thus multiple co-existing mixed solid phases. Considering the melting behavior of PO indicated by DSC it is not surprising to find a significant amount of liquid in PO at 5 °C (Che Man *et al.*, 1999). Compared to the samples of FHPO and PHPO, the obtained crystals are smaller indicating further differences in nucleation and growth characteristics (Verstringe *et al.*, 2013).

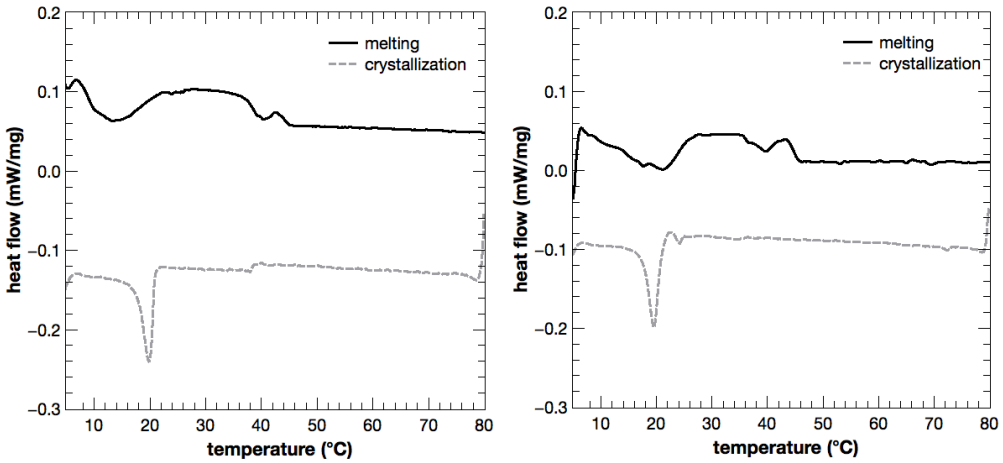

Figure 7.10: DSC results of PO cooled and heated at 2 °C/min; left: stabilized at -50 °C for 10 min; right: stabilized at 5 °C for 30 min.

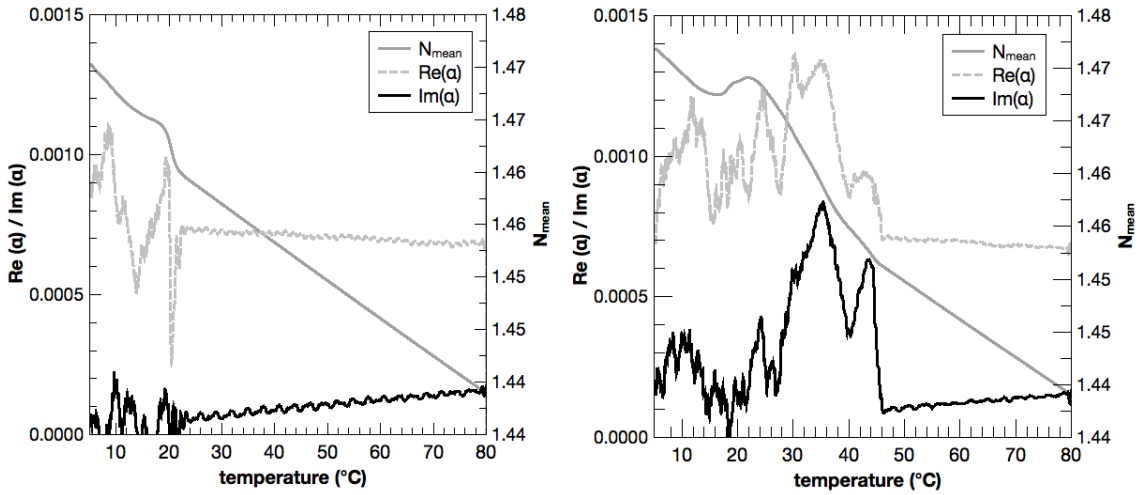

Figure 7.11: PO melting behavior determined with TMOR at 2 °C/min; left: crystallization; right: melting. Sample was stabilized at 5 °C for 30 min prior to melting.

The crystallization behavior of PO determined by DSC is displayed in Figure 7.10 and the one identified by TMOR in Figure 7.11. The crystallization peak temperature measured with the DSC is at 19.90 ± 0.30 °C which is quite close to the peak temperature determined with TMOR at 21.02 ± 1.26 °C. Another crystallization peak at 8.26 ± 0.98 °C was identified with TMOR probably due to the more direct measurement. This peak was not found in the DSC measurement, which was only conducted until 5 °C due to the aforementioned thermal lag. In contrast, DSC measurements on cooling down to -50 °C showed this crystallization peak at a temperature of 2.60 ± 0.10 °C.

The melting behavior of palm oil observed by DSC is depicted in Figure 7.10. PO showed a broad melting range with different melting peaks at 0.80 ± 0.10 °C, 3.95 ± 0.15 °C, 25.05 ± 3.15 °C, and 42.55 ± 0.05 °C when stabilized at -50 °C for 10 min and at 32.50 ± 2.10 °C and 42.45 ± 0.75 °C for the sample stabilized at 5 °C for 30 min, respectively. The high standard deviations for the melting peak between 25 °C and 32 °C occur due to the difficulty to determine the peak temperature of the broad peak. The first melting peak at approximately 5 °C was not considered here, because this peak cannot be evaluated for TMOR due to its limited temperature range. The thermograms confirm the complex crystallization behavior known for PO. Detailed indexing of the peaks by deconvolution is beyond the scope of this work. In Figure 7.11, the TMOR data of the melting behavior of PO is shown. Considering all signals, the melting peak temperatures were identified to be 11.24 ± 0.67 °C, 35.80 ± 1.17 °C, and 43.83 ± 0.51 °C.

The multiple peaks appeared most distinguished in the TMOR thermogram even though the identification and assignment of temperatures remains difficult. However, considering the changes in the RI signal to identify transitions combined with temperature identification for the thermal expansion data yields good results. Differently the lower resolution of the DSC resulted in a broad bump without clearly separated peaks. The four peaks probably relate to the different solid phases and thus different TAG compositions of the crystalline phases. The dissimilarities between the different stabilization temperatures for the DSC measurements were due to complicated recrystallization behavior typical for PO (Braipson-Danthine and Gibon,

2007). The low melting fraction investigated by TMOR has a higher melting point compared to the literature (6.0 °C) whereas the melting point of the high melting fraction is in alignment with the literature (Ng, 1990). Comparing the melting points assessed by TMOR and DSC it is again found that the favorable heat transfer in TMOR yielded lower melting temperatures. In the case of PO, the slip melting point temperature as state by the manufacturer is lower than these temperatures. This is possibly due to the high amount of liquid material in PO. Table 7.4 summarizes the obtained onset, peak and offset temperatures of melting and crystallization of palm oil measured by DSC and TMOR in duplicate and triplicate, respectively. The onset of crystallization is detected at higher temperatures for TMOR than for DSC as already seen for FHPO and PHPO. This is also valid for the detected onset of melting temperature.

Table 7.4: Onset, offset and peak temperatures during the phase transitions of palm oil (PO) determined via DSC and TMOR measurements at 2 °C/min, DSC stabilization temperatures of 5 °C and -50 °C, TMOR stabilization temperature of 5 °C.

	$T_{stab.}$	phase transition	T_{onset} (°C)	T_{peak} (°C)	T_{offset} (°C)
PO	DSC -50 °C	crystallization	21.30 ± 0.40	20.20 ± 0.30	18.00 ± 0.10
			4.40 ± 0.00	2.60 ± 0.10	-8.80 ± 1.00
		melting	-9.15 ± 0.35	0.80 ± 0.10	2.55 ± 0.05
			3.25 ± 0.05	3.95 ± 0.15	8.85 ± 0.25
			21.15 ± 4.45	25.05 ± 3.15	38.05 ± 1.35
			41.50 ± 0.20	42.55 ± 0.05	44.75 ± 0.45
	DSC 5 °C	crystallization	21.15 ± 0.15	19.90 ± 0.30	17.85 ± 0.05
		melting	20.55 ± 1.75	32.50 ± 2.10	33.25 ± 2.45
			40.40 ± 0.30	42.45 ± 0.75	44.75 ± 0.95
	TMOR 5 °C	crystallization	23.87 ± 0.39	21.02 ± 1.26	17.70 ± 1.28
			10.41 ± 1.51	8.26 ± 0.98	7.74 ± 1.21
		melting	11.37 ± 0.92	11.24 ± 0.67	8.94 ± 1.36
			32.60 ± 0.46	35.80 ± 1.17	39.84 ± 0.48
			41.62 ± 1.28	43.83 ± 0.51	45.84 ± 0.78

In a previous study, the extrapolation of the DSC data at different scan rates was done to generate comparable data at a scan rate of 0.5 °C/min, which is too slow for the DSC to detect a proper signal (Häupler and Floeter, 2018). This is different for TMOR, which gives better signals at lower scan rates, below 5 °C/min. Preliminary results, which are not shown, indicate, that the thermal lag is not as crucial for the TMOR method as for DSC measurements. DSC data showed, that the peak melting temperature increases with increasing heating rate. For TMOR, the relationship between the scan rate and the melting point temperature identified is vice versa for fast heating rates compared to the DSC. Decreasing the heating rate from 10 °C/min to 5 °C/min results in a slight increase of the melting point temperature. However, the differences between the peak melting temperature at 5 °C/min and 0.5 °C/min are small (0.3 °C). This little variation found for the results of TMOR caused by different scan rates lead to the conclusion that thermal lag has little significance for the TMOR method. This is supposedly due to the smaller sample volume considered for the determination.

In general, the differences found between the stabilization at -50 °C and 5 °C for DSC samples verified that these stabilization regimes are practically interexchangeable. The most pronounced differences were found for PO followed by PHPO and FHPO. This phenomenon can be explained by the different TAGs present in each fat. FHPO is known for its TAGs mainly composed of the saturated fatty acids palmitic and stearic acid (Masuchi *et al.*, 2014). These align faster and denser in a crystalline structure and are therefore already solidified at 5 °C. Considering PHPO, a higher amount of oleic acid and thus a higher degree of unsaturation is present in the TAGs (Sakata, Takahashi and Sonehara, 1985). Due to the increased variation of the fatty acid moieties, the alignment of the TAGs is more difficult yielding a slower and more complex crystallization process. Considering PO, the crystallization behavior gets even more complex due to a much broader number of different TAGs present (mainly PPP, POP, PPO, PLP, POO, PLO, OOO) (Basiron, 2005). This leads to lower crystallization temperatures of multiple solid phases and therefore, a stabilization temperature of -50 °C delivers increasingly different results compared to a stabilization at 5 °C.

It should be pointed out, that the differentiation between recrystallization and melting is difficult from TMOR data because a phase change always results in a positive

peak in contrast to the DSC thermograms, where negative peaks represent exothermal events in this study. To determine recrystallization by TMOR it is recommendable to consider the RI instead of the resulting peaks of the thermal expansion coefficient. An abrupt change in the slope during melting could be an indication for a recrystallization phenomenon indicating a change in the physical properties. In addition, the direct heat transfer of TMOR and thus the absence of extensive thermal lag could lead to an overlap of the recrystallization and the melting process. This compensation of the simultaneous processes possibly signifies a real transition temperature.

7.4 Conclusions

For the first time, temperature modulated optical refractometry was used to study fat crystallization and delivered good results. The advantage of the method is its direct thermal contact of the heat transfer surface, the easy sample preparation, the robustness of the device, as wells as the sample volume considered for measurement. The thermal lag of the technique is hence significantly reduced compared to the DSC and thus limits metastable states. Dispersions were investigated during crystallization and melting, which results in a varying level of a solid/liquid prism surface coverage. Even though this appears not to be suited for Abbe-refractometers a systematic evolution of the refractive index was detected in all three systems investigated. Furthermore, a change in the slope of the refractive index was always related to a change of the state of aggregation. Even polymorphic transitions could be determined by TMOR but further investigations of more systems are inevitable. The surprisingly positive results found for the inhomogeneous samples studied could relate to the fact that the actual measurement is processing the average value gathered over a defined surface area of the prism.

The authors would like to admit that the real and imaginary part of the thermal expansion coefficient are of limited value as a number itself but give valuable information about the temperatures of phase transitions at this point. To index multiple peaks like seen for PO an improved data analysis will be necessary in the future to enhance the applicability of TMOR for precise fat crystallization measurements. In addition, a proper measurement routine could lead to the possible determination of

polymorphic transitions using TMOR. However, the differentiation between endothermic and exothermic phase transitions is not straightforward with TMOR because no distinct signals are shown. The direct thermal contact changes the observation of polymorphic transition with TMOR compared to the sequential occurrence in DSC because simultaneous exo- and endothermal processes might compensate each other. Therefore, proper measurement routines to determine polymorphic transformation are the focus of future work.

In summary, the new TMOR method is already applicable for edible fats if the contact between the sample and the prism is ensured. Until today, a disadvantage is the limited temperature range from 4 °C to 90 °C but work is ongoing to extend the application to lower temperatures to improve the applicability in fat technology. TMOR could be a good enhancement of the DSC measurement, where fast cooling and heating rates lead to smoother curves whereas the TMOR method achieves better results at slow scan rates. The additional undulation could give an even more precise insight in the phase behavior of fats and oils due to stimulation of phase transitions. Thus, TMOR is a promising and cost effective method but further studies on different systems are necessary to enhance the understanding and robustness of the application of TMOR.

Acknowledgements

The authors would like to thank Anton Paar OptoTec GmbH for the support providing the prototype and space for discussion. In addition, the authors are grateful for the financial support of the Elsa Neumann scholarship of the federal state of Berlin and Anton Paar OptoTec GmbH. The authors have declared no conflict of interest.

8 FEASIBILITY STUDY ON THE DETERMINATION OF THE SOLID FAT CONTENT OF FATS USING TEMPERATURE MODULATED OPTICAL REFRACTOMETRY

Michaela Häupler*, Valeska Hutschenreuter, Susanne Rudolph, Eckhard Flöter

TU Berlin, Department of Food Process Engineering, Seestrasse 13, 13353 Berlin, Germany

Submitted to the European Journal of Lipid Science and Technology (2018)

The following chapter is a submitted manuscript.

Abstract

The solid fat content (SFC) of fat compositions is typically determined by pulsed nuclear magnetic resonance (pNMR). Alternatives, such as dilatometry, which has been used historically, or differential scanning calorimetry (DSC) find less application due to e.g. inferior robustness, more analytical effort. In this contribution the feasibility to determine the SFC with temperature modulated optical refractometry (TMOR) is discussed. The validity of the Lorentz-Lorenz equation is a necessary prerequisite for this approach. This was proven based on measurements of refractive indices and densities for fat systems indicating that the specific refractivity is independent of temperature in the temperature range studied. Materials studied were rapeseed oil, coconut oil, palm oil, and partially hydrogenated palm oil. The determination of the SFC with TMOR was based on linear combination of refractive indices of solid and liquid phases. Refractive indices of these phases were assumed to be linearly depending on temperature. The SFC values determined by TMOR were in good agreement with reference data. The optimized stabilization method developed allows to execute the determination with limited effort. However, these first promising results need to be substantiated before considering TMOR a viable alternative method to determine SFC values.

Keywords: *Fat crystallization, solid fat content, temperature modulation, refractive index, NMR*

Graphical Abstract

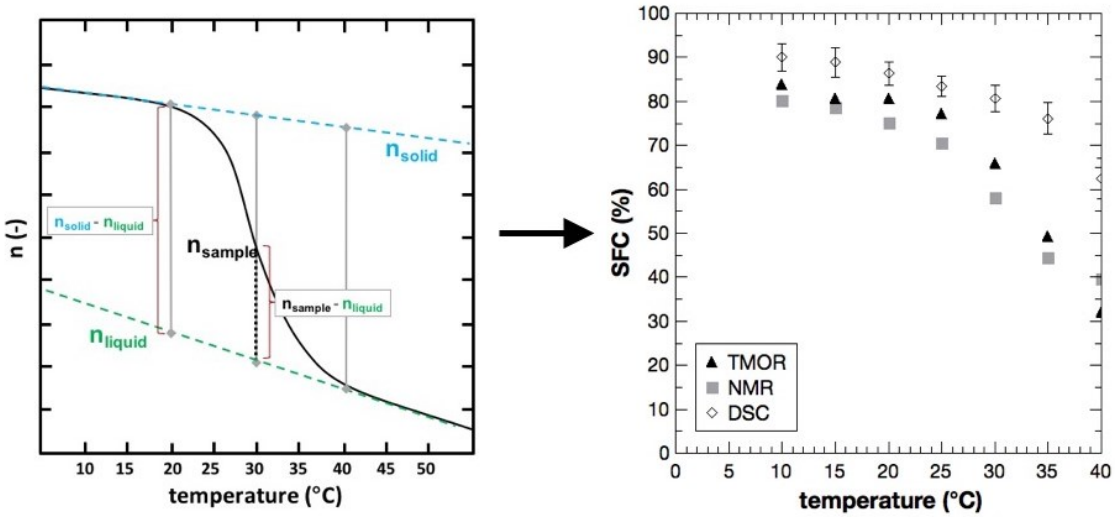

Practical applications

The mainly used pulsed nuclear magnetic resonance could be extended by the temperature modulated optical refractometry to determine the solid fat content in lipid systems. Since the device is robust and affordable it could be used during quality control in fat technology.

8.1 Introduction

The solid fat content (SFC) value describes the amount of crystalline material present in a fat composition at a given temperature. It is a very important characteristic of fat compositions. This is so, because it is regarded as an important specification in the trade of fat compositions. Even though not unique to a specific composition, it contributes with other properties to a unique fingerprint. Furthermore, the knowledge of the solid fat content as a function of temperature corresponds very well with the physical functionality of fats. The SFC line indicates the mouthfeel of a product, its spreadability at a certain temperature or stability of the matrix against temperature challenges. Hence, the knowledge of the SFC line is an important input to product developers and crucial for successful applications.

Decades ago, the main method to determine the amount of solids in a fat sample was dilatometry. It determines the volume expansion of a substance on temperature

change (Bekkedahl, 1949). Two assumptions are made in dilatometry. First, the thermal volume expansion of different fats is the same and second it is equal in the liquid and the solid state (Mills and van de Voort, 1981b). However, the dilatometric method is time-consuming and cumbersome and is only valid for a solid fat index below 50 % (Pohle, Taylor and Gregory, 1965; Madison and Hill, 1978; Mills and van de Voort, 1981b, 1981a; Van Duynhoven *et al.*, 2002).

Therefore, an easier way to determine the amount of solids present in a fat could be the use of a density meter which delivers similar results to dilatometry. Nevertheless, fats with a high content of solids can cause problems in applying this method due to the contraction of the sample during crystallization which might lead to a partial loss of contact between the inner wall and the sample (Mills and van de Voort, 1981b).

Another alternative is the differential scanning calorimetry (DSC), which monitors the heat flow during thermal processes. To determine the fraction of solids in a fat sample, it is melted, cooled and again melted, taking the second heating cycle into account. The calculated partial areas under the DSC peak can be used to determine the SFC (Menard and Sichina, 2000). This can either be done by relating the energy of a specific event to the heat of fusion of this specific event in the pure reference system or by treating the thermogram analog to a chromatogram.

In the 1970s, the use of pulsed nuclear magnetic resonance (pNMR) to determine the SFC became popular (Timms, 1984). This method is commonly used today. Its principle is based on the determination of the mobility of the hydrogen atoms. It determines the time for the rearrangement of H^1 atoms in a magnetic field after excitation by an electromagnetic pulse. Since these atoms are more mobile in the liquid than in the solid state this difference in the relaxation time can be used to calculate the solid fat content (Shahidi, 2005). Disadvantages of the method are the costs of the required device and the time-consuming stabilization procedure. However, for any method to determine the solid fat content a standardized stabilization method will be required in order to achieve reproducible results. Since different polymorphic forms of the crystals show differences in their relaxation characteristics, it is necessary to account for the polymorphic form for most accurate results. In general, even with neglecting the effect of different polymorphs the pNMR method is a sufficiently accurate and reliable method.

In this work we report on the study of the feasibility to determine the SFC by temperature modulated optical refractometry (TMOR). This is useful because the TMOR application could be a less costly, simpler, and faster alternative to the pNMR application. Therefore, the density and refractive indices of different oils were determined first to evaluate the validity of the Lorentz-Lorenz equation for the samples investigated. Secondly, a method to calculate the SFC based on the TMOR data was established. Additionally, samples were measured at different temperatures and data compared to DSC and pNMR results. Finally different procedures of temperature variation to stabilize the samples were evaluated in order to optimize the duration of the SFC determination.

To apply TMOR for the determination of the SFC special attention has to be paid to the important correlation between density and refractive index. Both the mass density and the refractive index are temperature dependent. For samples in the liquid state the refractive index decreases with increasing temperature. The same is true for the density (Beysens and Calmettes, 1977; Esteban *et al.*, 2012). In the solid state, the progress of the slope for the specific volume over temperature (inverse to the density) is half as steep as in the liquid state but still temperature dependent (Van Putte and Van Den Enden, 1974). The measurement of the refractive index in the solid state is quite difficult which is why Kaufmann and Thieme (1954) assumed the same temperature dependency for the solid phase as for the liquid phase. This temperature dependency definitely needs to be taken into account for the further analysis.

The mass density ρ of a substance is its mass per volume. It can be determined by a density meter which e.g. measures the oscillation of a sample in a flexural resonator in relation to a calibration substance. The refractive index of a substance is its ability to diffract light. It is also referred to as the optical density.

The Lorentz-Lorenz equation gives the relation between the refractive index, n (optical density) and the mass density, ρ:

$$\frac{\mathbf{n^2 - 1}}{\mathbf{n^2 + 2}} = \mathbf{r \cdot \rho} \qquad \textbf{Eq. 8.1}$$

and is used as base for the calculations when applying TMOR. Here it was examined if the Lorentz-Lorenz equation can be used assuming the specific refractivity

r is constant on temperature variation (Müller *et al.*, 2013). From literature it is known that this could be valid for oils and fats but not for other components (Aleksandrova *et al.*, 2014). Müller *et al.* (2013) assumed that the specific refractivity *r* is independent of the measurement temperature and thus of the state of aggregation of the material. Aleksandrova *et al.* (2014) stated for the demixing of a polymer solution that their specific refractivity *r* is strongly depending on the state of the material. They showed a temperature dependence of *r* for a polymer solution.

Hence, the Lorentz-Lorenz equation was applied for oils to check whether the specific refractivity is temperature-dependent for these systems. To prove this is of prime importance because a temperature independent constant *r* is a required prerequisite for the application of the equation used to determine the thermal expansion coefficient.

8.2 Materials and Methods

The fats used were coconut, rapeseed, and palm oil as well as partially hydrogenated palm oil. All fats were provided by ADM (Hamburg, Germany).

The density was determined using a density meter (DMA 58, chempro/PAAR, Austria). Since it was only possible to determine the densities of liquid oils, the temperatures were chosen above the melting points of the three investigated high melting materials which were 50 °C, 55 °C, and 60 °C, respectively.

A device of Netzsch (DSC 204 F1 Phoenix, NETZSCH-Geraetebau GmbH, Selb, Germany) was used to determine the SFC using differential scanning calorimetry. 5-10 mg of sample was weighed into aluminum pans and an empty pan was used as a reference. Data was received at a scan rate of 5 °C/min. The area under the peak was subdivided at the desired temperatures and partially integrated. The relation between the partial area and the complete area under the peak was defined as the amount of solids at the specific temperature (Bentz and Breidenbach, 1969; Nassu and Guaraldo Gonçalves, 1995).

Beside the DSC also pNMR was used as a reference method. A device from Bruker optics was used to determine the SFC (Bruker minispec mq20 NMR analyzer, Bruker Optics, Milton, Canada). The 10-mm diameter glass NMR tube was filled with

approximately 9 mL of melted fat. A pulse of 6 s length was applied as recommended by the AOCS Official Method Cd 16b-93 for non-stabilizing fats (AOCS, 2009b).

Temperature modulated optical refractometry (TMOR) was performed with a prototype device from Anton Paar OptoTec GmbH (Seelze-Letter, Germany). The respective sample was heated and cooled directly on the accurately temperature controlled prism. This minimized laboratory work during the SFC determination and guaranteed good heat transfer.

In order to verify that TMOR can be used for the determination of the SFC in fat/oil samples, the following approach was applied. For the systems coconut, palm and rapeseed oil the density and the refractive index were experimentally determined at various temperatures. From this data the specific refractivity *r* was obtained using the Lorentz-Lorenz equation.

Then, experimental data of the refractive index at different stabilization temperatures was obtained using TMOR for coconut oil, for which the SFC was known. For this measurements, the AOCS temperature profile for non-stabilizing fats was applied (AOCS, 2009a). The fat was heated up to 80 °C and kept at this temperature for 10 min. After cooling to 60 °C and a stabilization time of 10 min, the sample was cooled down to 0 °C. This temperature was held for 60 min before the sample was heated to the desired temperature, respectively 10 °C, 15 °C, 20 °C, …, 60 °C. The stabilization time at each temperature was 30 min during which the undulation was applied with a period of 30 s and an amplitude of 0.5 °C. The mean values of the refractive index data were taken during the temperature modulated isothermal measurement period. Before each measurement, the heating to 80 °C with the following stabilization steps at 60 °C and 0 °C was performed with each sample.

The TMOR data in the two-phase region was processed by a pseudo mass balance or lever rule such that the SFC of the given sample could be obtained. These data were compared for coconut oil to literature SFC data which showed that the method can be applied.

Additionally, it was tested if the time necessary for the analysis could be shortened. Therefore, the sample had to undergo different temperature profiles during analysis. First, a stepwise heating was applied after 30 min of stabilization at each temperature. Second, the time for stabilization was decreased from 30 min to 5 min. Third, the

stepwise concept was done starting at 60 °C for 30 min before the sample was cooled stepwise in 5 °C steps to respectively 55 °C, 50 °C, 45 °C, …, 0 °C.

8.3 Results and Discussion

The validity of the Lorentz-Lorenz equation for the investigated oils was investigated in this work. In addition, the SFC calculation based on TMOR data was performed and validated against reference data. Furthermore, the work at hand reports an attempt to optimize the stabilization method.

8.3.1 Temperature Dependency of Density and Refractive Index

In Figure 8.1, the density is plotted over temperature for the three oils. The values are in accordance to the literature (Timms, 1985; Noureddini, Teoh and Clements, 1992; Codex, 2001; Esteban *et al.*, 2012). The density decreases linearly with increasing temperature. Coconut oil shows the highest density over the complete temperature range which can be explained by its fatty acid composition. In comparison to the other two investigated systems it is composed of shorter fatty acids which contribute to a higher density than the longer fatty acids. The higher density of rapeseed oil in comparison to palm oil is related to the higher amount of unsaturated fatty acids. Commonly, unsaturated fatty acids have a higher density than saturated fatty acids in the liquid state (Noureddini, Teoh and Clements, 1992).

The trend lines in Figure 8.1 were used to guide the eye to show the linear progression of the density over temperature. In addition, the lines help to see the agreement of the measurement data with the literature data. For the experimental determination of the refractive index the same temperatures as for the density measurements were applied. The data of the refractive index and the density were used to calculate the specific refractivity applying, Eq. 8.1.

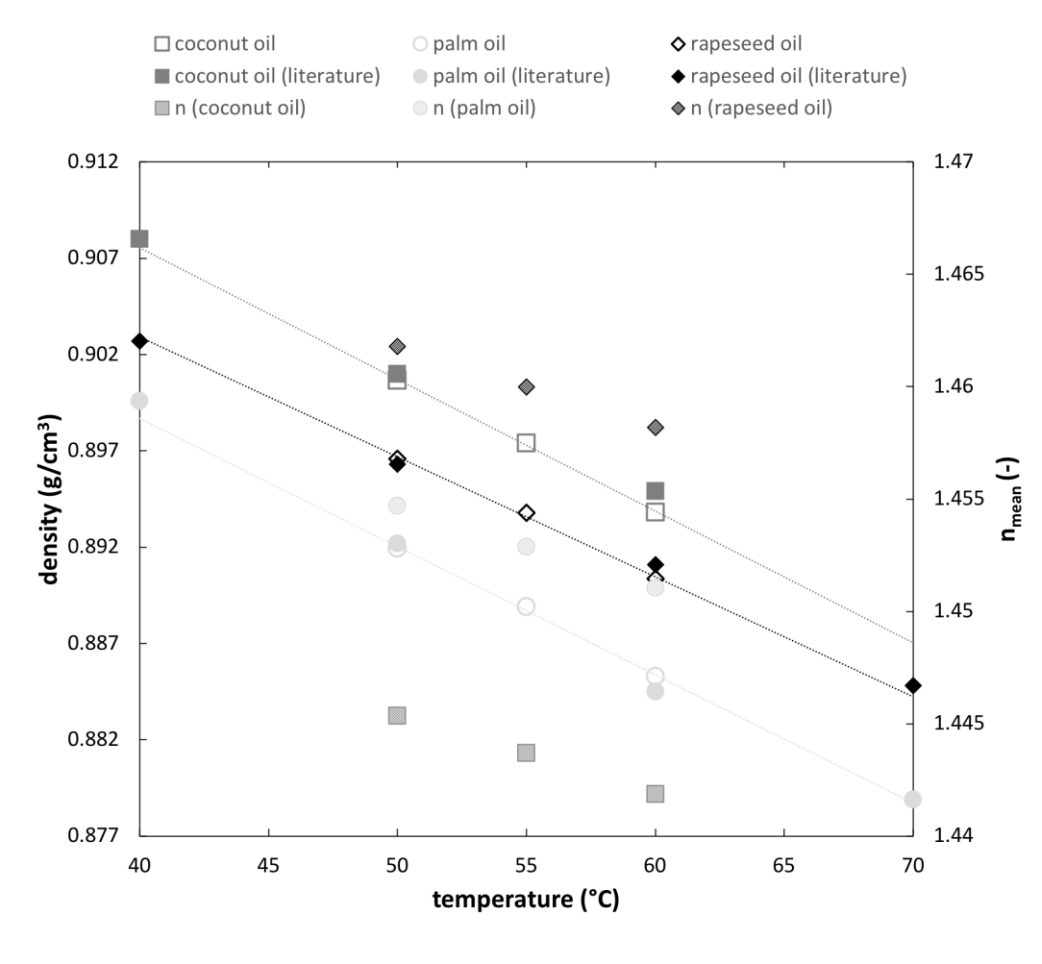

Figure 8.1: Temperature dependency of density (empty symbols) and refractive index (patterned symbols) determined for coconut oil (violet squares), palm oil (grey circles) and rapeseed oil (blue diamonds), the filled symbols represent literature data of densities.

The specific refractivity *r* of the investigated oils does not seem to be affected by temperature (see Table 8.1). Comparison of specific refractivity *r* of the fats leads to the assumption that the fatty acid composition has an effect because *r* of coconut oil is smaller than for the other fats. It could be concluded that *r* increases with increasing fatty acid chain length and the number of double bonds. To validate this finding in more detail is out of the scope of the work reported here.

Table 8.1: Summary of calculated specific refractivity *r* based on the densities and refractive indices of rapeseed, palm, and coconut oil.

T (°C)	n_{mean} (-)	ρ (measured, g/cm³)	r (cm³/g)
		rapeseed oil	
50	1.46180	0.89659 ± 0.00001	0.30651 ± 0.00000
55	1.45999	0.89380 ± 0.00022	0.30643 ± 0.00010
60	1.45818	0.89037 ± 0.00004	0.30656 ± 0.00002
		palm oil	
50	1.45469	0.89193 ± 0.00004	0.30401 ± 0.00002
55	1.45286	0.88891 ± 0.00017	0.30399 ± 0.00008
60	1.45107	0.88528 ± 0.00002	0.30418 ± 0.00001
		coconut oil	
50	1.44535	0.90065 ± 0.00002	0.29571 ± 0.00001
55	1.44368	0.89741 ± 0.00004	0.29582 ± 0.00002
60	1.44186	0.89382 ± 0.00004	0.29594 ± 0.00002

Assuming that the specific refractivity is temperature independent further investigations are based on mean values of the specific refractivity *r* ($r_{mean, coconut} = 0.296$; $r_{mean, palm} = 0.304$; $r_{mean, rapeseed} = 0.307$).

8.3.2 Solid Fat Content Calculation

The experiments described above were conducted to prove that the Lorentz-Lorenz correlation is suitable for fats and oils and that the assumption that the specific refractivity is temperature-independent is true. Next, experimental data of the refractive index were determined. These TMOR data for the SFC calculations were obtained applying the AOCS temperature profile for non-stabilizing fats (AOCS, 2009a). The use of TMOR for the SFC determination requires the measurement of the refractive index at three different temperatures. The calculative approach based on the refractive indices is depicted in Figure 8.2 together with a typical curve of refractive indices when changing from the solid to the liquid state. The determination of the SFC at a certain temperature requires the measurement of n_{sample} at this very temperature (e.g. 30 °C). In addition, an extrapolation of n_{liquid} and n_{solid} to this temperature is needed to apply the lever rule for the calculation. All measured properties are a function of temperature.

$$\mathbf{n_{sample} = SFC \cdot n_{solid} + (1 - SFC) \cdot n_{liquid}} \quad \textbf{Eq. 8.2}$$

$$\mathbf{n_{sample} - n_{liquid} = SFC \cdot (n_{solid} - n_{liquid})} \quad \textbf{Eq. 8.3}$$

$$\mathbf{SFC}\ (\%) = \frac{\mathbf{n_{sample} - n_{liquid}}}{\mathbf{n_{solid} - n_{liquid}}} \cdot \mathbf{100} \quad \textbf{Eq. 8.4}$$

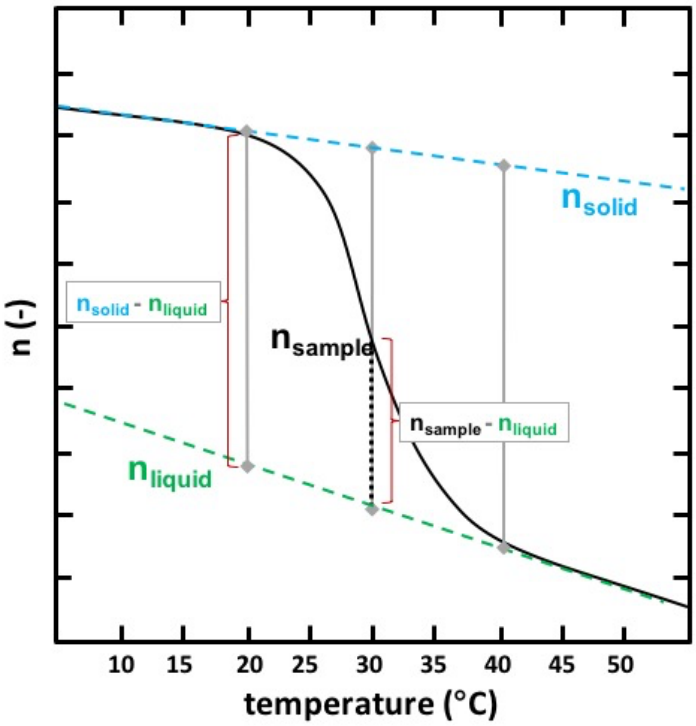

Figure 8.2: Schematic refractive index curve (black solid line) and calculation approach (dashed lines) of the SFC based on the measurement of the refractive indices at the sample temperature (n_{sample}, black), after melting of the sample (n_{liquid}, green) and after solidification of the sample (n_{solid}, blue).

The determined refractive index gives the value of the fat in its liquid state. Figure 8.3 shows the progress of the refractive indices. For the three different fats the mean refractive index changes linearly with temperature. The values for the slopes of the trend lines describing n are practically constant with $-3.65\ 10^{-4}$. In contrast, the intercept depends on the specific fat. The more unsaturated fatty acids are present, e.g. in rapeseed oil, the higher the mean refractive index. This implies that for every fat only one value in the liquid phase is required as basis for the calculations of the SFC. This allows the determination of the refractive index of the fat in the liquid state at any temperature.

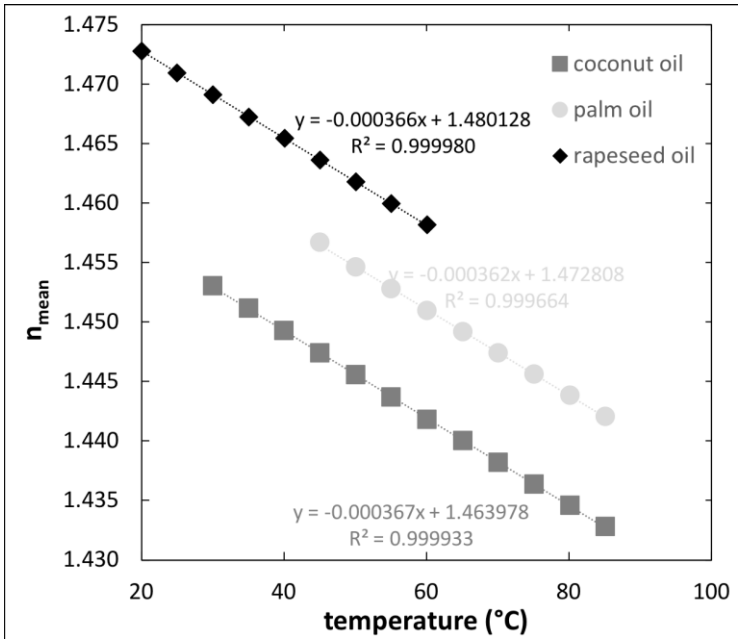

Figure 8.3: Mean refractive index of fats in the liquid state: palm oil (light grey circles), coconut oil (dark grey squares), rapeseed oil (black diamonds).

Van Putte and Van Den Enden (1974) deduced the relationship between the slopes in the liquid and the solid state from dilatometric measurements. They found that the slope for the liquid state is twice that of the solid state. This yields a value of -1.835 10^4 for the slope in solid phases.

The determination of n_{solid} is not possible for all fats due to the currently minimum achievable temperature of the device of 0 °C. Hence, Eq. 8.2 was used to calculate n_{solid} for a certain SFC based on the information given by the manufacturer. This approach was used for coconut oil, palm oil, and partially hydrogenated palm oil. The gained SFC values were compared to data taken from literature (Van Putte and Van Den Enden, 1974), data determined by pNMR and to the SFC calculated from the DSC data (Bentz and Breidenbach, 1969).

In Figure 8.4a the SFC values determined by TMOR, DSC, and literature data determined by pNMR are shown. The TMOR data shows a similar progress as the literature data of Van Putte and Van Den Enden (1974) while the DSC method

overestimates the SFC over the whole temperature range. This is also visible in the parity plot shown in Figure 8.4b.

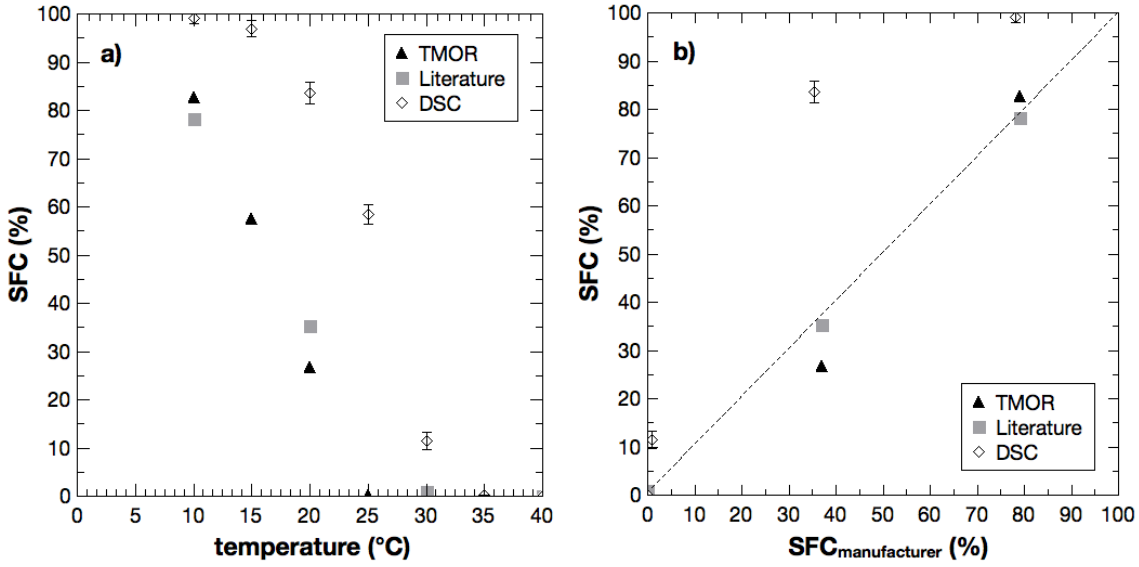

Figure 8.4: a) SFC of coconut oil plotted over temperature; TMOR data (black triangles), literature data (grey squares), DSC data (white diamonds); b) parity plot of SFC values of the manufacturer compared to TMOR, literature, and DSC data.

The applicability of TMOR as device to determine SFC was also investigated for palm oil and partially hydrogenated palm oil. These two fats were compared to pNMR data obtained experimentally instead of literature data.

Figure 8.5a shows the progress of the SFC of palm oil over temperature. The DSC values show big standard deviations because palm oil has a complex crystallization behavior. This makes the partial integration of the melting peaks difficult. The values determined by TMOR are in good agreement with the values obtained by pNMR. This is confirmed by comparison of the SFC values with the manufacturer's specifications (see Figure 8.5b). However, TMOR could only determine useful data for temperature as low as 20 °C, the calculation below this temperature yielded SFC values above 100 %.

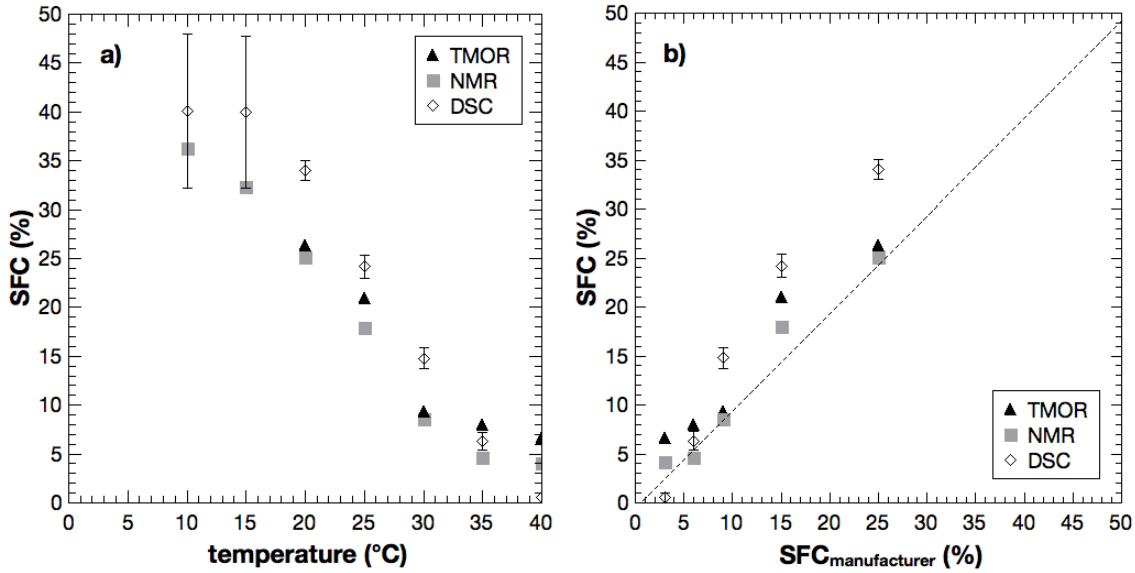

Figure 8.5: a) SFC of palm oil plotted over temperature; TMOR data (black triangles), literature data (grey squares), DSC data (white diamonds); b) parity plot of SFC values of the manufacturer compared to TMOR, literature, and DSC data.

The SFC of partially hydrogenated palm oil is displayed in Figure 8.6a. It shows that the progress of the SFC determined by pNMR and TMOR is quite the same. The DSC method overestimates the SFC over the whole temperature range. In Figure 8.6b, a parity plot of the SFC values gathered over the data given by the manufacturer is depicted. Both pNMR and TMOR data appear to match the supplier's information up to high solid levels.

Some authors advocate to determine SFC by DSC instead of pNMR. Currently however, the SFC values determined by DSC methods are usually higher compared to the pNMR method. These differences can be related to the nature of the measurement, DSC is dynamic while pNMR is static, and the respective stabilization methods (Márquez, Pérez and Wagner, 2013). Additionally it should be taken into account that for different mixed solid phases the variation of the heat of fusion is larger than the variation of respective relaxation characteristics. This renders the pNMR measurement less vulnerable to differences in the composition of solid phases or polymorphism. This tendency is generally confirmed by the results presented here. In contrast the SFC values determined by TMOR based on the assumptions made, linear temperature

dependency of the refractive indices of solid and liquid phases, show good agreement with the pNMR based data.

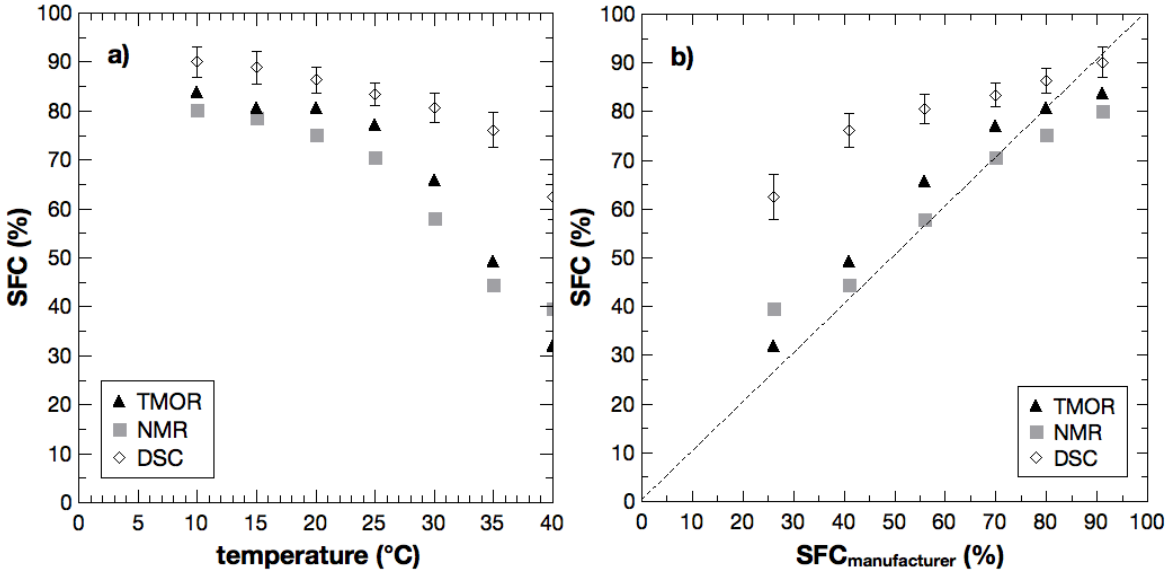

Figure 8.6: a) SFC of partially hydrogenated palm oil plotted over temperature; TMOR data (black triangles), literature data (grey squares), DSC data (white diamonds); b) parity plot of SFC values of the manufacturer compared to TMOR, literature, and DSC data.

8.3.3 Different stabilization procedures

In general it was shown that TMOR is applicable to determine the SFC. Next, it was investigated with which temperature profile the samples should be treated for the best determination. Four different temperature profiles were examined and coconut oil was used as sample. The temperature profile based on the AOCS method for pNMR was used as reference (AOCS, 2009b). This temperature profile was used for the experiments reported above.

In addition to the established AOCS temperature profile for non-stabilizing fats which is very time-consuming three temperature regimes with shortened measurement time were examined. One profile was a stepwise procedure after the stabilization time of 60 min at 0 °C to establish solid-liquid equilibrium. One approach was based on the stepwise partial melting at the measurement temperature. Holding times were 30 min or 5 min, respectively, beginning with 10 °C, followed by 15 °C, etc. until 60 °C were

reached. In particular, the procedure with the short stabilization time is based on the fact that the heat transfer in the TMOR is very good due to the very small volume of the sample that is considered for the determination (Häupler *et al.*, 2018). Alternatively, the samples were stabilized for 10 min at 60 °C and then cooled down stepwise, holding the stabilization temperatures for 30 min each. This approach was titled "backward". Taking into account that the prism is actually also the heat transfer surface this 'backward' method has the intrinsic risk to create a solid fat fouling layer on the prism falsifying the measurements due to inhomogeneities.

The comparison of the SFC values obtained using four different temperature profiles is depicted in Figure 8.7. The AOCS stabilization procedure serves as reference. The time-reduced forward-approach stabilizing the sample for 30 min at each step shows the best fit compared to the results from the AOCS procedure.

The reduction of the stabilization time to 5 min for this forward-procedure shows a reasonable match. Since the variation is rather random the differences encountered are most likely due to insufficient homogeneity of the sample after 5 minutes. The result of incomplete stabilization causes that the refractive index still changes during the measurement. The last procedure, the backward-approach, underestimates the present SFC systematically. This in particular at low SFC values. This is thought to be due to problems to initiate crystallization at low supersaturations and the above mentioned sample fractionation due to fouling. The data show, that a stepwise stabilization with increasing temperature allows to shorten the measurement time in TMOR procedures. Additional work is required to identify the optimal stabilization time.

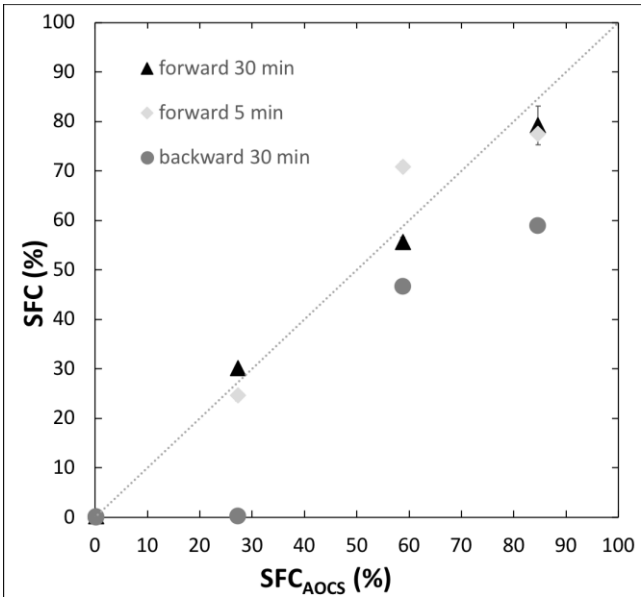

Figure 8.7: Parity plot for SFC determination by TMOR with different sample stabilization; comparison of reference AOCS procedure with three different temperature profiles: black triangles display a forward measurement with 30 min stabilization time, light grey diamonds represent a forward procedure with 5 min stabilization time, dark grey circles display stepwise profile with decreasing temperature and 30 min stabilization time.

8.4 Conclusion

This work illustrates that it is possible to determine the SFC of fats by TMOR. Results comparable to the established pNMR method were obtained. The data generation based on the lever rule or pseudo mass balance appears to be justified after the validity of the Lorentz-Lorenz equation for these systems was established. For complicated systems such as palm oil using TMOR was promising for temperatures higher than 20 °C. Also the SFC values obtained for partially hydrogenated palm oil showed good agreement with the established pNMR method.

The assumptions made for the calculation were that the refractive index in the liquid phase at any temperature can be determined by extrapolation. Using the generic slope, a single system specific data point is sufficient input. For the solid phases the generic slope is taken half that of the liquid state (Van Putte and Van Den Enden, 1974). To determine the anchor point for the refractive index of the solid phase is more complicated. It can be identified either for temperatures that relate to a fully crystalline sample or a single data point with known SFC at a given temperature.

In conclusion, the work reported here documents the feasibility of TMOR to determine the SFC of fats and oils. It was found that SFC curves could be generated with a single sample in a reasonably short period of time. Even though substantial additional work is needed to prove the general applicability of TMOR for SFC measurements in fats and oils it has the potential to become a versatile alternative to DSC of pNMR measurements.

Acknowledgements

The authors would like to thank Anton Paar OptoTec GmbH for the support providing the prototype and space for discussion. In addition, the authors are grateful for the financial support of the Elsa Neumann scholarship of the federal state of Berlin and Anton Paar OptoTec GmbH. The authors have declared no conflict of interest.

9 FEASIBILITY STUDY TO INVESTIGATE POLYMORPHIC TRANSITIONS USING TMOR

The following work presents the possibility to determine polymorphic forms using TMOR. Polymorphism is crucial in fat technology if products like chocolate or margarine are considered (Sato and Ueno, 2005). Usually it is determined using the established method of powder X-ray diffraction (XRD). This method is explained in detail in the experimental methods section (see chapter 3.6). Shortly, an X-ray beam is scattered by a sample in different directions if distinct polymorphic forms are under investigation. This method is used as a reference to investigate the applicability of TMOR to examine polymorphism. In this study, the polymorphic behavior of fully hydrogenated palm oil was investigated.

The aim of the work at hand was first to obtain two temperature profiles which result in distinct polymorphic forms. Second, the applicability of TMOR to determine different polymorphic forms was investigated.

9.1 Measurement Procedure

Before the treatment of the sample to achieve different polymorphic forms the fat was heated to 80 °C in a heating cabinet and kept at this temperature for approximately 30 min to remove all remaining crystals.

The XRD samples were prepared directly on the slides to avoid a change in the sample caused by subsequent treatment. Approximately 100 µl of the liquid fully hydrogenated palm oil were poured into the sample mold, where it was crystallized according to two different temperature profiles. A less stable polymorphic form was yielded by cooling the sample quickly to 4 °C and maintaining the temperature for 10 min. A more stable polymorphic form was generated by cooling the sample to 45 °C and hold the temperature for 60 min. The device measures the intensity of the reflected X-ray beam of the sample. The intensity plotted over the angle gives the typical XRD pattern. The generated XRD patterns are analyzed in two different regions depending on whether peaks occur in the small (< 6°) or the wide angle (> 6°) region. Depending on the peak position, conclusions are drawn about the unit cell structure and polymorphism (wide angle) as well as the crystal domain size and polytypism (small angle) (Peyronel and Marangoni, 2014b). Since polymorphism should be investigated the XRD patterns were analyzed in the wide angle region.

The temperature profile for TMOR was conducted directly on the prism of the device. The samples were cooled down with 10 °C/min and hold at 4 °C for 10 min for the less stable form and at 45 °C for 60 min to generate a more stable polymorph. During both stabilization procedures the temperature was modulated with and amplitude of 0.5 °C. Subsequently, the samples were heated at 2 °C/min for investigation with a modulation period of 30 s and an amplitude of 0.5 °C. This melting profile was used to determine if differences in the polymorphic forms are identifiable by TMOR.

The same temperature profile was performed with a DSC device from Netzsch (DSC 204 F1 Phoenix, NETZSCH-Geraetebau GmbH, Selb, Germany). 5-10 mg of sample was weighed into aluminum pans and an empty pan was used as a reference. Data was received at a scan rate of 2 °C/min. The DSC thermograms were used to check if TMOR is more accurate.

Only measurements without loss of contact were used for the analysis to guarantee the same temperature history like the samples analyzed in the XRD. The lack of contact between the sample and the prism can result in poor heat transfer due to the fact that the prism is the heat source.

9.2 Results and Discussion

Figure 9.1 shows the sample which was stabilized at 45 °C for 60 min. The pattern showed four peaks at 0.39 nm, 0.42 nm, 0.44 nm, and 0.46 nm. Characteristic peaks of the β' polymorph in the wide angle region are found at 0.42 nm and 0.38 nm. The polymorphic form β has its most characteristic peak at 0.46 nm (deMan, deMan and Blackman, 1989).

Hence, probably a mixture of both β' and β form is present. Another explanation could be that the existing POP in palm oil is converted into PSP during the hydrogenation process. It was stated, that this TAG only shows a β' polymorph as its most stable form. Hence, the yielded polymorphic form might already be the most stable one (D'Souza, DeMan and DeMan, 1990).

In comparison, the stabilization at 4 °C for 10 min lead to the XRD pattern depicted in Figure 9.2. A strong peak in the wide angle region at 0.41 nm was found which corresponds to the α polymorph (deMan, deMan and Blackman, 1989).

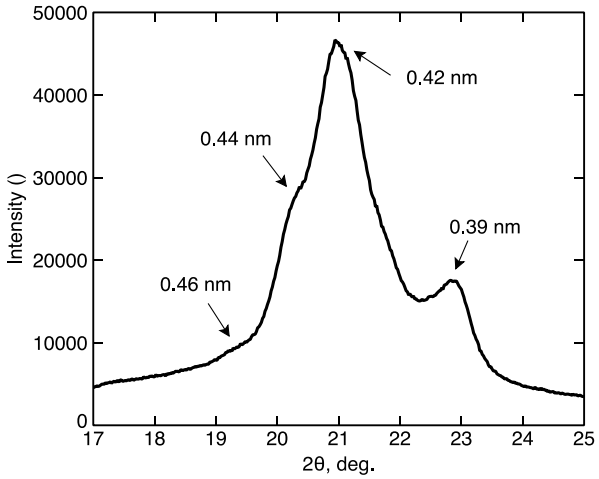

Figure 9.1: XRD pattern of fully hydrogenated palm oil stabilized at 45 °C for 60 min (left: small angle region; right: wide angle region).

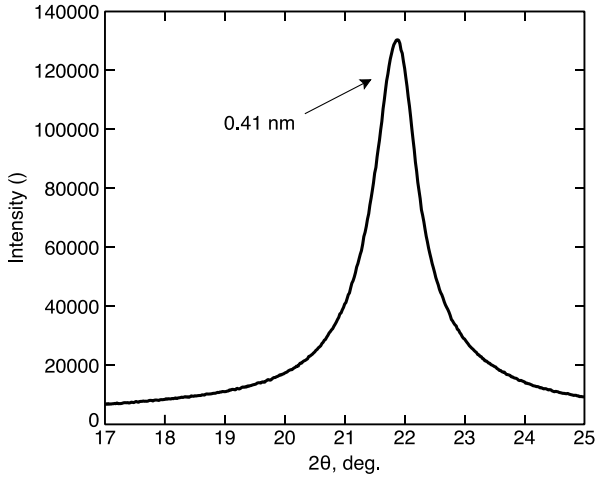

Figure 9.2: XRD pattern of fully hydrogenated palm oil stabilized at 4 °C for 10 min (left: small angle region; right: wide angle region).

In summary, the two different temperature profiles successfully yielded two distinct polymorphs. These were identified as the α and the, probably, β' form of fully hydrogenated palm oil. Hence, the two profiles were also used to conduct the experiments with TMOR.

The obtained TMOR graphs are shown in in Figure 9.3. The melting patterns show different developments. In the left graph, the sample was stabilized for 10 min at 4 °C. A small bump at approximately 48.0 °C and a large peak at 55 °C are visible. The small bump indicates that a less stable polymorphic form melts at this temperature. This is also visible in the refractive index which increases at temperatures higher than 48.0 °C indicating the recrystallization of the sample in a more stable polymorph. This polymorph starts to melt at around 52.0 °C and shows a peak temperature of 54.5 °C. This graph could be related to the XRD pattern received for the α polymorph.

The right graph of Figure 9.3 depicts the TMOR data after the stabilization of the sample at 45 °C for 60 min. The melting profile shows one melting peak and no kink in the refractive index. This leads to the conclusion that no unstable polymorph was formed and only the melting of the more stable polymorph occurred at around 55 °C. Hence, a differentiation between two distinct polymorphic forms is possible using TMOR even though the determination of the exact polymorph was so far not established.

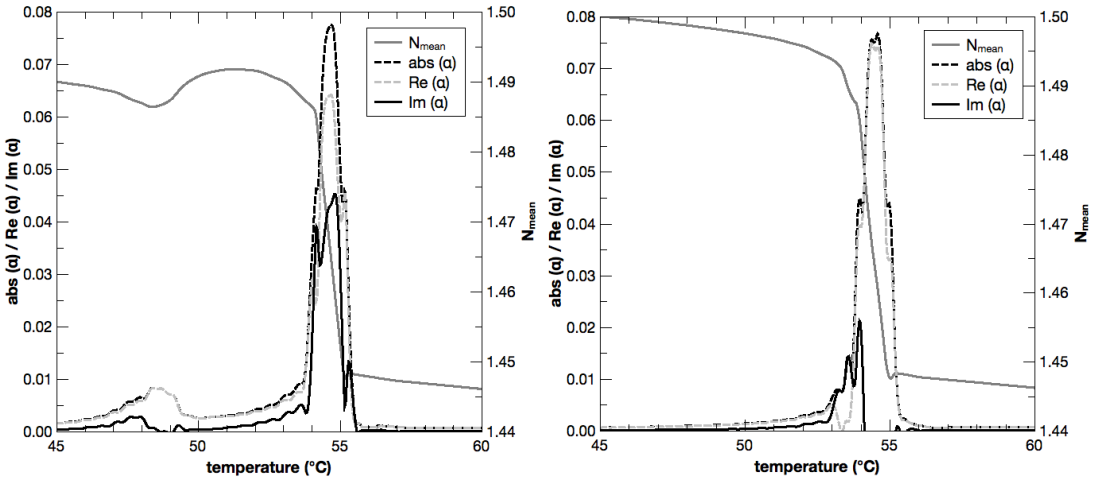

Figure 9.3: TMOR graphs of fully hydrogenated palm oil stabilized for 10 min at 4 °C (left) and for 60 min at 45 °C (right), both melted at a rate of 2 °C/min with a modulation period of 30 s and an amplitude of 0.5 °C.

The melting profile after the different stabilization regimes measured with DSC is depicted in Figure 9.4. The already explained recrystallization, concluded from the kink in the refractive index in Figure 9.3 (left graph), can be confirmed with the thermogram. The black solid line represents the less stable α polymorph which shows a recrystallization peak around 50 °C. The melting behavior of the more stable polymorph is given by the dashed grey curve.

For both stabilization procedure, DSC detects the peak temperatures at a higher temperature than TMOR. This confirms the above shown results that TMOR seems to have a higher sensitivity than DSC (see chapter 7).

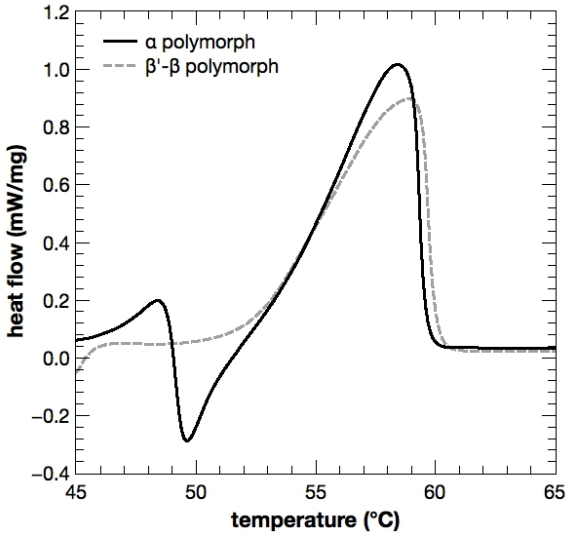

Figure 9.4: DSC thermogram of fully hydrogenated palm oil, stabilized for 10 min at 4 °C (α polymorph, black solid line) and for 60 min at 45 °C (β'-β polymorph, grey dashed line), both heated at 2 °C/min.

9.3 Conclusion

This work showed that differences in the TMOR data were obtained for distinct polymorphic forms. This shows the possibility that TMOR could be a device to investigate polymorphism. To obtain reliable data and procedures, more studies need to be conducted. Quasi-isothermal measurements which are conducted at one constant temperature with a predefined modulation amplitude and period should be conducted slightly below the polymorphic transition temperature. This means that the examination of the polymorphic transition is performed at one temperature only stimulated by a

small temperature modulation. This could be useful to generate more information about polymorphism using TMOR. These small temperature perturbations could force the crystals to rearrange in a more stable crystal structure at an even lower temperature than assumed at the moment. The results would be a more accurate statement to the correct transition temperature of polymorphic forms. Furthermore, the extension of the polymorphic investigations to cocoa butter would be helpful because its polymorphic behavior is widely studied. Since this fat shows only slight differences in some of its polymorphic forms the sensitivity of the TMOR equipment might help to get an even deeper insight.

10 FINAL CONCLUSION AND OUTLOOK

The conclusions of this thesis are given in two separated sub-chapters. One concludes the findings of the preliminary studies and the combined experiments of the new continuous emulsion fractionation process. The other gives a conclusion about the new determination method for phase transitions namely temperature modulated optical refractometry. In addition, an outlook on further experiments is given in each section.

10.1 Continuous emulsion fractionation

The idea behind the emulsion fractionation process was the design of a continuous fractionation process combining a continuous formation of a Pickering emulsion and a subsequent separation in a decanter centrifuge. The continuity of the process is desirable to decrease production costs and time. In addition, by the precise control of the process parameters it might be possible to fractionate specialty fats in one fractionation step instead of a two- or even three-step dry fractionation or the application of a solvent fractionation which is comparatively expensive.

The continuous emulsion fractionation process is a promising approach if the proper process window is found. There are three types of processes that need to be in balance: crystallization, flocculation, and emulsion break up. The amount of formed crystals must be enough to stabilize the water droplets in the Pickering emulsion during the whole process without emulsion break up. Simultaneously, the crystalline material should not extend a certain amount to avoid flocculation which would inter alia decrease the density difference and, thus, the separation efficiency.

Before the complete process of emulsion fractionation was studied, it was investigated how Pickering emulsions can be prepared using a cold water and a warm oil stream. Then, after having established stable Pickering emulsion, the separation was first tested using a benchtop centrifuge. Only if satisfying separation was established there, test runs were done in the decanter.

Three Pickering differently prepared emulsions were examined in this thesis. The dynamic preparation of the Pickering emulsion was done by simultaneously injecting the warm oil stream (10 % (w/w) hardstock) and the cold water stream (20 % (w/w)). Due to the contact of the cold water droplets, fat crystals originating from the warm liquid oil stream formed on the water droplet surface.

The static preparation meant that the Pickering emulsion was prepared with an Ultra-Turrax®, using a rotor-stator principle. The warm oil mixture (5 % (w/w) hardstock) and warm water (20 % (w/w) were emulsified and subsequently cooled down in an ice bath to induce crystallization of the high melting TAGs. Therefore, a Pickering stabilization was established.

The stored Pickering emulsion was commercially available and had almost the same composition as the statically prepared emulsion. Only the amount of hardstock was 2 % (w/w) instead of 5 % (w/w).

As mentioned above, to investigate the separation of the liquid oil phase and the water droplets stabilized by fat crystals, first, a benchtop centrifuge was used. Based on the findings of these separations, separation of these emulsions was tested in the decanter.

The dynamic prepared emulsion was stable for a short time but the droplets did not withstand the forces in the benchtop centrifuge so that a separation was not successful and the emulsion broke. The high amount of water and probably too large droplets could be the reason that the generated amount of fat crystals was not enough to stabilize the emulsion properly. A test run with a Pickering emulsion prepared dynamically in the decanter showed that there is no transport of solid fat crystals to the solid discharge. Due to the fact that the water droplets could not withstand the forces, they were destroyed probably leading to a water layer on the bottom of the decanter bowl. This layer prevented the solids from being transported by the screw and, thus, no solids exit the decanter.

The statically prepared emulsion was separated in the benchtop centrifuge into a liquid oil layer and a sediment composed of oil, fat crystals, and water. However, when testing the separation in the decanter the sediment was not transported to the solid discharge of the decanter but was again dispersed in the liquid phase and left the decanter in the liquid phase by both discharges.

It was already difficult to separate the stored Pickering emulsion in the benchtop centrifuge so that it was not expected that the decanter experiments would lead to a satisfying separation efficiency. Interestingly, in the decanter the solids were accumulated in the sample at the solid discharge. This leads to the conclusion that the stability of the emulsion was sufficient, the fat crystals remained attached to the surface

of the water droplets, and that the friction in the decanter was high enough to transport solids to the solid discharge. However, the ratio of solids discharged from the solid exit and the solids discharged with the liquid oil stream is not much larger than one, so that the separation efficiency is too low.

The studies described above show that the separation of a Pickering emulsion in the desired fractions was in general possible if crystallization and separation in a benchtop centrifuge were done separately. However, the continuous process in the decanter was not as successful. Here, the kinetics during crystallization and separation play an important role. As a result, either the fat crystals formed were not sufficient to occupy the surface of the water droplets stabilizing the emulsion or the crystals formed did rather form a network leading to flocculation which makes the separation very difficult. Thereby, the temperature is a crucial parameter because it influences the phase behavior and the kinetics. For example, if the surrounding liquid oil phase has a too high temperature, the fat crystals formed on the cold water droplets melt. If the temperature in the system is too low, too many fat crystals are formed causing a network formation. The temperature in the system is influenced on one hand by the starting temperatures of the liquid oil phase and the water phase in combination with the magnitude of these two streams and the dispersion and size of the water droplets, and on the other hand by the process conditions within the decanter.

In conclusion, the process sounds promising but the proper process conditions are hard to determine because of the complexity of the process. In particular, the kinetics of the crystallization and of the separation play an important role.

10.2 Temperature modulated optical refractometry

The rather new analytical method of temperature modulated optical refractometry (TMOR) uses refractometry in combination with temperature undulation to determine phase transitions. These transitions can either be glass or phase transitions (e.g. melting or crystallization). In both cases, a change in the thermal volume expansion coefficient α is determined from the phase shift which is caused by the temperature modulation.

The real part of α points to the kind of phase transition (step = glass transition, peak = melting or crystallization) at a given temperature which is indicated by the imaginary part.

The conducted studies applying TMOR to investigate the phase behavior of lipid mixtures showed that the results are as good as the ones obtained with the established DSC method. At the moment the temperatures at which the analysis can be done lay between 5 °C and 85 °C due to restrictions of the device. An extension of this range to lower temperatures would be desirable to make TMOR applicable even in a wider range to study fat and oil mixtures.

The easy sample handling and the possibility to analyze both transparent and opaque material make TMOR widely applicable. It was found that a proper combination of scan rate und modulation amplitude is crucial for all analysis so that they do not interfere and cause superimposed results. It seems that because the sample volume considered for measurement is smaller than for analysis by DSC, a higher sensitivity to phase changes was found. In addition, the prism is in direct contact with the sample which makes the heat transfer more direct than for the DSC measurement where the heat needs to permeate the aluminum crucible.

The verification of the method by investigating pure substances like *n*-hexadecane showed that the phase transition could be determined more accurately by TMOR than by DSC. This emphasizes the higher sensitivity of the measurement. The phase behavior of samples with increasing complexity like TAGs and fats (TAG mixtures) could also be determined using TMOR. Hence, it could be an extension or even replacement to the well-established DSC method to investigate crystallization and melting phenomena in fat and oil mixtures.

In addition, TMOR seems to work more accurate at smaller scan rates which allows the slower measurement resulting in more precise data or even discovering new phase transitions e.g. polymorphic transitions. So far, only preliminary studies were performed concerning the determination of polymorphism but give promising results for the differentiation between an α-polymorph and a β-polymorph.

Another application of the analytical method using TMOR was found to be the determination of the solid fat content in slurries. To prove this method, first, the validity of the Lorentz-Lorenz equation for fats was confirmed by separate density and refractive index measurements. From these, the so-called specific refractivity *r* could be determined for coconut oil, palm oil and rapeseed oil and was constant over the investigated temperature range. Since it was shown that an apparent refractive index of the slurry could be measured the SFC of this slurry could be computed using one value of the refractive index of the solid and the liquid phase. In this work, it was shown that this experimental determination of the SFC for coconut oil and partially hydrogenated palm oil was very accurate. The determination of the SFC for palm oil was not as accurate because it was not completely solid at a temperature of 0 °C so that the refractive index of the solid could not be determined. However, if the SFC together with the apparent refractive index of a slurry and of its constituent liquid phase is known, the method allows to compute the value of 100 % solids.

In summary, the determination of phase transitions of lipid mixtures and the SFC by TMOR was investigated in this thesis and found to be applicable. Preliminary tests showed that the investigation of polymorphic transitions can also be done using TMOR but further studies need to be conducted to verify the method.

10.3 Outlook

The work at hand shows that emulsion fractionation seems to be possible. Though to design a reliable process, more studies and modifications of the first set-up are required. To make the emulsion fractionation process more robust, water droplets could be replaced by particles of defined size and density. These particles are resistant against coalescence, their size stays the same over the processing time, and they are not deformed under force. However, it is difficult to find particles with a similar high heat capacity as water to ensure that the temperature of the particles is such that the desired fat crystals form at the surface of the particles. Additionally, the density of these particles needs to be higher than the one of water to improve the separation in the decanter.

The application of particles would decrease the number of processes which need to be controlled. The main process would be the crystallization of the fat at the surface while for water droplets also the stability of the emulsion due to the mentioned coalescence and fragility of the droplets under force need to be considered.

Further investigations of emulsion fractionation using water would imply to decrease the size of the water droplets during dynamic emulsion preparation. The smaller droplets ensure a larger surface at which the high melting fraction crystallizes. However, care needs to be taken since they heat up faster than larger droplets. In addition, the kinetics responsible for water droplets to coalesce and the kinetics of fat crystals to attach to the water droplet surface need to be studied. Only if the coalescence of the water droplets occurs slower than the attachment or formation of the crystals on the surface, the process can be successful

To further understand the underlying processes in the decanter, experiments only separating fat crystals from oil in the decanter should be conducted. Thereby, the device parameter (e.g. length of drying zone, retention time, acceleration, differential speed) influencing the separation efficiency could be obtained.

The next steps to further establish TMOR as an analytical tool in fat technology should be the investigations of a wide variety of fats differing in composition. The determined specific refractivity *r* was found constant for the investigated fats. Further investigations with different fats could lead to a correlation between the specific refractivity *r* and the fat composition (length/ saturation/ distribution of fatty acid residues at TAGs or iodine value). With these values known, the SFC value could be determined for more fats.

Another issue to be addressed is the extension of the achievable temperature range, in particular to lower temperatures. Then, the measurement of the refracitve index of 100 % solids would be possible for more fats. Hence, the application range of TMOR to determine SFC would be extended.

The future studies on polymorphism should include quasi-isothermal experiments at one temperature with additional modulation slightly below the known transition temperature of polymorphs. Due to the temperature undulation, the polymorphic transitions should then be accurately determined. For the development and later verification of the method cocoa butter should be used as a model system as it is known

for its high degree of polymorphism. In summary, both, continuous emulsion fractionation and temperature modulated optical refractometry, are applicable in fat technology and need to be studied intensively in the future to extend their field of application and reliability.

REFERENCES

Adomako, D. (1977) 'Fatty acid composition and characteristics of Pentadesma butyracea fat extracted from ghana seeds', *Journal of the Science of Food and Agriculture*, 28(4), pp. 384–386. doi: 10.1002/jsfa.2740280411.

Aini, I. N. and Miskandar, M. S. (2007) 'Utilization of palm oil and palm products in shortenings and margarines', *European Journal of Lipid Science and Technology*, 109(4), pp. 422–432. doi: 10.1002/ejlt.200600232.

Aleksandrova, R., Philipp, M., Müller, U., Rioboo, R. J., Ostermeyer, M., Sanctuary, R., Müller-Buschbaum, P. and Krüger, J. K. (2014) 'Phase instability and molecular kinetics provoked by repeated crossing of the demixing transition of PNIPAM solutions', *Langmuir*, 30(39), pp. 11792–11801. doi: 10.1021/la5026763.

Altieri, G., Di Renzo, G. C. and Genovese, F. (2013) 'Horizontal centrifuge with screw conveyor (decanter): Optimization of oil/water levels and differential speed during olive oil extraction', *Journal of Food Engineering*. Elsevier Ltd, 119(3), pp. 561–572. doi: 10.1016/j.jfoodeng.2013.06.033.

AOCS (2009a) 'Official Method Cd 16-81. Solid fat content (SFC) by low-resolution nuclear magnetic resonance - the indirect method.', in *Official Methods and Recommended Practices of the AOCS*. 6th edn.

AOCS (2009b) 'Official Method Cd 16b-93. Solid fat content (SFC) by low-resolution nuclear magnetic resonance - the direct method', in *Official Methods and Recommended Practices of the AOCS*. 6th edn.

Augusto, P. E. D., Soares, B. M. C., Chiu, M. C. and Gon??alves, L. A. G. (2012) 'Modelling the effect of temperature on the lipid solid fat content (SFC)', *Food Research International*. Elsevier Ltd, 45(1), pp. 132–135. doi: 10.1016/j.foodres.2011.10.026.

Awad, T., Hamada, Y. and Sato, K. (2001) 'Effects of addition of diacylglycerols on fat crystallization in oil-in-water emulsion Research Paper', *European Journal of Lipid Science and Technology*, 103, pp. 735–741.

Awad, T. and Sato, K. (2001) 'Effects of hydrophobic emulsifier additives on crystallization behavior of palm mid fraction in oil-in-water emulsion', *Journal of the American Oil Chemists' Society*, 78(8), pp. 837–842. doi: 10.1007/s11746-001-0352-6.

Awad, T. and Sato, K. (2002) 'Acceleration of crystallisation of palm kernel oil in oil-in-water emulsion by hydrophobic emulsifier additives', *Colloids and Surfaces B: Biointerfaces*, 25(1), pp. 45–53. doi: 10.1016/S0927-7765(01)00298-3.

Bailey, A. E. and Kraemer, E. A. (1944) 'Dilatometric investigations of fats I. Apparatus and techniques for fat dilatometry', *Oil & Soap*, 21(9), pp. 251–253. doi: 10.1007/BF02565466.

Bailey, A. E. and Singleton, W. S. (1945) 'Dilatometric investigations of fats: III. The density, expansibility, and melting dilation of some simple triglycerides and other fats', *Oil & Soap*, 22(10), pp. 265–271. doi: 10.1007/BF02638406.

Basiron, Y. (2005) 'Palm Oil', in Shahidi, F. (ed.) *Bailey's Industrial Oil and Fat Products*. Hoboken, New Jersey: John Wiley & Sons, Inc., pp. 333–429.

Beiser, M., Bennoit, H., Erk, A., Forster, P., Frost, S., Hoffner, B., Karolis, A., Langeloh, T., Mayr, C., Schuster, C. and Stiborsky, M. (2004) 'Dekantierzentrifugen', in Stahl, W. H. (ed.) *Industrie-Zentrifugen*. Männedorf: DRM Press, pp. 391–722.

Bekkedahl, N. (1949) 'Volume dilatometry', *Journal of research of the National Bureau of Standards*, 42(2), pp. 145–156. doi: 10.6028/jres.043.017.

Bentz, A. P. and Breidenbach, B. G. (1969) 'Evaluation of the differential scanning calorimetric method for fat solids', *Journal of the American Oil Chemists' Society*, 46(2), pp. 60–63. doi: 10.1007/BF02541208.

Berger, K. G. and Idris, N. A. (2005) 'Formulation of zero-trans acid shortenings and margarines and other food fats with products of the oil palm', *Journal of the American Oil Chemists' Society*, 82(11), pp. 775–782. doi: 10.1007/s11746-005-1143-9.

Beysens, D. and Calmettes, P. (1977) 'Temperature dependence of the refractive indices of liquids: Deviation from the Lorentz–Lorenz formula', *The Journal of Chemical Physics*, 66(2), p. 766. doi: 10.1063/1.433954.

van Boekel, M. A. J. S. (1981) 'Estimation of solid-liquid ratios in bulk fats and emulsions by pulsed nuclear magnetic resonance', *Journal of the American Oil Chemists' Society*, 58(7), pp. 2–6. doi: 10.1007/BF02887319.

Bot, A. and Flöter, E. (2013) 'Application of Edible Oils', in *Edible Oil Processing*, pp. 223–249.

Braipson-Danthine, S. and Gibon, V. (2007) 'Comparative analysis of triacylglycerol composition, melting properties and polymorphic behavior of palm oil and fractions', *European Journal of Lipid Science and Technology*, 109(4), pp. 359–372. doi: 10.1002/ejlt.200600289.

Calliauw, G. (2014) *Dry Fractionation*, *AOCS Lipid Library*. Available at: http://lipidlibrary.aocs.org/OilsFats/content.cfm?ItemNumber=40328 (Accessed: 31 October 2017).

Calliauw, G., Fredrick, E., Gibon, V., Greyt, W. De, Wouters, J., Foubert, I. and Dewettinck, K. (2010) 'On the fractional crystallization of palm olein: Solid solutions and eutectic solidification', *Food Research International*. Elsevier Ltd, 43(4), pp. 972–981. doi: 10.1016/j.foodres.2010.01.002.

Carlton, R. A. (2011) 'Polarized Light Microscopy', in *Pharmaceutical Microscopy*, pp. 7–64. doi: 10.1007/978-1-4419-8831-7.

Chaleepa, K., Szepes, a. and Ulrich, J. (2010) 'Dry fractionation of coconut oil by melt crystallization', *Chemical Engineering Research and Design*, 88(9), pp. 1217–1222. doi: 10.1016/j.cherd.2010.01.026.

Chapman, D. and Sunlight, P. (1959) 'A Nuclear Magnetic Resonance Study of the Liquid / Solid Content of Margarine Fat', *Journal of American Oil Chemists' Society*, 37, pp. 243–246.

Che Man, Y. B., Haryati, T., Ghazali, H. M. and Asbi, B. A. (1999) 'Composition and thermal profile of crude palm oil and its products', *Journal of the American Oil Chemists' Society*, 76(2), pp. 237–242. doi: 10.1007/s11746-999-0224-y.

Chiu, M. H. and Prenner, E. J. (2011) 'Differential scanning calorimetry: An invaluable tool for a detailed thermodynamic characterization of macromolecules and their interactions', *Journal of Pharmacy and Bioallied Science*, 3(1), pp. 39–59. doi: 10.4103/0975.

Codex (2001) 'Codex standard for named vegetable oils', *Codex Alimentarius*, 8, pp. 11–25.

Cornelius, J. A. (1977) 'Palm Oil and Palm Kernel Oil', *Prog. Chem. Fats other Lipids*, 15, pp. 5–27.

Costa, M. C., Rolemberg, M. P., Meirelles, A. J. A., Coutinho, J. A. P. and Krähenbühl, M. A. (2009) 'The solid–liquid phase diagrams of binary mixtures of even saturated fatty acids differing by six carbon atoms', *Thermochimica Acta*, 496(1–2), pp. 30–37. doi: 10.1016/j.tca.2009.06.018.

Coupland, J. N. and McClements, D. J. (1997) 'Physical properties of liquid edible oils', *Journal of the American Oil Chemists' Society*, 74(12), pp. 1559–1564. doi: 10.1007/s11746-997-0077-1.

Cowan, W. D. (2014) *Enzymatic Interesterification*, *AOCS Lipid Library*.

D'Souza, V., DeMan, J. M. and DeMan, L. (1990) 'Short spacings and polymorphic forms of natural and commercial solid fats: A review', *Journal of the American Oil Chemists' Society*, 67(1), pp. 835–843. doi: 10.1007/BF02540502.

Deffense, E., Tirtiaux, S. A. F. and Charleroi, C. De (1985) 'Fractionation of Palm Oil', *JAOCS, Journal of the American Oil Chemists' Society*, 62(2), pp. 376–385.

deMan, L., deMan, J. M. and Blackman, B. (1989) 'Polymorphic behavior of some fully hydrogenated oils and their mixtures with liquid oil', *Journal of the American Oil Chemists' Society*, 66(12), pp. 1777–1780. doi: 10.1007/BF02660746.

Dhaka, V., Gulia, N., Ahlawat, K. S. and Khatkar, B. S. (2011) 'Trans fats-sources, health risks and alternative approach - A review.', *Journal of food science and technology*, 48(5), pp. 534–41. doi: 10.1007/s13197-010-0225-8.

Dijkstra, A. J. (2014a) *Chemical Interesterification*, *AOCS Lipid Library*. Available at: http://lipidlibrary.aocs.org/OilsFats/content.cfm?ItemNumber=40323 (Accessed: 7 November 2017).

Dijkstra, A. J. (2014b) *Hydrogenation Mechanism*, *AOCS Lipid LibraryC*.

Dorset, D. L. (2005) 'Binary and multicomponent solids of n-paraffins', in *Crystallography of the Polymethylen Chain- an Inquiry into the Structure of Waxes*. New York: Oxford University Press, pp. 73–108.

Douaire, M., di Bari, V., Norton, J. E., Sullo, A., Lillford, P. and Norton, I. T. (2014) 'Fat crystallisation at oil-water interfaces.', *Advances in Colloid and Interface Science*. Elsevier B.V., 203, pp. 1–10. doi: 10.1016/j.cis.2013.10.022.

Van Boekel (1981) Estiation of solid-liquid ratios in bulk fats and emulsions by pulsed nuclear magnetic resonance, *Journal of the American Oil Chemists´ Society*, 768-772.

Van Duynhoven, J., Dubourg, I., Goudappel, G. J. and Roijers, E. (2002) 'Determination of MG and TG phase composition by time-domain NMR', *Journal of the American Oil Chemists' Society*, 79(4), pp. 383–388. doi: 10.1007/s11746-002-0493-7.

van den Enden, J. C., Haighton, A. J., van Putte, K., Vermaas, L. F. and Waddington, D. (1978) 'A Method for the Determination of the Solid Phase Content of Fats Using Pulse Nuclear Magnetic Resonance', *Fette, Seifen, Anstrichmittel*, 80(5), pp. 180–186. doi: 10.1002/lipi.19780800502.

Esteban, B., Riba, J. R., Baquero, G., Rius, A. and Puig, R. (2012) 'Temperature dependence of density and viscosity of vegetable oils', *Biomass and Bioenergy*. Elsevier Ltd, 42, pp. 164–171. doi: 10.1016/j.biombioe.2012.03.007.

Firestone, D. (1999) *Physical and Chemical Characteristics of Oils, Fats, and Waxes*. Washington D.C.: AOCS Press.

Floeter, E., Haeupler, M. and Sato, K. (2018) 'Molecular Interactions and Mixing Phase Behavior of Lipid Crystals', in Sato, K. (ed.) *Crystallization of Lipids: Fundamentals and Applications in Food, Cosmetics and Pharmaceuticals*. Wiley-Blackwell, pp. 61–104.

Flöter, E. (2009) 'The role of physical properties data in product development', *European Journal of Lipid Science and Technology*, 111(3), pp. 219–226. doi: 10.1002/ejlt.200800260.

Flöter, E. (2012) 'Phase Behavior of Fat Mixtures', in Marangoni, A. G. (ed.) *Structure-function analysis of edible fats*. Urbana: AOCS Press, pp. 107–126.

Flöter, E. (2014a) 'Crystallization', *Private Communication*, pp. 1–33.

Flöter, E. (2014b) 'Vorlesung Fraktionierung'. Berlin.

Frasch-Melnik, S., Norton, I. T. and Spyropoulos, F. (2010) 'Fat-crystal stabilised w/o emulsions for controlled salt release', *Journal of Food Engineering*. Elsevier Ltd, 98(4), pp. 437–442. doi: 10.1016/j.jfoodeng.2010.01.025.

Fulton, N. D., Lutton, E. S. and Wille, R. L. (1953) 'A Quick Dilatometric Method for Control and Study of Plastic Fats', *JAOCS, Journal of the American Oil Chemists' Society*, 31, pp. 98–103.

Ghosh, S. and Rousseau, D. (2011) 'Fat crystals and water-in-oil emulsion stability', *Current Opinion in Colloid and Interface Science*. Elsevier Ltd, 16(5), pp. 421–431. doi: 10.1016/j.cocis.2011.06.006.

Gleiss, M. and Nirschl, H. (2015) 'Modeling Separation Processes in Decanter Centrifuges by Considering the Sediment Build-Up', *Chemical Engineering & Technology*, 38(10), pp. 1873–1882.

Gunstone, F. D. (2013) 'Composition and Properties of Edible Oils', in Hamm, W., Hamilton, R. J., and Calliauw, G. (eds) *Edible Oil Processing*. Chister, UK: John Wiley & Sons, Ltd., pp. 1–39.

Hajj Ali, H., Michaux, F., Bouelet Ntsama, I. S., Durand, P., Jasniewski, J. and Linder, M. (2016) 'Shea butter solid nanoparticles for curcumin encapsulation: Influence of nanoparticles size on drug loading', *European Journal of Lipid Science and Technology*, 118(8), pp. 1168–1178. doi: 10.1002/ejlt.201500348.

Hamm, W. (1986) 'Fractionation - With or without Solvent?', *Fette, Seifen, Anstrichmittel*, 88(1 S), pp. 533–537. doi: 10.1002/lipi.19860881310.

Harris, J. (2014) *Solvent Fractionation*, *AOCS Lipid Library*. Available at: http://lipidlibrary.aocs.org/OilsFats/content.cfm?ItemNumber=40338 (Accessed: 10 August 2017).

Hartel, R. W. (2013) 'Advances in food crystallization.', *Annual review of food science and technology*, 4, pp. 277–92. doi: 10.1146/annurev-food-030212-182530.

Häupler, M. and Floeter, E. (2018) 'Determination of the Crystallization Behavior of Lipids by Temperature Modulated Optical Refractometry', *submitted to Food Analytical Methods*.

Häupler, M., Savitri, R. A., Hutschenreuter, V. and Flöter, E. (2018) 'Application of Temperature Modulated Optical Refractometry for the Characterization of the Crystallization Behavior of Palm Oil', *European Journal of Lipid Science and Technology*, 1700511, p. 1700511. doi: 10.1002/ejlt.201700511.

Hernqvist, L. (1988) 'Crystal Structures of Fats and Fatty Acids', in *Crystallization and Polymorphism of Fats and Fatty Acids*, pp. 97–137.

Himawan, C., Starov, V. M. and Stapley, A. G. F. (2006) 'Thermodynamic and kinetic aspects of fat crystallization.', *Advances in Colloid and Interface Science*, 122(1–3), pp. 3–33. doi: 10.1016/j.cis.2006.06.016.

Hodge, S. M. and Rousseau, D. (2005) 'Continuous-phase fat crystals strongly influence water-in-oil emulsion stability', *Journal of the American Oil Chemists' Society*, 82(3), pp. 159–164. doi: 10.1007/s11746-005-5166-4.

Ikeda, E., Ueno, S., Miyamoto, R. and Sato, K. (2010) 'Phase behavior of a binary mixture of 1,3-dipalmitoyl-2-oleoyl-sn-glycerol and 1,3-dioleoyl-2-palmitoyl-sn-glycerol in n-dodecane solution', *Journal of Physical Chemistry B*, 114(34), pp. 10961–10969. doi: 10.1021/jp101821c.

Illers, K.-H. (1974) 'Die Ermittlung des Schmelzpunktes von kristallinen Polymeren mittels Wärmeflusskalorimetrie (DSC)', *European Polymer Journal*, 10(10), pp. 911–916. doi: 10.1016/0014-3057(74)90027-5.

Jacobsberg, B. and Ho, O. C. (1976) 'Studies in palm oil crystallization', *Journal of the American Oil Chemists' Society*, 53(10), pp. 609–617. doi: 10.1007/BF02586272.

Kang, K. K., Kim, S., Kim, I. H., Lee, C. and Kim, B. H. (2013) 'Selective enrichment of symmetric monounsaturated triacylglycerols from palm stearin by double solvent fractionation', *LWT - Food Science and Technology*. Elsevier Ltd, 51(1), pp. 242–252. doi: 10.1016/j.lwt.2012.08.009.

Kaufmann, H. P. and Thieme, J. G. (1954) 'Zur Refraktometrie der Fette II: Das Prinzip der Mehrphasen-Refraktometrie *', *Fette, Seifen, Anstrichmittel*, 56(12), pp. 990–996.

Kaufmann, H. P., Thieme, J. G. and Wöhlert, U. (1955) 'Zur Refraktometrie der Fette III: Mehrphasen-Rafraktometrie der polymorphen Kakaobutter-Glyceride', *Fette, Seifen, Anstrichmittel*, 57(1), pp. 21–24.

Kellens, M. and Calliauw, G. (2013) 'Oil Modification Processes', in Hamm, W., Hamilton, R. J., and Calliauw, G. (eds) *Edible Oil Processing*. 2nd edn. Chichester: John Wiley & Sons Ltd., pp. 153–196.

Kellens, M., Gibon, V., Hendrix, M. and De Greyt, W. (2007) 'Palm oil fractionation', *European Journal of Lipid Science and Technology*, 109(4), pp. 336–349. doi: 10.1002/ejlt.200600309.

Kellens, M., Meeussen, W., Gehrke, R. and Reynaers, H. (1991) 'Synchrotron radiation investigations of the polymorphic transitions of saturated monoacid triglycerides. Part 2: Polymorphism study of a 50:50 mixture of tripalmitin and tristearin during crystallization and melting', *Chemistry and Physics of Lipids*, 58(1–2), pp. 131–144. doi: 10.1016/0009-3084(91)90119-V.

Kloek, W., Walstra, P. and van Vliet, T. (2000) 'Crystallization kinetics of fully hydrogenated palm oil in sunflower oil mixtures', *Journal of the American Oil Chemists' Society*. Springer-Verlag, 77(4), pp. 389–398. doi: 10.1007/s11746-000-0063-z.

Koyano, T., Hachiya, I. and Sato, K. (1990) 'Fat Polymorphism and Crystal Seeding Effects on Fat Bloom Stability of Dark Chocolate', *Food Structure*, 9(9), pp. 231–240. Available at: http://digitalcommons.usu.edu/foodmicrostructure%0Ahttp://digitalcommons.usu.edu/foodmicrostructure/vol9/iss3/6.

Koyano, T., Hachiya, I. and Sato, K. (1992) 'Phase Behavior of Mixed Systems of SOS and OS0', *American Chemical Society*, 96(25), pp. 10514–10520.

Lin, S. W. (2011) 'Palm Oil', in Gunstone, F. D. (ed.) *Vegetable Oils in Food Technology: Composition, Properties and Uses*. 2nd edn. Blackwell Publishing Ltd., pp. 25–58. doi: 10.1002/9781444339925.ch2.

Lopes, D. G., Becker, K., Stehr, M., Lochmann, D., Haack, D., Zimmer, A. and Salar-Behzadi, S. (2015) 'Role of Lipid Blooming and Crystallite Size in the Performance of Highly Soluble Drug-Loaded Microcapsules', *Journal of Pharmaceutical Sciences*, 104(12), pp. 4257–4265. doi: 10.1002/jps.24660.

Madison, B. L. and Hill, R. C. (1978) 'Determination of the solid fat content of commercial fats by pulsed nuclear magnetic resonance', *Journal of the American Oil Chemists' Society*, 55(3), pp. 328–331. doi: 10.1007/BF02669922.

Marangoni, A. G., Acevedo, N., Maleky, F., Co, E., Peyronel, F., Mazzanti, G., Quinn, B. and Pink, D. (2012) 'Structure and functionality of edible fats', *Soft Matter*, 8(5), p. 1275. doi: 10.1039/c1sm06234d.

Márquez, A. L., Pérez, M. P. and Wagner, J. R. (2013) 'Solid fat content estimation by differential scanning calorimetry: Prior treatment and proposed correction', *JAOCS, Journal of the American Oil Chemists' Society*, 90(4), pp. 467–473. doi: 10.1007/s11746-012-2190-z.

Masuchi, M. H., Gandra, K. M., Marangoni, A. L., de Sá Perenha, C., Chiu, M. C., Grimaldi, R. and Gonçalves, L. A. G. (2014) 'Fats from Chemically Interesterified High-Oleic Sunflower Oil and Fully Hydrogenated Palm Oil', *Journal of the American Oil Chemists' Society*, 91, pp. 859–866. doi: 10.1007/s11746-014-2420-7.

Menard, K. F. and Sichina, W. J. (2000) 'Prediction of Solid Fat Index (SFI) Values of Food Fats Using DSC', *Thermal Analysis*.

Metin, S. and Hartel, R. W. (2005) *Crystallization of Fats and Oils*, *Bailey's Industrial Oil and Fat Products*. doi: 10.1002/047167849X.bio021.

Mills, B. L. and van de Voort, F. R. (1981a) 'Comparison of the Direct and Indirect Wide-Line Nuclear Magnetic Resonance Methods for Determining Solid Fat Content', *JAOCS, Journal of the American Oil Chemists' Society*, pp. 776–778.

Mills, B. L. and van de Voort, F. R. (1981b) 'Determination of Solid Fat Index of Fats and Oils Using the Anton Paar Density Meter', *JAOCS, Journal of the American Oil Chemists' Society*, pp. 618–621.

Moens, K., De Clercq, N., Verstringe, S. and Dewettinck, K. (2015) 'Revealing the Influence of Tempering on Polymorphism and Crystal Arrangement in Semicrystalline Oil-in-Water Emulsions', *Crystal Growth and Design*, 15(12), pp. 5693–5704. doi: 10.1021/acs.cgd.5b00665.

Mondieig, D., Rajabalee, F. and V. Metivaud, V., Oonk, H. A. J. and Cuevas-Diarte, M. A. (2004) 'n-Alkane Binary Molecular Alloys', *Chemistry of Materials*, 16(5), pp. 786–798.

Mozaffarian, D. and Clarke, R. (2009) 'Quantitative effects on cardiovascular risk factors and coronary heart disease risk of replacing partially hydrogenated vegetable oils with other fats and oils', *European Journal of Clinical Nutrition*. Nature Publishing Group, 63, pp. 22–33. doi: 10.1038/sj.ejcn.1602976.

Mozaffarian, D., Pischon, T., Hankinson, S. E., Rifai, N., Joshipura, K., Willett, W. C. and Rimm, E. B. (2004) 'Dietary intake of trans fatty acids and systemic inflammation in women', *Am J Clin Nutr*, 79, pp. 606–612.

Mozaffarian, D., Rimm, E. B., King, I. B., Lawler, R. L., McDonald, G. B. and Levy, W. C. (2004) 'trans Fatty acids and systemic inflammation in heart failure', *American Journal of Clinical Nutrition*, 80, pp. 1521–1525.

MPOB (2009) *Pocketbook of Palm Oil uses*.

Müller, U., Philipp, M., Thomassey, M., Sanctuary, R. and Krüger, J. K. (2013) 'Temperature modulated optical refractometry: A quasi-isothermal method to determine the dynamic volume expansion coefficient', *Thermochimica Acta*. Elsevier B.V., 555, pp. 17–22. doi: 10.1016/j.tca.2012.12.011.

Nassu, R. T. and Guaraldo Gonçalves, L. A. (1995) 'Solid fat content determination: Comparison between pNMR and DSC techniques', *Grasas y Aceites*, 46(6), pp. 337–343. doi: 10.3989/gya.1995.v46.i6.949.

Nassu, R. T. and Guaraldo Gonçalves, L. A. (1999) 'Determination of melting point of vegetable oils and fats by differential scanning calorimetry (DSC) technique.', *Grasas y Aceites*, 50(1), pp. 16–21. doi: 10.3989/gya.1999.v50.i1.630.

Netzsch (2017) *Funktionsprinzip einer Wärmestrom-DSC*. Available at: https://www.netzsch-thermal-analysis.com/de/landing-pages/funktionsprinzip-einer-waermestrom-dsc/ (Accessed: 23 November 2017).

Ng, W. L. (1990) 'A study of the kinetics of nucleation in a palm oil melt', *Journal of the American Oil Chemists' Society*, 67(11), pp. 879–882. doi: 10.1007/BF02540510.

Ng, W. L. and Oh, C. H. (1994) 'A kinetic study on isothermal crystallization of palm oil by solid fat content measurements', *Journal of the American Oil Chemists' Society*, 71(10), pp. 1135–1139. doi: 10.1007/BF02675908.

Normann, W. (1931) 'Die Schmelzausdehnung der Fette', *Chemische Umschau auf dem Gebiet der Fette, Öle, Wachse und Harze*, 2, pp. 17–22.

Noureddini, H., Teoh, B. C. and Clements, L. D. (1992) 'Densities of Vegetable Oils and Fatty Acids', *Chemical and Biomolecular Engineering Research and Publications*, 69(12), pp. 1184–1188. doi: 10.1007/BF02637678.

Ostwald, W. (1897) 'Studien über die Bildung und Umwandlung fester Körper', *Zeitschrift für Physikalische Chemie*, 22, pp. 289–293.

Pawlik, A., Kurukji, D., Norton, I. and Spyropoulos, F. (2016) 'Food-grade Pickering emulsions stabilised with solid lipid particles', *Food Funct.* Royal Society of Chemistry, 7(6), pp. 2712–2721. doi: 10.1039/C6FO00238B.

Petersson, B., Anjou, K. and Sandström, L. (1985) 'Pulsed NMR Method for Solid Fat Content Determination in Tempering Fats, Part I: Cocoa Butters and Equivalents', *Fette, Seifen, Anstrichmittel*, pp. 225–230.

Peyronel, F. and Marangoni, A. G. (2014a) *Differential Scanning Calorimetry*, *AOCS Lipid Library*.

Peyronel, F. and Marangoni, A. G. (2014b) *X-Ray Powder Diffractometry*, *AOCS Lipid Library*. doi: 10.21748/lipidlibrary.40299.

Pickering, S. U. (1907) 'Emulsions', *Journal of the Chemical Society*, 91, pp. 2001–2021.

Vanden Poel, G. and Mathot, V. B. F. (2006) 'High-speed/high performance differential scanning calorimetry (HPer DSC): Temperature calibration in the heating and cooling mode and minimization of thermal lag', *Thermochimica Acta*, 446(1–2), pp. 41–54. doi: 10.1016/j.tca.2006.02.022.

Pohle, W. D., Taylor, J. R. and Gregory, R. L. (1965) 'A comparison of nuclear magnetic resonance and dilatometry for estimating solids content of fats and shortenings', *Journal of the American Oil Chemists Society*, 42(12), pp. 1075–1078. doi: 10.1007/BF02636912.

Przybylski, R. (2011) 'Canola/Rapeseed Oil', in Gunstone, F. D. (ed.) *Vegetable Oils in Food Technology: Composition, Properties and Uses, Second Edition*. 2nd edn. Blackwell Publishing Ltd., pp. 107–136. doi: 10.1002/9781444339925.ch4.

Van Putte, K. and Van Den Enden, J. (1974) 'Fully automated determination of solid fat content by pulsed NMR', *Journal of the American Oil Chemists Society*, 51(7), pp. 316–320. doi: 10.1007/BF02633005.

van Putte, M. and van den Enden, J. (1973) 'Pulse NMR as a quick method for the determination of the solid fat content in partially crystallized fats', *Journal of Physics E: Scientific Instruments*, 6, pp. 910–912. doi: 10.1088/0022-3735/6/9/031.

Ricci-Rossi, G. and Deffense, E. (1984) 'Erfahrungen mit der Fraktionierung von Fetten nach dem Tirtiaux-Verfahren', *Fette, Seifen, Anstrichmittel*, 86(1), pp. 500–505.

Richardson, M. J. and Savill, N. G. (1975) 'Temperatures in differential scanning calorimetry', 12, pp. 213–220.

Saeed, R. M., Schlegel, J. P., Castano, C. and Sawafta, R. (2016) 'Uncertainty of Thermal Characterization of Phase Change Material by Differential Scanning Calorimetry Analysis', *International Journal of Engineering Research and Technology*, 5(Volume. 5-Issue. 01, January-2016), pp. 405–413.

Sakata, M., Takahashi, Y. and Sonehara, M. (1985) 'Quality of fried foods with palm oil', *Journal of the American Oil Chemists' Society*, 62(2), pp. 449–454. doi: 10.1007/BF02541421.

Salas, J. J., Bootello, M. a., Martínez-Force, E. and Garcés, R. (2009) 'Tropical vegetable fats and butters: properties and new alternatives', *Oléagineux, Corps gras, Lipides*, 16(4-5–6), pp. 254–258. doi: 10.1051/ocl.2009.0278.

Sarma, P. V. V. R., Sailaja, B. B. V., Rao, T. A. S. and Rao, G. N. (2011) 'Physico chemical studies on texturized and partially hydrogenated RBD palm oil samples', *Annals of Biological Research*, 2(4), pp. 439–446.

Sato, K. (2001) 'Crystallization behaviour of fats and lipids — a review', *Chemical Engineering Science*, 56(7), pp. 2255–2265. doi: 10.1016/S0009-2509(00)00458-9.

Sato, K. and Garti, N. (1988) 'Crystallization and Polymorphic Transformation-An Introduction', in *Crystallization and Polymorphism of Fats and Fatty Acids*, pp. 3–7.

Sato, K., Goto, M., Yano, J., Honda, K., Kodali, D. R. and Small, D. M. (2001) 'Atomic resolution structure analysis of beta' polymorph crystal of a triacylglycerol: 1,2-dipalmitoyl-3-myristoyl-sn-glycerol.', *Journal of lipid research*, 42(3), pp. 338–345.

Sato, K. and Ueno, S. (2005) 'Polymorphism in fats and oils', in *Bailey's Industrial Oil and Fat Products*, pp. 77–120. Available at: http://onlinelibrary.wiley.com/doi/10.1002/047167849X.bio020/full.

Sato, K. and Ueno, S. (2011) 'Crystallization, transformation and microstructures of polymorphic fats in colloidal dispersion states', *Current Opinion in Colloid & Interface Science*. Elsevier Ltd, 16(5), pp. 384–390. doi: 10.1016/j.cocis.2011.06.004.

Sato, K., Ueno, S. and Yano, J. (1999) 'Molecular interactions and kinetic properties of fats', *Progress in Lipid Research*, 38(1), pp. 91–116. doi: 10.1016/S0163-7827(98)00019-8.

Schuchmann, H. P. and Köhler, K. (2012) *Emulgiertechnik: Grundlagen, Verfahren und Anwendungen*. 3rd edn. Hamburg: B. Behr´s Verlag GmbH & Co. KG.

Shahidi, F. (ed.) (2005) *Bailey´s Industrial Oil and Fat Products*, *Wiley interscience*. Hoboken, New Jersey: John Wiley & Sons, Inc. doi: 10.1002/047167849X.

Shi, Y., Liang, B. and Hartel, R. W. (2005) 'Crystal morphology, microstructure, and textural properties of model lipid systems', *Journal of the American Oil Chemists' Society*, 82(6), pp. 399–408. doi: 10.1007/s11746-005-1084-3.

Sirota, E. B. and Herhold, A. B. (1999) 'Transient Phase – Induced Nucleation', *Science*, 283, pp. 529–533. doi: 10.1126/science.283.5401.529.

Sirota, E. and Herhold, A. (2000) 'Transient rotator phase induced nucleation in n-alkane melts', *Polymer*, 41(25), pp. 8781–8789. doi: 10.1016/S0032-3861(00)00221-4.

Smith, K. W., Bhaggan, K., Talbot, G. and van Malssen, K. F. (2011) 'Crystallization of Fats: Influence of Minor Components and Additives', *Journal of the American Oil Chemists' Society*, 88(8), pp. 1085–1101. doi: 10.1007/s11746-011-1819-7.

Stöver, H.-M., Eggers, R. and Stein, W. (1983) 'Speiseölfraktionierung', *Fette, Seifen, Anstrichmittel*, 85(1), pp. 534–538.

Takeuchi, M., Ueno, S. and Sato, K. (2003) 'Synchrotron Radiation SAXS / WAXS Study of Polymorph-Dependent Phase Behavior of Binary Mixtures of Saturated Monoacid Triacylglycerols', *Crystal Growth & Design*, 3(3), pp. 369–374. doi: 10.1021/cg025594r.

Talbot, G., Smith, K. W. and Cain, F. W. (2006) 'Solvent fractionation of palm oil', *Inform*, 17(5), pp. 324–326.

Tan, C. P. and Che Man, Y. B. (2002a) 'Comparative differential scanning calorimetric analysis of vegetable oils: I. Effects of heating rate variation.', *Phytochemical analysis : PCA*, 13(3), pp. 129–41. doi: 10.1002/pca.633.

Tan, C. P. and Che Man, Y. B. (2002b) 'Differential scanning calorimetric analysis of palm oil, palm oil based products and coconut oil: effects of scanning rate variation', *Food Chemistry*, 76(1), pp. 89–102. doi: 10.1016/S0308-8146(01)00241-2.

Timms, R. E. (1984) 'Phase behaviour of fats and their mixtures', *Progress in Lipid Research*, 23(1), pp. 1–38. doi: 10.1016/0163-7827(84)90004-3.

Timms, R. E. (1985) 'Physical properties of oils and mixtures of oils', *Journal of the American Oil Chemists' Society*, 62(2), pp. 241–249. doi: 10.1007/BF02541385.

Timms, R. E. (1997) 'Fractionation', in Gunstone, F. D. and Padley, F. B. (eds) *Lipid Technologies and Applications*. New York: Marcel Dekker, pp. 199–222.

Timms, R. E. (2005) 'Fractional crystallisation - the fat modification process for the 21st century', *European Journal of Lipid Science and Technology*, 107(1), pp. 48–57. doi: 10.1002/ejlt.200401075.

Timms, R. E. (2006) 'Fractionation of palm oil: Current status, future possibilities', *Inform*, 18(1), pp. 59–62.

Uauy, R., Aro, A., Clarke, R., Ghafoorunissa, R., L'Abbé, M., Mozaffarian, D., Skeaff, M., Stender, S. and Tavella, M. (2009) 'WHO scientific update on trans fatty acids: Summary and conclusions', *European Journal of Clinical Nutrition*, 63, pp. 68–75. doi: 10.1038/ejcn.2009.15.

Vanhoutte, B., Dewettinck, K., Vanlerberghe, B. and Huyghebaert, A. (2003) 'Monitoring milk fat fractionation: Filtration properties and crystallization kinetics', *Journal of the American Oil Chemists' Society*, 80(3), pp. 213–218. doi: 10.1007/s11746-003-0679-z.

Verstringe, S., Danthine, S., Blecker, C., Depypere, F. and Dewettinck, K. (2013) 'Influence of monopalmitin on the isothermal crystallization mechanism of palm oil', *Food Research International*. Elsevier Ltd, 51(1), pp. 344–353. doi: 10.1016/j.foodres.2012.12.034.

Walker, R. C. and Bosin, W. A. (1971) 'Comparison of SFI, DSC and NMR methods for determining solid-liquid ratios in fats', *Journal of the American Oil Chemists Society*, 48(2), pp. 50–53. doi: 10.1007/BF02635684.

Wentzel, N. and Milner, S. T. (2010) 'Crystal and rotator phases of n -alkanes: A molecular dynamics study', *Journal of Chemical Physics*, 132(4), pp. 1–10. doi: 10.1063/1.3276458.

Wille, R. L. and Lutton, E. S. (1966) 'Polymorphism of Cocoa Butter', *J Am Oil Chem Soc*, 43, pp. 491–496.

Wright, A. J., Narine, S. S. and Marangoni, A. G. (2000) 'Comparison of experimental techniques used in lipid crystallization studies', *Journal of the American Oil Chemists' Society*, 77(12), pp. 1239–1242. doi: 10.1007/s11746-000-0194-2.

Xie, B., Liu, G., Jiang, S., Zhao, Y. and Wang, D. (2008) 'Crystallization behaviors of n-octadecane in confined space: Crossover of rotator phase from transient to metastable induced by surface freezing', *Journal of Physical Chemistry B*, 112(42), pp. 13310–13315. doi: 10.1021/jp712160k.

Yan, W. (2017) 'A makeover for the world's most hasted crop', *Nature*, 543, pp. 306–308.

Zhou, Y. and Hartel, R. W. (2006) 'Phase behavior of model lipid systems: Solubility of high-melting fats in low-melting fats', *Journal of the American Oil Chemists' Society*, 83(6), pp. 505–511. doi: 10.1007/s11746-006-1233-8.